# The Role Of MicroRNAs In The Peripheral Circadian Rhythms Of Cartilage

## **Molly-Kay Bridget Bailey**

THESIS SUBMITTED FOR THE DEGREE OF DOCTOR OF PHILOSOPHY

University of East Anglia School of Biological Sciences 100275254/1

2025

This copy of the thesis has been supplied on condition that anyone who consults it is understood to recognise that its copyright rests with the author and that use of any information derived there-from must be in accordance with current UK Copyright Law. In addition, any quotation or extract must include full attribution.

### **ABSTRACT**

Osteoarthritis (OA) is a chronic joint disease characterised by gradual loss of the articular cartilage (AC), OA affects 7.6% of the global population and clinical interventions have been limited OA's complex pathogenesis. The peripheral circadian clock and microRNAs (miR) are mediators of chondrocyte gene expression and, their deregulation is associated with AC degeneration in OA. An informed understanding of their intrinsic regulators may aid the development of novel therapies. Therefore, the purpose of this study has been to characterise co-regulation between the time keeping mechanism and microRNAs using an *in-vitro* and *in-vitro* model of AC.

Time keeping mechanisms pivots around core clock proteins oscillating in an autoregulatory transcriptional/translational feedback loop. In this study, clock genes *CLOCK*, *RORα PER2 CRY2* were targeted by miR-455-5p and *NPAS2* was targeted by mir-455-3p in 3'UTR luciferase reporter assays. No significant changes in the expression of circadian genes was identified in RNA-seq data of *miR-455* KO mouse AC or miR-455 overexpression in SW1353 cells. miRNAs are likely subtle modulators of the clock gene expression with roles in determining circadian phase and amplitude.

Using a circadian small RNA sequencing model, 19.5% of chondrocyte miRNAs exhibit autonomous 24-hour oscillations in knee AC. Two-thirds of rhythmic miRNAs peaked within the animal's rest-phase including miR-23a-5p and miR-30b-5p, miR-30d-3p and miR-30c-2-3p of the miR-30 family. The 5p arms of the miR-30 family share a conserved 6-mer seed region, though were differentially regulated by the clock diversifying their biological function. miR-17-5p and miR-18a-5p of the miR-17/92 cluster, were co-regulated and peaked at CT12. Circadian regulation of miR-17-5p was a conserved mechanism between knee and hip AC and transcripts oscillated in antiphase. miR-140-5p was stably expressed in knee AC, whilst miR-140-5p oscillated in SW1353 cells *in-vitro*. This demonstrates that the miRNAomes are differentially regulated between human and mouse and may evolve to accommodate different biophysical tissue demands. The miRNAome hosted miRNAs involved in AC physiology and putative targets were enriched for cartilage development and extracellular matrix ontologies. Thus, the miRNAome emerges as an effector of the clock mechanism. and future work will study the implications of daily fluctuations in miRNA abundance as on AC homeostasis.

i

#### **Access Condition and Agreement**

Each deposit in UEA Digital Repository is protected by copyright and other intellectual property rights, and duplication or sale of all or part of any of the Data Collections is not permitted, except that material may be duplicated by you for your research use or for educational purposes in electronic or print form. You must obtain permission from the copyright holder, usually the author, for any other use. Exceptions only apply where a deposit may be explicitly provided under a stated licence, such as a Creative Commons licence or Open Government licence.

Electronic or print copies may not be offered, whether for sale or otherwise to anyone, unless explicitly stated under a Creative Commons or Open Government license. Unauthorised reproduction, editing or reformatting for resale purposes is explicitly prohibited (except where approved by the copyright holder themselves) and UEA reserves the right to take immediate 'take down' action on behalf of the copyright and/or rights holder if this Access condition of the UEA Digital Repository is breached. Any material in this database has been supplied on the understanding that it is copyright material and that no quotation from the material may be published without proper acknowledgement.

# TABLE OF CONTENTS

ABSTRACT	I
TABLE OF CONTENTS	II
List of Figures	VII
LIST OF TABLES	X
LIST OF APPENDICES	XI
DEDICATIONS	XII
CHAPTER 1:INTRODUCTION	
1.1 STRUCTURES OF THE SYNOVIAL JOINT	1
1.1.1 The articular capsule	1
1.1.2 Articular Cartilage	2
1.1.2.1 Extracellular Matrix	2
1.1.2.1.1 Zones	3
1.1.2.1.2 Collagens	6
1.1.2.1.3 Proteoglycan	6
1.1.2.1.4 Water	7
1.1.2.1.5 Chondrocytes	7
1.2 Osteoarthritis	9
1.2.1 OA pathogenesis	9
1.2.1.1 Mechanisms of cartilage destruction	
1.2.1.1.1 Matrix degrading enzymes	
1.2.1.1.2 Altered catabolic signalling	
1.2.2 OA risk Factors	14
1.2.2.1 Non-modifiable risk factors	14
1.2.2.1.1 Ageing	14
1.3 CIRCADIAN RHYTHMS	16
1.3.1 Central circadian oscillators	16
1.3.2 The molecular clock	17
1.3.3 Tissue-specific clock	20
1.3.4 Cartilage circadian clocks	21
1.3.4.1 Evidence of circadian clocks in cartilage	21
1.3.4.1.1 Autonomous clock gene expression	21

1.3.4.1.2	The chondrocyte circadian transcriptome	22
1.3.4.1.3	Cartilage clock entrainment factors	23
1.3.4.2	Osteoarthritis and circadian rhythms	25
1.4 M	ICRORNAS	27
1.4.1	miRNA biogenesis	27
	miRNA mechanism of action	
1.4.3	miRNAs and the molecular circadian clock	31
1.4.3.1	Circadian miRNAs	31
1.4.3.2	Regulation of the circadian clock by miRNAs	32
1.4.4	Cartilage miRNAs	34
1.4.4.1	miRNAs in cartilage development	34
1.4.4.2	miRNAs, cartilage homeostasis and disease	35
1.4.4.3	miRNAs and cartilage circadian rhythms	37
1.4.5	Hypothesis and Aims	37
CHAPTE	ER 2:MATERIALS AND METHODS	39
2.1 M	ATERIALS	39
	Cell models	
2.1.1.1	E.coli Strains	
2.1.1.2	Mammalian cell lines	
2.1.2	Murine models	
2.2 M	ETHODS	40
	Cell culture	
2.2.1.1	Bacterial growth conditions	
2.2.1.2	Mammalian cell culture conditions	
2.2.2	Molecular methods	
2.2.2.1	Isolation of human genomic DNA	41
2.2.2.2	Polymerase chain reaction (PCR)	
2.2.2.2.1	Total RNA isolation from cultured cells	41
2.2.2.2.2	Total RNA isolation from murine tissues	42
2.2.2.2.3	Total RNA quantification	42
2.2.2.2.4	Reverse Transcription	42
2.2.2.3	Quantitative real time polymerase chain reaction (qRT-PCR)	42
2.2.2.3.1	Universal Probe library qRT-PCR	42
2.2.2.3.2	SYBR ® Green qRT-PCR	43
2.2.2.4	Small-RNA sequencing	44
2.2.2.5	Subcloning	45
2.2.2.5.1	Circadian gene 3'UTR pmirGLO constructs	45

2.2.2	2.5.2 Primer design	45
2.2.2	2.5.3 Amplification of 3'UTR	46
2.2.2	2.5.4 Agarose gel purification	47
2.2.2	2.5.5 Plasmid digestion	47
2.2.2	2.5.6 E.coli transformation	47
2.2.2	2.5.7 Plasmid verification	47
2.2.2	2.5.8 Site directed mutagenesis of pmirGLO	49
2.2.3	3 Cell culture and cell-based assays	50
2.2.3	3.1 SW1353 circadian time series model	50
2.2.3	3.2 Cell viability assay (Presto Blue)	50
2.2.3	3.3 Identifying clock gene targets of hsa-miR-455-3p and hsa-miR-455-5p	51
2.2.3	3.3.1 Transient transfection of circadian 3'UTR constructs and miR-455 mimic	51
2.2.3	3.3.2 Dual-GLO luciferase assay	51
2.2.4	4 Mouse models	52
2.2.4	4.1 Wild-type mouse circadian time series model	52
2.2.3	5 In-silico	53
2.2.3	5.1 Identification of microRNA circadian gene targets	53
2.2.0	6 Data analysis	54
2.2.0	6.1 Quantitative RT-qPCR	54
2.2.0	6.1.1 Housekeeper gene	54
2.2.0	6.2 Relative gene expression- comparative $C_t$ method	54
2.2.6	6.3 Analysis of NGS data	54
2.2.6	6.4 Detection of circadian rhythmicity	55
2.2.6	6.4.1 Parametric model	55
2.2.6	6.4.2 Non-parametric model (RAIN)	55
2.2.6	6.5 Gene set enrichment analysis	55
2.2.0	6.6 Statistical analysis	56
CHAI	PTER 3:EXPLORING CIRCADIAN REGULATION OF	MIRNA
EXPR	RESSION IN CARTILAGE (IN-VITRO)5	7
3.1	Introduction	57
3.2	AIMS	59
3.3	Results	60
3.3.	1 Developing a statistical model for detection of oscillating components in-vitro	60
3.3.2		
3.3.3		
	ck by oscillation of BMAL1	
3.3.4		

3.3	.5	Determining oscillation of positive, negative, and auxiliary limb circadian genes in SW1353
syn	chr	onised in dexamethasone
3.3	.6	Identifying circadian miRNAs in SW1353 chondrosarcoma cells
3.3	.7	Exploring regulatory mechanisms of circadian miRNA expression
3.3	.8	Evaluating the utility of the 'rest-phase' in the SW1353 circadian time series protocol 84
3.4	Ι	DISCUSSION
СНА	PT	ER 4:REGULATION OF THE CHONDROCYTE CIRCADIAN CLOCK BY
HSA	-M	IR-45591
4.1	I	NTRODUCTION91
4.2	A	AIMS
4.3	F	RESULTS93
4.3	.1	Exploring expression of core clock genes in-vivo and in-vitro miR-455 data sets93
4.3	.2	Identification of miR-455-3p and miR-455-5p predicted targets95
4.3	.3	miRNA-455-3p and miRNA-455-5p directly target the circadian clock
4.4	Ι	DISCUSSION
СНА	PT	ER 5:DEFINING THE MOUSE CARTILAGE MIRNAOME 105
5.1	I	NTRODUCTION
5.2	A	AIMS
5.3	F	RESULTS107
5.3	.1	Optimising RNA extraction from murine cartilage
5.3	.2	Identifying stably expressed housekeeper gene
5.3	.3	Validating an autonomous molecular clock in a mouse cartilage model111
5.3	.4	Identifying circadian miRNAs by small-RNA-sequencing in mouse knee cartilage
5.3	.4.1	Developing a statistical model for identifying circadian miRNAs in small RNA sequencing
dat	ta se	ets in-vivo.
5.3	.4.2	Global analysis of small-RNA-sequencing data
5.3	.4.3	RAIN analysis
5.3	.4.4	Time dependent expression of miRNAs by RT-qPCR in knee, hip, and xiphoid cartilage 129
5.3	.4.5	GO-term analysis of rhythmic miRNA targets
5.3	.4.6	
5.4	Ι	DISCUSSION
		ER 6:GENERAL DISCUSSION AND FUTURE DIRECTION 143
СПА	1 1	ER U.GENERAL DISCUSSION AND FUTURE DIRECTION 143
6.1	(	CIRCADIAN REGULATION OF MIRNA EXPRESSION IN CARTILAGE 143

APP	EN	NDICES	179
BIBI	I(	OGRAPHY	153
6.2	Τ	THE ROLE OF MIRNA-455 IN THE CHONDROCYTE CIRCADIAN CL	оск 147
6.1.	2	In-vivo	145
6.1.	1	In-vitro	144

## LIST OF FIGURES

Figure 1. 1 Structures of articular cartilage
Figure 1. 2 Mechanisms of synovial joint destruction in osteoarthritis13
Figure 1. 3 Molecular mechanisms of the circadian clock
Figure 1. 4 Canonical biogenesis of miRNAs in mammals29
Figure 2. 1 Map of the pmirGLO plasmid. Generated from SnapGene viewer45
Figure 3. 1 Parameters of circadian rhythms
Figure 3. 2 Stepwise protocol for the evaluation detection of oscillating components in articular cartilage in by parametric models RT-qPCR and smallRNA sequencing data
Figure 3. 3 Expression levels of candidate housekeeper genes in SW1353 synchronized in 50% FCS or 100nM dexamethasone
Figure 3. 4 Determining efficacy of serum shock as a cell synchronising agent by induction of <i>BMAL1</i> oscillation
Figure 3. 5 Determining efficacy of Dexamethasone as a cell synchronising agent by induction of <i>BMAL1</i> oscillation
Figure 3. 6 Cosinor analysis of BMAL1 abundance in SW1353 following dexamethasone synchronisation
Figure 3. 7 Comparing parameters of <i>BMAL1</i> oscillation across the SW1353 time series
Figure 3. 8 Measuring the viability of SW1353 in a 72-hour circadian time series mode by PrestoBlue
Figure 3. 9 Rhythmic expression of positive and negative limb genes of the molecular circadian clock in SW1353
Figure 3. 10 Average abundance of miR-140 and miR-455 in SW1353 chondrosarcoma cells

Figure 3. 11 Time dependent expression of miR-140-3p79
Figure 3. 12 Time dependent expression of miR-455-3p and miR-455-5p80
Figure 3. 13 Diurnal expression of <i>DICER1</i> and <i>DROSHA</i> in SW1353 chondrocytes.82
Figure 3. 14 Phase relationships of <i>BMAL1</i> , <i>SOX9</i> and miR-140-3p transcripts in SW1353 chondrocytes
Figure 3. 15 Revised model for the detection of circadian microRNAs in cartilage <i>in-vitro</i>
Figure 3. 16 Oscillation of <i>BMAL1</i> mRNA in the rest phase of circadian protocol86
Figure 3. 17 Determining immediate effects of dexamethasone on cartilage gene expression
Figure 4. 1 Identifying miR-455-5p clock targets by dual-glo luciferase assay99
Figure 4. 2 Identifying miR-455-3p clock targets by dual-glo luciferase assay100
Figure 5. 1 Optimising murine cartilage RNA extraction
Figure 5. 2 Demonstrating autonomous <i>Bmal1</i> oscillation in mouse tissues by RT-qPCR.
Figure 5. 3 Evaluating bone and muscle contamination in hip AC113
Figure 5. 4 Schematic diagram for the statistical analysis of time series data determined by qPCR and small-RNA-sequencing in mice
Figure 5. 5 Quality control of knee AC samples for small-RNA seq analysis117
Figure 5. 6 Distribution of small RNAs in knee articular cartilage119
Figure 5. 7 Principal component analysis of small-RNA sequencing data. Axes of variation in small-RNA sequencing data was determined by PCA and clustering analysis
Figure 5. 8 Average abundance of key miRNAs in mouse cartilage121
Figure 5. 9 Periodic functions of circadian microRNAs in mouse knee cartilage126
Figure 5. 10 Circadian expression of miR-30 family in mice

Figure 5. 11 Cosinor analysis of miR-30.
Figure 5. 12 Determining time dependent expression of miR-196a-5p, miR-17-3p, miR-
30c-2-3p in mouse knee and hip AC by RT-qPCR130
Figure 5. 13 Diurnal expression of <i>dicer1</i> and <i>drosha</i> mRNA in mouse cartilage and liver.
137
Figure 5. 14 Diurnal expression of pre-miR-30c-2 in mouse knee cartilage138
Figure 5. 15 Oscillating microRNAs target key regulators of cartilage development,
homeostasis, and diseases
Figure 6. 1 Schematic of the proposed output mechanisms of the circadian clock in
chondrocytes
Figure 6. 2 Schematic of the proposed interactome of miR-455 in chondrocytes and its
associated physiological processes

## LIST OF TABLES

Table 1 Post-transcriptional regulation of circadian clock genes by microRNAs33
Table 2. 1 Temperature cycles for universal probe library quantitative PCR reactions.43
Table 2. 2 miRNA RT-qPCR assay ID
Table 2. 3 PCR reaction for 3'UTR amplification
Table 2. 4 PCR thermal cycles for amplification of 3'UTR inserts
Table 2. 5 Reaction for QuikChange Lightning mutli-site directed mutagenesis kit .49
Table 2. 6 PCR protocol for QuikChange Lightning mutli-site directed mutagenesis kit
Table 2. 7 Outline of Presto Blue assay experimental conditions
Table 3. 1 Ranking of candidate reference genes by RefFinder software66
Table 4. 1 Circadian clock genes abundance in miR-455 RNA seq datasets94
Table 4. 2 Predicted circadian targets of miR-455-3p and miR-455-5p96
Table 5. 1 Determining expression stability of housekeeper genes in mouse tissues.110
Table 5. 2 Identification of the circadian miRNAome in mouse knee cartilage <i>in-vivo</i> .
Table 5. 3 GO term analysis oof miR-30-2-3p targets
Table 5. 4 GO term analysis of miR-17-5p targets
Table 5. 5 GO term analysis oof miR-196a-5p targets

## LIST OF APPENDICES

Appendix Table 1. 1 RT-qPCR primer and probe universal probe library
Appendix Table 1. 2 Human RT-qPCR primer and probe Sybr green
Appendix Table 1. 3 Mouse RT-qPCR primer and probe Sybr green
Appendix Table 1. 4 Circadian clock gene 3'UTR cloning Wild-type and mutant primers for miR-455-5p assay
Appendix Table 1. 5 . Circadian clock gene 3'UTR cloning Wild-type and mutant primers for miR-455-3p assay
Appendix Figure 2. 1 Comparing cosinor analysis of <i>BMAL1</i> abundance in non-synchronised and synchronised SW1353 cells
Appendix Figure 2. 2 Rhythmic expression of NPAS2 and RORα genes of the molecular circadian clock in SW1353
Appendix Figure 2. 3 Average abundance of miR-140 and miR-455 in SW1353 chondrosarcoma cells
Appendix Figure 2. 4 Effects of dexamethasone on DICER1 and DROSHA abundance in chondrocytes
Appendix Figure 2. 5 Oscillation of BMAL1 in SW1353 chondrosarcoma cells synchronised in 50% FCS
Appendix Figure 3. 1 Identifying miR-455-5p clock targets by dual-glo luciferase assay191
Appendix Figure 4. 1. Circadian expression of miR-17/92 cluster in knee AC
Appendix Figure 4. 2. Cosinor analysis of circadian miRNA identified by RAIN
Appendix Table 4. 1 Abundance of microRNAs in mouse knee AC determined by small-RNA sequencing
Appendix Table 4. 2 Identification of the circadian miRNAome in mouse knee cartilage in-vivo (P>0.05)

## **DEDICATIONS**

For my wonderful dad,
Until the lines on my skin tell the tales without you,
and then we'll be together again forever more.

Love Doshy x

#### **Chapter 1:** Introduction

Osteoarthritis (OA) is a chronic degenerative disease of the synovial joints, causing pain, deformity, and gradual loss of function. OA a leading cause of disability in older adults and affect 500million individuals worldwide – posing a sizable healthcare burden (1). However, despite its prevalence, there is no effective treatment for OA. Existing treatments include a trajectory of palliative pharmacological drugs for control of pain and invasive surgeries for end-stage OA (e.g. joint arthroplasty and replacement). Clinical outcomes of these therapies are variable and, often affected by different localisations of disease(2). This has created demand for alternative interventions, capable of addressing the pathophysiological and biochemical disease mechanisms. Whilst the risk factors of OA have been explored (e.g. age, gender, injury, and genetics); the aetiology and pathogenesis remain largely undefined. Recently, microRNAs (miRNAs) and the molecular circadian clock have emerged as mediators in joint health and disease. However, few studies have focused on crosstalk between these two factors and their co-regulation of joint homeostasis. Here, our current understandings of the roles of circadian rhythms and microRNAs in tissue homeostasis is reviewed and their roles in the rebranding of joint tissues in OA.

#### 1.1 Structures of the synovial joint

Synovial joints (diarthroses) are freely movable and function to protect articulating bones during movement by absorbing loads and reducing friction. Synovial joints are found within the knee, hip, wrist, and elbow and are characterised by an articular capsule, enclosing a joint cavity filled with synovial fluid (SF)(3). Here, the ends of bones are protected by a thin layer of hyaline cartilage (articular cartilage) which, unlike most tissues, is avascular and aneural (4). Osteoarthritis is a degenerative disease of the synovial joints and, is driven by dysfunction in its components(5). Therefore, an informed understanding of the biological and mechanical characteristics of the synovial joints is essential in the development of preventative and curative therapies.

#### 1.1.1 The articular capsule

The articular capsule is divided into an outer capsular ligament and inner synovial membrane. The capsular ligament is continuous with the periosteum, composed of dense collagen fibrils which hold articulating bones together(6).

The role of the synovium is to support joint homeostasis by synthesising the SF. SF functions as a biological lubricant and biochemical pool for the exchange of nutrients, regulatory elements, and waste between the perichondral circulation and the avascular AC (4). Structurally, the synovium a is highly vascular areolar tissue made of two layers; the intimal and subintimal. The *intimal layer* is 1-4 cell layers thick with no basement membrane. This configuration enables ultrafiltration of blood plasma molecules (<10kDa) into the synovial cavity, forming the SF(6). Cell types of the intima include synovial macrophages (type A synoviocytes) and synovial fibroblasts (type B synoviocytes)(7,8). Type B synoviocytes synthesise lubricants of the SF including high-molar mass hyaluronans and lubricin. Lubricin functions to maintain a low friction coefficient and, its deficiency has been linked with progressive wear and pain in OA patients (9). In contrast, the *subintimal layer* is vascularised and relatively acellular; composed of fibrous, areolar, or adipose tissues. Vasculature of the subintimal layers is derived from branches of epiphyseal arteries running at the periosteum junction – forming the perichondral circulation(4,10).

#### 1.1.2 Articular Cartilage

AC is a highly specialised tissue, overlaying bone surfaces in synovial joints where it reduces friction during movement. It is composed of a dense extracellular matrix (ECM), maintained by specialised cells termed chondrocytes (Figure 1.1). These components form the origins the of compressive and tensile strength of AC and, their preservation is essential for joint function. Despite this, AC has a low regenerative capacity partially due to its avascular and aneural status. As result, degeneration of the AC often follows injury and is a common artefact in joint diseases including secondary OA (11).

#### 1.1.2.1 Extracellular Matrix

The ECM of AC is primarily composed of water, collagen, and proteoglycan. Together, these components from a complex fibrillar network permitting the compressive and tensile strength required for smooth articulation. Anatomically, the ECM can be divided into four zones: superficial, transitional, deep, and calcified cartilage. Each zone can be further divided into 3 regions – the pericellular region, the territorial region, and the interterritorial region(12). Here, chondrocyte morphology and fibrillar networks differ in organisation to meet the biomechanical requirements of the tissue.

#### 1.1.2.1.1 Zones

As shown in Figure 1, the superficial (tangential) zone (SZ) forms the outer layer of AC (10% - 20% of total thickness) and is covered by a thin layer of lubricin for surface lubrication(13). This zone has the highest water content and hosts a tangential arrangement of collagen fibres (type I, II and IX), providing tensile and sheer strength. Here, chondrocytes are ellipsoid and populate an ECM high in collagens and low proteoglycan.(14) As result, the SZ has a lower resistance to compressive forces, though still essential in the overall mechanical behaviour of AC. Indeed, degradation of the superficial zone is an early artefact of OA.

Immediately deep to the SZ is the middle (transitional) zone (MZ), representing 40% - 60% of AC volume. MZ chondrocytes are spherical, lower in density and show robust matrix production, consistent with a higher number of synthetic organelles. Morphologically, this zone is an intermediate of the SZ and DZ; defined by an oblique arrangement of thicker collagen fibrils and a higher density of proteoglycans (i.e. aggrecan). This composition facilitates hydration of the ECM, acting as the first line of resistance to compressive forces(15).

The deep zone (DZ) is responsible for providing the greatest resistance to compressive forces; characterised by a greater range of fibril diameters in a radial position and, the highest proteoglycan content. Typically, chondrocytes are arranged in a columnar orientation, parallel to collagen fibres(16). Though lower in density, the biosynthetic activity of chondrocytes in the DZ is 10-fold higher, comparative to the SZ, evidenced by assessing incorporation of {3H}proline and [35S]sulphate.(17) A 'tidemark' represents the interface between the DZ and calcified cartilage(18). This boundary is considered a resting mineralisation front and, its duplication (therefore, advancement) is an early feature OA, likely driven by reactivation of endochondral ossification pathways(19).

The calcified cartilage zone (CCZ) lies between the tide mark and the cement line, consisting of dispersed hypertrophic chondrocytes within a calcified matrix of type I collagen, sodium hyaluronate and nanohydroxyapatite.(20) Here, perpendicular collage type II fibres couple with collagen type I; cementing uncalcified cartilage to subchondral bone; thus, diffusing load (20,21). As reviewed by *Boushell et al* (22), the CCZ may aid AC nourishment by transportation of small solutes between the subchondral bone and DZ, stabilising chondrocytes in the hypoxic environment of the DZ(23). Enlargement of the CCZ is regarded as an artefact

of ageing and also primary OA(24). In this way, pathological changes in the CCZ may contribute to degeneration of AC.

4

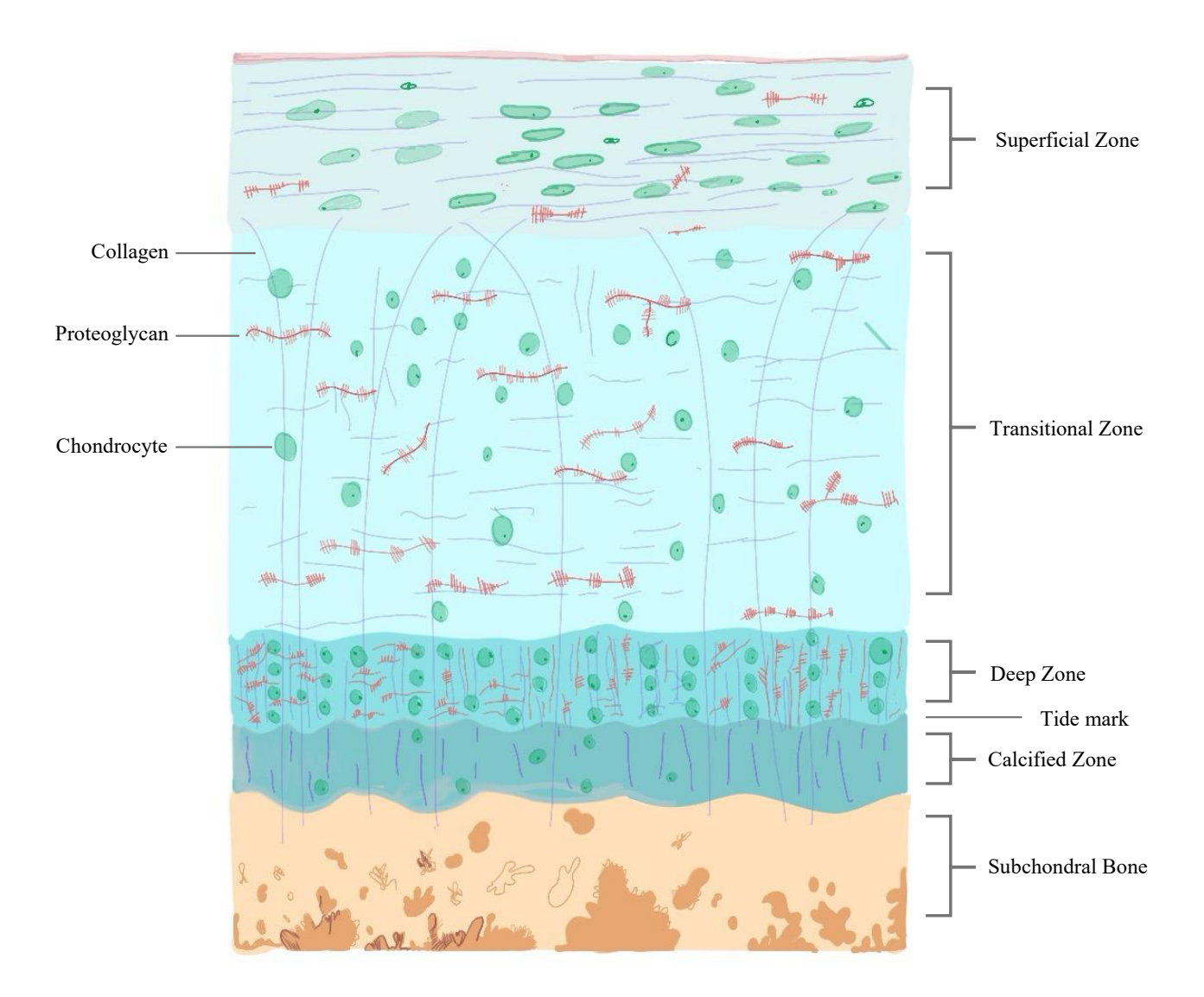


Figure 1. 1 Structures of articular cartilage.

Articular cartilage can be divided into 4 zones. Superficial zone: chondrocytes are ellipsoid, collagen fibrils are parallel to the articular surface. Transitional zone: chondrocytes are spherical, and collagens are randomly orientated. Deep Zone: chondrocytes are arranged in columns and collagen fibrils are perpendicular to articular surface. Calcified zone is formed of dispersed hypertrophic chondrocytes in a calcified collagen matrix. Tide mark separates deep zone and calcified bone.

#### **1.1.2.1.2** Collagens

Collagen fibrils form the structural backbone of the ECM in AC, accounting for approximately two-thirds dry weight(25). This is composed mainly of Type II collagen, transcribed from the *COL2A1* gene by chondrocytes. Other collagens (types I, VI, IX, X, XI, XII and XIV) are present in lesser quantities, though their precise function is under discussion (26). Initially, collagens are secreted into the ECM as a pro-collagen molecule, formed of three α-chains in a helix. Mature collagen results from C- and N- termini cleavage by specific proteases (e.g. ADAMTS2, 3 14 and BMP-1) and subsequently, assemble into a heavily crosslinked heteropolymers. The surface of the fibrils is stabilised by type IX and XI collagen, as well as leucine-rich proteoglycans including decorin, fibromodulin and biglycan (27,28). As mentioned, AC tensile strength depends on extensive collagen crosslinking and its zonal changes in fibril architecture. Despite this, AC chondrocytes show a poor recapitulative capacity following injury, posing a fundamental flaw in AC. Indeed, type II collagen denaturation is an artefact in early OA and a prelude to SZ fibrillation(29). Similarly, *COL2A1* mutations have been associated with spondyloepiphyseal dysplasia and, early lethality is reported in *col2a1* double knockout mice(30,31).

#### 1.1.2.1.3 Proteoglycan

Proteoglycans are the second largest load bearing molecule in AC; formed of a protein core covalently bound to glycosaminoglycans (GAGs). Aggrecan is the major proteoglycan in AC and is characterised by its capacity to associate with hyaluronan (HA) and link proteins to form hydrated immobilised aggregates in interfibrillar spaces of the ECM(32). The core protein of aggrecan is composed of 3 globular domains (G1, G2,G3) and three extended domains (IGD, KS, CS). Functionally, G1 is responsible for interaction with hyaluronan and link protein, forming stable ternary complexes in the ECM. G1 and G2 are separated by an interglobular domain (IGD), containing proteolytic cleavage sites. A long-extended region, decorated with chondroitin sulphate (CS) and keratan sulphate (KS) chains, divides G2 and G3. The fixed anionic groups of the GAGs account for aggrecans polyanionic charge, attracting freely diffusible ions (i.e. sodium cations (Na+) and chloride anions (Cl-)) and in turn, water(33). Absorption of water from the synovial fluid results in swelling of collage fibrils to form a hydrated gel-like structure capable of resisting compressive loads.

#### 1.1.2.1.4 Water

Water accounts for 80% of AC wet weight. Despite this, defining the mechanical significance of water in AC has been controversial. Current models argue AC stiffness may originate from the distribution and fluidity of water, in a three-phase mechanical model of AC (34). Here, water is partitioned between intrafibrillar (IF) and extrafibrillar (EF) spaces and its division serves mechanical significance. IF water is defined as the volume between collagen fibrils – where it supports the tertiary structure of mature collagen. In unloaded AC, IF accounts for 30% of total water and can be exchanged with EF under osmotic stress (35). In contrast, EF exists as a diffusible electrolyte gel in the pore space of the ECM, aiding the transport of essential nutrients to chondrocytes and AC swelling pressure. Indeed, appropriate hydration of collagen fibrils and extrafibrillar space is a determinant of its load bearing capacity and, altered hydration is a hallmark of OA, preluding radiographic artefacts (36,37).

#### 1.1.2.1.5 Chondrocytes

In mature AC, chondrocytes are the sole cell type and are responsible for matrix synthesis and its maintenance. AC chondrocytes originate from mesenchymal stem cells (MSCs) in the developing embryo during endochondral ossification. As reviewed by Goldring *et al*, this is process has 4 steps; chondrogenesis, chondrocyte differentiation and hypertrophy, bone cell invasion and matrix mineralisation and bone formation (38). Briefly, chondrogenesis begins with the aggregation and condensation of loose mesenchyme to form cartilage analgen. SRY-box 9 (SOX9) is a pivotal transcription factor in this process, prompting rapid differentiation of condensations into early-stage chondrocytes followed by their active proliferation, maturation, and synthesis of ECM macromolecules(39). Meanwhile cells near the analgen's centre undergo hypertrophy, terminal differentiation, and apoptosis. Bone is formed when the residual cartilage matrix becomes vascularised and serves as a scaffold for mineral deposition by invading osteoclasts and osteoblasts.

In mature AC, matrix generation and maintenance is dependent on homeostasis between ECM synthesis (i.e. anabolism) and turnover (i.e. catabolism) (40). Indeed, proteomic analysis of the secretome in healthy AC reflects this (Reviewed (41)). Collagens (type II, VI and XII) and proteoglycans are most abundant ECM molecules, alongside proteoglycan aggrecan, HPLN-1 (proteoglycan link protein), COMP and chitinase-3-like-protein 1 (CHI3L1). Concomitantly, concentrations of catabolic enzymes, including the matrix-metalloproteinase family (MMP),

were low or only identified following stimulation with IL-1 $\beta$ . Given AC is avascular and therefore hypoxic, chondrocytes rely on diffusion for the receipt of metabolites and anaerobic respiration (i.e. glycolysis)(42).

#### 1.2 Osteoarthritis

As a 'whole joint' disease, pathologies of OA include AC degradation, synovial inflammation, and osteophyte formation (Figure 1.2). Generally, OA can be classified as either idiopathic (i.e. the causes is unknown) or secondary due to risks factors including injury, age, genetic predisposition, and systemic factors(43). Though, determining case aetiologies is challenging given dissociation between clinical symptoms and radiographic findings. For instance, 40% of patients with moderate radiographic knee OA were asymptomatic(43). Here, interplay between OA risk factors and its key molecular mechanisms are discussed.

#### 1.2.1 OA pathogenesis

In both idiopathic and secondary incidences of OA, disease progression is driven by imbalance in catabolic and anabolic pathways in the joint, favouring a state of low-grade inflammation. This is characterised by increased expression of pro-inflammatory mediators (e.g. IL-1β, TNF-α, TGF-β, CCL2, CCL4) and matrix degrading enzymes (e.g., MMP13, ADAMTS5) which, in turn, prompts degradation of the ECM, vascularisation, cartilage calcification and tissue degeneration. (44) Marked changes in chondrocyte phenotype are also observed beginning with activation, proliferation, and the assumption of a hypertrophic-like phenotype. This is evidenced by the downregulation of AC markers (*ACAN*, *COL2A1* and *PRG4*) and upregulation of hypertrophy markers (*IHH*, *COL10A1* and *RUNX2*) expression(45,46). Progression of OA is also marked by decreased transcription of anti-angiogenic factors (chondromodulin and troponin-C) leading to increased AC vascularisation, cartilage mineralization and osteophyte formation. Notably, these cascades resemble those observed in endochondral ossification and as reviewed by Jaswal *et al*, several OA therapies have been reexamined from a developmental biology perspective (47).

#### 1.2.1.1 Mechanisms of cartilage destruction

#### 1.2.1.1.1 Matrix degrading enzymes

MMPs and ADAMTSs are families of zinc-containing endopeptidases and are the major catabolic metalloproteases involved in cleavage of ECM proteins in OA; specifically, type II collagen and aggrecan(48). Notably, the presence of these enzymes alone does not constitute pathology, rather, a balance in their activity is required for maintenance of the anabolic and catabolic pathways central to joint health. Under normal physiological conditions, both families regulate chondrocyte behaviour (e.g. ECM biosynthesis, proliferation, differentiation, and

apoptosis) and their abundance and activity is tightly modulated by action of hormones (e.g. estrogen), growth factors (TGF- $\beta$ ) and cytokines (IL-1 $\beta$ ) (49–51). Thus, altered expression of MMP and ADAMTSs is an effector and indicator of pathological state in AC, making them plausible OA biomarkers for diagnosis and assessment of OA.

#### 1.2.1.1.1.1 MMPs

In human AC, MMPs are classified based on their sub-cellular location (i.e. secreted or membrane type) and target macromolecules (i.e. collagenases, gelatinases, stromelysins). In healthy AC, Kevorkian *et al* reported high expression of *MMP2*, *MMP12*, *MMP14* and *MMP19* and moderate expression of *MMP1*, *MMP9*, *MMP13*, *MMP16*, *MMP23* and *MMP24*. Significantly, MMP-1, MMP-2, MMP-13, and MMP-14 were constitutively expressed in AC, whereas MMP-3, MMP-8 and MMP-9 were detected under pathologic circumstances(52). Further, regulation of MMPs may be specific to the anatomical location of AC; MMP-1 is higher in healthy knee AC compared to the hip though, endogenous inhibitors of the MMP family (i.e. TIMP-3) were more abundant in the latter(53).

MMP-13, a secreted collagenase, is the primary collagenase in OA given its capacity to cleave type collagens type II, IV and IX, proteoglycans, perlecan and osteonectin. *In-vivo*, a high expression of MMP-13 and has been associated with AC degradation in human and murine OA models and, progression of meniscal injury-induced OA was decelerated in *Mmp13*<sup>Col2ER</sup> mice(54). Further, administration of a specific MMP13 inhibitor (CL82198) had chondroprotective effects, via reduced loss of collagen type II and chondrocyte apoptosis.

Mechanistically, inflammatory cytokines associated with OA regulate MMP gene expression. *In-vitro*, IL-1 $\beta$  and TNF-  $\alpha$  act synergistically to positively regulate expression of *MMP1* and *MMP13* and, both are overexpressed in OA joints(55). Indeed, increased secretion of IL-1 $\beta$  by chondrocytes and synoviocytes is a known effect of mechanical injury to the joint and prompts activation of MMP-13 by intracellular cascades involving NF- $\kappa\beta$  and MAPK(56,57). Similarly, methylation of histone 3 and STAT3 binding mediated increased *MMP1*, *MMP3* and *MMP13* expression in IL-6 stimulated synovial fibroblast(58).

#### 1.2.1.1.1.2 ADAMTS

The aggrecanases (ADAMTS-1,4, 5, 8, and -15) are a subcategory of the ADAMTS family and mediate ECM degradation early stages of OA(59). Several studies have evidenced this by

detection of C-terminal fragments with a 374ARGSVIL N-terminus neoepitope in the SF of OA patients and in culture media of IL-1\beta treated AC explants. Such fragments are formed by cleavage between amino acid residues Glu<sup>373</sup>-Ala-<sup>374</sup> in aggrecans IGD. Indeed, ADAMTS4 and ADAMTS5 aggrecanases, preferentially cleave aggrecan at Glu<sup>373</sup>-Ala<sup>374</sup> and, polymorphisms in the Adamts5 gene have been correlated to OA susceptibility(60). Significantly, *Adamts 4* is overexpressed in OA and may play a role in oxidative and mechanical stress induced ECM degradation(61). Mechanistically, mRNA and activity levels of ADAMTS4, but not ADAMTS-5 were increased in chondrogenic cultures following addition of H<sub>2</sub>O<sub>2</sub>, IL-1, TNF-α and TGF-β and applied force *in-vitro* indicating ADMATS-4 may have a more prominent role in human OA(62,63). Interestingly, a study reported increased activity of both aggrecanases but no alteration in mRNA levels following retinoic acid treatment in healthy AC; suggesting catabolic role of aggrecanases maybe regulated post-transcriptionally in OA(64). In murine DMM models, the protective effects of Adamts 5 gene knockout and adamts5-specific antibodies were comparable to the Adamts4/Adamts5 double knockout models, emphasizing Adamts5 as the major aggrecan degrading enzyme in mouse OA models, though ADAMTS-4 in humans(65). However, therapeutic utility of ADAMTS5 is limited by the aggrecanases chondroprotective roles in AC. For example, Adamts 5 is constitutively expressed in healthy AC tissue and deleterious accumulation of proteoglycan was observed in the cardiovascular system of Adamts 5 knockout mice(66,67). Therefore, insight into the molecular regulation of aggrecanases may be necessary.

#### 1.2.1.1.2 Altered catabolic signalling

Chronic low-grade inflammation is a well-established mediator of ECM degradation in OA. This is, in part, catalysed by deregulation of inflammatory cytokines (i.e. IL-1 $\beta$ , TNF- $\alpha$  and TGF- $\beta$ )(68). Mechanistically, effects of these cytokines are facilitated through activation of signalling pathways involved in the pathogenesis of OA. Examples include Runx2, Nf- $\kappa$ B, Notch and Wnt signalling(69,70). These pathways, themselves, go on to activate expression of additional cytokines and modulators of AC destruction including matrix metalloproteases and their inhibitors. Here, the role of IL-1 $\beta$  is discussed in the context of knee OA pathogenesis.

In OA, several members of the interleukin-1 superfamily are overexpressed including the proinflammatory cytokine IL-1 $\beta$  and the receptor agonist IL-1RA. The destructive effects of IL-1 $\beta$  begins by binding to transmembrane type I IL-1 receptors (IL-1RI) and activation of signalling cascades such as MAPK and Nf- $\kappa$ B pathways(71,72). Here, IL-1RA acts to supress

cytokine induced catabolism by competing for binding sites in the IL-1R. Martel-Pelletier *et al* reported increased abundance of IL-1RI in human OA chondrocytes and, plasma levels of IL-1RA correlated with the radiographic stage of symptomatic knee OA suggesting a state of constant competition between anti-inflammatory and proinflammatory factors in knee AC(73,74). Thus, increased IL-RA may be a chondroprotective response to IL-1 $\beta$  mediated inflammation in OA.

As reviewed by Molnar *et al*, mitogen-activated protein kinase (MAPK) consists of three families: extracellular signal-regulated kinases (ERKs), c-Jun N-terminal kinases (JNKs) and p38 MAPKs (68). In human chondrocytes, ERK pathway activation by IL-1β reduced AC ECM production via downregulation of aggrecan and type II collagen gene expression. In parallel, IL-1β exacerbated ECM catabolism by induction of MMP-1 (via ERK, P38, JNK), MMP3 (via ERK), MMP13 (via ERK, P38, JNK) and ADAMTS-5 (via ERK) (75). Effects of IL-1β are perpetuated by MAPK stimulated secretion of IL-6, PGE-2, NO and COX-2. Aside from enhancing IL-1β secretion, these mediators are drivers of synovial inflammation, chondrocyte hypertrophy and apoptosis. In this way IL-1β upregulates its own expression in a positive feedback loop to aggravate OA progression.

Given IL-1β has the capacity to activate several OA signalling pathways, suppression of IL-1β action has been explored as a therapeutic target. Interestingly, a study in bovine AC showed that IL-1β induced MMP-1, MMP-3, ADAMTS-4 and ADAMTS-5 expression decreased under mechanical loading and the expression of metalloprotease inhibitor *TIMP3* increased (76). Though, IL-1β inhibition failed to prevent the progression of OA in other models. Therefore, OA pathology is interpreted as a multifactorial process and, the pathogenesis of disease is likely to vary depending on disease aetiology and its risk factors.

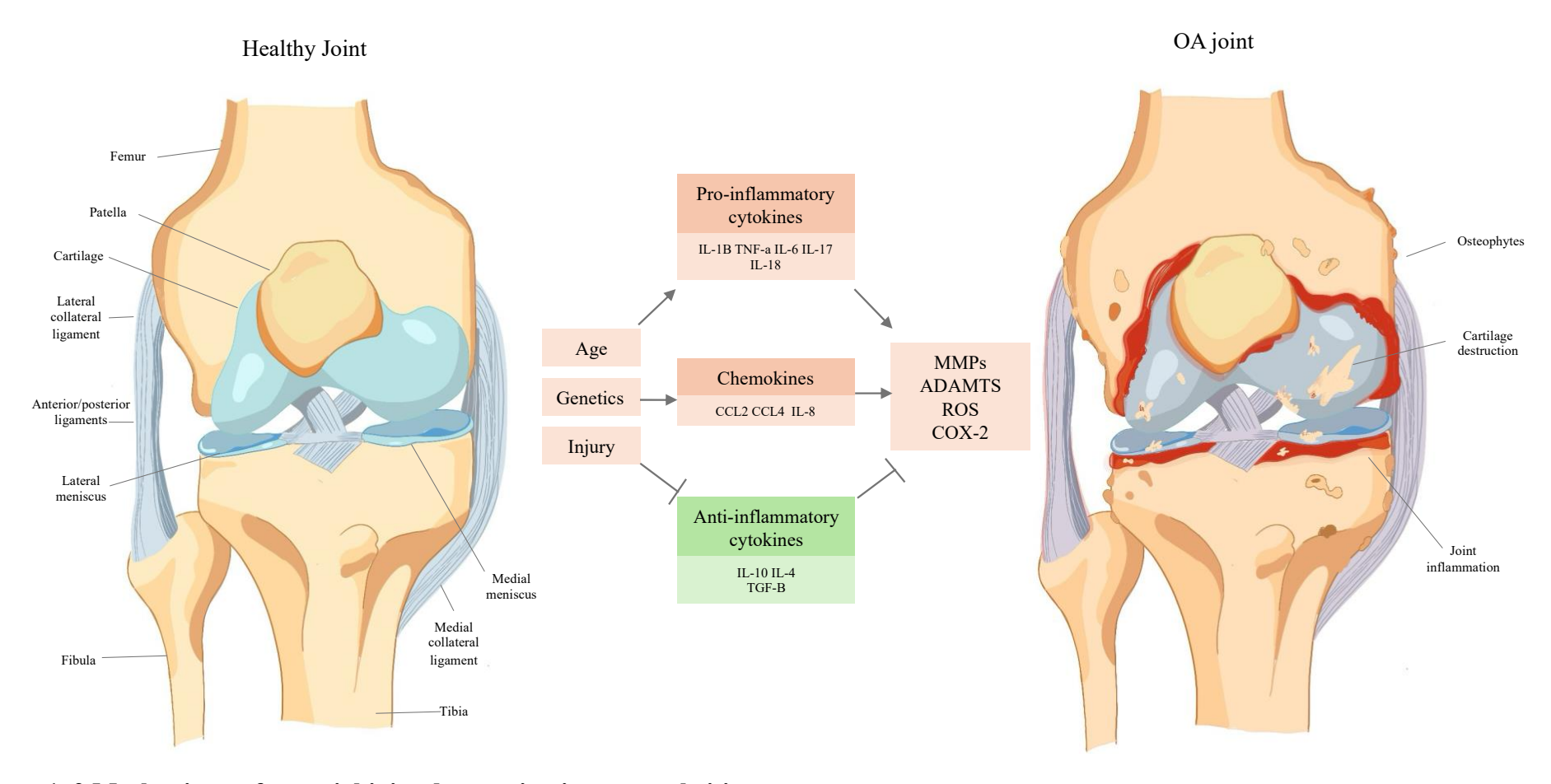


Figure 1. 2 Mechanisms of synovial joint destruction in osteoarthritis.

Schematic representation of healthy joint physiology (left) and OA pathology (right). Synovial joints allow for smooth movements between adjacent joints. Risk factors such as age, genetics and joint injury increase susceptibility to OA. OA can be characterised by osteophyte formation, cartilage degradation and joint inflammation, driven by increased expression of pro-inflammatory cytokines and chemokines.

#### 1.2.2 OA risk Factors

Risk factors for the onset of OA are considered either non-modifiable (i.e. age, gender, and genetics) or modifiable (i.e. smoking and obesity) and, determining the impact of these factors is highly relevant in the prevention of OA. Currently, epidemiological are a standard model for quantifying OA risk factors, though outcomes vary widely in the literature. For instance, estimates of heritability of radiographic knee OA in longitudinal twin studies ranges from 6%-80%(77–81). Therefore, variation in study setting, definitions of OA and mode of data collection must be considered(82). Here the relationship between the non-modifiable risk factor, aging, and joint degeneration in secondary OA is discussed.

#### 1.2.2.1 Non-modifiable risk factors

#### 1.2.2.1.1 Ageing

Ageing is the most prominent risk factor for the development OA in all joints, though likely not a direct cause. For instance, age-associated morbidities may contribute to joint disorganisation observed in OA (i.e. systemic inflammation) (83). As reviewed in (84) higher incidences of knee, hip, and hand OA are reported in older cohorts. Indeed, in a study of 3000 participants, cases of radiographic knee OA increased from 26.2% in the 55-64 age range, to 50% in the 75+ group (85,86). Significantly, both studies reported higher incidences of hip and knee OA in women compared to men. Indeed, age-associated estrogen deficiency is linked with increased OA severity(87).

#### **1.2.2.1.1.1 Inflamm-aging**

Advanced age is associated with several pathologies that are known to contribute to the disorganisation of the joint and OA development: including genomic instability, mitochondrial dysfunction, autophagy, and senescence (88). Collectively, these processes prompt a state of chronic low-grade inflammation in the joint which, in the context of advanced age, is termed 'inflamm-ageing'. Indeed, systemic inflammation markers including C-reactive protein (CRP), IL-6, IL-18 and TNF-α increase with age and, are elevated in people with OA of the knee (89–91) Conversely, lower innate production of IL-1β, and IL-6 correlated to an absence of OA in a cohort of 90-year-olds and, IL-6 null mice has more severe age-related OA (92,93). The contributions of age-associated chondrocyte senescence to inflamm-ageing and OA has been reviewed (94,95). Indeed, increased beta-galactosidase expression and decreased telomere length is observed in aged human articular chondrocytes (HAC). Further, beta-galactosidase

staining was only evident in OA cartilage compared to healthy AC in older patients (*in-situ*), suggesting an accumulation of senescent chondrocytes in aged and OA AC(96). In addition to growth arrest, senescent cells display a senescence-associated secretory phenotype (SASP), associated with overexpression of cytokines (IL-1β and IL-6), growth factors (EGF, TGF-β) and matrix degrading enzymes (MMP-3, MMP-13) (96,97). Interestingly, high levels of these SASP factors have been found in OA tissues and synovial fluid (reviewed in (88)) suggesting age-associated senesce may contribute to ECM degeneration in OA.

#### 1.3 Circadian rhythms

Circadian clocks temporally regulate key behavioural, physiological, and metabolic outputs with a period of ~ 24 hours. In complex organisms, rhythmicity originates from an intrinsic molecular clock that runs in synchrony to the light and temperature cycles-produced by earth's rotation (i.e. Zeitgebers)(98). Here, gene expression is regulated to create diurnal peaks in mRNA and protein expression relative to when a physiological process is most active. For example, the neural mechanisms that regulate cognition and attention are upregulated in daytime in mammals. In this way, organisms achieve temporal homeostasis with their environment, providing a fitness and survival advantage. The mammalian 'circadian clock' can be discussed on a cellular and systemic level (99).

#### 1.3.1 Central circadian oscillators

At the systemic level, phases of peripheral tissue clocks are organised into coherent behavioural rhythms by a 'master clock' in the hypothalamic suprachiasmatic nuclei (SCN). The SCN is necessary for circadian behaviour, as shown by disruption of daily rhythms following ablation of the SCN either surgically or by pituitary tumours(100). Recently it has also been demonstrated that peripheral tissue clocks also preferentially entrain to localised factors such as daily rhythms in food availability and mechanical loading (101,102). Thus, peripheral clocks are coordinated by both systemic and localised factors.

Formed of ~10,000 neurons, the SCN integrates extrinsic into intrinsic time by transducing photic stimuli into entrainment factors for peripheral tissue clocks. Anatomically, the SCN can be subdivided into a dorsomedial shell (DS) and ventrolateral core (VC) responsible for rhythm generation and input of photic stimuli respectively. Photic cues are transduced through two retinofugal routes; direct projections from the melanopsin-expressing retinal cells of the retinohypothalamic tract (RHT) and indirectly via the retinorecipient intergeniculate leaflet (IGL) via the geniculohypothalamic tract. Following this, the DS relays timing information to neighbouring cortical, hypothalamic and extrahypothalamic regions through diffusible mediators (e.g. vasopressin and gamma-aminobutyric acid)(103). As reviewed by Hastings *et al*, cycles in spontaneous firing rates (SFR), oscillating between >10 and <1Hz both *in-vivo* and in culture, are a key mediator in this model. Here, light pulses induce the acute depolarisation of SCN neurons leading to the activation of cAMP response element—binding protein (CREB)—mediated induction of circadian clock genes. Of the core clock genes, *Per1* 

and *Per2* are particularly sensitive to photic entrainment. Indeed, efferent pathways used by the SCN to coordinate the periphery (i.e. neuroendocrine) are observed in a pattern reflective of the SFR(104).

Architecturally, molecular clocks of the SCN neurons and periphery are highly conserved though clocks of the SCN neurons are more robust. Dispersed in culture, molecular clocks in individual SCN neurons maintain autonomous rhythms in SFR and intracellular calcium concentrations. Further, in organotypic slice culture, rhythmicity is maintained indefinitely, permitted by intercellular coupling to resist phase disturbances from internal cues(105,106). Thus, allowing the SCN to stay coordinated the solar cycle.

#### 1.3.2 The molecular clock

At the cellular level, intrinsic rhythmicity is driven by interlocked transcription/translation feedback loops (TTFL) found in all cells (i.e. the molecular clock). The TTFL can be divided into a positive and negative limb (Figure 1.3), formed of transcription factors with short half-lives, allowing periodic rise and fall of their levels within a 24-hour day. The positive limb is driven by the transcriptional activators, CLOCK, and its heterodimer BMAL1. Here, CLOCK:BMAL1 heterodimers activate the expression of PERIOD genes (*PER1*, *PER2* and *PER3*), CRYPTOCHROME genes (*CRY1* and *CRY2*) and nuclear receptors (REV-ERBα and RORα) through promotor E-box binding. When at sufficient concentrations, PER and CRY proteins form a complex and translocate to the nucleus to repress their own expression by interacting with CLOCK:BMAL1. This forms the negative limb of the TTFL, creating a self-sustaining oscillating circuit(107).

In order to modulate repression, PER and CRY are targeted for proteasome degradation by specific E3 ubiquitin ligase complexes (i.e. β-TrCP and FBXL21); gradually decreasing inhibition of the positive limb, enabling a new circadian cycle to begin(108). In a separate auxiliary feedback loop, REV-ERBα and RORα regulate *Bmal1* transcription through ROR regulatory elements (109,110). Interestingly, though BMAL1 is essential for circadian pacemaking in the SCN and peripheral tissues, NPAS2 (Neuronal PAS domain protein 2) can functionally substitute for CLOCK in the SCN, highlighted by rhythmicity in CLOCK-deficient rodents(111).

17

Beyond the TTFL, clock transcription factors regulate expression of output genes (i.e. clock-controlled genes (CCGs)) through cis-element binding (E-box, RORE and D-elements) or circadian regulation of chromatin remodelling (i.e. Sirtuin1 and CBP/p300) and RNA polymerase recruitment. Collectively, CCGs form a tissue-specific 'circadian transcriptome', hosting genes of key pathways including cell signalling, kinase activity and energy production. In this way, ~24-hour rhythms in diverse biological processes are generated(112).

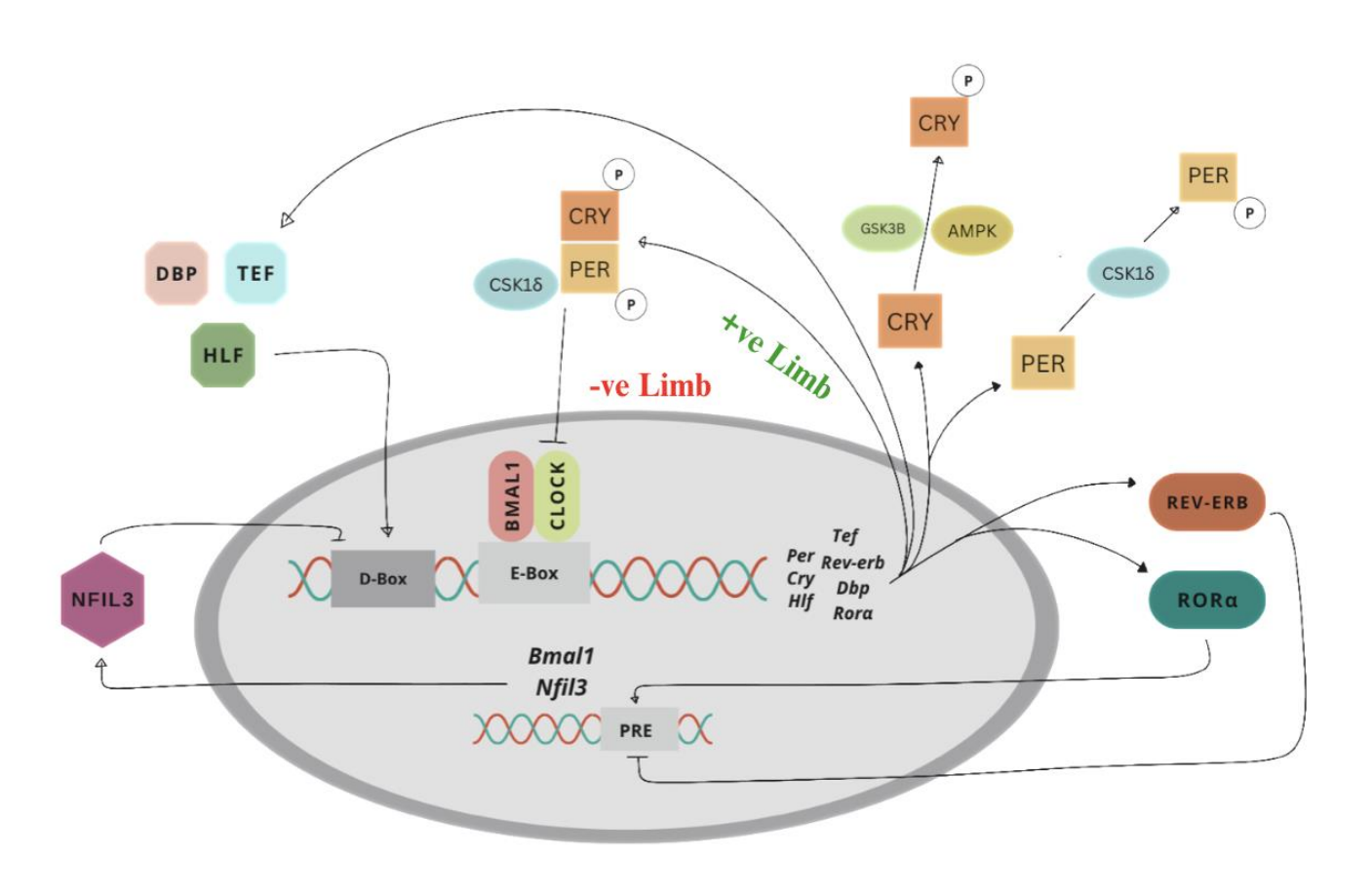


Figure 1. 3 Molecular mechanisms of the circadian clock.

The circadian clock is a conserved transcriptional-translational feedback loop with a delay. Transcriptional activators BMAL1 and CLOCK heterodimerise and bind to E-box elements in the promotor region of conserved clock genes including PER1/2/3, CRY1/2, REV-ERB, RORα, DBP, HLF. Resulting PER1/2 and CRY1/2 proteins heterodimerise and are phosphorylated by CK1ε This forms the transcriptional repressors of the negative limb, which return to nucleus to supress BMAL1 and CLOCK expression. Suppression is moderated by proteasomal degradation of PER and CRY by CK1ε AMPK and GSKβ respectively.

#### 1.3.3 Tissue-specific clock

As reviewed by Herzel *et al*, circadian transcriptomes are highly tissue specific and often, adopt a differential peak phase distributions to neighbouring tissues in order to meet physiological needs(98). In a comparison of circadian transcriptomes in mice, Yeung *et al* identified 9995 oscillating genes of which, 41 were shared in at least 8 of the 14 tissues analysed(113,114). Given the flexibility of the circadian transcriptome, it is likely that peripheral clocks are entrained by relevant physiological zeitgebers within their environment. Indeed, the uncoupling of the circadian clock in liver and other tissues has been reported following restricted feeding cycles(115,116). Considering this, the array of pathologies reported in clockgene mutant mice is unsurprising. For example, a premature ageing phenotype is observed across various tissues in global *Bmal1* KO mice, correlating to pathologies such as arthropathy and sarcopenia. Similarly, the *Clock*  $\Delta$ 19 and *Clock/Npas2* double KO mice develop attenuated energy balance and, spontaneous tendon calcification, supporting the importance of local clocks in physiology and disease (117,118).

#### 1.3.4 Cartilage circadian clocks

#### 1.3.4.1 Evidence of circadian clocks in cartilage

Due to daily cycles in joint loading, chondrocytes are known to experience diurnal changes in their biomechanical and biophysical environment. Therefore, temporal segregation of key metabolic processes in chondrocyte homeostasis will be advantageous. Indeed, the hallmarks of a robust molecular clock have been illustrated in murine cartilage and neighbouring tissues including (1) autonomous CG rhythmicity, (2) entrainment by periodic cues and (3) oscillation in downstream targets (i.e. cartilage circadian transcriptome). However, translation of these findings into human models is hampered by limited availability of human circadian time series tissues.

#### 1.3.4.1.1 Autonomous clock gene expression

Early observations of diurnal activity in chondrocytes were demonstrated in 1962. Stevenson *et al* reported changes in the mitotic index of growth plate chondrocytes in rats over the 24hour day(119). Here, proliferation was highest in the 'rest phase' (ZT 0600), correlating to a peak in growth plate height at noon (ZT 1200). Further, daily fluctuations in collagen production have been identified in chondrocytes of bone forming sites (e.g. mandible) by modelling uptake of [3H] proline and, such observations persist in the absence of external stimuli(120). Indeed, *Bmal1* is expressed in pre-hypertrophic chondrocytes in the growth plate and, the molecular clock is a regulator of the Tgf-β and Wnt pathway; both required for prevention of chondrocyte terminal differentiation (121–123)Global deletion of *Bmal1* in mice lead to decreased cranial calcification and smaller mandibular chondrocytes and, Col2a1 Bmal1–/– mice exhibit endochondral ossification-like phenotypes in the IVD(121,124,125). Negligible differences in bone volume or thickness is reported in the *Bmal1*-KO mice; proposing a functional and dynamic role for Bmal1 in the development of different skeletal components(126).

The generation of circadian reporter, and transgenic mouse models has aided demonstration of a functional molecular clock in mature AC particularly *Period2*::Luciferase (*Per2*::Luc) knockin mice. Here, a *Luc* gene is fused in-frame to the 3'end of the endogenous *Per2* gene on chromosome 1 creating a fusion reporter (127). Gossan *at al* observed strong oscillations in *Per2*::Luc activity within different cartilage subtypes (i.e. growth plate, femoral head, knee, and xiphoid cartilage) in explant culture. *In-vivo*, *Per2* oscillations persisted for several months and met the criteria for the temperature compensation theory (not discussed here). Interestingly,

differences in the clock properties of xiphoid and femoral head cartilage were not significant (mean period+/-SD: 24.18 +/- 0.3 hours and 23.4 +/-0.5 hours, respectively). Critically, abolition of *Per2*::Luc activity is reported in femoral head and xiphoid cartilage of offspring of the chondrocyte-specific *Bmal1*-KO (*Col2a1 Bmal1*-/-) and *Per2*::Luc mice; supporting a role of an autonomous functional circadian clock in cartilage(126,128).

Comparable findings have been demonstrated in *in-vitro* human chondrocyte models by time-series microarrays, and generation of circadian reporter cell lines by lentiviral transduction. In a human (malignant) chondrocyte derived cell line (SW1353) *PER2*:luc and *BMAL1*:luc reporters oscillate robustly over several days, in antiphase to one another. Time dependent expression of canonical clock genes including *BMAL1*, *NPAS2*, *PER1* and *NR1D1* mRNA was also reported by RT-qPCR; demonstrating oscillations in components of the positive and negative limb of the molecular clock in human chondrocytes(126).

# 1.3.4.1.2 The chondrocyte circadian transcriptome

Recently, the extent of circadian transcriptional control in AC been explored in mature xiphoid cartilage of mice kept in constant darkness by time series microarray. Notably, oscillation in total darkness is required to be deemed 'autonomous' given its persistence in the absence of the main zeitgeber: light. Here, 615 transcripts (~4% of expressed genes) displayed 11 distinct patterns of circadian expression, including those involved in chondrocyte lineage (Sox9, Ihh and Nfatc2) ECM remodelling (Tgf-β, Timp4) and apoptosis (Xiap)(128). 332 genes were allocated to the 'early day' group (ZT 03:00) and 78.6% of genes related to ''proteolysis' peaked during rodents 'rest phase'. Amongst these were transcripts associated with ECM homeostasis; including Fbn1, Col2a1, Agc1, Adamtss4/9 and Mmp14. Mmp-14 has a role in chondrogenic differentiation and activation of other MMPs including Mmp-13; a key collagenase in OA pathogenesis(129). *Timp4*, an inhibitor of MMP, oscillated in antiphase (i.e. 'Early night' group ZT 1900) to Mmp-14. Indeed, the temporal segregation of anabolic and catabolic enzymes may permit more effective tissue maintenance following nocturnal activity. Interestingly, only 16 common transcripts were identified between circadian transcriptomes in other musculoskeletal tissues (e.g. muscle, tendon, and intervertebral disc (IVD)). Though, several ECM related transcripts were common between mouse and rat cartilage; supporting the hypothesis of evolutionary conserved tissue specific clock function in cartilage(117). Similar temporal expression patterns have been extended into human chondrocyte models, including the newly identified OA susceptibility gene *Gnl3* (130).

Circadian transcriptional control is likely mediated by locally expressed clock genes in chondrocytes. Significantly, 132 of the genes identified by Dudek *et al* had previously determined Bmal1 binding sites in E-box domains and, chondrocyte-selective deletion of *Bmal1* lead to constant expression levels of rhythmic genes identified in WT mice(128). Further, Per2 and Adamts4 oscillation is abolished in  $Clock \Delta 19$  mutant mice. *In-vitro*, BMAL1 moderated expression of catabolic genes by crosstalk with Mapk/Erk pathways in temporomandibular chondrocytes(131). Here, overexpression of *Bmal1* by intra-articular adenoviral injection decreased Erk phosphorylation and minimised effects of IL-6 as shown by increased expression of *Mmps*, *Adamts5* and *Col2*.

Recently, dynamics in protein abundance in mature mouse AC have been explored by mass spectrometry. Though composition of the ECM is considered relatively stable, abundance of 145 proteins (12.5% of total identified) exhibited daily rhythms including 17 matrix proteins (i.e. Ctgf Pai-1, Fbln7, Col6a2 and Plod1). Further, pathways involved in protein synthesis, cytoskeleton and glucose metabolism displayed time-of-day specific temporal segregation (132). Chang J *et al* has reported similar findings showing ~10% of tendon proteome is rhythmic(133). Importantly, 21.4% of rhythmic AC proteins showed rhythmicity at the transcript level in mouse RNA-seq data including Ctgf, Matrilin 1 and Serpine 1. Notably, there is considerable disparity between oscillation at the mRNA and protein level suggesting that circadian regulation of gene expression extends to the post-transcriptional level in AC.

## 1.3.4.1.3 Cartilage clock entrainment factors

Given that AC is avascular and not innervated, understanding how chondrocyte molecular clocks build and sustains coherent time with the external environment is of interest. As discussed in-depth by Rogers et al(134), entrainment is likely mediated by both systemic zeitgebers coordinated by the SCN (i.e. body temperature and hormones) and physiological cues in their local environment (i.e. periodic mechanical loading). Indeed, glucocorticoid signalling by the SCN displays daily rhythms and, dexamethasone is a well-defined clock resetting agent in chondrocytes(117). Endocrine signalling may also moderate the chondrocyte clock, particularly melatonin signalling. Melatonin receptors Mt1 and Mt2 are coordinated by the circadian clock in primary murine chondrocytes. Further, addition of melatonin regulated the expression of *bmal1* and *per2* and increased expression of *col2a1*, *Acan* and *Sox9*. Interestingly, though primarily synthesised in the pineal gland, chondrocytes appear to

themselves, cyclically synthesise melatonin; indicating that exogenous and endogenous melatonin work in synergy in chondrocytes to adjust rhythmic expression to the central suprachiasmatic nucleus clock(135).

## 1.3.4.2 Osteoarthritis and circadian rhythms

Given the relationship between the chondrocyte clock and the cartilage homeostasis, it is unsurprising that its disruption has a role in the pathogenic rebranding of AC in OA. In human OA, altered expression of *BMAL1*, *NPAS2*, *NR1D1*, *PER2* and *CRY2* has been reported in chondrocytes(123,136,137). Notably, disparity between data sets is a common theme in chronobiology, imparted by variation in sampling techniques and by the nature of gene oscillation itself.

Limitations such as those mentioned above, may be ameliorated by use of transgenic mice and circadian reporter models. Here, gain and loss of function models enable the exploration of clock gene function and monitoring of clock gene dynamics. For example, RNA-seq revealed 53 differentially expressed genes in knee AC of *Cry2-KO* mice, including ECM turnover genes(138). Similarly, *Col2a1*-targeted deletion of *Bmal1* in mice AC abolished chondrocyte circadian rhythms leading to reduced Tgf-β and Nfatc2 signalling, decreased expression of ECM genes (i.e. *Sox9*, *Acan* and *Col2a1*) and progressive cartilage degeneration(126). As reviewed by Dernie *et al*, *Nfatc2* expression is directly regulated by the Bmal1/Clock heterodimer and downregulation has been shown to induce ECM catabolism and OA(139).

In chondrocytes, TGF-β signalling occurs via two opposing routes: ALK5/SMAD-2/3 which promotes a chondrocyte phenotype and ALK1/SMAD-1/5/8 which stimulates chondrocyte terminal differentiation (140). In aged and OA chondrocytes, TGF-β signalling is skewed towards ALK1/SMAD-1/5/8 pathway; characterised by *COL10A1* and *MMP13* expression. Akagi *et al* reported similar findings following knockdown of *BMAL1* and *NR1D1* in primary human chondrocytes; indicating that deregulation of clock gene expression may contribute to altered cytokines signalling in OA (123). Conversely, several studies have implicated altered cytokine expression with circadian dysfunction observed in OA. Exposure to IL-1B dampened rhythmic expression of *Cry1* in cartilage explants of the *Cry1*-luc reporter mouse and, disruption was inhibited by pre-study treatment with IKK1/2 inhibitor indicating involvement of the NFκB pathway (141). Similarly, Pferdehirt *Et al* reported a rapid loss of *Per2* oscillation in *Per2*:luc explants following IL-1α and ECM degradation (142). Both studies report little impact of TNFa exposure on clock gene expression, revealing a differential role of IL-1 and TNFα in cartilage clock-related pathways.

Significantly, global *bmal1*<sup>-/-</sup> mice demonstrate a premature ageing phenotype and, circadian amplitude is dampened by ~40% in AC explants of aged *Per2*::Luc mice(143). Indeed, given that ~4% of AC genes are CCGs, deregulated rhythmicity likely has a profound impact on chondrocytes capacity to control AC homeostasis. *SIRT1* is a clock-controlled gene and has been identified as a potential pathway linking aging, clock disruption and OA. *In-vivo*, defective Sirt-1 enzymatic activity led to increased Mmp proteins (i.e. Mmp-8,Mmp-9 and Mmp-13), chondrocyte apoptosis and, increased cartilage degradation with age(144). With respect to time keeping, SIRT1 is both a regulator and a target of the molecular clock(145). Separate studies have shown SIRT1 directly regulated B*mal1* expression and, deacetylates PER2 and BMAL1 proteins (146,147). Further, Sirt1 activity is regulated by the clock through coordination of Nampt expression(148). Gossan *et al* reported that Nampt, the rate limiting enzyme controlling synthesis of the Sirt1 substrate NAD+, is rhythmically expressed in xiphoid cartilage(128). Therefore, it has been proposed that deregulation of SIRT1 expression observed in ageing and circadian dysfunction increase susceptibility to OA.

Ageing has also been associated with the deterioration of extrinsic regulators of the chondrocyte clock; including inflammation and systemic entrainment factors(149). Rhythmic secretion of cortisol and parathyroid hormones by the SCN are known regulators of the chondrocyte clock. Sherman *et al* reported a phase advance in cortisol levels in older patients aged (40+) and separately, serum levels of PTH is significantly higher in postmenopausal women(150,151). Further, 'inflamm-aging' contributes to the onset of OA and may catalyse deregulation of the circadian rhythms in chondrocytes. *In-vitro*, IL-1β stimulation reduces *BMAL1* expression via NF-kB activation and increases peak expression of PER2 levels in human chondrocytes(152). Thus, age-related change in endocrine signalling and catabolic cytokines may compromise chondrocytes clocks capacity to remain synchronised to its external environment. These, and other studies pose the question of whether interventions targeting circadian function (i.e. light, dietary, or physiological therapies) ought to be explored as a therapy for patients with OA. However, our capacity to develop OA chronotherapies is limited by a lack of understanding towards the intrinsic regulators of the intrinsic clock mechanism and, the extent of interplay between the clock and mediators of AC homeostasis.

#### 1.4 MicroRNAs

Mature microRNAs (19-25nt) are a class of small non-coding RNAs (ncRNAs) that function at a post-transcriptional level to regulate gene expression. Complementary matching between the miRNA and target mRNA 3/5' UTR can take place at the miRNA seed sequence (nucleotides 2-8), the non-seed sequence (nucleotide 8+) or a combination of both to induce translational repression (animals) and/or degradation (degradation). At least 60% of human protein coding genes are predicted to have conserved miRNA target sites in their 3'UTR; including those involved in chondrocyte proliferation, differentiation, ECM biosynthesis and more recently, the chondrocyte circadian clock(153). In this way, miRNAs have emerged as key regulators in the homeostasis of cartilage and their dysregulation has been associated OA(154). Given this, a comprehensive understanding of the regulation of miRNA expression and mechanisms of action may aid identification of putative therapeutic targets for cartilage disease.

# 1.4.1 miRNA biogenesis

Over half of identified miRNAs are intragenic and processed from introns of protein genes(155). Within the microRNA-induced silencing complex (miRISC), mature miRNAs act as a guide strand for the recognition of target RNAs by AGO proteins. Here, base pairing between the miRNA seed sequence (i.e. nt 2-7 or 8) and the 3'UTR of target mRNA induces the recruitment of additional factors by RISC to destabilise or impede mRNA translation(156).

Over half of conserved miRNAs in vertebrates are organised into genomic clusters formed of 2 or more miRNAs arranged in tandem, indicating an evolutionary pressure to maintain these genes and their organisation. Given their proximity, clusters are likely processed as polycistrons, with one pri-miRNA carrying multiple pre-miR(157). Often, miRNA within clusters are functionally related and their co-expression may potentiate a more-robust downregulation of multiple targets. Interestingly, miRNA within clusters are known to follow differential expression patterns in response to physiological stimuli. This suggests action of post-transcriptional regulation of miRNA expression. Such regulation has been identified at multiple levels in the canonical pathway including Dicer/Drosha processing, RNA editing, methylation and Argonaute modification (158).

In the nucleus, canonical biogenesis of microRNAs begins with the generation of primary-miRNA (pri-miR) transcripts by RNA polymerase II (Figure 1.4). Pri-miRNA folds into a

stem-loop structure followed by recognition and cleavage into preliminary-miRNAs (pre-miRNA) by the microprocessor complex formed of the RNase III DROSHA and a dimer of Pasha/DGCR8 (Di George syndrome critical region 8). Using the Exportin 5 factor (a Ran-GTP dependent transporter), pre-miRs are transported into the cytoplasm for subsequent cleavage by a second RNase III – DICER. The resulting miRNA duplex (20-24nt long) is loaded into an Argonaute (AGO) protein, and a guide strand is selected; forming the miRNA induced silencing complex (miRISC). Guide strand selection is largely determined by thermostability at the 5' end of the miRNA duplex. Here, the strand with the highest stability is deemed the 'passenger' strand and degraded – leaving the guide strand incorporated into the miRISC(159). Interestingly, it has been hypothesised that both strands may be used differentially under different physiological conditions or in different tissues.

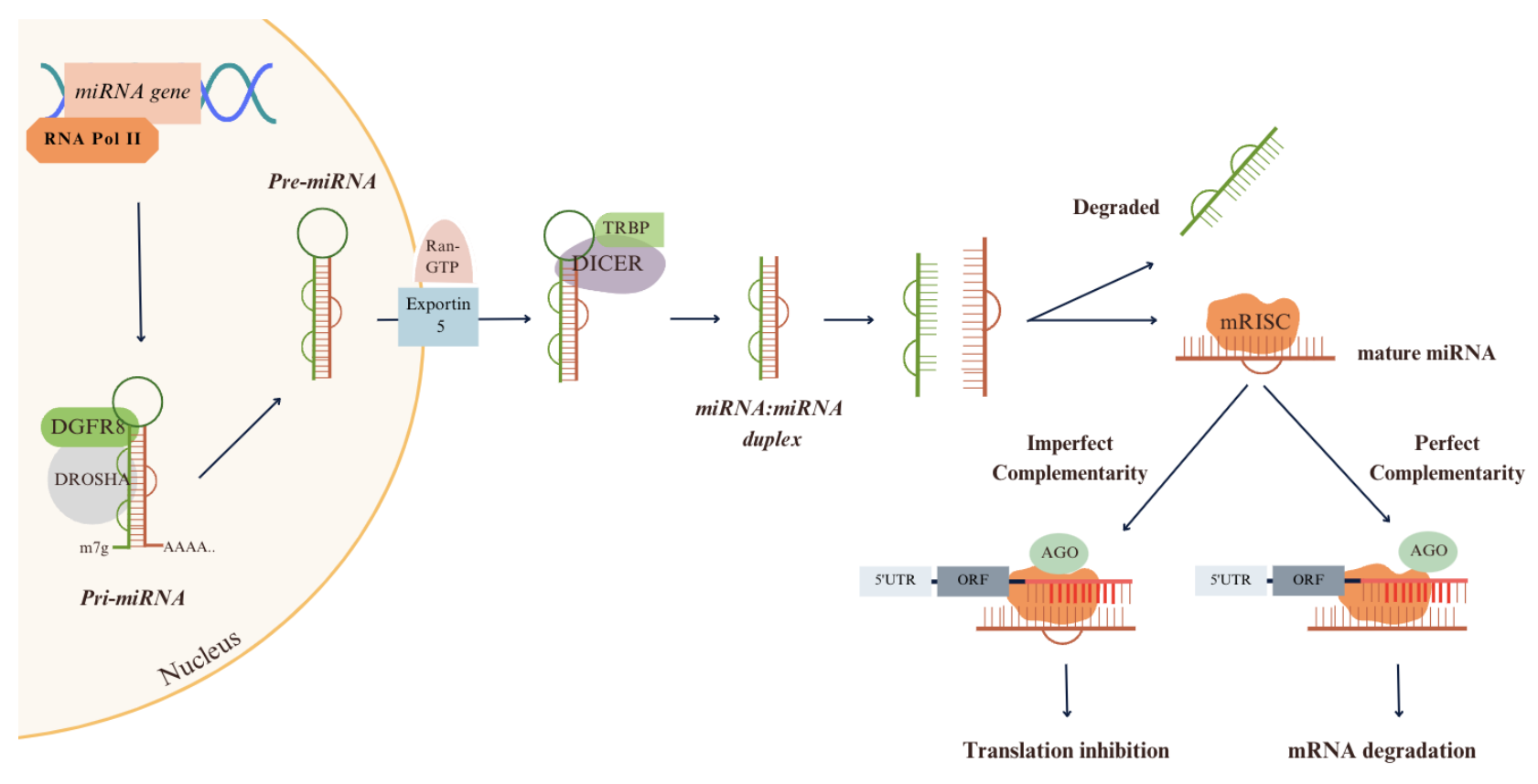


Figure 1. 4 Canonical biogenesis of miRNAs in mammals.

Primary transcripts are synthesized by RNA polymerase II, forming a hairpin pri-miRNA with a poly(A) tail and 5'cap. Pri-miRNA are cleaved by a microprocessor complex to form a shorter, pre-miRNA transcript. After being exported to the cytoplasm, pre-miRNA transcripts are processed by Dicer1to form a small, double stranded miRNA duplex. The passenger strand is degraded, and guide strand loaded onto an AGO protein before forming the miRISC complex. Seed regions in the miRNA bind to MRE in the 3'UTR of target mRNAs to regulate mRNA translation, instigating translational inhibition or mRNA degradation.

#### 1.4.2 miRNA mechanism of action

miRNA-mediated regulation of gene expression is a broad and dynamic processes, dependent on factors such as subcellular locations and the abundance of both mRNA and guide miRNA. Predominantly, miRNA regulate gene expression by binding to complementary sequences in the 3'UTR of target mRNAs(160). Importantly, miRNA binding sites have been identified in the 5'UTR and promotor regions(161). For example, miRNA miR-10a has been shown to interact with the 5'UTR of mRNA encoding ribosomal proteins to alleviate translational repression; though further studies are required to fully understand the functional significance of this interaction(162).

Within the miRISC complex, miRNAs function as a guide by binding to MREs in the 3'UTR of target mRNAs via their 'seed' region (residues 2-8 at the 5'end). The seed region contributes to the miRNA specificity and thermal stability of the mRNA interaction. As reviewed by MacFarlane *et al*, the degree of complementarity between miRNA:mRNA determines the mechanism of gene silencing by AGO proteins. Extensive base-pairing favours AGO2 endonuclease cleavage (i.e. slicer-dependent silencing); beginning with deadenylation and degradation by either the exosomes or, decapping by Dcp1 and Dcp2 enzymes(163). However, this interaction destabilises the association between AGO and the 3' end of the miRNA promoting its degradation(164). In the event of imperfect base-pairing, a bulging in the RNA duplex inhibits AGO2 activity and induces mRNA translational inhibition (i.e. slicer-independent silencing)(165).

## 1.4.3 miRNAs and the molecular circadian clock

Circadian clock genes are regulated by a variety of behavioural and biochemical factors. Recently miRNAs have been shown to participate in time keeping mechanisms in the central clock and peripheral oscillators in mammals. Conversely, expression of several precursor and mature miRNAs exhibit circadian rhythms and have been reported to contain the circadian ciselements E-Box and RORE in their upstream regions. However, as discussed here, the extent of this interplay and mechanisms remains unclear.

## 1.4.3.1 Circadian miRNAs

In the SCN of Dicer-deficient mice (and thus miRNA deficient), robust rhythms were observed with shortened periods (~2hours); suggesting miRNA regulation is not essential in the circadian feedback loop but regulates the pace of the clock(166). In the central clock, miR-132 and miR-219 positively regulated light-inducible clock entrainment and circadian period length, respectively(167). Interestingly, miR-132 itself is induced by photic entrainment cues via a Mapk/Creb-dependent mechanism and regulates transcripts involved in modulation of Period gene expression including chromatin remodelling (MeCP2, Ep300) and translational control (Btg2, Paip2a) genes(168,169). Significantly, promotors of Per1 and Per2 are transcriptionally activated by MeCP2 and translation of Period proteins is repressed by Paip2a (170). *In-vitro*, pre-miR-219-1 is regulated by Clock/Bmal1, peaking in the mid-subjective day of rodents (CT 6). Similarly, expression of miR-122 is regulated by REV-Erbα acting on two RORE in its promoter and, miR-142-3p oscillated in immortalised SCN cells and in cultured fibroblasts following serum shock(171,172). Indeed, in-vitro models such as this indicate the entrainment capacity of microRNA expression. However, given that not all miRNAs host circadian cis-elements in their promotors; it is likely that the temporal regulation of miRNAs is regulated by several pathways. For example, diurnal expression of Dicer1 has been demonstrated in in mammalian tissues (e.g. SCN, liver, bone marrow and retina). In this model, phase shifts and dampening in oscillation of Dicer1, miR-146a and miR-125a-5p was observed in aged mice. This suggests circadian regulation of these miRNA is perhaps, in part, due to oscillation in miRNA biogenesis pathways(173).

31

## 1.4.3.2 Regulation of the circadian clock by miRNAs

As shown in Table 1, core clock genes have been experimentally validated as miRNA targets. In mammals, the Period genes, *Per1*, *Per2 and Per3* are regulated by miR-30a, the miR-29 family (miR-29a, miR-29b and miR-29c) and miR-24a(166,174,175). These miRNAs are broadly expressed in several cell types and likely regulate peripheral clocks in several tissues. Conversely, interplay between miRNAs and circadian genes is also highly tissue specific and may account for variability in rhythmic proteomes(167,176). For example, miR-103 supresses *PER3* expression in colorectal cancer cells and, is induced by *BMAL1* in vascular smooth muscle(177,178). In serum, pre-miR-494 is rhythmically expressed and, pre-miR-494 and pre-miR-142-3p decreased translation of *Bmal1* in the SCN of mice(172,179). In the liver, rhythmicity of *Bmal1* is regulated by miR-155 and miR-27b and, miR-155 also directly targets *Bmal1* in macrophages to regulate circadian control of the innate immune system(180). *Clock* is a known target of several miRNAs including miR-17-5p and miR-206, though the circadian regulation of *Clock* is still debated. Interestingly, *Npas2* is a functional substitute for *Clock* in the SCN of mice and, is regulated by miR-17-5p(181,182).

miRNAs may simultaneously regulate the expression of clock gene and mediate biological processes. For instance, in breast epithelial cells miR-5188 directly targets *FOXO1* and, interacts with β-catenin in the cytoplasm to stimulate WNT signalling pathways involved in cancer (e.g. N-cadherin, Slug, Oct2, c-Jun and c-Myc)(183) In human chondrocytes, FOXO1 transcription factor has chondroprotective roles in the regulation of clock and ECM genes and, is reduced with ageing and OA(184). Outside of the core clock genes, miRNAs have also been shown to regulate entrainment pathways used by the SCN to coordinate the periphery. For example, Adenylyl cyclase VI (Adcy6), is a rhythmically expressed factor in melatonin production and is a predicted target of both miR-96 and miR-182(184). These studies identify a role for microRNAs as regulators of the molecular clock and its capacity to remain synchronised to the external environment. However, further research is needed to determine the extent of this relationship and its potential role in diseases.

	MicroRNA	Clock Target	Model	Cell line	Ref
HSA	miR-29a/b/c	PER1	Luciferase Reporter Assay	A549	(174)
	miR-192/194	PER1 PER2 PER3	Luciferase Reporter Assay	HeLA	(185)
	miR-103	PER3	Lentiviral Transduction	SW480	(186)
	miR-199b-5p	NPAS2	Lentiviral Transduction	SNU-368	(187)
	miR-503-5p		Luciferase Reporter Assay	HeLA	(188)
	miR-27a-3p				
	miR-183-5p	RORA			
	miR-450b-5p				
	miR-181a-5p				
	miR-142-3p	BMAL1	Luciferase	HeK293T	(179)
	miR-494		Reporter Assay		
	miR-24	Per2	Luciferase Reporter Assay	NIH 3T3	(175)
	miR-449	Per3	Mir-449 Overexpression	NIH 3T3	(189)
	miR-27b-3p	Bmal1	Luciferase	AML-12	(180)
101	miR-155	Ditail	Reporter Assay	7111112 12	
MMU	miR-10a	Bmal1	Luciferase	HUH-7	(190)
	mix rou	Rora	Reporter Assay		
	miR-17-5p	Clock Npas2	Luciferase Reporter Assay	HEK2935 NIH3T3	(181)
	miR-185	Cry1	Luciferase Reporter Assay	NIH3T3	(191)

Table 1 Post-transcriptional regulation of circadian clock genes by microRNAs.

## 1.4.4 Cartilage miRNAs

The development and maintenance of cartilage depends on the dynamic balance between anabolic and catabolic pathways. Recently, regulation of cartilage homeostasis by microRNAs has received increased attention. Indeed, a global reduction in miRNAs by conditional ablation of *Dicer1* lead to a decrease in proliferating chondrocytes, skeletal defects, and premature death in mice(192). However, further studies are required to understand the extend of miRNA mediated regulation and, the mechanisms that govern this process.

# 1.4.4.1 miRNAs in cartilage development

It is understood that cartilage development in humans is, in part, regulated by miRNA driven mechanisms. A study using human embryonic cartilage, reported differential expression of miRNAs between precursor (PC), differentiated (DC) and hypertrophic (HYP) chondrocytes. For example, expression of miR-138, miR-193b and miR-365 was greater in the HYP and DC compared to PC suggesting functional roles in terminal differentiation(193). Specifically, Let-7 and miR-140 are abundantly expressed in developing and mature chondrocytes and coordinately regulate skeletal development(194). In-vivo, miR-140 deficiency accelerated premature hypertrophic chondrocyte differentiation, though had no effect on chondrocyte proliferation. Conversely, overexpression of Lin28, a let-7 inhibitor, upregulated Sox9 transcription and increased expression of regulators of cell cycle (Cdc34) and proliferation (Hmag2) (195). Conditional deletion of Lin28 in AC resulted in a mild skeletal phenotype. compound miR-140 deficient/Lin28a (Col2-Whereas transgenic models Cre:Lin28a<sup>c</sup>:Mir140<sup>-/-</sup>) show dramatic growth defects. Significantly, similar phenotypes were observed in simultaneous miR-140 knockdown and Lin28a overexpression in Zebrafish, suggesting a conserved role for miR-140 and Let-7 as negative regulators of skeletogenesis in vertebrates(196).

As mentioned, the SOX9 transcription factor regulates cartilage formation and is required for chondrocyte phenotype. Several miRNAs are regulated by SOX9 and/or, regulate SOX9 itself including miR-140 and miR-455(197). Both examples are intronic miRNAs, residing in host genes *WWP2* and *COL27A1* respectively(198,199). In ATDC5 chondrogenesis models, SOX9 regulated the expression of both miRNA and hosts transcripts. *SOX9* 3'UTR is one of several developmental genes regulated by miR-140 including: *HDAC4*, *SMAD3* and *RALA(200–202)*. Notably, *SMAD3* expression is only regulated at the protein level. As mentioned, SMAD3 is a

key transcription factor of the TGF- $\beta$  pathway and, TGF- $\beta$  has been shown to suppress accumulation of miR-140; forming a negative feedback loop(203). Similarly, miR-574-3p is regulated by SOX9 and targets retinoid X receptor alpha gene (RXR $\alpha$ ). Since RXR $\alpha$  was previously shown to inhibit SOX9 activity, miR-574-3p may be part of a positive feedback loop that promotes chondrogenesis(204). Together these reports support the physiological significance of miRNAs in skeletal development.

## 1.4.4.2 miRNAs, cartilage homeostasis and disease

Several studies have experimentally verified miRNAs as contributors to AC homeostasis and their role in the pathogenesis of OA. Notably, there is little overlap in the differentially expressed miRNAs in OA amongst transcriptomic data. Likely, this is due to heterogeneity in diseased and healthy tissue control samples between studies. In a bioinformatic analysis of 57 human miRNA-OA studies, Cong *et al* reported 46 differentially expressed miRNAs involved in chondrocyte metabolism, autophagy, apoptosis, inflammation, and ECM degradation(205). Later, Almeida *et al* devised a miRNA-OA interactome of 62 differentially expressed miRNAs with 238 mRNA targets, using lesioned and preserved OA AC in a single patient(206). Here, 14 DE miRNA were specific to hip (e.g. miR-455-5p) and 5 specific to knee (e.g. let-7c-5p). Significantly, miR-143-3p was allocated an interactome of 16 DE genes (e.g. *SMAD3*, *CDAKD* and *AMIGO1*) and regulated chondrocyte proliferation by regulating the Ras/p38 MAPK signalling pathways *in-vitro*(207). These reports broadly demonstrate miRNAs capacity to regulate multiple metabolic and inflammatory networks in OA. As summarised by Zacharjasz, these investigations have directed more in-depth *in-vitro* and *in-vitro* studies(208).

## 1.4.4.2.1 miRNAs and ECM degradation

Chronic inflammation is a known contributor to the degradation of AC ECM observed in OA. It is now understood that deregulation of miRNA may play a role in inflammatory response in the joint. For instance, miR-26a and miR-130a are downregulated in OA chondrocytes and regulate Il-1β mediated catabolism by targeting the 3'UTR of *NF-k*B and *TNF-α* respectively(209,210). *In-vitro*, miR-26a overexpression suppressed saturated NEFA-induced NF-kB activity in obesity-related chronic inflammation in human chondrocytes(211). Similarly, miR-22 and miR-103 expression is correlated with an elevated BMI in OA patients; linking an OA risk factors with deregulation of miRNA expression(212).

Individual miRNAs may play a dual role in OA, by regulating several catabolic pathways. For example, miR-146a is downregulated and, mediates expression of TRAF6 by impairing NF-Kβ activity in synoviocytes of OA patients(213,214). Additionally, miR-146a regulates translation of *BCL-2* and *SMAD4* to coordinate autophagy and, apoptosis following mechanical injury in human chondrocytes, respectively(215,216).

Functional assays indicate miR-140 regulates the translation of catabolic enzymes (e.g. *MMP13* and *ADAMTS5*) and mediators (e.g. *TLR4* and *IL1B*)(200,217,218). Indeed, costal chondrocytes isolated from miR-140 null mice show increased expression of predicted targets of miR-140-5p and 140-3p(219). Further, miR-140 overexpression rescued loss of proteoglycan and type II collagen after antigen induced joint inflammation and, loss of miR-140 exacerbated early onset OA in aged mice. Zhang *et al.* reported an inverse correlation between miR-140 abundance and disease severity in the synovial fluid of knee OA(220). In this way, miR-140 likely plays chondroprotective role in AC and poses as a promising biomarker for joint ageing and disease detection. Considering this utility of intra-articular injection of miR-140 therapeutically has been proposed, though unprotected miR-140 is rapidly degraded by endogenous nucleases in inflammatory disease, such as OA(221). Alternatively, pre-clinical data supports the use of miR-140-5p delivery by exosomes, with TAO *et al* demonstrating AC regeneration and OA prevention in human synovial MSCs(222).

However, there is notable contrast between studies regarding the kinetics of miRNA expression in OA particularly; miR-455 and miR-140. For example, expression of both miRNA were upregulated in human hip OA cartilage in a study by Swingler *et al*, whereas other studies in miR-140-null mice and human knee OA reported their downregulation (200,223). These observations are likely due to use of different AC models within which disease stage, type of OA, gender and age may vary. Alternatively, discrepancies may reflect differential regulation of miRNA expression between knee and hip AC to meet tissue specific needs in different anatomical locations. Therefore, the utility of miRNA therapeutically might be examined on a joint specific basis. Further, given the extend of circadian regulation of miRNA in other tissues, it is plausible that differences in study findings may be influenced by patient chronotype and the time of collection.

# 1.4.4.3 miRNAs and cartilage circadian rhythms

As discussed, the altered miRNA secretion and circadian rhythms disruption in chondrocytes contributes to progressive damage and loss of AC. However, the extent of the crosstalk between these factors in AC has only been preliminarily explored. For example, the miR-195/497-5p cluster regulated the chondrocyte circadian rhythms of mice by indirect modulation of Per2 protein, resulting in degradation of AC(224). Here, miR-195/497-5p directly regulated the expression of Dusp3, a regulator of Creb and Erk1/2 phosphorylation. Concomitantly, Per2 transcription is upregulated by both Creb and Erk1/2. In another study, mice with cartilage specific-KO of miR-128a exhibited decelerated suppression of Nr1d2 and reduced OA severity in DMM models. Kuo et al forecasted 3 MRE for miR-128a in the 3'UTR of NR1D2 by insilico analysis and, NR1D2 agonist rescued suppressed expression of cartilage anabolic factors and ECM synthesis caused by miR-128a precursor(225)(226). These early models begin to identify regulatory mechanisms connecting chondrocyte miRNAs to maintenance of the circadian clock and cartilage homeostasis. With respect to oscillating miRNAs in AC, Swingler et al suggested the temporal abundance of cartilage miRNAs miR-455 may be regulated by the molecular clock in SW1353 chondrosarcoma cells(226). However, further work is required to understand the extend of the circadian microRNAome and, the functional effects of oscillating microRNAs in maintaining cartilage homeostasis.

## 1.4.5 Hypothesis and Aims

This thesis aims to explore the interplay between the circadian molecular clock and miRNAs in cartilage tissues. We hypothesise that daily abundances of AC miRNAs are regulated by the molecular clock and, microRNAs may directly regulate core clock genes of the TTFL. As discussed here, the circadian clock and miRNAs are key regulators of gene expression in AC and are deregulated in OA. Therefore, exploring interplay between these two factors may improve our understanding of AC physiology and regulators of its disease.

The following aims will be explored throughout this thesis:

- To develop *in-vitro* and *in-vivo* time series model for the evaluation of circadian mRNA and miRNA expression in cartilage.
- To determine a stepwise protocol for the statistical evaluation of oscillating miRNAs in small RNA sequencing and RT-qPCR data sets.

- To explore the implication of daily fluctuation of key cartilage miRNAs on AC physiology and homeostasis by enrichment analysis.
- To predict and evaluate putative circadian clock targets of miR-455-3p and miR-455-5p by luciferase reporter assays.

## **Chapter 2:** Materials and Methods

#### 2.1 Materials

## 2.1.1 Cell models

## **2.1.1.1** *E.coli* Strains

For cloning of pmirGLO luciferase constructs, *E. coli* were either Stellar<sup>TM</sup> competent cells (Clonetech) or DH5-alpha chemically competent cells. Cell used were dependent upon availability.

### 2.1.1.2 Mammalian cell lines

SW1353 is an immortalised human chondrosarcoma cell line generated in 1977 from a primary grade II chondrosarcoma of the humerus (ATCC, #HTB-92)). C28/I2 are an immortalised juvenile costal chondrocyte cell line established by transduction of primary cultures with vectors encoding simian virus 40 large T antigen (Goldring). DF1 is a spontaneously immortalised chicken dermal fibroblast cell line (a gift from Dr.Lingzi Niu, UEA).

#### 2.1.2 Murine models

All mice, used throughout had a C57/BL6 wild-type (WT) background. All experimental procedures were conducted within the law of the 1986 UK Home Office Animal Procedures Act. Mice were bred in-house and housed in individually ventilated cages in 12-h light/12-h dark (LD) photoperiod under a constant temperature (22-23°C), except where stated (section 2.2.41). Mice were maintained on standard chow and water ad-lib. All mice were sacrificed by exposure to rising concentrations of carbon dioxide followed by cervical dislocation in accordance with the schedule 1 licensing act 1981.

#### 2.2 Methods

#### 2.2.1 Cell culture

# 2.2.1.1 Bacterial growth conditions

*E. coli* were plated on lysogeny broth (LB) agar (agar 15m/L, tryptone 10g/L, yeast extract 5g/L, NaCl 5 g/L) containing 100ug/ml ampicillin (Sigma-Aldrich) and incubated at 37°C overnight. For liquid culture, LB was inoculated with *E. coli* and incubated at 37°C, shaking at 180 g for 12 hours.

## 2.2.1.2 Mammalian cell culture conditions

Mammalian cell lines were maintained in Dulbecco's modified Eagle Medium (DMEM) plus GlutaMAX (Life Technologies) supplemented with 10% (v/v) heat-inactivated fetal bovine serum (Life Technologies), 100 IU/ml penicillin and 100μg/ml streptomycin at 37°C and 5% (v/v) CO<sub>2</sub>. Both cell lines were passaged at 70-80% confluency by washing with Hanks Balanced Salt Solution (HBSS; life technologies) followed by incubation in 0.25% trypsin/EDTA (TE) at 37°C for 3-5 minutes. The enzymatic reaction was terminated by diluting the trypsin with complete media in a 1:10 ratio. For plating, cells were counted using a haemocytometer and diluted to the desired concentration in complete media.

## 2.2.2 Molecular methods

## 2.2.2.1 Isolation of human genomic DNA

Genomic DNA (gDNA) was extracted from SW1353 cells using an extraction buffer containing 10mM Tris-HCL pH 8, 100mM NaCl, 50nM EDTA, 1% (w/v) SDS and 200 μg/ml Proteinase K (Sigma-Aldrich). SW1353 cells were harvested from a 75cm2 flask by incubation in 0.25% (w/v) trypsin-EDTA and pelleted by centrifugation at 500 x g for 3 minutes. The cell pellet was washed Dulbecco's phosphate-buffered saline (DPBS) (Life Technologies) and resuspended in 500μL of extraction buffer before incubation at 55°C for 3 hours. 500μL of PCI (phenol: chloroform: isoamyl Alcohol, 25:24:1) was added to lysates and centrifuged at 12000 x g at 4°C for 12 minutes. The top aqueous phase was transferred to a new collection tube and equal volumes of chloroform (Sigma Aldrich) added, vortexed and centrifuged as before. The upper phase was added to 2 volumes of 100% (v/v) ethanol, precipitated overnight at -20°C and centrifuged as before. DNA pellets were washed with 70% (v/v) ethanol followed by centrifugation as before. The supernatant was discarded, and pellets were dried on a hot block at 35°C before resuspending in warmed nuclease free water (Sigma Aldrich).

## 2.2.2.2 Polymerase chain reaction (PCR)

## 2.2.2.2.1 Total RNA isolation from cultured cells

Growth medium was removed from adherent cells before washing twice with 500μL ice cold Dulbecco's phosphate-buffered saline (DPBS, Thermo Fisher Scientific). 500μL of Trizol<sup>TM</sup> reagent (Invitrogen, thermofisher) was added to each well, incubated at 37°C for 15 minutes and transferred to a 1.5mL collection tube. 250μL of chloroform was added per 500ul Trizol<sup>TM</sup> reagent, vortexed for 15 seconds and incubated at room temperature for 15 minutes. Reaction mix was centrifuged at 14,000g at 4°C for 15 minutes and the upper aqueous phase transferred to a fresh 1.5mL collection tube. 500μL of isopropanol (Sigma-Aldrich, Merck) was added, incubated at room temperature for 15 minutes followed by centrifugation at 14,000g at 4°C for 15 minutes. Supernatant was discarded and RNA pellets were washed with 400μL 70% (v/v) ice cold ethanol before centrifuging at 7000g at 4°C for 10 min. The supernatant was removed and resuspending in 30μL of warmed nuclease free water. RNA was stored at -80°C until further use.

#### 2.2.2.2. Total RNA isolation from murine tissues

Murine tissues were micro-dissected, snap frozen in liquid nitrogen and homogenised using a sterile pestle. Total RNA isolation was performed using either the miRVANA<sup>TM</sup> miRNA isolation kit (Invitrogen) or the miRNEASY<sup>TM</sup> tissue/cell advanced micro-Kit (Qiagen) according to manufacturer's instructions.

## 2.2.2.3 Total RNA quantification

Total RNA concentration was quantified using a Nanodrop<sup>TM</sup> spectrophotometer (Thermo-Scientific). The ratio between absorbance at A260 (nm) and A280 (nm) (A<sub>260</sub>/A<sub>280</sub>) was used as an indicator of RNA purity.

# 2.2.2.4 Reverse Transcription

# 2.2.2.4.1 SuperScript<sup>TM</sup> III reverse transcriptase cDNA synthesis

Total RNA isolated from cultured cells and murine tissues was reverse transcribed into cDNA using SuperScript<sup>TM</sup> III reverse transcriptase (Invitrogen). In a total volume of 11uL, 1ug total RNA and 0.2ug random primers (Invitrogen) was incubated at 70°C for 10 minutes. On ice, a master mix containing 1μL SuperScript<sup>TM</sup> III reverse transcriptase (200units/uL), 4μL First Strand Buffer (5X) (Invitrogen), 2μL 0.1M dithiothreitol (DTT) (Invitrogen), 1μL RNasin ribonuclease inhibitor (40units/ uL) (Invitrogen) was added to a final volume of 20μL and incubated at 42°C for 60 minutes and 70°C for 5 minutes. Reactions were prepared omitting reverse transcriptase as negative controls to control for genomic DNA amplicons. cDNA was diluted to 0.5ng/μL in nuclease free water and stored at -20°C.

# 2.2.2.3 Quantitative real time polymerase chain reaction (qRT-PCR)

# 2.2.2.3.1 Universal Probe library qRT-PCR

Expression of genes of interest (GOI) was quantified using the Universal Probe Library (UPL) (Roche) and normalised to housekeeper gene for variations in total RNA. Short hydrolysis probes (8-9 nucleotides) containing a 3' fluorescein (FAM<sup>TM</sup>) and 5' quencher dye (TAMRA) were designed using the Roche universal probe library assay design centre. Primers were designed using Probe Finder software and confirmed as 'exon spanning' manually using Ensembl (Appendix table 1.1). All primers were supplied lyophilised from Sigma Aldrich and reconstituted to 100uM in nuclease free water. To 5μL of 0.5ng/μL cDNA, a master mix containing 200nM Universal Probe (Roche), 200nM forward and reverse primer, 8.33μL

qPCRBIO Probe Mix Lo-ROX (PCR biosystems) was added to a final volume of 20uL). Reactions omitting cDNA were prepared as negative controls. Quantification of gene expression was performed using an Applied Biosystem<sup>TM</sup> 7500 Real-Time PCR System with MicroAmp optical 96-well plates (Applied biosystems) using standard qRT-PCR cycle conditions (Table 2.1).

Step	Temperature (°C)	Time	Cycles
Initial denaturation	50°C	2 minutes	1
Denaturation	95°C	10 minutes	1
Annealing/Extension	95°C	15 seconds	40
	60°C	1 minutes	

Table 2. 1 Temperature cycles for universal probe library quantitative PCR reactions.

# 2.2.2.3.2 SYBR ® Green qRT-PCR

SYBR® green dye fluorescence was used with specific primers to detect expression of GOI, pre-miRNA and mature miRNA (Table 2.2, Appendix table 1.2-1.3). To a final volume of 20uL, 5μL of 0.5ng/μL cDNA, 0.2ul SYBR® green I dye, 10μL qPCRBIO Probe Mix Lo-ROX (PCR biosystems) and 100nM final concentration of forward and reverse primers were added. Reactions omitting cDNA were prepared as negative controls. The PCR cycles were as above.

Assay name	Assay ID
hsa-miR-455	001280
hsa-miR-455-3p	002244
hsa-miR-140-3p	002234
mmu-miR-196a-5p	241070
mmu-miR-17-5p	2308
mmu-miR-30c-2-3p	2110
mmu-pre-miR-30c	Mm03306701_pri

Table 2. 2 miRNA RT-qPCR assay ID

## 2.2.2.4 Small-RNA sequencing

Total RNA was extracted from the knee cartilage of adult WT mice as per section 2.2.2.2.2. Small RNA sequencing was performed by TAmiRNA (https://www.tamirna.com/). RNA integrity and concentration of knee cartilage samples was analysed using Agilent Bioanalyzer RNA 6000 Nano Chip (Agilent Technologies). Small RNA libraries were prepared by TAmiRNA with equal amounts of total RNA (100ng) and with fixed volume (8.5uL) (N=3 biological replicates per time point). For libraries, adapter-ligated libraries were amplified with 19 PCR cycles using barcoded Illumina reverse primers in combination with the Illumina forward primer (Illumina, San Diego, CA). cDNA libraries were quantified using the Bioanalyzer Agilent DNA 1000 kit (Agilent Technologies) and equimolar pools of tissue samples were prepared. Pools were purified using a microfluidic 3% agarose gel cassette (Sage Bioscience), selecting for a size range between 130 and 160bp. Sequencing was performed on an Illumina NovaSeq 6000 (Illumina).

## 2.2.2.5 Subcloning

# 2.2.2.5.1 Circadian gene 3'UTR pmirGLO constructs

The pmirGLO dual-luciferase vector is designed to quantitatively evaluate miRNA regulation (Promega). This is achieved by insertion of miRNA target sites downstream of the firefly luciferase primary reporter gene (lu2). Renilla luciferase (hRluc-neo) was used as a control reporter for normalisation.

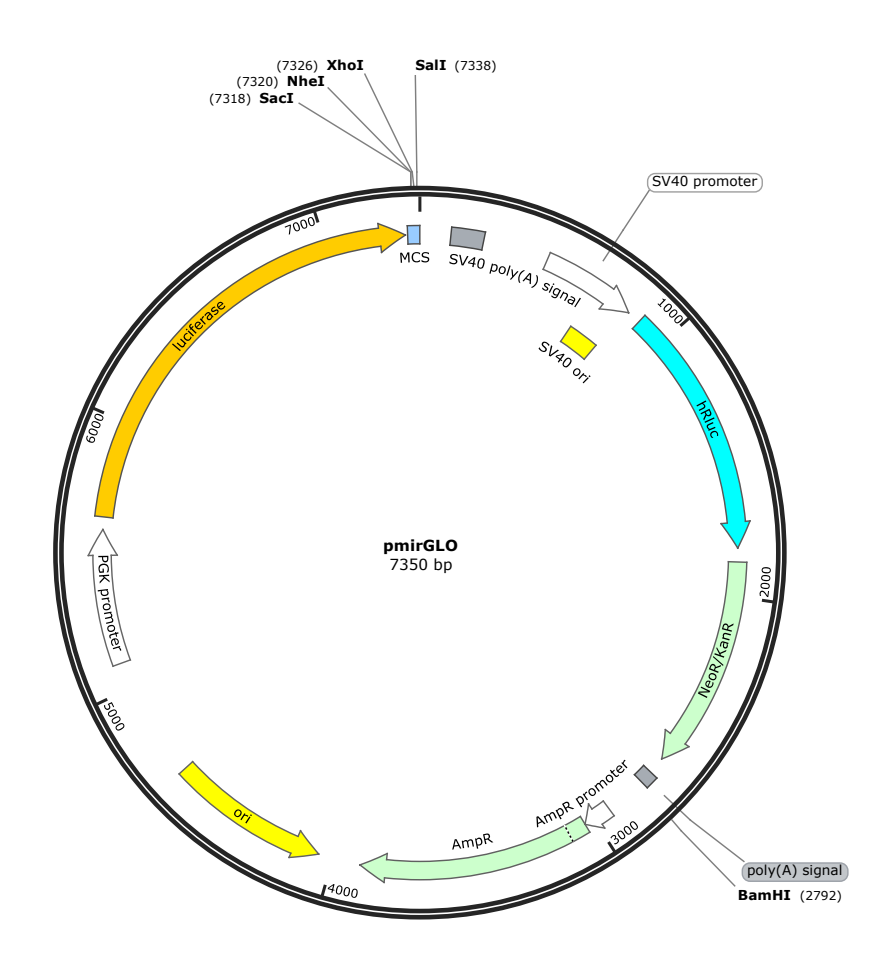


Figure 2. 1 Map of the pmirGLO plasmid. Generated from SnapGene viewer.

## 2.2.2.5.2 Primer design

Predicted targets of miR-455-3p and miR-455-5p were identified by manually searching the 3'UTR of putative genes. For 3'UTRs with multiple seed sites spanning <1500bp, additional primers were designed to amplify the 3'UTR in multiple parts. Restriction sites for *Sac1* (5' TTGTTTAAACGAGCTC3') and *Xho1* (5' CGACTCTAGACTCGAG3') were added to the 5' ends of the forward and reverse primers respectively (Appendix table 1.4 & 1.5)). For sequencing of 3'UTR pmirGLO constructs, primers were designed to amplify regions spanning

Xho1 and Sac1 restriction sites and a 10-15 base pair region of new the new 3'UTR inserts. All primers were supplied lyophilised from Sigma Aldrich and reconstituted to 100uM in nuclease free water.

## 2.2.2.5.3 Amplification of 3'UTR

3'UTR amplicons of predicted target genes were amplified using PCR from human genomic DNA isolated from the SW1353 cell line (section 2.2.2.1). Amplicons were amplified using Q5® High-Fidelity DNA Polymerase (New England Biolabs) according to manufacturer's protocol (Table 2.3) using PCR protocol (Table 2.4). Amplification was confirmed by gel electrophoresis. Agarose gels were prepared by heating 1% agarose (w/v) in TAE buffer (Trisacetate 40nM, EDTA 1mM) 3μL of PCR product was loaded onto 1% (w/v) agarose gels and run at 100V. Gels were stained with ethidium bromide solution (Sigma-Aldrich) for 15 minutes. Products were imaged with Bio-Rad Gel Doc <sup>TM</sup> EZ Gel Documentation System or UVP ChemiDoc-It2T<sup>M</sup> 810 Imager.

Component	Quantity
gDNA	100ug
10μM Forward Primer	2.5μL
10μM Reverse Primer	2.5μL
25 mM dNTPs	0.4μL
5x Q5 reaction buffer	10μL
Q5® High-Fidelity DNA Polymerase	0.5μL
Nuclease-free water	Το 50μL

Table 2. 3 PCR reaction for 3'UTR amplification

Step	Temperature (°C)	Time	Cycles
Denaturation	98	30 seconds	1
	98	5-10 seconds	
Annealing/extension	50-72	10-30 seconds	30
	72	20-30 seconds/Kb	
Final extension	72	2 minutes	1

Table 2. 4 PCR thermal cycles for amplification of 3'UTR inserts

## 2.2.2.5.4 Agarose gel purification

3'UTR amplicons were isolated by gel electrophoresis. The PCR mix was applied to 1% (w/v) agarose gel and run at 140V. DNA fragments were stained with ethidium bromide solution (Sigma-Aldrich) and excised from the gel by scalpel under UV-Light. DNA amplicons were purified using the QIAquick PCR purification kit (Qiagen). Briefly, 3 volumes of buffer QC were added to each volume of excised agarose gel and incubated at 50°C for 10 minutes. 1 volume of isopropanol was added to the dissolved agarose solution, transferred to a QIAquick spin column, and centrifuged at full speed for 3 minutes. To wash columns, 750μL of buffer PE was added and centrifuged at full speed for 30 seconds. DNA was eluted with 30μL of warmed nuclease free water, quantified using a NanoDropTM spectrophotometer (Thermo Scientific) and stored at -20°C.

# 2.2.2.5.5 Plasmid digestion

pmirGLO was digested with Xho1 and Sac1 FastDigest restriction enzymes (Thermo Scientific) at 37°C for 30 minutes (500ng plasmid DNA, 2μL 10X fast digest green buffer,1μL FastDigest Xho1, 1μL Fast digest Sac1, nuclease free water to 20 μL). Linearised vectors were purified using agarose gel purification described in section 2.2.2.5.4.

## 2.2.2.5.6 E.coli transformation

To 100μl of *E. Coli* cells either 100ng of ligation reaction or control was added. For transformation, cells were incubated on ice for 30 minutes, heat shocked at 42°C for 50 seconds before incubation on ice for a further 5 minutes. 500μl of SOC media was added to the transformed cells before shaking in an incubator at 180g for 1 hour at 37°C. 100μL of transformed cells were plated on selective LB agar containing 100mg/μL ampicillin (Sigma-Aldrich) and grown overnight at 37°C.

#### 2.2.2.5.7 Plasmid verification

Colony PCR was used to identify E.coli colonies containing desired 3'UTR pmirGLO constructs. Colonies were picked and incubated in 5mL LB broth supplemented with 100mg/µL ampicillin at 180g for 12 hours at 37°C. Colony PCR was performed using Q5® High-Fidelity DNA Polymerase as described in section 2.2.2.5.3 substituting gDNA for 1.5µL of transformation medium. Reactions were analysed by agarose gel electrophoresis. Positive recombinant clones were verified by Sanger sequencing (Source BioScience). Results were analysed using SnapGene viewer software. Positive recombinant colonies were used to

inoculate 5mL LB with 100mg/mL ampicillin before shaking in an incubator at 180g at 37°C overnight. Bacterial cultures were pelleted by centrifugation at maximum speed for 5 minutes. Plasmids were isolated using QIAprep spin miniprep kit (Qiagen).

## 2.2.2.5.8 Site directed mutagenesis of pmirGLO

Single or multiple 6mer miR-455-3p (GGACTG) or miR-455-5p (GCACAT) target sites within the 3'UTR pmirGLO constructs were mutated to one of three restriction sites (BamHI; GGATCC, SaII; GTCGAC, Nhel; GCTAGC) using the QuikChange Lightning Multi-site directed mutagenesis kit (Agilent). Reactions were prepared as per table 2.5. Mutant strands were synthesised using thermal cycles shown in table 1.6. Parental DNA templates were removed from amplification products by incubation at 37°C for 1 hour with *Dpn-I* restriction enzyme (10units/uL). 10µL *Dpn-I* treated reaction was transformed into DH5α competent cells as described in section 2.2.2.5.6. Recombinant colonies purified as described in section 2.2.2.5.7. Positive recombinant colonies were identified by restriction digestion and verified by Sanger sequencing (Source BioScience).

Component	Quantity
Plasmid DNA	50ng
QuikChange Lightning Multi reaction buffer (10X)	1μL
dNTPs (25nM)	0.4μL
Mutagenic primer (10uM)	1μL
QuikSolution	0.3μL
QuikChange Lighting multi enzyme blend	0.4μL
Nuclease free water	Το 10μL

Table 2. 5 Reaction for QuikChange Lightning mutli-site directed mutagenesis kit

Step	Temperature (°C)	Time	Cycles
Denaturation	95	2 seconds	1
	96	20 seconds	
Annealing/extension	55	30 seconds	30
	65	30 seconds/Kb	
Final extension	65	5 minutes	1

Table 2. 6 PCR protocol for QuikChange Lightning mutli-site directed mutagenesis kit

## 2.2.3 Cell culture and cell-based assays

#### 2.2.3.1 SW1353 circadian time series model

# **Cross sectional study**

SW1353 chondrosarcoma cells were plated in 6-well plates (6 x 105 SW1353/well) in 3mL complete media (DMEM plus GlutaMAX supplemented with 10% (v/v) FCS) and left to adhere overnight. For cell synchronisation, cells were synchronised in either 50% (v/v) FCS (DMEM plus GlutaMAX supplemented with 50% FCS (v/v)) for 2 hours or 100mM Dexamethasone (Sigma-Aldrich) for 1 hour. For a non-synchronised control, culture media was replaced with fresh complete media for 1 hour. After allotted time, synchronisation media was removed and replaced with low serum media (DMEM plus GlutaMAX supplemented with 0.5% (v/v) FCS). Total RNA was harvested from cells either 0 hours or 24 hours post synchronisation and the first collection point nominated as Circadian time zero (CT0). At CT0, culture media was removed, cells were washed in HBSS followed by ice cold-PBS. 500μL of TrizolTM reagent (Invitrogen, Thermofisher) was added to each well and incubated at room temperature 15 minutes. Dishes were scraped with a sterile cell scraper before aspiration into 1.5mL sterile Eppendorf tubes and stored at -80°C. Samples were collected every 4 hours for 48 hours. Once sample collection was complete total RNA was extracted as described in section 2.2.2.2.1.

## 2.2.3.2 Cell viability assay (Presto Blue)

The metabolic activity of SW1353 cells within the cross-sectional model (section 2.2.3.1) was evaluated based on resorufin fluorescence Presto Blue (PB) assays (ThermoFisher). Briefly, SW1353 cells were plated in 96-well plate (6.6x10³ cells/well) and left to adhere. Cell viability under 4 experimental conditions (table 2.7) was evaluated. Synchronisation of group A and vehicle control group B was as per section 2.2.3.1. Following synchronisation groups A-C were placed into fresh 0.5% media and group D was placed in 10% media. At time points 0H, 24H, 48H and 72H 10µL of PB solution (10X) was added to wells containing 90µL fresh media, incubated in darkness for 20 minutes at 37°C. The fluorescence of resorufin was measured using a EnVisionTM 2103 multilabel microplate reader (Perkin-Elmer) with excitation and emission wavelength set at 560nm and 590nm respectively. The cell viability was normalised to 10% (w/v) FCS and 0.5% (w/v) FCS background media controls, expressed as logarithmic base 10. (N=6).

Group	Condition
A	Dexamethasone Synchronised (100nM)
В	Dexamethasone vehicle control (0.1%
	EtOH)
С	DMEM plus GlutaMAX 0.5% (v/v) FCS
D	DMEM plus GlutaMAX 10% (v/v) FCS

Table 2. 7 Outline of Presto Blue assay experimental conditions

# 2.2.3.3 Identifying clock gene targets of hsa-miR-455-3p and hsa-miR-455-5p

## 2.2.3.3.1 Transient transfection of circadian 3'UTR constructs and miR-455 mimic

SW1353 and DF1 cells were plated in 96-well plates (5 x 10<sup>4</sup> SW1353/well) in 100μL complete media (DMEM plus GlutaMAX supplemented with 10% (v/v) FCS) and grown to 90% confluency. DF1 cells were used to ameliorate the limitations of high endogenous expression of hsa-miR 455 in the SW1353 model. For microRNA transfection, 50nM miRCURY LNA miRNA mimic and 50nM miR-miRCURY LNA miRNA mock negative control were diluted in 5μL Opti-MEM<sup>TM</sup> medium (Gibco, Thermo Fisher Scientific). For each condition, a solution containing 0.2μL Lipofectamine<sup>TM</sup> 3000 diluted in 5μL Opti-MEM<sup>TM</sup> medium was added and incubated at room temperature for 15 minutes. To each well, 90μL of fresh complete media was added and 10μL of either condition. Transfected cells were incubated for 24 hours at 37°C in 5% (v/v) CO<sub>2</sub>. For 3'UTR pmirGLO transfection, 100ng 3'UTR pmirGLO vectors and 0.2ul P3000 (Invitrogen, ThermoFisher Scientific) was added to 5μL of Opti-MEM<sup>TM</sup> medium. 3'UTR pmirGLO solutions were prepared with Lipofectamine<sup>TM</sup> 3000 as before and added wells in a total volume of 90μL fresh complete media. Cells were incubated at 37°C in 5% (v/v) CO<sub>2</sub> for 48hours until luciferase assay.

## 2.2.3.3.2 Dual-GLO luciferase assay

Relative luciferase activity was measured using the Dual-Glo Luciferase Assay system (Promega). Media was replaced with 50μL fresh complete media (DMEM plus GlutaMAX supplemented with 10% (v/v) FCS). For luciferase, 50μL Dual-Glo reagent was added to each well and incubated at room temperature for 15 minutes. Luciferase activity was measured using an EnVision 2013 multilabel microplate reader (Perkin Elmer). For Renilla luminescence, 50μL Dual-Glo Stop & Glo reagent was added to each well, incubated for 15 minutes and

Renilla luciferase activity measured. Luciferase activity was normalised to Renilla luciferase internal control.

## 2.2.4 Mouse models

# 2.2.4.1 Wild-type mouse circadian time series model

3-month-old C57BL male and female mice (WT) were obtained for the murine circadian time series models. 36 hours prior to tissue harvest, mice were released into total darkness (DD). DD conditions were maintained for the duration of the study in order to identify free running oscillations. Animals were sacrificed by cervical dislocation, followed by harvest of liver and the femoral head, knee and xiphoid cartilage using a sterile scalpel. Tissues were snap-frozen in liquid nitrogen and stored at -80°C until use. The first tissue harvest was nominated as circadian time zero (CT0). Tissues were collected every 4 hours for 48hours. Once sample collection was complete, total RNA was extracted as described in section 2.2.2.2.2.

## 2.2.5 In-silico

# 2.2.5.1 Identification of microRNA circadian gene targets

Three types of canonical 3'UTR seed matches were considered when identifying miRNA target. Typically, 6-mer seed matches are 6nt in length and complementary to nucleotides 2-7 in the miRNA response element (MRE). 7-mer seed matches are 7nt in length and complementary to nucleotides 1-6 or 2-7; 8 mer seed matches are 8nt in length and complementary to nucleotides 1-8 with an 'A' at nucleotide 1 in the miR. Predicated target of miRNAs were identified by either manually searching the 3'UTR for seeds in Ensembl or using miRabel target prediction software (bioinfo.univ-rouen.fr/mirabel/).

2.2.6 Data analysis

2.2.6.1 Quantitative RT-qPCR

2.2.6.1.1 Housekeeper gene

Expression stability of candidate housekeeper genes (HKG) GAPDH, YWHAZ, 18S and SDHA

across time series models determined using Refinder software was

(https://www.ciidirsinaloa.com.mx/RefFinder-master/). All calculations are performed using

raw Ct values form time series models.

2.2.6.2 Relative gene expression- comparative C<sub>t</sub> method

Raw fluorescence data was analysed using an Applied Biosystem<sup>TM</sup> 7500 Real-Time PCR

System and expressed as threshold cycle (Ct). The Ct is the cycle at which the fluorescence

generated within a reaction crosses the fluorescence threshold. Relative expression (RE) of

mRNA and miRNAs was determined using the Comparative C<sub>T</sub> method:

 $RE = 2 - \Delta CT$ 

Where  $\Delta Ct =$ 

mRNA/miRNA: GOI Ct – HKG Ct

2.2.6.3 Analysis of NGS data

MicroRNA identification and annotation was performed using the miRNA next generation

sequencing (NGS) discovery (miND) pipeline (227) NGS data quality was evaluated using

FastQC V0.11.9(228) and multiQC v1.10 (229) Sequencing reads were adapter trimmed using

Cutadapt v3.3 and filtered for low-quality reads (Q<30) with a minimum length of 17nt.

Sequencing data was mapped against the murine genome reference GRCm38.p6 provided by

Ensembl (230) using bowtie V1.3.0 and miRDeep2 v2.0.1.2 (231) allowing one mismatch and

filtered for mmu miRNA only. For a general RNA composition overview, non-miRNA mapped

reads were mapped against RNAcentral v19.0 (232) and then assigned to various RNA species

of interest. Data analysis was kindly performed by Dr Michal Dudek (University of

Manchester, UK) using R v4.0. DESeq2 ((233)) was used to remove low abundance miRNAs

(>=10), normalise raw counts and generate principal component analysis plots. Batch effect

54

adjustment was performed using ComBat-seq (234). Data sets were investigated for circadian periodicity using the RAIN package, cosinor rhythmometry and ANOVA.

# 2.2.6.4 Detection of circadian rhythmicity

#### 2.2.6.4.1 Parametric model

Two parametric models were used for the detection of rhythmicity in GOI and miRNA abundance in RT-qPCR and NGS time-series data. One-way ANOVA with Tukey's multiple comparisons and Cosinor rhythmometry. All analysis was performed in GraphPad Prism (version 10). For **ANOVA**, data obtained across two consecutive days (cycles) was stacked into time bins, absence of rhythmicity is inferred when P>0.05 and amplitude was deduced by Tukey's multiple comparisons. For **Cosine rhythmometry**; data is fitted with a cosine curve with a 24-hour period constraint by least squares model. The cosine model can be written according to the equation:

$$x_i = M + A\cos(\theta_i + \varphi) + e_i$$

Whereby the value of each point (Xi) is a function of the average value under investigation, the MESOR (M, the rhythmic mean), the amplitude of oscillation (A) and the phase of the maximum in relation to a fixed reference time ( $\varphi$ , Acrophase). Given that the period (P) is known (24hours), the trigonometric angles ( $\theta$ i) corresponding to sampling times (t, time at which samples Xi were collected) is obtained by  $\theta$ i =( $2\pi$  ti)/P.

## 2.2.6.4.2 Non-parametric model (RAIN)

Statistical analysis was kindly performed by Dr Michal Dudek in discussion with Prof Qing Jun Meng (University of Manchester). The RAIN algorithm is a robust nonparametric method for the detection of rhythms of specified periods in biological data that can detect arbitrary wave forms(235). Circadian periodicities were defined by a period of 24 hours. A Benjamini-Hochberg adjusted p-value of <0.1 or a P-value of <0.05 was considered significant.

## 2.2.6.5 Gene set enrichment analysis

Putative mRNA targets of miRNAs were identified by miRTarBase and Targetscanmouse. Gene set enrichment analysis was performed using Enrichr software, a freely available online analysis tool (<a href="https://maayanlab.cloud/Enrichr/">https://maayanlab.cloud/Enrichr/</a>)(236). Enriched biological processes were deemed significant at FDR p-<0.05 corresponding to  $-\log(p-adj)\sim1.3$ .

# 2.2.6.6 Statistical analysis

Unless otherwise stated, data sets were normally distributed and a students unpaired t-test or one-way ANOVA with Tukey's multiple comparisons to compare differences between two groups. Statistical analysis was performed with Microsoft Excel (2006) or GraphPad Prism (version 10). Data is presented as mean +/- standard deviation (SD).

# Chapter 3: Exploring circadian regulation of miRNA expression in cartilage (invitro)

## 3.1 Introduction

In chondrocytes, the molecular clock temporally organises the expression of ~4% of cartilage mRNAs, including those involved in development (i.e. *Sox9*) and homeostasis (*Col2a1*, *Acg1*, *Adamts4*). Dynamic expression of these genes ensures key processes are executed at an optimal time of day. For instance; *Col2a1* and *Timp4* abundance is greatest in the 'early-night' period and, oscillates in antiphase to *Mmp14* in mouse cartilage(237). In this way, proteolysis of the ECM is segregated to the rodent's 'rest-phase', permitting more effective tissue maintenance. Given this, circadian dysfunction likely has a profound impact on chondrocyte capacity to coordinate cartilage homeostasis. Indeed, altered expression of *Bmal1*, *Per* and *Cry* is reported in several human OA models and, targeted deletion of *Bmal1* resulted in decreased transcription of ECM macromolecules, altered cytokine signalling and cartilage degeneration in mice(126).

Similarly, microRNAs are important regulators of cartilage physiology and play a role in the pathologic rebranding of AC in OA. Broadly, cartilage specific ablation of Dicerl lead to decreased chondrocyte proliferation and skeletal defects(192). miR-140 is the most abundant microRNA in cartilage and directly regulates translation of catabolic enzymes (MMP-13, ADAMTS5) and mediators (SOX9, SMAD3, IL1B). Therefore, an OA-like phenotype was observed in miR-140 KO mice and, overexpression of miR-140 protected mice from cartilage degeneration(194,200,219). Previous research in the Clark lab has illustrated similar roles for miR-29 and miR-455. In vitro, miR-29b-3p directly regulated translation of ADAMTS2, 9,12,15,16,18 and 20 and, incidences of OA were greater in a double KO miR-29 mice comparative to control littermates. miR-455-3p and miR-455-5p co-ordinately regulate expression of AC development (RUNX-2, HDAC2, HDAC8) and degeneration-related genes (SIRT1, HIF-2a)(223,238,239). Significantly, both 'arms' of mir-455 are deregulated in OA and, their overexpression protected cartilage degeneration in a mouse OA model, demonstrating their therapeutic potential(238). Indeed, extracellular vesicles (EV) derived from TGF-b-preconditioned BMSCs rich in miR-455 promoted AC regeneration by activation of the SOX11/FOXO signalling pathway(240).

Given the relevance of microRNAs in cartilage homeostasis, understanding the molecular regulators of microRNA expression and activity are of value. Considering the extent of the circadian transcriptome in AC, we propose a role for the chondrocyte molecular clock in the regulation of cartilage microRNAs. To evaluate this, an *in-vitro* model for the preliminary analysis of cartilage circadian microRNAs has been developed. Here, the diurnal expression of miR-140 and miR-455 in SW1353 chondrocytes were quantified by RT-qPCR analysis.

## 3.2 Aims

- Develop an *in-vitro* time-series model for the evaluation of circadian mRNA and miRNA expression in SW1353 chondrocytes by RT-qPCR
- Evaluate the time-dependent expression of miR-140 and miR-455
- Discuss mechanisms of circadian regulation of miR-140-3p

### 3.3 Results

## 3.3.1 Developing a statistical model for detection of oscillating components in-vitro

Given that studies investigating circadian regulation of mRNA and miRNA expression in cartilage are limited, devising an effective model for the detection and evaluation of this phenomena in time-series data is a major aim. Here, we report procedures for the statistical evaluation of oscillating transcripts in the SW1353 RT-qPCR datasets. Notably, this model may be applied to larger transcriptomic data sets obtained by small-RNA seq in chapter 5.

### Numerical and statistical analysis

Figure 3.1 shows the four parameters by which circadian components may be defined: amplitude, phase, period and MESOR. Therefore, an analysis workflow capable of identifying rhythmicity with statistical significance, parameter estimation and visually modelling data sets was devised (Fig 3.2). For this, data has been interpreted using two parametric models: **cosinor fit analysis** and **one-way ANOVA**. In cosinor rhythmometry, a curve is fitted to data by least squares routine to estimate the shape and parameters of a rhythm. Notably, as a parametric model we assume circadian components are 24hour synchronised (i.e. has a 24hour period), that rhythms follow a sinusoidal waveform, and that the rhythm is stationary (i.e. a rhythms parameters constant over time). Under these assumptions we have interpreted rhythms as significant when the fitted curve has an amplitude statistically greater than zero. Hear in, this is indicted graphically by absence of overlap between the 95% confidence interval at the peak/trough of the curve and the MESOR (Fig 3.2A). We evaluate this alongside the goodness of fit statistic (R-squared statistic (R<sup>2</sup>)) though no lower threshold is set for this value given this method increased exclusion of oscillating components in noisy data.

In instances where visually oscillating components failed cosinor tests, additional parameter tests were utilised. A one-way ANOVA is applied to distinguish noisy rhythms from random oscillations and, multiple comparisons are applied to time bins to reveal circadian amplitude in absence of a difference in MESOR (Fig 3.2B). Therefore, through this thesis, statistical outputs are loosely interpreted, and rhythmic components are identified by multiple data processing methods.

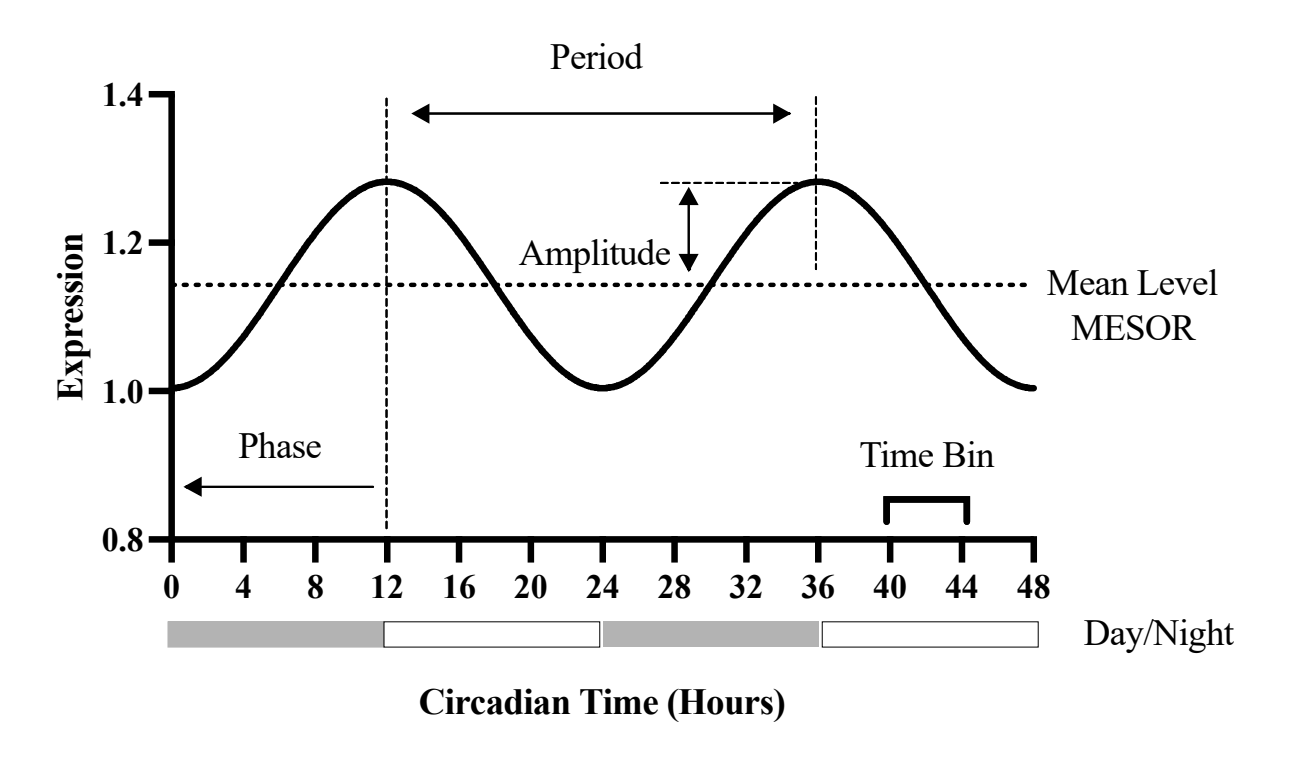


Figure 3. 1 Parameters of circadian rhythms.

A representative circadian rhythm in which expression of a particular measure (e.g. mRNA or microRNA) varies according to time. In a symmetrical oscillation MESOR (or mean level) is the central value around which the oscillation occurs. Period is the duration of a full cycle. Amplitude is half the range of excursion in a given period. The timing of a reference point (e.g. the peak) relative to a fixed event (e.g. beginning of the dark period) is the Phase.

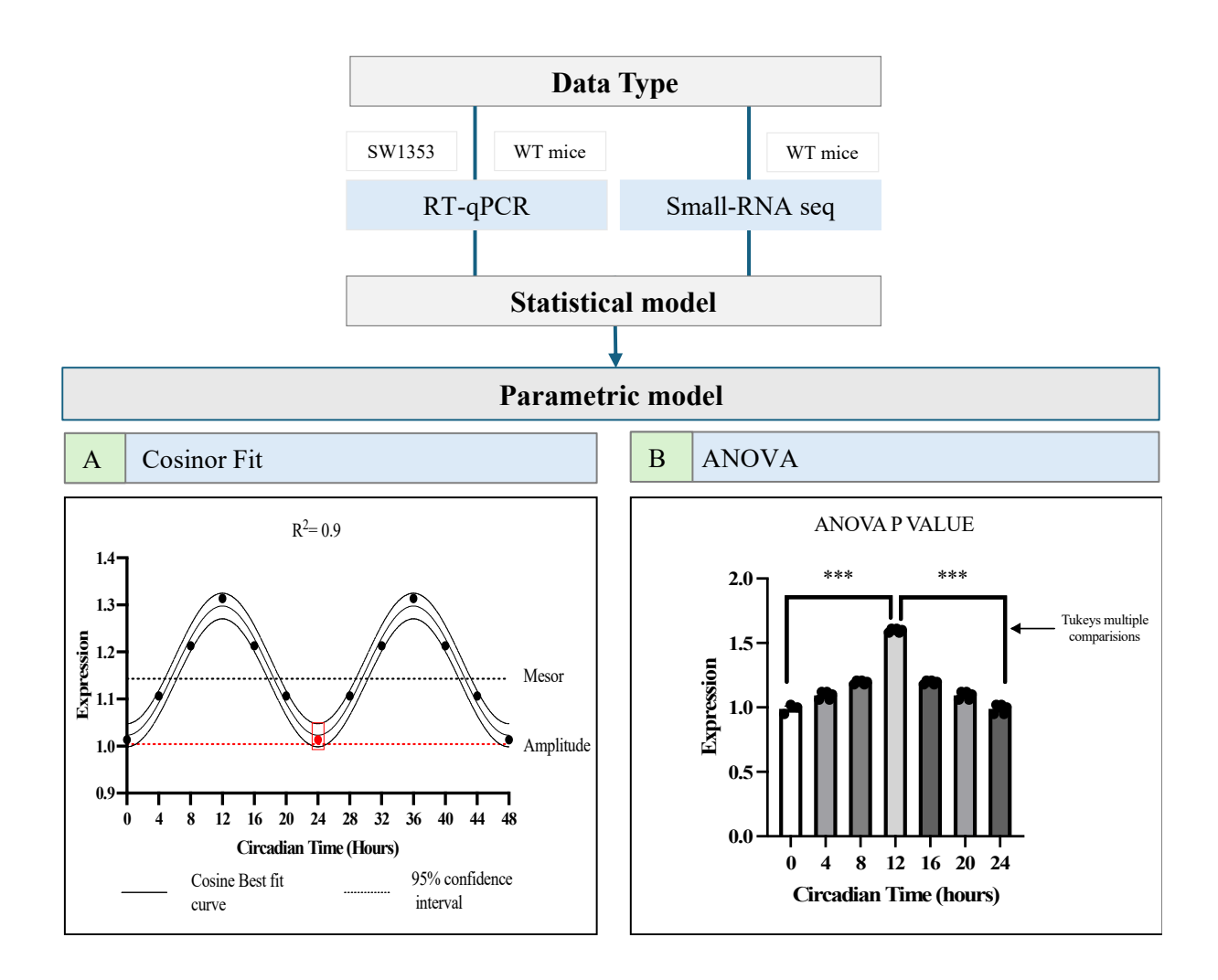


Figure 3. 2 Stepwise protocol for the evaluation detection of oscillating components in articular cartilage in by parametric models RT-qPCR and smallRNA sequencing data.

(A) Cosinor fit. Rhythmicity detected by Cosinor fit analysis. Red line and black line depict predicted amplitude and MESOR respectively. Red data points indicate amplitudes significantly greater than MESOR. Data presented relative to circadian time (CT) 0. (B) Oneway ANOVA. Absence of rhythmicity determined by one-way ANOVA with Tukeys multiple comparisons test.

# 3.3.2 Evaluating housekeeper gene expression stability by RT-qPCR and RefFinder software

Figure 3.3 depicts the Ct values of 18S, GAPDH, SDHA and YWHAZ in 50% or 100nM dexamethasone synchronised SW1353 across a 48-hour period, as determined by RT-qPCR. A Ct value represent the number of cycles at which PCR products appear to affectively increase. Therefore, they may be used to compare mRNA abundance of candidate HKG as a factor of circadian time and experimental condition. In the 50% FCS group, Ct values for four candidate gene varied from 16 to 35 and the full range varied from 6 to 10. Of the four genes, expression levels of 18S rRNA (18S) was the highest whilst YWHAZ was the lowest with an average Ct value of 16 and 35 respectively. Comparatively, Ct values in the 100nM dexamethasone group varied from 16 to 33 with a range of 6 to 13. In descending order, average mRNA abundance of 18S was highest (Ct=16), followed by GAPDH (Ct=24), SDHA (Ct=28) and YWHAZ (Ct=33). The CT values of the HKG genes varied across the time series in both experimental conditions. Preliminarily, expression stability of HKG across the time series is indicated by the Ct values coefficient of variation (CV), the greater the coefficient the more unstable the gene expression. In both conditions, time dependent expression of YWHAZ was most stable (50%) CV= 4 ,100nM CV=4). Though, variability of GAPDH was two-fold greater between conditions (50% CV= 10,100nM CV=5) and the gene with the greatest variance was SDHA in the dexamethasone group.

Expression stability of HKG was further evaluated by RefFinder software(241). RefFinder ranks genes based on the geometric mean of the individual rankings determined by GeNorm, NormFinder, BestKeeper software and the comparative delta-Ct method. The rankings and characteristic stability parameters for candidate HKG in 50% FCS and 100nM dexamethasone groups are shown in Table 3.1. For both experimental conditions, analysis was conducted separately. The comprehensive ranking identified *18S* as the most stable reference gene in the 50% FCS group, followed by *GAPDH*, *SDHA* and *YWHAZ*. Significantly, *18S* was ranked most stable across all 4 analysis methods in this group, though had the greatest variation (CV=14) and the greatest geometric mean in the 100nM dexamethasone group. These differences are likely to due to insufficient synchronisation by 50% FCS, as discussed later.

In 100nM dexamethasone YWHAZ and GAPDH both ranked equally as the most stable HKG. GAPDH was ranked highly throughout all softwares whilst YWHAZ is ranked of 4<sup>th</sup> by

BestKeeper. These analyses suggests that though the average expression of candidate genes is unaffected by synchronising agent, the abundance of each gene is variable across the time course and under different treatment conditions in-vitro. Therefore, HKG stability should be assessed and selected independently in circadian models. Here-in, 18s and GAPDH will be used to normalised RT-qPCR data in 50% FCS and 100nM dexamethasone time series models.

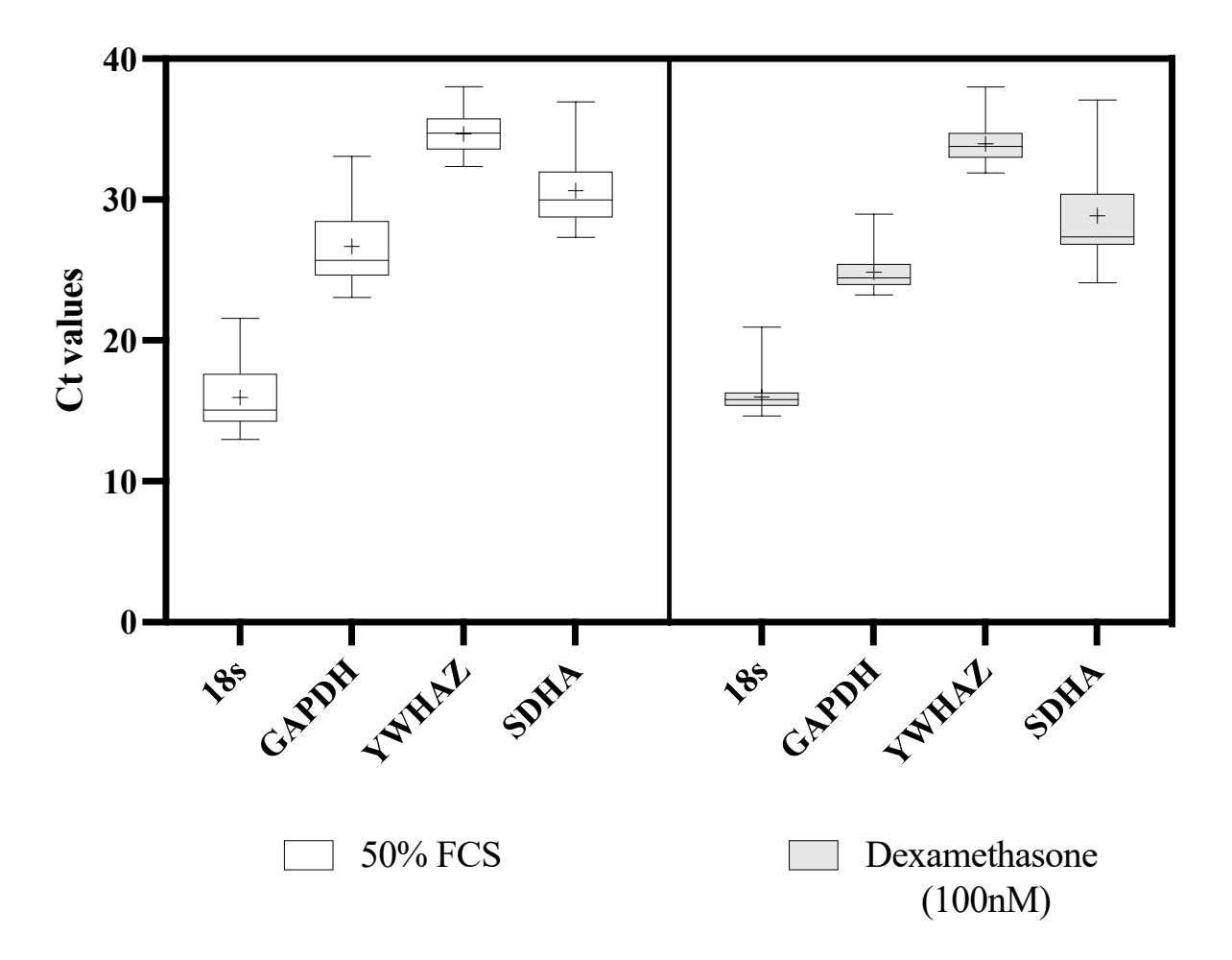


Figure 3. 3 Expression levels of candidate housekeeper genes in SW1353 synchronized in 50% FCS or 100nM dexamethasone.

Expression data displayed as raw Ct values for each housekeeper gene over a 48hours in 50% FCS or Dexamethasone synchronized samples. A line across the box depicts the median expression value from across the time series. A (+) represents the mean. Whiskers represent the maximum and minimum values. Box represent the 25th and 75th percentiles (N=13)

Comprehensive Rank	Gene symbol	GeNorm		Comparative Delta Ct		NormFinder		BestKeeper		Geometric
		Rank	M value	Rank	Mean SD	Rank	Stability value	Rank	Stability value	Mean
50% FCS										
1	18S	1	3.5	1	6.7	1	1.7	1	1.8	1
2	GAPDH	1	3.5	2	7.9	3	4.4	2	2.1	1.9
3	SDHA	2	4.9	3	8	2	5	3	2.5	2.7
4	YWHAZ	3	8.9	4	12.94	4	12.5	4	7.8	4
100nM Dexamethasone										
1	YWHAZ	1	6.3	1	11.9	2	7.8	4	9.8	1.57
2	GAPDH	2	9.7	2	12	1	4.8	1	4.7	1.57
3	SDHA	1	6.3	3	12.2	3	8	3	9.9	2.45
4	18S	3	13.3	4	16.8	4	15.5	2	5.1	3.36

Table 3. 1 Ranking of candidate reference genes by RefFinder software.

The comprehensive rank for each housekeeper gene is generated based on the geometric mean of ranks across GeNorm, NormFinder, BestKeeper software and comparative delta Ct.

# 3.3.3 Confirming synchronisation of SW1353 chondrosarcoma cells by dexamethasone and serum shock by oscillation of *BMAL1*

*In-vitro*, the SW1353 chondrocyte-like cell line requires synchronisation with artificial zeitgebers to reset the phase of the population's molecular clocks. Confluent cells were synchronised in either 50% FCS or 100nM dexamethasone 24hours prior to the first RNA harvest (Circadian time (CT) 0). Vehicle controls (VC) were run in parallel, and all cultures were maintained in low serum for the experiment's duration. We sought to confirm effective resetting in both conditions by monitoring oscillation of *BMAL1* transcripts across the duration of the time series by RT-qPCR (N=3). Notably, a western-blot time series was run in parallel to both models to confirm oscillation at the protein level. However, this model was unsuccessful due to an ineffective batch of RIPA buffer.

In the 50% FCS group, expression of *BMAL1* peaked at CT20 comparative to CT0 (multiple comparisons, P=0.008) and variance between the time bins was significantly greater than that of the bin's biological replicates (ANOVA, P=0.007) (Fig 3.4A). By cosinor analysis, *BMAL1* abundance peaked at CT20 and, 24 hours later at CT44 though, these amplitudes were not significantly greater than the MESOR (Fig 3.4B). We speculate that large inter-sample variation contributed to the absence of statistical rhythmicity. Standard deviation (SD) may be used to discuss data spread within time bins. In the 50% group SD ranged from +/-0.1-0.6. Notably, CT 16 (SD=+/-0.5) deviates considerably from fitted wave. Exclusion of CT16 improved the R² statistic from 0.46 to 0.70 and amplitudes of CT20 and CT40 were significant. However, exclusion of CT16 was deemed unnecessary given all time bins were exposed to the same method of synchronisation, to the best of our knowledge. Therefore, though the absence of rhythmicity can be rejected by ANOVA analysis, *BMAL1* oscillation failed formal models of rhythmicity in the 50% FCS. Given this, we chose not to analyse the VC model for the 50% FCS in favour of pursuing 100nM Dexamethasone samples for further investigations.

Dexamethasone improved the synchronicity between molecular clocks of the cellular population, without influencing the baseline abundance of core clock gene *BMAL1*. As shown in figure 3.5A, grouping the data shows 100nm dexamethasone had no significant effect on the global expression of *BMAL1*, though overall variance within the population decreased significantly compared to VC (Fig 3.5A, F=0.006). Between time bins, variation in the average expression of *BMAL1* was improved comparative to VC but, not to the level of significance as

shown in figure 3.5 B and C ((ANOVA (100nM Dex, P=0.3) (VC, P=0.8)). Further, under ANOVA analysis, dynamic expression of *BMAL1* visually improves, but a peak CT could not be deduced in the synchronised model due to large SD in the CT16 and CT20 time bins.

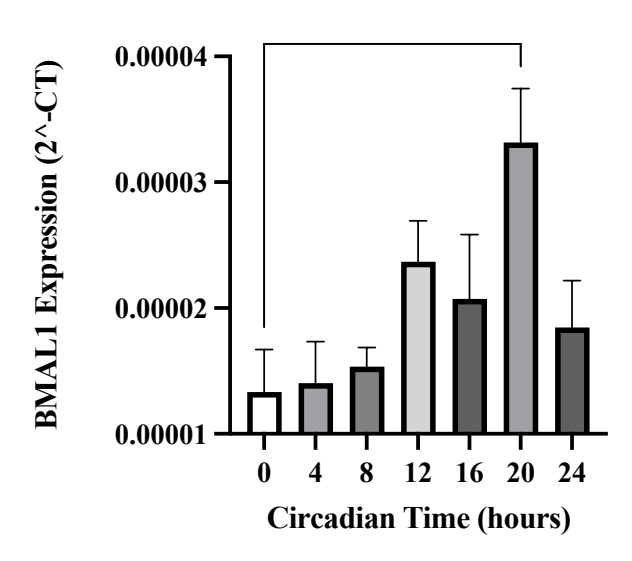
Figure 3.6 depicts cosinor analysis of *BMAL1* abundance in VC and dexamethasone synchronised models. Notably, we were unable to combine the outcomes of cosinor analysis of VC and dexamethasone on a single graph due to large differences in the fitted curve and confidence intervals. An example of this is shown in appendix Figure 2.1. Therefore, VC and Dexamethasone models are presented separately. As shown, no oscillation was identified in the abundance of *BMAL1* in the VC (Fig 3.6A). Cosinor analysis identified circadian regulation of *BMAL1* expression following dexamethasone synchronisation. Here, transcript abundance of *BMAL1* oscillated across two circadian cycles. Expression peaked at CT20 and CT40 and, both amplitudes were significantly greater than the MESOR (Fig 3.6B). In the dexamethasone model, variation increased across the time series as indicated by the SD. In the first circadian cycle (24A), SD ranged from +/- 0.03-1.3. In the second cycle (24B), SD range increased to 0.4-2.1 and is greatest in the final 3-time bins.

To better understand the implications of this, 24A and 24B were analysed by ANOVA and cosinor models individually. As shown in figure 3.7 A and B, variation between time bins was only significant in 24A (P=0.01) and, *BMAL1* expression was significantly different between CT0 and its peak at CT20 (Fig 3.7A (Multiple comparisons, P=0.03)). Further, the rhythm estimates and parameters of the cosine model were a better fit to the 24A data, indicated by an R<sup>2</sup> of 0.8 comparative to an R<sup>2</sup> of 0.6 in 24B (Fig 3.7 C-D). Indeed, relative *BMAL1* expression at CT 20 in 24A was significantly greater than the estimated MESOR, whilst the peak expression of *BMAL1* at CT40 in 24B failed formal tests of rhythmicity. These observations suggest a decrease in the cell synchronicity in the second cycle of our model. This may be due the absence of external zeitgebers in culture media to maintain and entrain the molecular clocks or decreases in cell viability.

Therefore, we can confirm that dexamethasone is an effective synchronising agent in-vitro and circadian regulation of *BMAL1* expression is more robust in first circadian cycle of the time series. Here-in, mRNA and miRNA analysis will be performed on the samples of 24A in order to avoid false negative results.



A



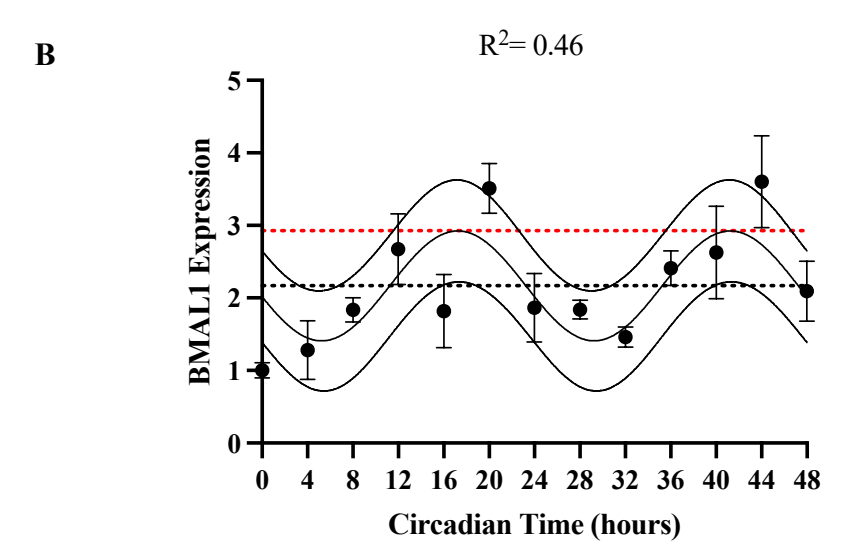


Figure 3. 4 Determining efficacy of serum shock as a cell synchronising agent by induction of *BMAL1* oscillation.

SW1353 chondrosarcoma cells were synchronised in DMEM containing 50% foetal calf serum for 2 hours and rested in low serum. 24hours post synchronisation, RNA was extracted by TRIZOL every 4 hours for 48hours. The first harvest was designated circadian time 0. Expression of BMAL1 mRNA was measured by RT-qPCR, normalised to 18S housekeeper gene mRNA. (A) Absence of rhythmicity determined by one-way ANOVA with Tukeys multiple comparisons test (data presented as mean +/- SD, N=6 biological replicates per bin). (B) Rhythmicity detected by Cosinor fit analysis. Red line and black line depict predicted amplitude and MESOR respectively. Data presented relative to circadian time 0 mean +/- SD, N=3 Biological replicates per time point. \*p<0.05 \*\*P<0.005 \*\*\*P<0.001.

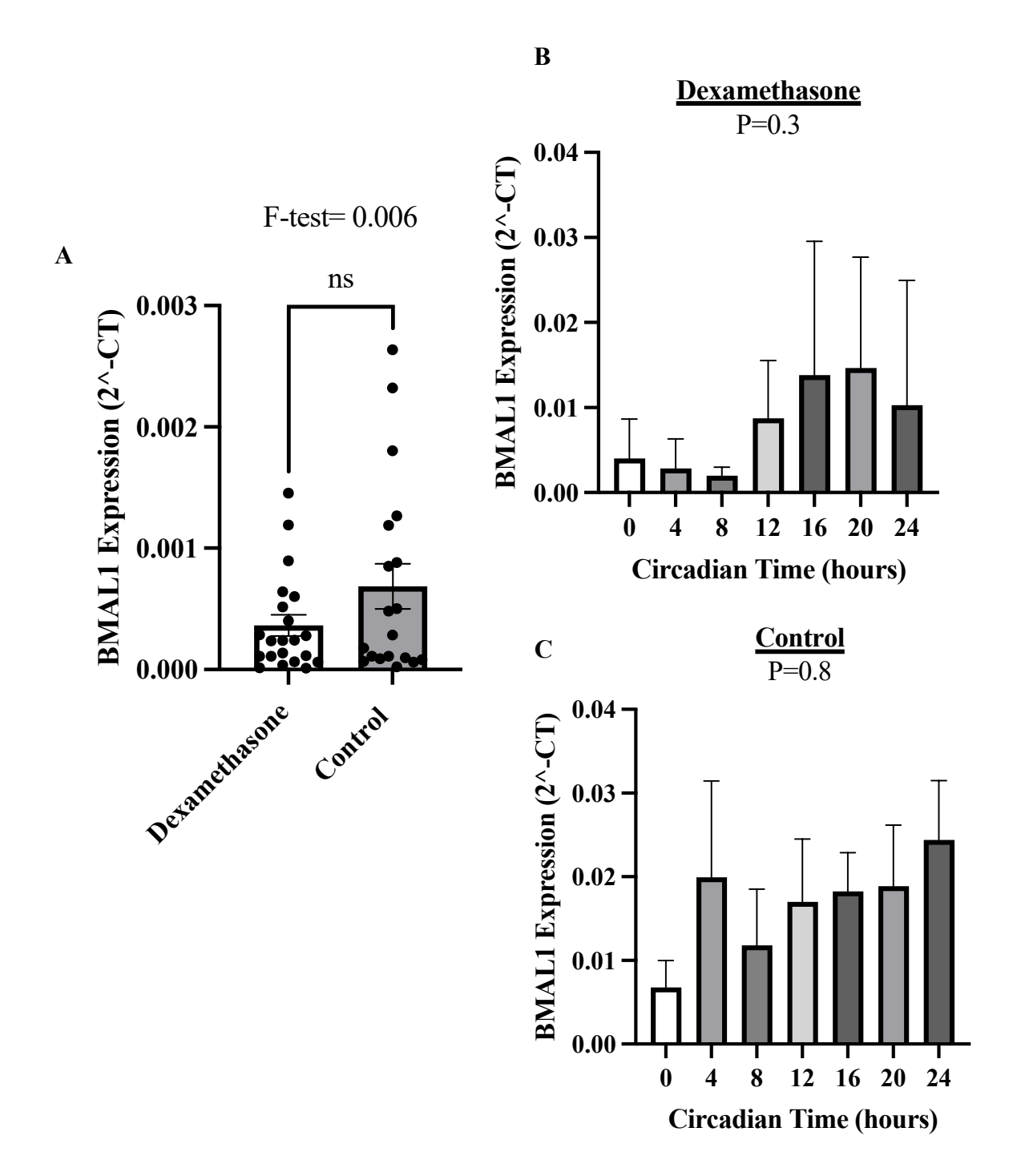
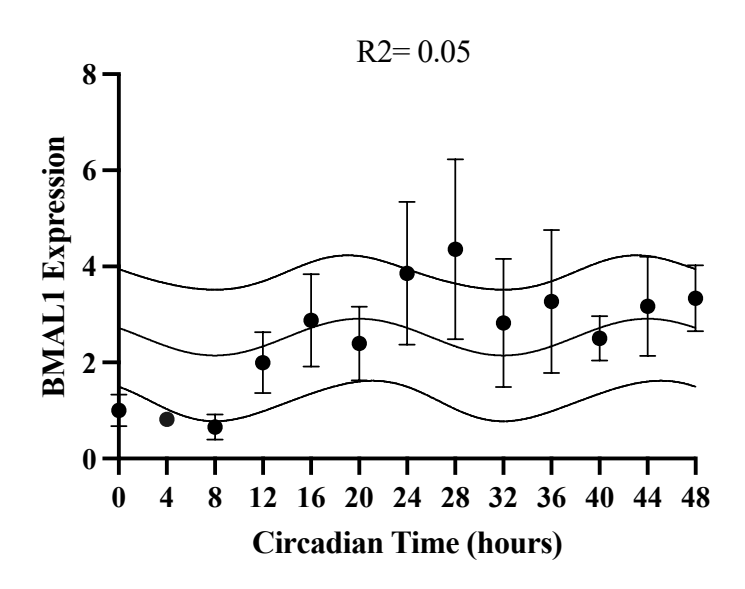


Figure 3. 5 Determining efficacy of Dexamethasone as a cell synchronising agent by induction of *BMAL1* oscillation.

SW1353 chondrosarcoma cells were synchronised in DMEM containing 100nM dexamethasone for 1 hour. After 24hours in low serum RNA was extracted every 4 hours/48hours for 48hours. *BMAL1* mRNA was measured by RT-qPCR, normalised to *GAPDH*. (A) Average *BMAL1* expression between 100nM dexamethasone and VC compared by Students T-test (data presented as mean +/- SD, (N=39). Absence of rhythmicity in dexamethasone (B) and VC (C) determined by one-way ANOVA with multiple comparisons (Data presented as mean+/- SD(N=6))

A



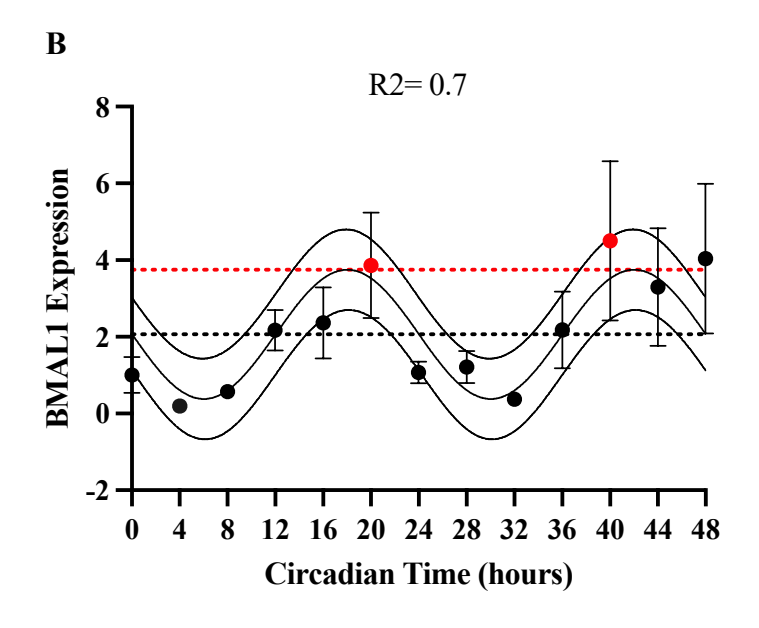


Figure 3. 6 Cosinor analysis of BMAL1 abundance in SW1353 following dexamethasone synchronisation.

Rhythmicity in (A) VC and (B) dexamethasone detected by Cosinor fit analysis. Red line and black line depict predicted amplitude and MESOR respectively. Red data points indicate amplitudes significantly greater than MESOR. Red line and black line depict predicted amplitude and MESOR respectively. Data presented relative to circadian time 0 mean +/- SD, N=3 Biological replicates per time point.

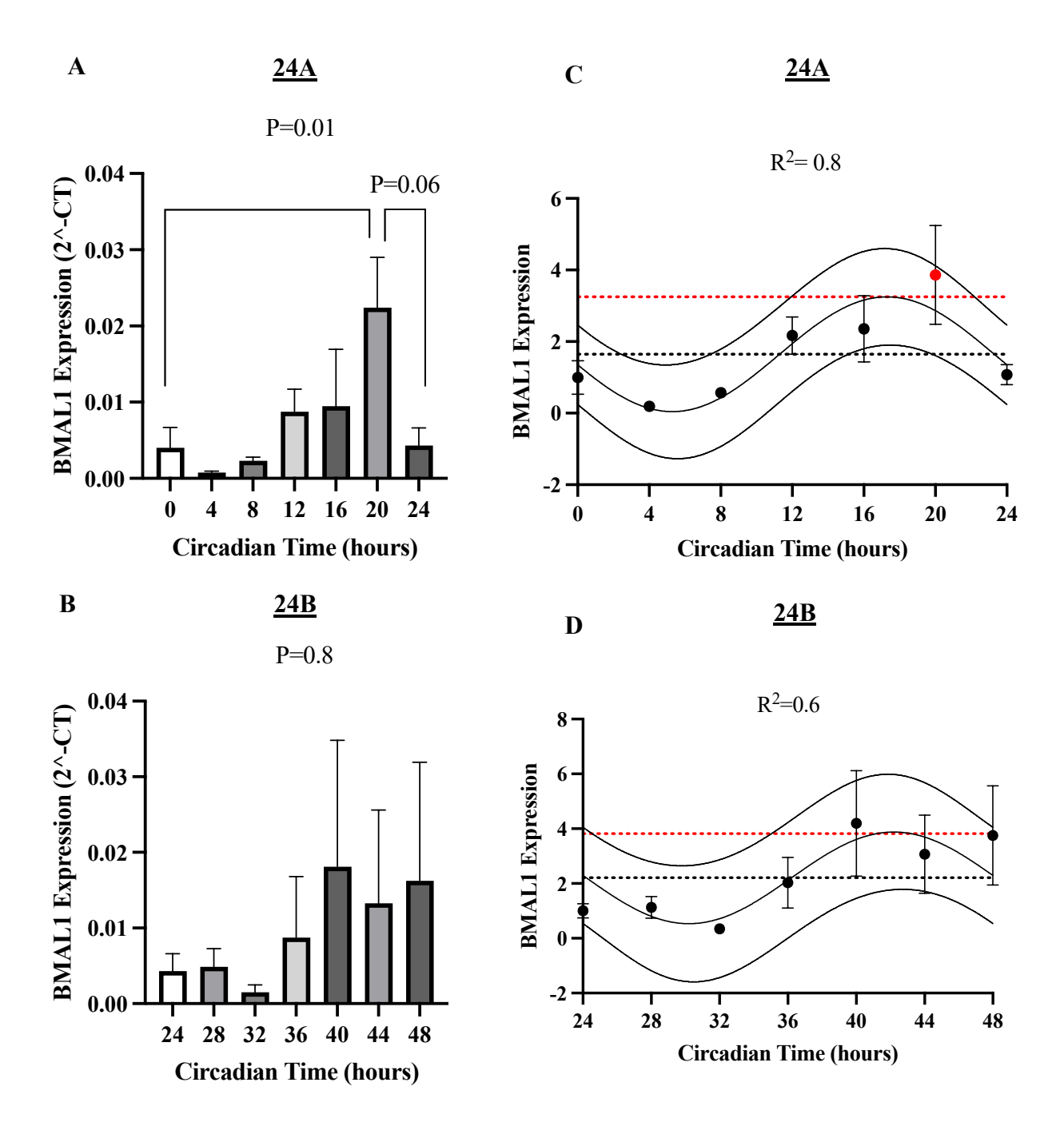


Figure 3. 7 Comparing parameters of *BMAL1* oscillation across the SW1353 time series.

Robustness of *BMAL1* mRNA rhythmicity was compared between two full circadian cycles of the SW1353 time series model. Absence of rhythmicity in 24A (A) and 24B (B) determined by one-way ANOVA and Tukeys post hoc test (data presented as mean  $\pm$ -SD(N=3)). Predicted shape of the *BMAL1* curves were fitted by cosinor analysis (C,D). Red data points indicate amplitudes significantly greater than MESOR. Red line and black line depict predicted amplitude and MESOR respectively. Data presented relative to circadian time 0 mean  $\pm$ -SD, N=3 Biological replicates per time point. Statistical significance between groups represented as  $\pm$ 0.05 \*\* $\pm$ 9<0.005 \*\* $\pm$ 9<0.001

# 3.3.4 Determining SW1353 cell viability within a circadian time series model by PrestoBlue

We have shown that the robustness of *BMAL1* mRNA rhythmicity decreases in the second circadian cycle of the SW1353 time series model. We hypothesises that this is, in-part, an effect of changes to cell viability. This has been quantified as a factor of both time and experimental treatment using a fluorometric (Presto-Blue(PB)) assay. Here, conversion of resazurin to resorufin is proportional to the number of viable cells(242). Notably, we have not compared fluorescence between experimental groups, given variability in time point 0 data. For example, fluorescence at time-point 0 for group C and D 6.0 +/- 0.02 and 5.8+/- 0.04. This could indicate differences in cell densities or, error in addition of PB. Therefore, we are unable to confirm if statistical difference between groups are a factor of experimental treatments or, cell number.

The first 24-hour period represents the 'rest-phase' of cell synchronisation protocols. In all four groups, fluorescence significantly increased in this interval (Group A-D, p<0.0001)(Figure 3.8 A-D). On average, non-synchronised cells (NCS) in 10% FCS had the greatest fold change (Group D, FC=2.3), followed by NSC in 0.5% FCS (Group C, FC=2.1), dexamethasone synchronised cells in 0.5% FCS (Group A, FC=2.0) and NSC VC in 0.5% FCS (Group B, FC=1.7). Regions highlighted in grey represent the window in which samples are collected during in-vitro circadian models. From time point 24 to 48, fluorescence increased in Groups A-D though not significantly, with group C having the largest fold change of 1.7. Importantly, significant decreases were observed in all groups between time point 48 and 72 (Groups A-D, P<0.0001). Given fluorescence correlates with cell number and metabolically active cells, we infer that cell death increases in the second circadian cycle. This observation occurs irrespective of the utility of dexamethasone or low serum, suggesting that cells viability is decreasing as a factor of time. This further supports our decision to use the first 24 hours of our in-vitro models to analysis mRNA and miRNA expression.

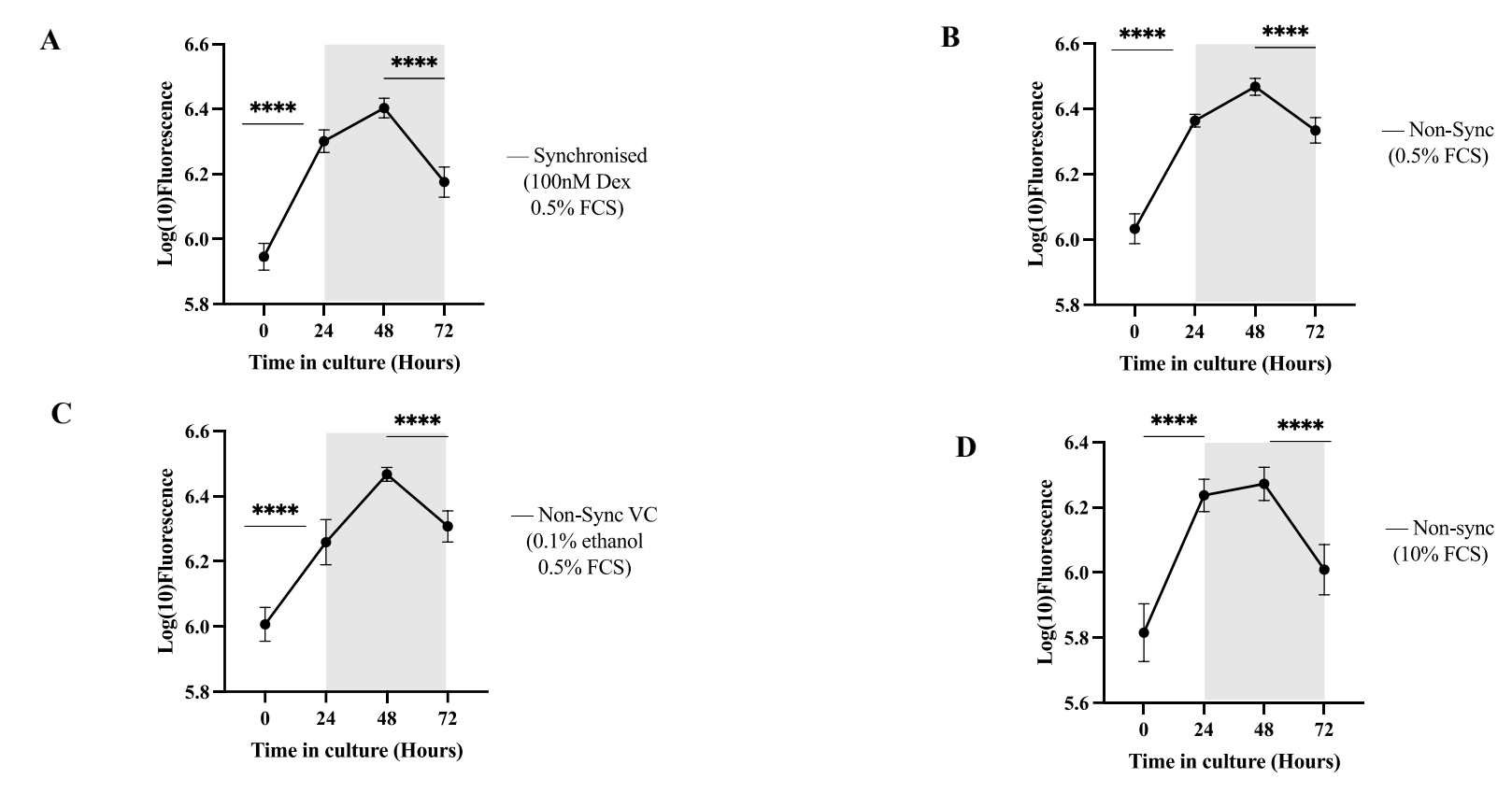


Figure 3. 8 Measuring the viability of SW1353 in a 72-hour circadian time series mode by PrestoBlue.

Viability of SW1353 cells was monitored as a factor of experimental group and time. Grey regions represent time frame in which data is collected in circadian experiments. Experimental groups consisted of: (A) Group A, 100nM DEX synchronised (B) Group B 0.1% Ethanol non-synchronised Vehicle control, (C) Group C 0.5% FCS non-synchronised and (D) Group D 10% FCS non synchronised. After 1 hour, cells were placed into either 0.5% FCS or 10% FCS for the duration of the experiment, Fluorescence intensity of resorufin was measured at 0 24 48- and 72-hour intervals, normalised to either 0.5% or 10% media controls. Differences between time points determined by students t-test, represented as \*p<0.05 \*\*\*p<0.005 \*\*\*p<0.001.. Data expressed as mean +/- SD(N=6 replicates per time point.

# 3.3.5 Determining oscillation of positive, negative, and auxiliary limb circadian genes in SW1353 synchronised in dexamethasone

Though we have demonstrated robust oscillation of BMAL1 mRNA in our model. It is unclear whether other conserved clock regulators of the TTFL show circadian expression with correct phase relations. This has been addressed by measuring time dependent expression of positive limb (CLOCK), negative limb (CRY, PER) and auxiliary loop ( $ROR\alpha$ ) transcripts by RT-qPCR.

BMAL1:CLOCK heterodimer enhances expression of CRY1 and PER2 by binding to E-box elements in their promotor. As discussed by Gossan *et al*, *CLOCK* mRNA and proteins are not rhythmically expressed in most mammalian tissues though, are essential for rhythm generation in AC(243). Data in Fig 3.9 A and B agrees with this. Here, no significant changes were observed in the time dependent (Multiple comparisons, P=NS) or the average (T-test, P=NS) expression of *CLOCK* mRNA comparative to controls. Though, variance within synchronised groups decreased (F-test =<0.0001). This may be an effect of synchronisation of the transcriptional activators and suppressors of *CLOCK*, resulting in less randomised transcription and translation comparative to control. In the SCN, the *NPAS2* transcription factor is rhythmically expressed and, functionally substitutes for CLOCK protein and, ROR $\alpha$  is an enhancer of positive limb gene expression. Here, transcripts of *NPAS2* and *ROR* oscillated robustly in SW1353, peaking significantly at CT16 (Appendix Fig 2.2A and B). Confirming presence oscillation of positive and auxiliary limb transcription factors in our model.

Negative limb genes, *CRY* and *PER*, supress BMAL1:CLOCK expression and have differing expression kinetics in the SW1353 model. *CRY1* and *CRY2* abundance peaked at CT12, though not significantly, with an average fold change of 4.1 and 4.4 respectively. In other models, CRY proteins are a stronger *BMAL1* suppressor due to its higher affinity. Here, both *CRY* transcripts peaked 8 hours prior to *BMAL1* (section 3.3.3), suggesting positive limb inhibition by CRY1 is progressively reduced to enable a new circadian cycle to begin (244). Comparative to PER1, PER2 plays a more dominant role in the negative limb and is the only negative limb protein that targets *CLOCK*(245). *PER2* passed the formal tests of rhythmicity by cosinor analysis, peaking at CT16 (FC=4.3). Notably, *PER2* transcripts peaked 4 hours later than *CRY*, likely reflecting their differing roles in the negative limb. These findings demonstrate the induction of an auto-regulatory feedback loop in the SW1353 chondrocyte model.

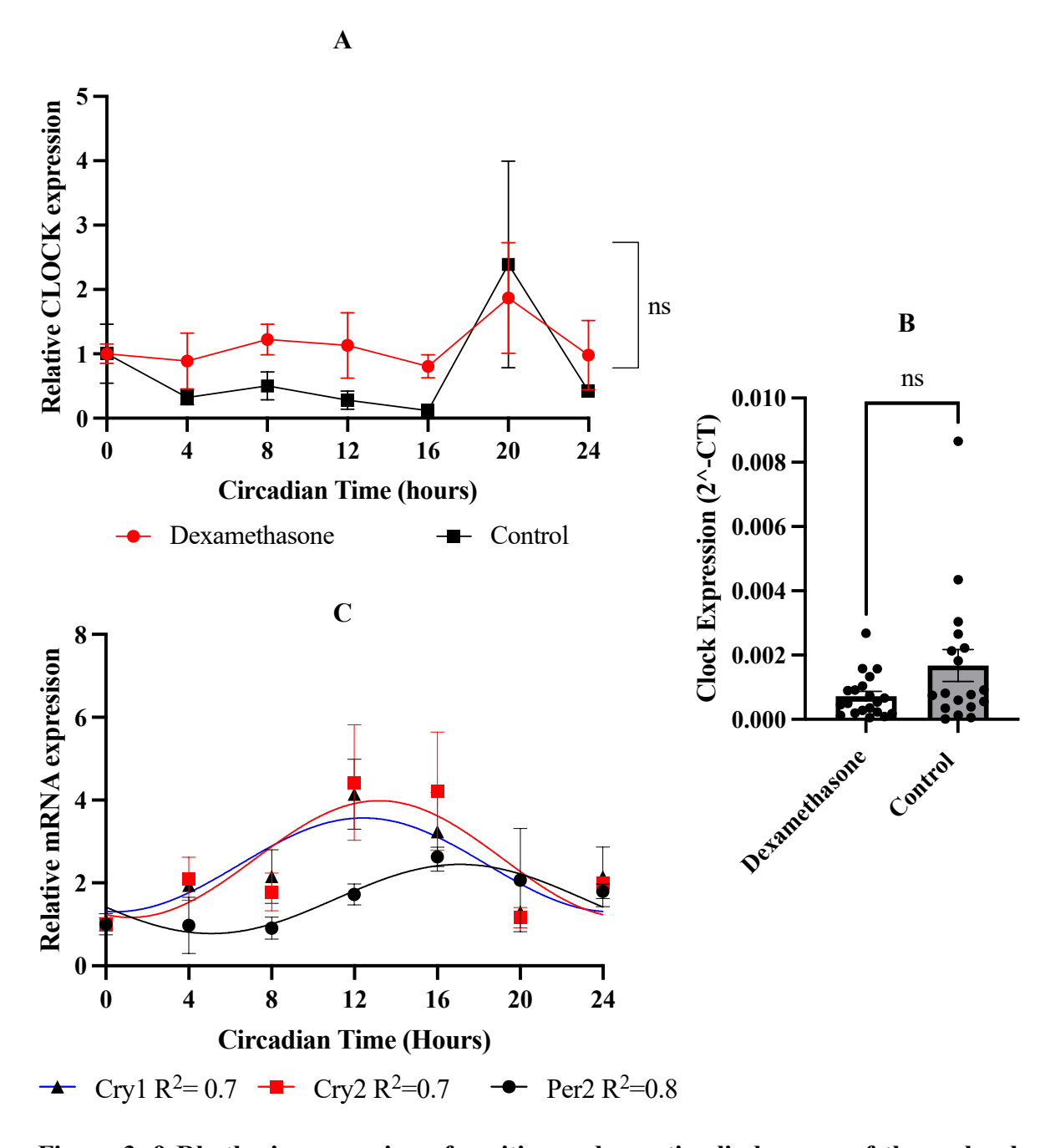


Figure 3. 9 Rhythmic expression of positive and negative limb genes of the molecular circadian clock in SW1353.

A robust circadian molecular feedback loop in SW1353 cells synchronised in 100nM dexamethasone was validated by RT-qPCR. (A) Depicts time dependent expression of the positive limb genes *CLOCK* in synchronised and non-synchronised controls. Differences determined by two-way ANOVA and multiple comparisons. (B) Average expression of *CLOCK* mRNA between 100nM dexamethasone and VC compared by Students T-test (data presented as mean +/- SD, (N=39). (C) expression dynamics of negative limb genes *CRY1*, *CRY2* and *PER2* determined by cosinor analysis. All data normalised to GAPDH housekeeper gene, presented relative to circadian time 0, mean+/- SD(N=3).

### 3.3.6 Identifying circadian miRNAs in SW1353 chondrosarcoma cells

Pertinent roles for microRNAs and circadian rhythms have been reported in cartilage homeostasis and OA pathogenesis, though interplay between the two has yet to be explored. Here, we have evaluated circadian regulation of two cartilage miRNAs in SW1353 chondrocytes: hsa-miR-140 and hsa-miR-455. miR-140 is highly expressed in chondrocytes(246). Both candidates have previously been shown to regulate expression of cartilage genes and are deregulated in OA. Therefore, understanding their temporal regulation would be physiologically relevant.

Mature miR-140-3p is most abundant miRNA in human cartilage and miR-455-3p expression is greater than miR-455-5p (246). Figure 3.10 confirms these findings in-vitro. Here miR-140-3p had the greatest average expression across the time series (N=39) comparative to miR-455 and abundance of miR-455-3p was greater than the 5p arm (P=0.04). These relationships persisted in non-synchronised control (Appendix Fig 2.3). As shown in figure 3.11 C and D, miR-140-3p showed circadian expression, peaking at CT16 comparative to CT0 (FC=5.7). Indeed, abundance at CT16 passed both formal tests of rhythmicity and considering the goodness of fit statistic (R<sup>2</sup>=0.8), we can assume miR-140-3p transcription is temporally regulated in chondrocytes with a ~24hour period. Concomitantly, rhythmicity was not observed in either arm of miR-455 and, no significant differences were observed between CT0 and CT12 (Fig 3.12 C-D). In the interval between CT0 and CT12, miR-455-3p abundance decreased (CT4 FC=0.2, CT8 FC=0.1) whereas miR-455-5p increased (CT4 FC=1.6, CT8 FC=2) likely indicating divergent functions between both arms in chondrocytes.

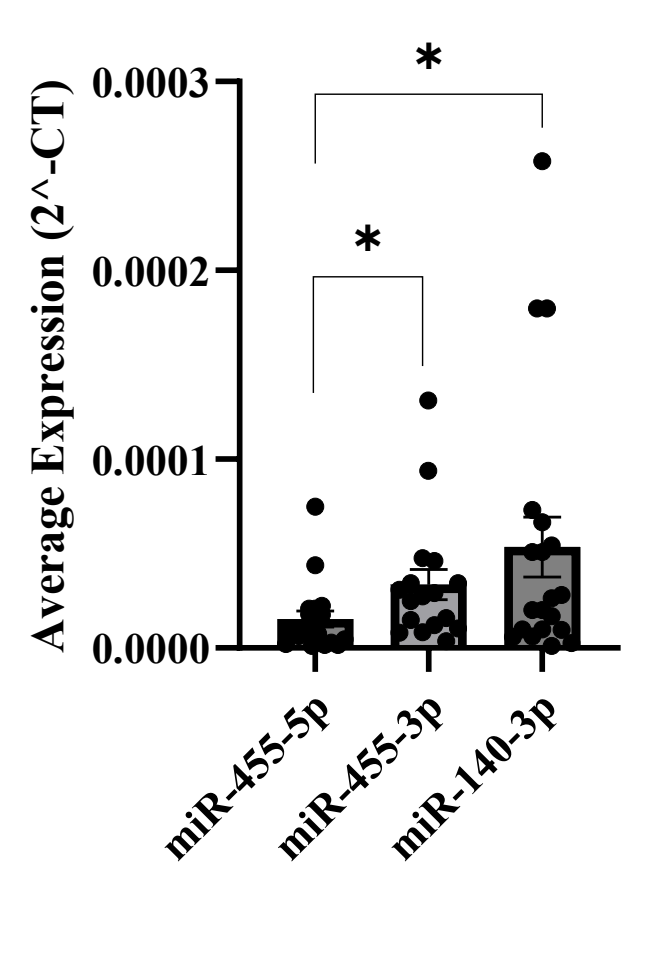


Figure 3. 10 Average abundance of miR-140 and miR-455 in SW1353 chondrosarcoma cells.

Average expression of microRNAs in SW1353 cells synchronized in dexamethasone and vehicle control over a 48hours. Expression of hsa-miR-455-3p, hsa-miR-455-5p and hsa-miR-140-3p was determined by RT-qPCR, normalized to GAPDH housekeeper gene. Data presented as mean  $\pm$ -SD, Difference determined by multiple comparisons test P<0.05, \*\*P<0.01\*\*\*\* p < 0.001.(N=39)

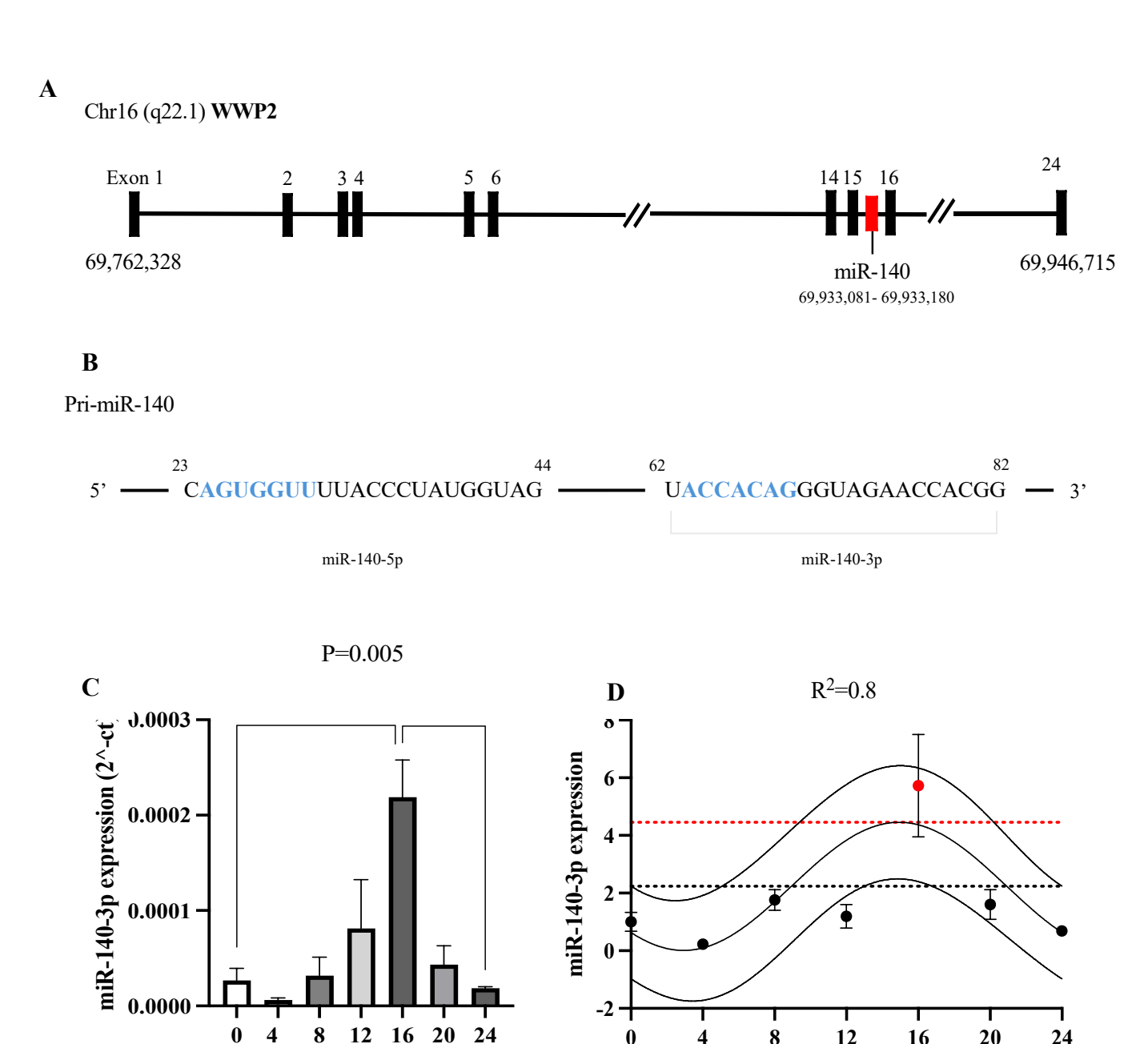


Figure 3. 11 Time dependent expression of miR-140-3p.

8

**Circadian Time (hours)** 

(A) miR-140 is located on chromosome 16 in the 15th in intron of the WWP2 gene. (B) sequences of miR-140-5p and miR-140-3p, blue nucleotides represent 7-mer miRNA seed sequences. (C) Absence of oscillation were determined by one-way ANOVA with Tukeys posthoc test (data presented as mean +/- SD(N=3)). Time dependent expression of mature miR-140-3p in SW1353 chondrocytes was evaluated by (D) cosinor analysis. Red data points indicate amplitudes significantly greater than MESOR. Red line and black line depict predicted amplitude and MESOR respectively Data presented relative to circadian time 0 mean +/- SD, N=3 Biological replicates per time point. Statistical significance between groups represented as \*p<0.05 \*\*P<0.005 \*\*\*P<0.001.

0

4

12

**Circadian Time (hours)** 

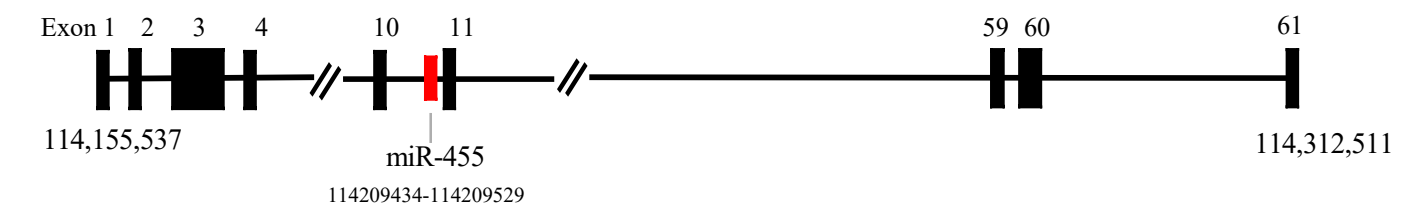
16

**20** 

24

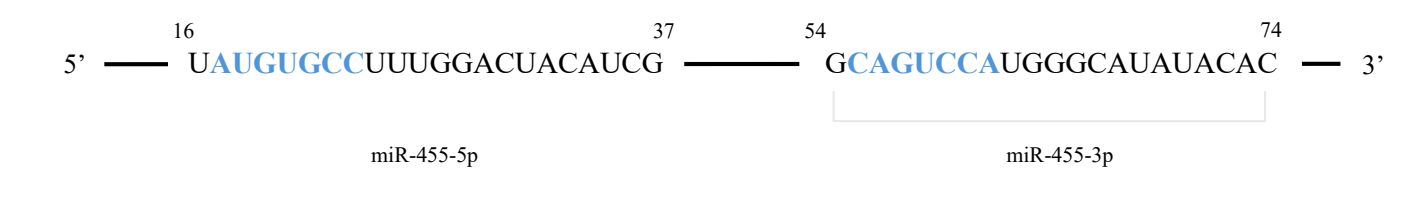
### A

# Chr9 (q32) COL27A1



B

Pri-miR-455



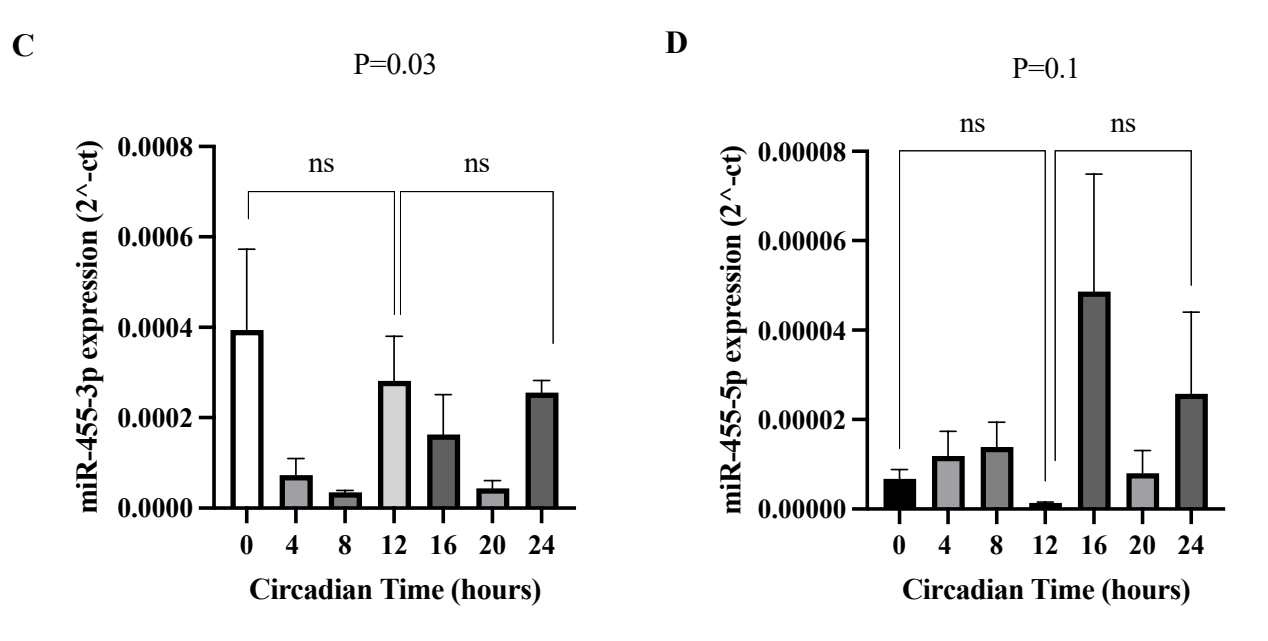


Figure 3. 12 Time dependent expression of miR-455-3p and miR-455-5p.

(A) miR-455 is located on chromosome 9 in the  $10^{th}$  in intron of the *COL27A1* gene. (B) sequences of miR-455-5p and miR-455-3p, blue nucleotides represent 7-mer miRNA seed sequences. (C,D) Absence of oscillation were determined by one-way ANOVA with Tukeys post-hoc test (data presented as mean +/- SD(N=3). Statistical significance between groups represented as \*p<0.05 \*\*P<0.005 \*\*\*P<0.001.

## 3.3.7 Exploring regulatory mechanisms of circadian miRNA expression

RNA interference genes, *DROSHA* and *DICER1* are critical in miRNA processing. Mature miR-140 is derived from an intron-retained transcript and is co-expressed with its host gene, *WWP2*. Expression of pre-miR-140 and *WWP2* is directly induced by the SOX9 transcription factor (199). To understand the mechanisms behind miR-140-3p rhythmicity, expression dynamics were compared to those of *DROSHA*, *DICER1*, *WWP2* and *SOX9*.

In -vivo, diurnal expression patterns in the expression of Dicer1 are observed in the SCN, liver, retina, and bone marrow of mice. 24hour rhythmicity was not observed in our chondrocyte model in either *DICER1* or *DROSHA* abundance (Fig 3.13) and dexamethasone synchronisation had no effect on average expression (Appendix Fig 2.4); supporting the tissue specificity of the circadian interactome. In murine xiphoid cartilage, *Sox9* is rhythmically expressed whilst *Wwp2* is not temporally regulated at the mRNA or protein level (237). These findings were conserved in human chondrocytes. Here, *SOX9* was rhythmically expressed and oscillated in antiphase to miR-140-3p; with *SOX9* peaking 12 hours prior to miR-140-3p at CT4 (Fig 3.14). This suggests oscillation of miR-140 is likely not an effect of rhythmicity in upstream regulators of biosynthesis or its expression and, rhythmicity is likely directly regulated by clock transcription factors.

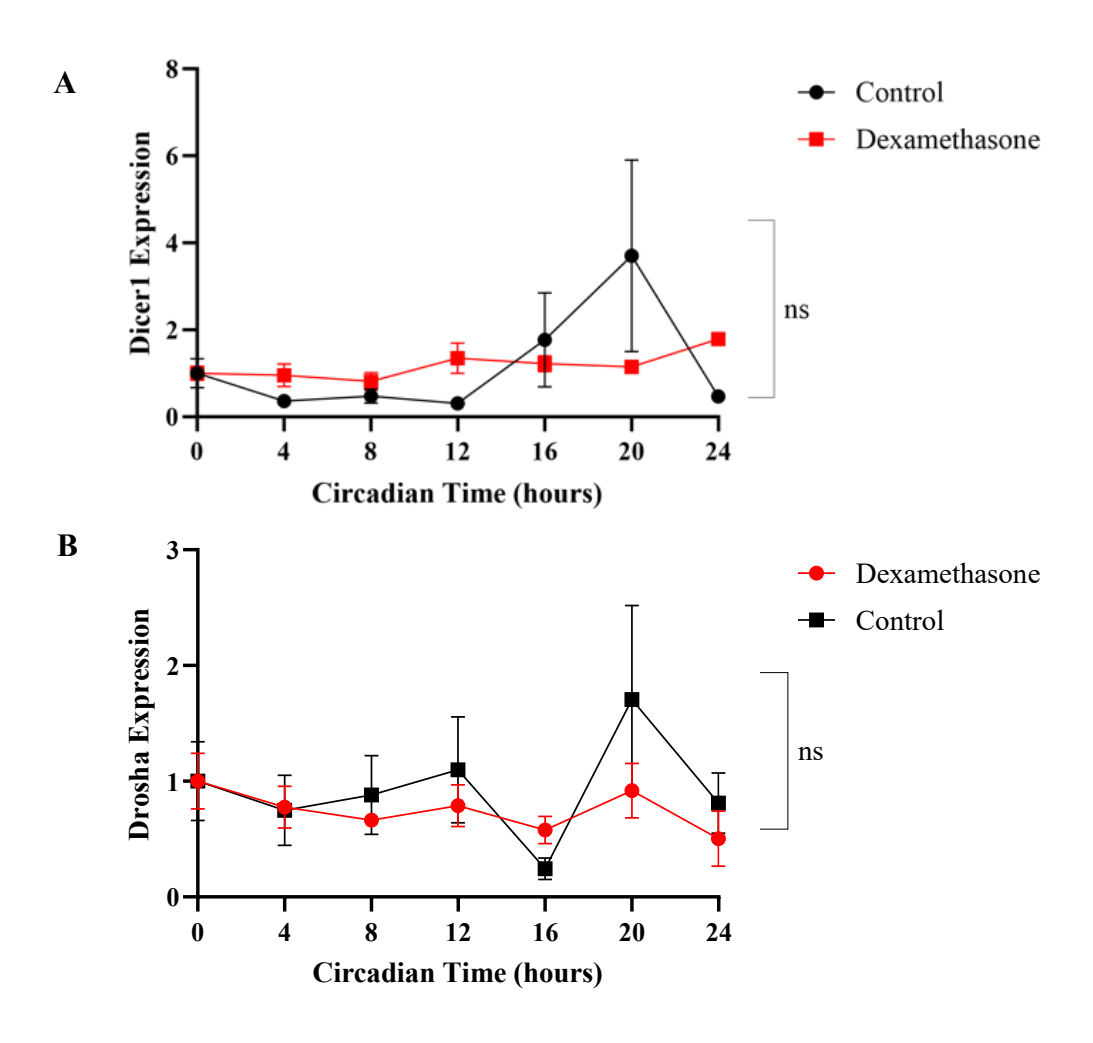


Figure 3. 13 Diurnal expression of *DICER1* and *DROSHA* in SW1353 chondrocytes.

Time dependent expression of miRNA biogenesis enzymes (A) *DICER1* and (B) *DROSHA* in SW1353 cells synchronized in dexamethasone and vehicle control over a 48hours. Expression normalized to *GAPDH* housekeeper gene. Data presented as mean +/- SD, Difference determined by two-way ANOVA. NS, P>0.05 (N=3).

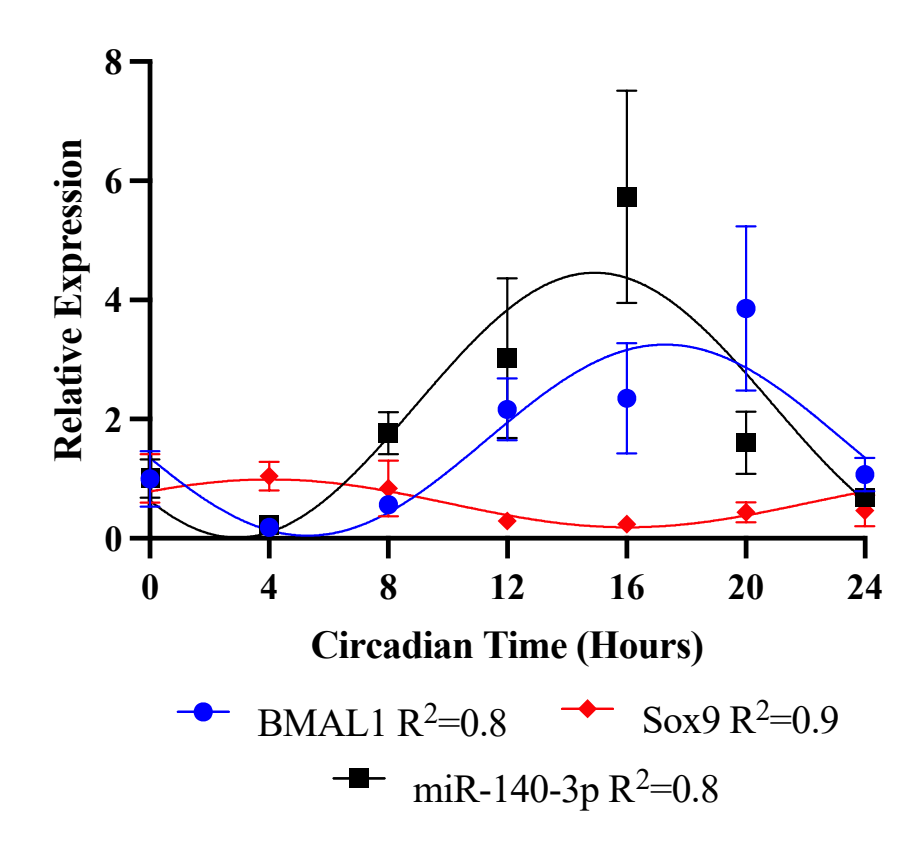


Figure 3. 14 Phase relationships of *BMAL1*, *SOX9* and miR-140-3p transcripts in SW1353 chondrocytes.

Expression of *BMAL1*, *SOX9* and miR-140-3p was determined by RT-qPCR, normalized to *GAPDH* housekeeper gene. Data fitted with a cosinor curve by cosinor analysis, presented as mean +/- SD.

# 3.3.8 Evaluating the utility of the 'rest-phase' in the SW1353 circadian time series protocol

It is common practice to 'rest' cells for a full circadian cycle following phase resetting to allow gene expression to equilibrate. Given that the viability of SW1353 cells decreases in the second circadian cycle of our model, we explored the possibility of removing the rest-phase and commencing circadian harvests immediately after synchronisation (Fig 3.15). In this section the 'rest-phase' is annotated as 24A. In the 50% (v/v) FCS group, oscillation of BMAL1 mRNA failed all formal tests of rhythmicity (Appendix 1.4). Synchronisation was deemed unsuccessful, and no further analysis was performed on these samples.

As shown by Figure 3.16 A, expression of *GAPDH* housekeeper gene in dexamethasone groups were unstable comparative to our early investigations. Though differences between 12-hour time bins were not significant (ANOVA, P=0.4) all results are interpreted without normalisation. Figure 3.16 B depicts robust oscillation of *BMAL1* mRNA within both circadian cycles of the time series. In 24a and 24b, the amplitude was significantly greater than the MESOR peaking at CT16 and CT36, respectively. Goodness of fit for both models was also comparable (24a R<sup>2</sup>=0.9, 24b R<sup>2</sup>=0.8), suggesting core clock genes oscillate robustly in the rest-phase period. To ensure these observations are not artificial fluctuations induced by exposure to dexamethasone, abundance of clock transcripts (BMAL1), cartilage ECM genes (MMP13), chondrocyte phenotype genes (SOX9) and miRNAs of interest (hsa-miR-455-3p) were compared to PRE synchronisation control. For all transcripts, no significant differences between PRE and CT0 were found (Figure 3.17). Notably, the abundance of *BMAL1* and *SOX9* is greater at CT12 comparative to PRE, though this likely reflect regulation by the chondrocyte clock. Therefore, dexamethasone had negligible effects on genes that regulate circadian rhythms, ECM, and chondrocyte phenotype. However, investigations towards circadian regulation of miRNA were not conducted in these samples, given we were unable to normalise these data sets.

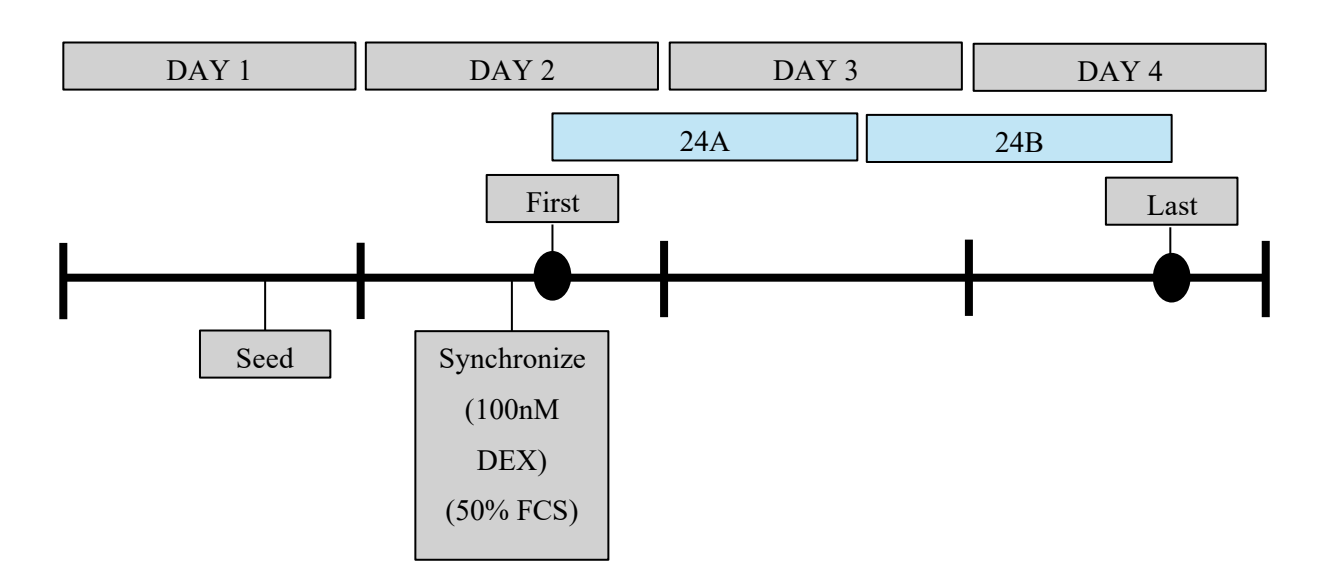


Figure 3. 15 Revised model for the detection of circadian microRNAs in cartilage *in-vitro*.

SW1353 chondrosarcoma cells were seeded in a 6-well plate prior to phase resetting in dexamethasone or 50% FCS. After synchronisation, cells were placed in low serum (DMEM+0.5% FCS) before RNA extraction every 4 hours for 48hours. The first harvest is designated circadian time 0.

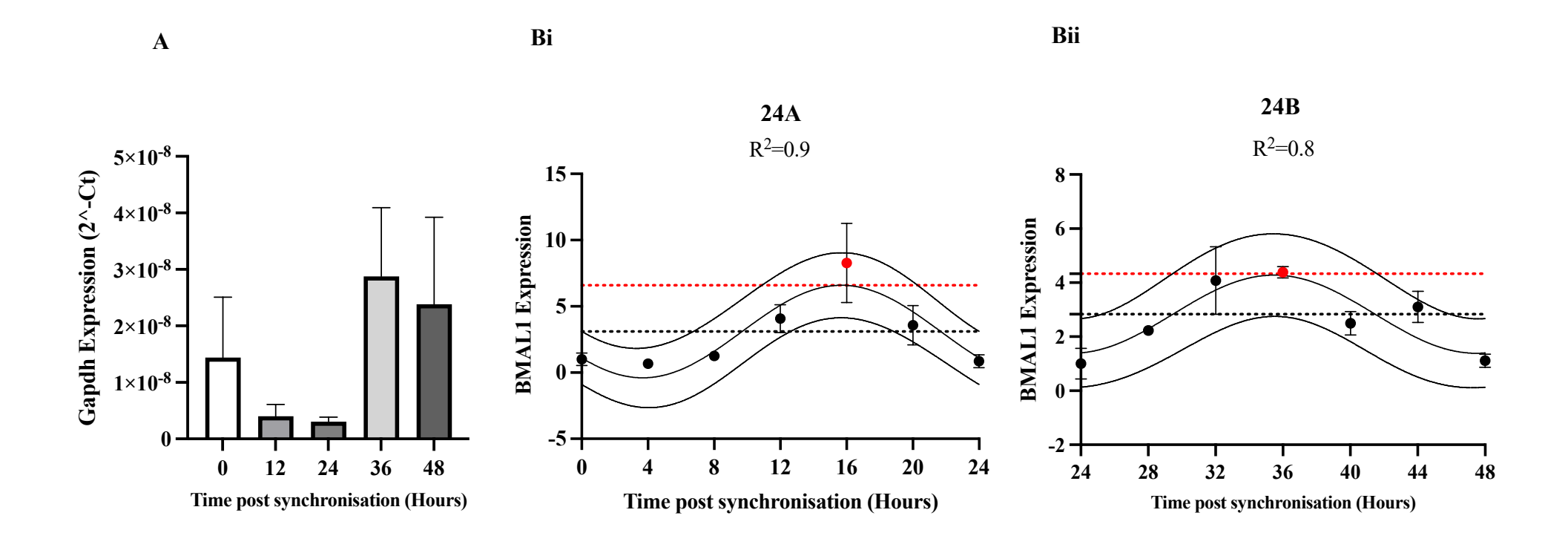


Figure 3. 16 Oscillation of BMAL1 mRNA in the rest phase of circadian protocol.

SW1353 chondrosarcoma cells were synchronised in 100nM dexamethasone and time dependent abundance of (A) *GAPDH* and (B) *BMAL1* was measured every 4hours/48hours post synchronisation. Oscillation in BMAL1 abundance in 24A (Bi) and 24B (Bii) evaluated by cosinor analysis. Red data points indicate amplitudes significantly greater than MESOR. Red line and black line depict predicted amplitude and MESOR respectively Data presented relative to circadian time 0 mean +/- SD, N=3.

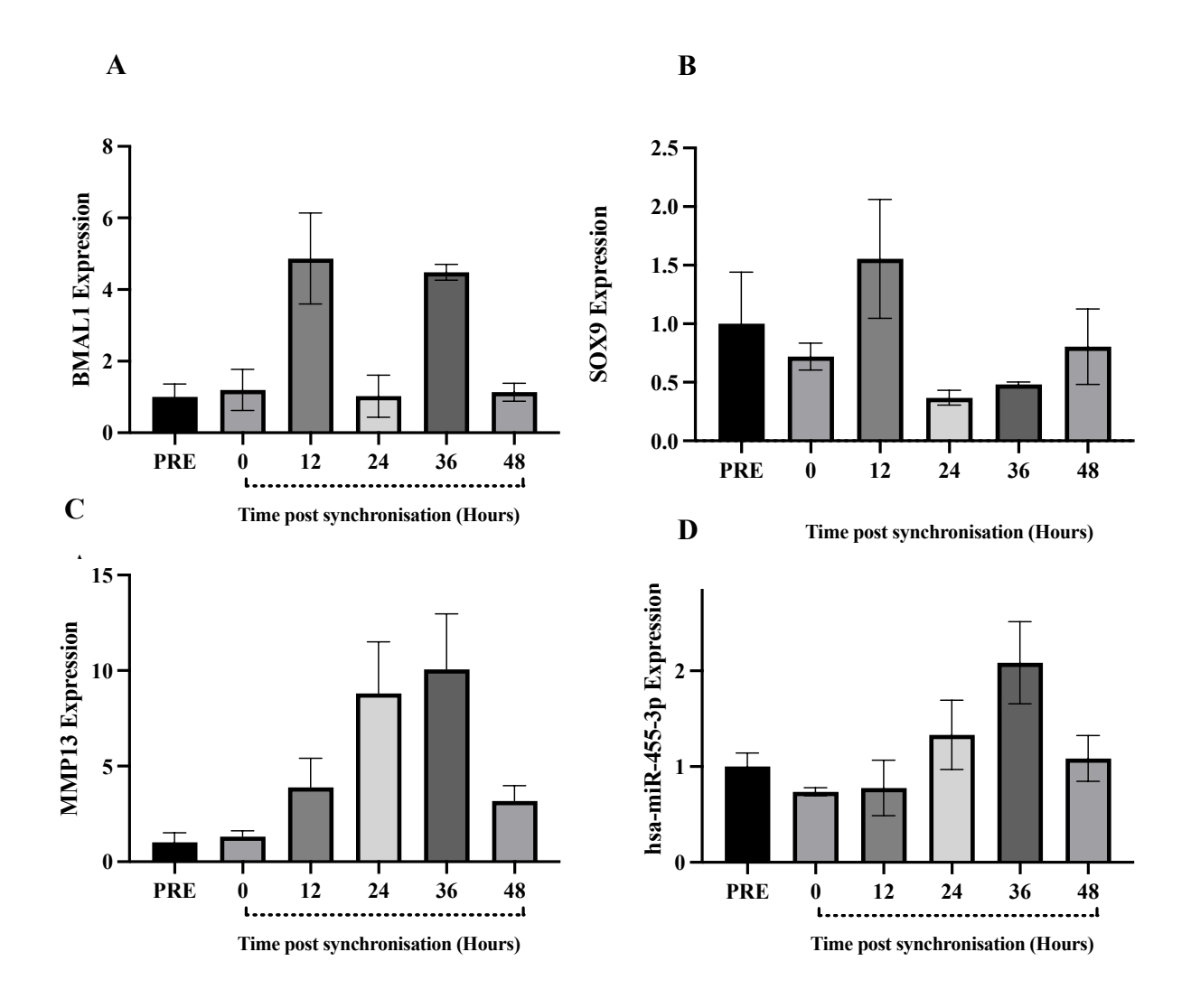


Figure 3. 17 Determining immediate effects of dexamethasone on cartilage gene expression.

SW1353 chondrosarcoma cells were synchronised in 100nM dexamethasone and time dependent abundance of (A) *BMAL1* (B) *MMP13* (C) *SOX9* (D) hsa-miR-455-3p measured every 12hours for 48 hours. Statistical difference determined by students t-test. Data presented relative to PRE synchronisation control. Presented as mean +/- SD. (N=3)

### 3.4 Discussion

The aim of this chapter has been to devise an *in-vitro* model for the detection of oscillating miRNAs in AC. As discussed, regulation of gene expression by the circadian clock and microRNAs is implicated in AC development, homeostasis, and OA pathology. However, whilst the rhythmic expression of microRNAs has been observed in the central oscillator of mice, interplay between these factors has yet to be explored in cartilage (247).

This study provides preliminary evidence that regulation of miRNA expression is an additional output function of the chondrocyte molecular clock. Thus, identifying an additional pathological mechanism by which circadian dysfunction contributes to OA pathogenesis. Here, miR-140-3p oscillated robustly in SW1353 cells synchronised in dexamethasone and, expression was greatest within the mammalian 'subjective day' (i.e. CT12). miR-140-3p is a direct regulator of catabolic factors in AC (*MMP-13*, *ADAMTS5*, *SOX9*, *SMAD3*, *IL1B*) and, therefore we speculate its circadian production may aid segregation of ECM turnover to periods of non-activity(194,200,219). However, this is largely dependent upon the miR-140 half-life and, the sensitivity of the chondrocyte transcriptome to repression by miR-140.

Given this, understanding the mechanisms responsible for circadian regulation of miR-140-3p is relevant. Previously, oscillation in *Dicer1* has been reported in comparable time-series models in the mouse SCN and liver; suggesting rhythmicity is induced during miRNA biogenesis(192). Concomitantly, abundance of *DICER1* and *DROSHA* were not transcriptionally regulated by the circadian clock in this model, as shown by no significant changes in temporal and globalised expression following phase-resetting. Further, the abundance of neither miR-455-3p or miR-455-5p passed tests for rhythmicity. Thus, oscillation of miR-140-3p is not a reflection of rhythmic processing and, circadian regulation of *Dicer1* is likely not conserved between man and mouse. Notably, statistical models utilised here assume the rate of transcription and degradation of oscillating components are comparable, thus conform to a cosine curve. However, given that half-lives of guide miRNAs is highly variable (i.e. 4hours - >24hours in mammalian cells), the detection power of this model is likely low, and a non-parametric model may be more applicable in analysis of larger data-sets(248).

In light of this, the rhythmic accumulation of *SOX9* was determined, given primary transcripts of miR-140 are directly induced by SOX9 binding to the intron 10 of the *wwp2* gene(197). In

agreement with Vágó *et al* (249), *SOX9* was regulated by the chondrocyte clock though, oscillated in antiphase to miR-140-3p. To add, daily rhythmicity in the abundance of SOX9 was not identified in a time-series proteomics model in mouse hip AC; suggesting *Sox9* oscillation is not imparted on its miRNA targets(132). Further, rhythmicity was not identified in accumulation of *WWP2* transcripts in agreement with previous in-vivo models (237). Therefore, we propose that miR-140 oscillation may be regulated at an independent promoter to that of WWP2 in chondrocytes.

Predominantly, oscillation of circadian mRNAs is driven directly by the periodic binding of core clock genes within E-box or RORE sequences in their promotors(250). Recently, studies have extended this model include regulation of miRNAs *in-vitro*. For instance, abundance of miR-17-5p is regulated by CLOCK in human fibroblasts and, Rev-Erbα regulated miR-122 expression in mouse hepatocytes (171,181) . Here, a phase delay was observed between the peak abundance of miR-140-3p and *BMAL1*, whereas *CRY1* and *CRY2* expression peaked 4 hours prior. This indicates that transcriptional activity of miR-140 may be regulated by mechanisms of the negative limb transcription factors. For instance, CRY1 directly interacts with several nuclear receptors in mammals, including steroid hormone and vitamin D receptors. Concomitantly, vitamin D receptor has been shown to regulate miR-140 expression during bone development, though confirming this mechanism in chondrocytes would require additional research(251,252).

Notably, several limitations were incurred in this chapter and, areas of optimisation have been explored. Initially, this study aimed to quantify miRNAs expression over two circadian cycles using two different phase-resetting stimuli (i.e. serum shock and dexamethasone). In our hands, serum shock was an in-effective method, likely due to a low-quality FCS batch. Dexamethasone was effective, though cell synchronicity was not maintained in the second cycle. This was determined to an effect of decreased viability of SW1353 as a factor of time. To this end, the feasibility of excluding the 'rest-phase' was explored by commencing RNA extraction immediately after synchronisation. Historically, rest-phases are recommended to enable coupling of population clocks and equilibration of gene expression. Concomitantly, no immediate effects on the transcription of key circadian and AC genes was identified and, robust oscillation in *BMAL1* is detectable. Importantly, anomalous expression of our HKG was detected in this model, highlights a broader issue with reproducibility in circadian cell models.

Therefore, replicating this model on a larger scale *in-vivo* whereby tissues are under the stable entrainment of a strong synchronising agent (i.e. the light/dark cycle) would be beneficial.

## Chapter 4: Regulation of the chondrocyte circadian clock by hsa-miR-455

### 4.1 Introduction

Degeneration of cartilage is a key pathology of OA, characterised by increased catabolic signalling leading to the degradation of matrix macromolecules. This process is largely irreversible and therefore, understanding the mechanisms involved is of value. The molecular clock and miRNAs are prominent regulators of chondrocyte gene expression; and have been dually associated with AC degeneration in OA. For instance, ablation of miR-455 in chondrocyte disrupted homeostasis resulting in OA-like damage in mice. Significantly, overexpression of miR-455-3p and miR-455-5p protected mice form AC degeneration; posing miRNAs as a novel therapeutic agent for OA(238). Understanding these observations on a molecular level has been aided by advances in luminescence-based technologies; enabling us to identify direct targets microRNAs. Indeed, seed sites within the 3'UTR of modulators of chondrocyte phenotype (Col2a1, Sirt1, Sox9, Hdac2, Hdac8) and inflammation (PKA2, HIF- $2\alpha$ ) have been validated as direct targets of miR-455(198,238,253,254). Similarly, globalised expression of BMAL1 is decreased in human OA chondrocytes and ECM degradation and lesion development is observed in cartilage-specific BMAL1 KO mice(126,255). Given this, exploring the extent of the circadian regulation in AC and, the intrinsic regulators of the chondrocyte clock is of value. In chapter 3, the reach of the cartilage circadian interactome was extended to include the temporal regulation of microRNA abundance and here, we propose that miRNAs regulate the chondrocyte clock at a post-transcriptional level.

# **4.2** Aims

- Identify putative targets of miR-455-3p and miR-455-5p in existing RNA-seq data sets and in-silico models
- Evaluate direct regulation of the chondrocyte circadian clock by miR-455-3p and miR-455-5p by luciferase assay,

### 4.3 Results

## 4.3.1 Exploring expression of core clock genes in-vivo and in-vitro miR-455 data sets

Deregulated expression of miR-455 and circadian genes is a hallmark of OA. To capture the extent of miR-455-mediated regulation, abundance of circadian genes was quantified in three existing RNA-sequencing (RNA-seq) data sets: 'miR-455 knockout Vs wild-type cartilage 'and 'SW1353 chondrosarcomas + miR-455-3p mimic or miR-455-3p inhibitor'. Notably, neither models were optimised for the detection of oscillating transcripts. For instance, microdissection of WT and KO mouse cartilage was not isolated to the same circadian time and, SW1353 cultures were not synchronised prior to RNA extraction.

The miR-455 null mouse was created by Dr.Tracey Swingler in the Clark Lab at UEA using the CRISPR Cas (Clustered Regularly interspaced short Palindromic Repeats) genome editing technique(256). For mRNA-seq, RNA was extracted and from the knee AC of 3-month-old WT and KO mice (N=3, 6 knee joints in total). Here, circadian genes of the positive limb (*Clock, Bmal1, Npas2*), negative limb (*Per, Cry*) and auxiliary limbs (*RORα, NR1D1, DBP, HLF, CSNK1E*) were detected but no significant difference in expression were observed in the absence of miR-455-3p and miR-455-5p (table 4.1 A). Notably, abundance of several clock genes had an upward trend including; *Clock* (FC=1.3), *Cry1* (FC=1.2), *Per1* (FC=1.8), *Per2* (FC=1.3) and *Hlf* (FC=1.2)

Comparable findings were observed in mRNA-seq data from the SW1353 miR-455-3P overexpression and inhibitor models (N=6). Here, SW1353 chondrosarcomas were transfected with 50nM of miR-455-3p mimic or inhibitor or respective control for 48hours prior to RNA harvest. Table 4.1B&C, indicates that the abundance of *BMAL1* and *DBP* significantly increased following overexpression though an upward trend was also observed following inhibition. Similarly, *PER1* and *NR1D1* was significantly lower following miR-455-3p overexpression while increased expression of *NR1D1* and *PER1* following miR-455 inhibition was not observed. Often genes are regulated by multiple miRNAs. Thus, absence or overexpression of a single miRNA likely does not affect the overall expression of a single target gene to the level of significance. Further, given that the phase resetting was not included in this model, we propose that gene expression analysis of this nature is insufficient in capturing miRNA-mediated circadian gene expression and a more specific targeted approach is required.

		IN-	VIVO	IN-VITRO							
Gene	A miR-455 KO vs v			В	SW1353+		С	SW1353+			
name					miR-455 mimic		C	miR-455 i	nhibitor		
		FC	P.VAL		FC	P.VAL		FC	P.VAL		
CLOCK	1.3		0.105	1.2		0.284	0.9		0.232		
ARNTL	0.9		0.352	1.6		0.004	1.2		0.206		
PER1	1.8		0.202	0.6		0.017	0.8		0.231		
PER2	1.3		0.210	1.0		0.928	0.6		0.067		
PER3	0.9		0.376	0.9		0.316	0.8		0.019		
CRY1	1.2		0.196	1.2		0.200	0.9		0.373		
CRY2	1.1		0.689	0.8		0.203	0.8		0.207		
NPAS2	0.7		0.858	1.0		0.771	1.0		0.701		
NR1D1	1.1		0.814	0.7		0.000	1.0		0.983		
RORα	1.1		0.701	0.8		0.439	0.9		0.748		
DBP	1.1		0.749	1.1		0.046	1.1		0.802		
CSNK1E	1.1		0.582	1.1		0.916	1.0		0.530		

Table 4. 1 Circadian clock genes abundance in miR-455 RNA seq datasets.

Summarises expression of core clock genes in RNA-seq data from (A) WT and miR-455 KO mouse knee cartilage (N=3), (B) SW1353 chondrosarcomas + miR-455 mimic (N=6) and (C) SW1353 chondrosarcomas + miR-455 inhibitor (N=6). Fold change determined relative to control. Significant difference determined by Students T-test.

## 4.3.2 Identification of miR-455-3p and miR-455-5p predicted targets

Two methods were used to identify putative targets of both miR-455-3p and miR-455-5p including miRabel target prediction software (bioinfo.univ-rouen.fr/mirabel/) and by manually identifying 6mer sequences in the 3'UTR of circadian genes (miR-455-3p (GGACTG) miR-455-5p (GCACAT)). Results are summarised in table 4.2.

miRabel aggregates the target prediction results from miRanda, PITA, TargetScan and SVmicrO databases to generate a miRabel score which indicates the significance of the proposed interaction with a recommended threshold of  $\leq$  0.05. Comparatively, miR-455-3p had a greater number of predicted targets genes (Total entries= miR-455-3p (10,494), miR-455-5p (7304)), though, only 13 and 11 of these predictions were below the threshold for miR-455-3p and mir-455-5p respectively. BMAL1,CLOCK, PER2, CRY2, RORa, CSKN1E and NPAS2 were predicted miR-455-3p targets, though no significant miRabel scores were identified. Similarly, BMAL1, CLOCK, RORa, CSNK1E and NPAS2 were predicted targets of miR-455-5p alongside PER3 and HLF – though not significant. In contrast, at least 1 seed site was manually identified in the 3'UTR of 11 and 6 circadian transcripts for mir-455-3p and miR-455-5p, respectively. Discrepancies were observed in frequency of seed sites in the 3'UTR of clock genes. For instance, multiple miR-455-3p seed sites were identified in PER1, CSKN1E, DBP and DEC2; suggesting differing roles for miR-455-3p and miR-455-5p modulating the circadian clock, despite being derived from the same pri-miRNA.

	Hs	a-miR-455-3p		Hsa-miR-455-5p				
Gene	miRabel	Algorithm	6mer	miRabel	Algorithm	6mer		
	score	riigoriumi	seeds	score	riigoriumi	seeds		
CLOCK	0.30	P, M,T	9	0.56	P,M	11		
BMAL1	0.83	M,T		0.96	M			
PER1			1					
PER2	0.49	P, M, T	7			1		
PER3			2	0.33	P,M,T	2		
CRY1						1		
CRY2	0.41	P, M , T	8			2		
NR1D1								
RORa	0.84	M, T	5	0.95	P,M	2		
CSNK1E	0.97	M	2	0.89	M,T			
DBP			2					
HLF			3	0.99	P			
NPAS2	0.59	P, M T	2	0.99	P			
DEC2			3					

Table 4. 2 Predicted circadian targets of miR-455-3p and miR-455-5p.

MiRanda (M) PITA (P) TargetScan (T).

## 4.3.3 miRNA-455-3p and miRNA-455-5p directly target the circadian clock

Several core clock genes contain ≥1 seed sites for miR-455-3p and/or miR-455-5p. To investigate whether miR-455 directly regulates circadian clock genes, a dual-GLO luciferase assay system was used. Here, wild-type (WT) plasmids were constructed by cloning regions of the 3'UTR hosting miRNA seeds into the pmirGLO reporter plasmid. Recombinant plasmids were obtained by *E.coli* transformation and, transiently transfected into either SW1353 human chondrosarcoma or DF1 chicken fibroblast cells with 50nM miRNA mimic or non-targeting miRNA mimic for 48hours. Direct targets are identified by a significant reduction in luciferase activity in WT comparative to control, followed by mutagenesis of the seed site to negate function and validate specificity.

For miR-455-5p assays, regions of CLOCK, PER2, PER3, CRY1, CRY2 and RORα 3'UTR's where cloned downstream of the firefly luciferase in pmirGLO plasmids by SacI and Xho1 restriction sites. In cases where seeds within the 3'UTR spanned >1000bp, separate constructs were generated. For instance, Clock A plasmid hosts 2 6mer seed sites at positions 4148-4155 and 4730-4736 in the 3'UTR, whilst Clock B hosts 1 seed at location 5729-5725 (Fig 4.1A). With the exception of CRYI constructs, recombinant plasmids were verified by Sanger sequencing. In DF1 cells, miR-455-5p overexpression significantly reduced luciferase expression for CLOCK A, CLOCK B, RORa A, PER2, CRY2 A, CRY2 B (Figure 4.1B). Luciferase expression was not reduced in *PER3* or in the  $ROR\alpha$  B assay (Appendix Figure 3.1); suggesting miR-455-5p regulates  $ROR\alpha$  translation by directly targeting the seed regions within RORA A (location 5519-5525 in the UTR). Notably, this model was replicated in the SW1353 cell line though, no significant changes in luciferase activity were observed. Indeed, endogenous expression of miR-455 is high in human chondrocytes and transfection protocol in this model was likely ineffective against background expression of miR-455. Thus, luciferase experiments were performed in the DF1 fibroblast cell line. Here limitations of endogenous 455 expression are ameliorated given a single base-pair difference between ggamiR-455-5p and hsa-miR-455-5p.

To confirm specific targeting of the seed sites by the miR-455-5p mimic in the DF1 model, target site(s) were mutated using the QuickChange Multi-site mutagenesis kit. Here, seeds are converted into either BamHI (GGATCC) or Nhell (GCTAGC) restriction sites and validated by restriction digest and sequencing. Mutagenesis of miR-455-5p seeds in the 3'UTR of *PER2*,

*ROR*α A, *CRY2* A and *CRY2* B rescued the suppression of luciferase activity in DF1's by miR-455-5p mimic. This demonstrates that the miR-455-5p specifically binds to the 6mer sequence in the 3'UTR, validating the predicted target sites as miR-455-5p activation sites. For *CLOCK*, conversion of the second seed of *CLOCK* A was unsuccessful and, transformation of E.coli with *CLOCK* B mutant constructs was ineffective. Though, as shown, mutation of the first seed was sufficient rescue the effects of miR-455-5p. Therefore, we suggest that the miR-455-5p seed sequence (GCACAT) exerted function in the 3'UTR of Clock by binding with the 6mer sequence at position 4148-4155 in the 3'UTR.

For miR-455-3p assays, WT plasmids were constructed for *CLOCK* B, *NPAS2*, *PER1*, *PER2* A, *PER3*, *CRY2*, *RORA* A, *RORA* B and *HLF*. Figure 4.2 A-D indicates that the overexpression of miR-455-3p in DF1s significantly reduced luciferase activity in *PER1* and *NPAS2* assays; with repression being greatest in the *PER1* 3'UTR (FC=0.5+/-0.04). Conversion of 6mer seeds within the *NPAS2* WT into a BAMHI rescued repression of luciferase activity, indicating miR-455-3p regulates *NPAS2* expression by directly targeting the 6mer seed site at position 412-417 in the 3'UTR. Luciferase expression was greater in *PER1* mutant's comparative to the WT plasmids; but not to the level of significance. As shown in figure 4.2 D, luciferase activity in *CLOCK* B, *PER1*, *RORA* A assays was reduced by miR-455-3p overexpression. However, mutagenesis assays for both constructs was unsuccessful and require repetition in order to determine if repression is specific to the miR-455-3p seed site.

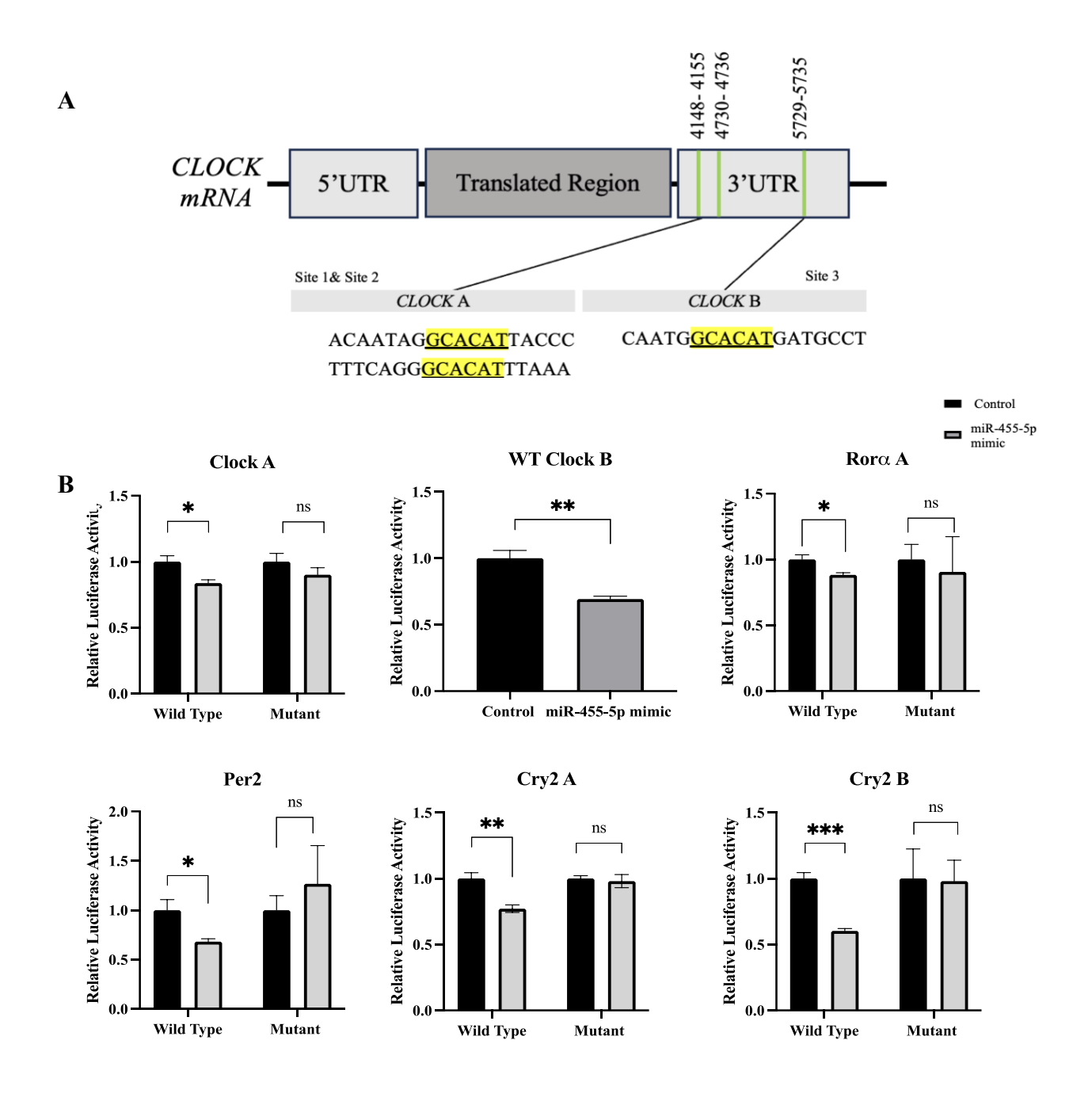


Figure 4. 1 Identifying miR-455-5p clock targets by dual-glo luciferase assay.

Dual-luciferase reporter assays were performed to assess interaction of hsa-miR-455-5p and targeting sequences in the 3'UTR of circadian gene mRNA. (A) Schematic of circadian pmirGLO reporter plasmids containing sections of the 3'UTR with predicted miR-455-5p seed sites. (B) Wild-type and mutant clock gene 3'UTR reporter plasmids were transfected into DF1 cells with miR-455-5p or negative control for 48hours. Relative luciferase activity was normalised to Renilla luciferase. Results presented as miR-455-5p fold change over negative control. Data presented as mean +/ SD(N=5), two-tailed unpaired t-test. \* p < 0.05, \*\* p < 0.01, \*\*\* P<0.005

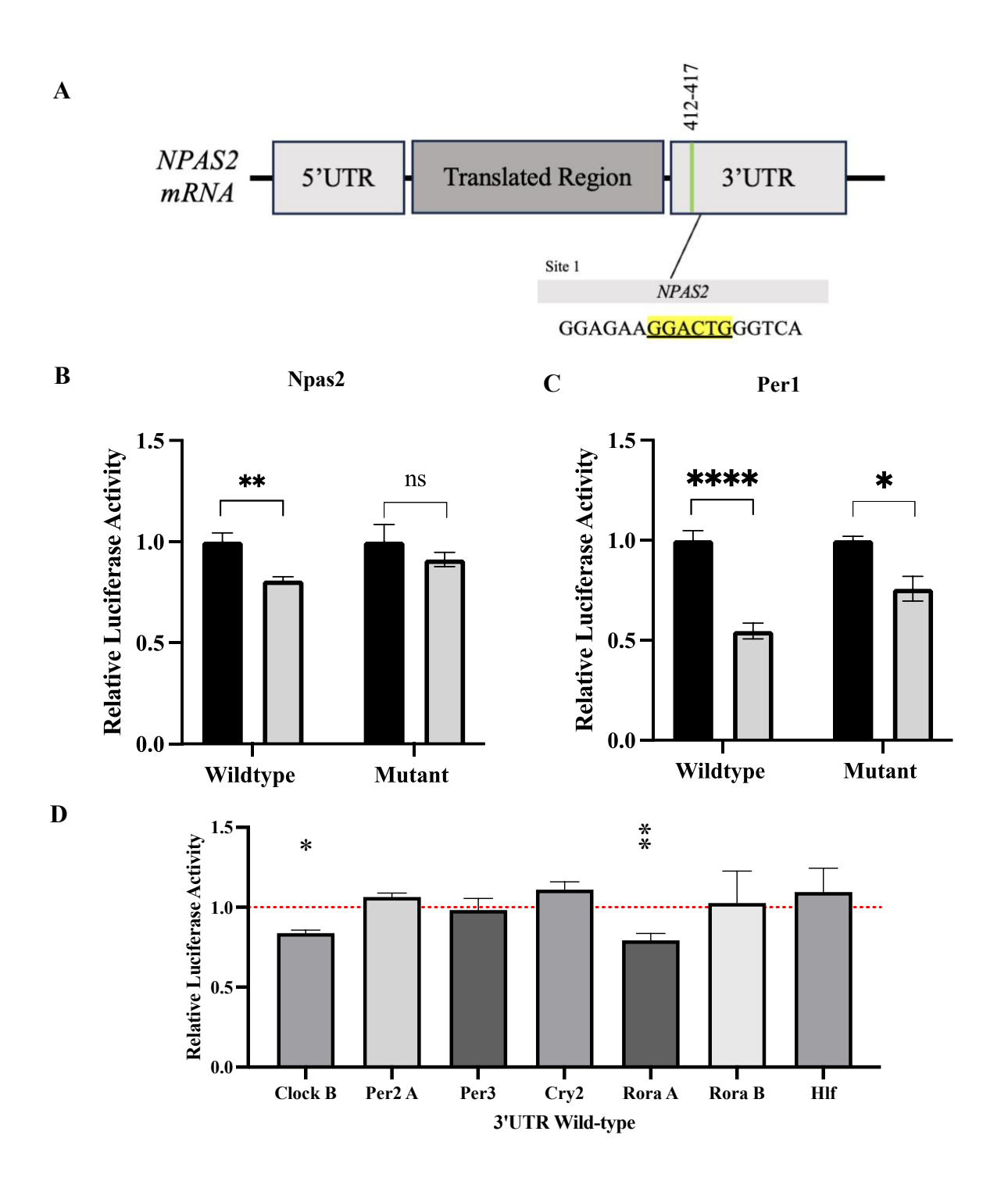


Figure 4. 2 Identifying miR-455-3p clock targets by dual-glo luciferase assay.

Dual-luciferase reporter assays were performed to assess interaction of hsa-miR-455-3p and targeting sequences in the 3'UTR of circadian mRNA. (A) Schematic of circadian pmirGLO reporter plasmids containing sections of the 3'UTR with predicted miR-455-3p seed sites. Direct targeting of predicted seed sites in the 3'UTR plasmids for (B) NPAS2 (C) PER1 validated by BAMHI mutagenesis. (D)Wild-type luciferase assays for CLOCK B, PER2 A, PER3, CRY2, ROR $\alpha$ , ROR $\alpha$  B and HLF 3'UTR reporter plasmids. Relative luciferase activity was normalised to Renilla luciferase. Results presented as miR-455-3p fold change relative to control (red line) \* p < 0.05, \*\* p < 0.01, \*\*\* P<0.005.

#### 4.4 Discussion

Often, individual microRNAs regulate multiple mRNAs, belonging to several pathways. Therefore, their deregulation likely has a profound impact on disease initiation and progression. In a study, 114 DE miRNAs were identified in human OA cartilage and their predicted targets were associated with AC development, cell cycle and collagen fibril organisation(257). Recently, the reach of the miRNA interactome has been extended to include circadian clock genes tissues. For instance, *RORa* was cooperatively regulated by miR-27a-3p, miR-503-5p and miR-183-5p in oral squamous cell carcinoma(188). Alterations in the circadian rhythms of cartilage is an emerging pathology of OA, in part, driven by deregulated expression of clock transcription factors. However, the pathologic mechanism leading to disruption is poorly understood and further exploration is of value in the search for interventions. This chapter aimed to explore posttranscriptional regulation of the chondrocyte clock in the context of microRNA-455. Here, a non-oscillating microRNA was selected to minimise the complexity of our model and preliminary data prior to this study suggested miR-455 may target the circadian machinery(226).

Initially, we explored putative clock targets of miR-455 by quantifying the abundance of circadian transcripts in existing RNA-seq data sets from miR-455 null mouse cartilage(258). Broadly, the absence of miR-455-3p and miR-455-5p had no significant effects on the expression of core clock genes, though increased expression of *Clock, Cry1, Per1, Per2* and *Hlf* was observed. As we understand, miRNAs fine-tune transcription rather than having a major influences on the expression of their target gene. Therefore, we might expect miRNAs aid the circadian clock by regulating the phase of gene oscillation. However, we were unable to quantify the impact of miR-455 deletion on the parameters the chondrocyte clock (i.e. amplitude, phase, period) due to the model's low temporal resolution. Thus, this model was insufficient for accurate prediction of miR-455 targets, particularly in the context of chronobiology.

Similarly, the overexpression of miR-455-3p in SW1353s repressed the expression of NR1D1 though other transcripts of the positive and negative limb were unaffected. Indeed, miR-455-3p is overexpressed in OA and, studies indicated the abundance of NR1D1 is decreased. (258,259)Functionally, 330 DE gene were identified following siRNA knockdown of nr1d1; including BMAL1 and mediators of TGF $\beta$ signalling(259). Further, miR-455-3p directly

regulates the expression of *SIRT1* and *HDAC4(253)*. Significantly, both targets and *NR1D1* are regulators of the core autophagy protein ULK1 and, deregulation of autophagy is a hallmark of ageing and OA(260). However, as this model was unsynchronised we are uncertain of its reliability in identifying oscillating targets of miR-455-3p.

To address mechanism of miR-455 regulation of the clock directly, an *in-silico* target prediction analysis and, dual glo-luciferase assay was utilised. Notably, no circadian targets were identified by prediction softwares MiRanda, PITA, TargetScan. This is likely due to lack of consideration for oscillating clock components in current protocols. Importantly, several putative clock targets of miR-455 were identified by manually searching the 3'UTR though, as shown, not all seed sites were deemed as functional locations for suppression.

The present study validated predicted binding sites of miR-455-3p in the 3'UTR of NPAS2. Downregulation of CLOCK and RORA by miR-455-3p mimic was also observed in our luciferase assay, though mutagenesis of these constructs was unsuccessful. The circadian interactome of mir-455-5p was broader; negatively regulating transcription factors of the positive (CLOCK), negative (CRY2,PER2) and auxiliary (RORA) limbs. These genes form the endogenous circadian clock in chondrocytes and, collectively coordinate the timely expression of cartilage genes (i.e. the circadian transcriptome). We propose that the timely accumulation of core clock proteins is fine-tuned at the post-transcriptional level by action of miR-455 and, miR-455-5p and miR-455-3p have distinct functional differences. Thus, altered expression of miR-455 could have pathological consequences and contribute to circadian dysfunction observed in OA.

As discussed, the expression of 4% of all chondrocyte genes is rhythmic and, *in-vitro*, CLOCK and NPAS2 transcription factors coordinated oscillation of *Col2a1*, *Col10a1* and *Acan* by binding to E-box regions within their promotors(237). In OA, the temporal secretion and breakdown of ECM macromolecules is deregulated and has a known impact on tissue homeostasis and disease progression. Several studies have reported reductions in CLOCK and NPAS2 protein abundance is in human OA cartilage; suggesting a role for post-transcriptional mechanisms(259). Therefore, we propose changes to miR-455 expression observed in OA may contribute to transcriptional dysregulation of positive limb genes. Interestingly, we were unable to replicate this model in our chondrocyte like cell line (SW1353). miR-455 is abundantly expressed in chondrocytes therefore, transfection with 50nM of mimic was likely insufficient

against background expression of miR-455. Future work may explore utility of replicating this model using a miR-455 inhibitor though this was beyond the financial reach of this project.

Our luciferase assays found both CRY2 and PER2 were downregulated by miR-455-5p. In somatic cells, CRY and PER proteins co-repress the transcription of BMAL1 to regulate circadian phase(261). Therefore, through post-transcriptional regulation of CRY and PER, miR-455-5p may play a key role in generating rhythmic accumulation of clock proteins of the positive limb. This hypothesis is in keeping with previous studies. In HeLa and NIH3T3 cells, miR-192/194 regulated the expression of the entire Per gene family and, its overexpression altered circadian periodicity(262). Paralogs of both proteins have distinct functional differences(263,264). *In-vitro*, the phase of circadian genes is reversed in *PER1* KO cells but largely unaffected by the absence of PER2; though PER2 is required by CRY2 to form stable repressive complexes with BMAL1/CLOCK. CRY1 is a potent repressor of BMAL1/CLOCK whilst CRY2 is a stronger modulator of auxiliary loop and homeostatic genes; including Nr1d1, Nr1d2, Dbp and Tef(265). In line with this, CRY2 but not CRY1 staining is decreased in human OA cartilage and, disease severity was greater in Cry2 vs Cry1 deficient mice. Therefore, direct regulation of PER2 and CRY2 by miR-455-5p likely influences the chondrocyte circadian transcriptome. Indeed 118 genes were downregulated following over-expression of miR-455 in SW1353 including those enriched for 'collagen-containing ECM' and 'skeletal development'(266).

The transcription factor ROR $\alpha$  directly activates transcription of BMAL1 and NPAS2 mRNA and is involved in generation of oscillation. *In-vitro*, loss of RORA $\alpha$  protein dampened circadian transcription of BMAL1; suggesting regulation at the post-transcriptional level has the capacity to moderate the circadian clock(267). Indeed, this study has shown that 3'UTR of ROR $\alpha$  was negatively regulated by miR-455-5p though, further investigations are required to understand the function of this suppression on the expression of positive limb proteins. It is understood that ROR $\alpha$  also broadly coordinates other metabolic processes in chondrocytes including abundance of proinflammatory mediators IL-6 and STAT3(268). In human OA, ROR $\alpha$  expression was positively correlated with OA severity and, elevated expression of type II collagen and aggrecan is observed following intraarticular injection of siROR $\alpha$ . Given this, it may be suggested that miR-455 exerts a chondroprotective influence through downregulation of ROR $\alpha$  in OA.

To summarise we have identified functional sites of suppression for miR-455 in the 3'UTR of core circadian genes. Despite this, overexpression and knockout models indicate that miR-455 likely does not moderate the globalised expression of these targets, rather, plays a role in fine timing the circadian phase of the clock. Understanding this on a functional level is the next iteration of this work.

Indeed, this study aimed to delineate this by developing a stably overexpressing miR-455 in a circadian reporter chondrocyte cell line (kindly donated by Prof Qing-Jun Meng, University of Manchester) using a third-generation Lenti-viral system. Theoretically, this model would enable the quantification clock gene dynamics without the limitations of transient transfection we observed in the SW1353 model. However, due to limited availability of luminescence machinery we were unable to complete this model within the thesis. Further, the dependency of the chondrocyte clock on miR-455 may be explored *in-vivo* by breeding the miR-455 null mouse generated by the Clark lab onto the PER2::Luciferase reporter mouse background(127); though this was beyond the financial reach of this project.

# Chapter 5: Defining the mouse cartilage miRNAome

#### 5.1 Introduction

Maintaining a balance between anabolic and catabolic pathways is essential for maintenance of homeostasis and therefore, cartilage physiology. In chondrocytes, mediators of these pathways are dually regulated by miRNAs and the molecular clock. For example, *in-vivo*, transcription of *MMP14* is tightly regulated by the circadian clock and, is also direct target of miR-150-3p in mouse knee cartilage(128,269). It is understood that alterations in both contribute to OA pathogenesis and therefore, pose as a therapeutic target. Indeed, miR-17 suppresses AC destruction by regulating pathological factors (*MMP3/13*, *ADAMTS5* and *NOS2*) and its deficiency contributes to OA progression(270). Similarly, deletion of *Bmal1* lead to decreased *Col2a1*, *Sox9* and *Acan* expression and progressive AC degeneration(271).

Despite this, intrinsic regulators of both remains elusive. In this thesis, the reach of the circadian interactome has been extended to include regulation of miR-140-3p abundance in a human chondrocyte model and, miR-455 has been shown to post transcriptionally regulate the core circadian machinery (i.e. *CLOCK*, *PER1*, *PER2*, *CRY*, *RORA* and *NPAS2*). Similar findings are reported in other central and peripheral tissues. Gao *et al* showed miR-17-5p is rhythmically expressed in cultured fibroblasts and directly supresses expression of *CLOCK*(181). Recently, development of small RNA library construction and sequencing techniques have aided expansion of these models to the analysis of circadian miRNAs on a genomic scale. Changyue et al, identified differential expression of 23 mature miRNAs in the eye-stalks of *Eriocheir sinensis* over a 24-hour period(272). To date, comparable models towards the mammalian miRNAome are not reported, in part, due to natural limitations of obtaining human tissue explants and underdevelopment of techniques for the detection of oscillating microRNAs.

To this end, this chapter aims to explore the relationship between the circadian clock and cartilage microRNAs on an organismal level by devising a time series model in 3-month-old WT mice. Here, cartilage explants were harvested every 4 hours for a 48-hour period and the time dependent abundance of cartilage microRNAs was investigated by small-RNA-sequencing.

# **5.2** Aims

- Devise an *in-vivo* model for the detection of oscillating miRNAs in mouse cartilage
- Evaluate statistical models for the analysis of oscillating miRNAs
- Explore the roles of circadian microRNAs in mouse cartilage and their implications on chondrocyte phenotype, homeostasis, and OA development

#### 5.3 Results

# 5.3.1 Optimising RNA extraction from murine cartilage

To explore the cartilage microRNAome, daily fluctuations in microRNA abundance were profiled using smallRNA sequencing and RT-qPCR. This model required high quality RNA samples that fulfil two criteria: high yield and high purity. Preparation of high-quality cartilage RNA from cartilage is limited by the tissue's low cellularity and high proteoglycan content(273). Further, proximity of cartilage to surrounding tissues (i.e. subchondral bone) challenges time-sensitive microdissection. Therefore, extraction of RNA has been optimised to maximise RNA quality during this time-series model.

RNA was extracted from the cartilaginous portions of the murine xiphoid process (xiphoid), femoral condyle (hip) and tibial plateau (knee) surfaces using commercially available extraction kits containing phenol (i.e. miRVANA) and excluding phenol (i.e. miRNeasy). As shown in figure 5.1A, whilst the concentrations of RNA extracted by either miRVANA or miRNEASY kits were not significantly different; knee cartilage explants had a consistently greater RNA concentration relative to the hip and xiphoid (miRVANA: 115ng/uL, miRNEASY:105ng/uL). Pooling hip explants from two animals only significantly increased RNA yield in the miRVANA group (P=0.0054). Though, given that the weight of explants prior to RNA extraction was not standardised; it is unlikely that this variation reflects a limitation of the miRNEASY model. In agreement with this, A<sub>260/280</sub> ratios were comparatively greater in the miRNEASY group indicating greater peptide/phenol contamination in the miRVANA protocols. Overall, RNA purity was greatest in knee explants with an average  $A_{260/280}$  ratio of  $2 \pm 0.01$  and  $A_{260/230}$  of  $0.7 \pm 0.01$  in the miRNEASY group. For hip and xiphoid explants RNA  $A_{260/280}$  ratios for were <2 and their  $A_{260/230}$  ratios were >0.3. Therefore, though inadequate for small-RNA sequencing, such tissues may be suitable for validating conservation of oscillating components in cartilage from different anatomical locations by RT-qPCR.

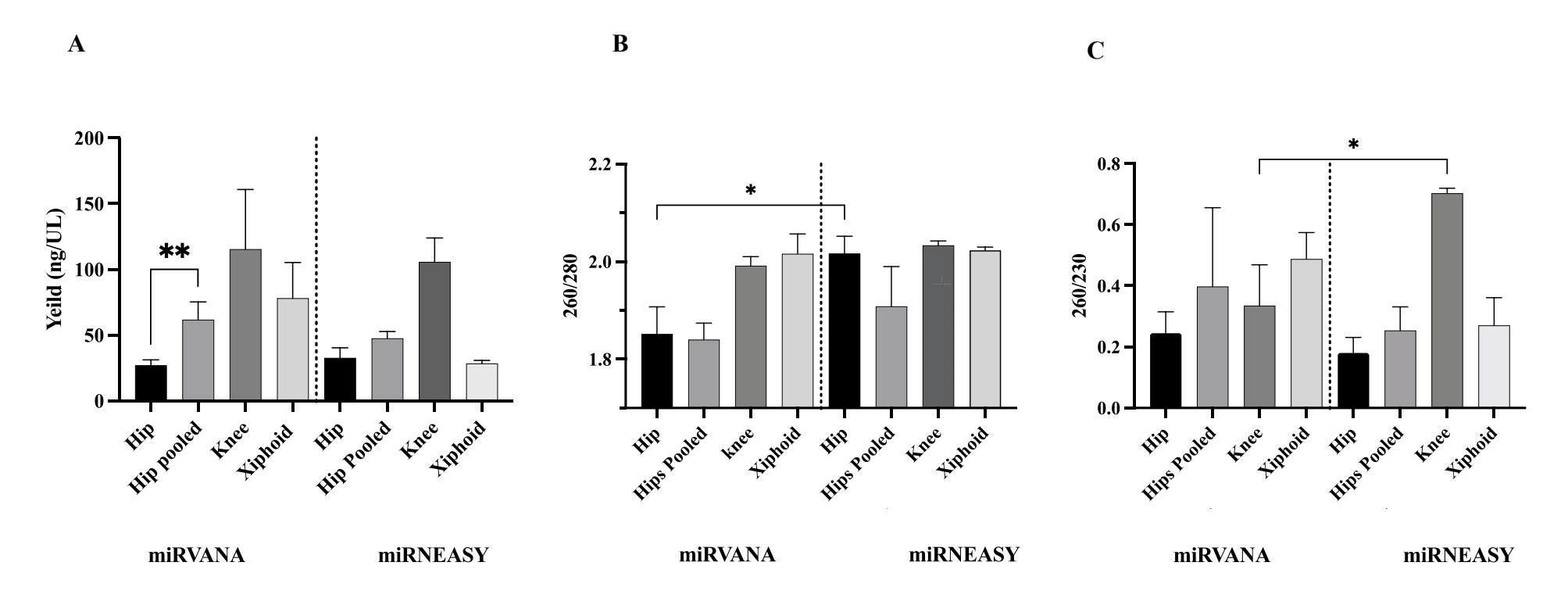


Figure 5. 1 Optimising murine cartilage RNA extraction.

Cartilaginous portions were microdissected from the femoral head, patella and xiphoid and rapid frozen. RNA was extracted using either miRVANA or the miRNEASY RNA extraction kit. (A) RNA yield and (B-C) purity was measured by nanodrop. (N=12 biological replicates mean+/- SD, two-tailed t-test \*p<0.05)

# 5.3.2 Identifying stably expressed housekeeper gene

Prior to identifying oscillating components in our mouse time series model, the expression stability of common endogenous housekeeper genes (HKGs: 18s rRNA, Gapdh) in the explants of the liver and in cartilage of the knee, hip and xiphoid was determined by RT-qPCR. As in section 3.3.2, this was achieved by evaluating HKG Ct values across two consecutive circadian cycles using RefFinder software. In all 4 tissues, the average Ct value for 18s rRNA was lower than Gapdh, though the variation in Gapdh mRNA expression was lower across the time series as indicated by the CV (Table 5.1). In line with this, expression stability of Gapdh mRNA was ranked higher than 18S rRNA in knee cartilage and liver tissue (Rankings (Knee: 18S rRNA: 1.4; Gapdh: 1.1) (Liver 18S rRNA: 1.7; Gapdh:1)). Interestingly, this was not conserved in the xiphoid and knee cartilage, where 18s rRNA was determined to be the most stable HKG.

Gene	Average Ct	SD±	CV (%)	RefFinder Rank	
Knee					
Gapdh	34	0.7	2.2	1	
18s rRNA	14	0.5	3.4	2	
Hip					
Gapdh	34	0.8	2.3	2	
18s rRNA	15	0.5	3.4	1	
Xiphoid					
Gapdh	33	1.1	3.5	2	
18s rRNA	19.7	0.9	4.6	1	
Liver					
Gapdh	34	0.3	0.7	1	
18s rRNA	12	0.3	2.8	2	

Table 5. 1 Determining expression stability of housekeeper genes in mouse tissues.

Expression stability of common housekeeper genes was determined by evaluating variance in gene expression and RefFinder software. The comprehensive rank for each housekeeper gene is generated based on the geometric mean of ranks across GeNorm, NormFinder, BestKeeper software and comparative delta Ct.

## 5.3.3 Validating an autonomous molecular clock in a mouse cartilage model

Diurnal rhythmicity of the circadian pacemaker, *Bmal1*, may be used to infer the presence of a functional molecular clock in tissues harvested in time series models. Therefore, prior to exploring circadian regulation of cartilage miRNAs, time-dependent expression of *Bmal1* mRNA was quantified by RT-qPCR in cartilage and liver explants. Here, tissues were harvested every 4hours/48hours beginning at CT0 from mice maintained under constant darkness (DD). In this way, oscillating components that are identified are referred to as 'free-running' (i.e. autonomous), given that oscillation persists in the absence of photic entrainment.

In knee AC chondrocytes, *Bmal1* abundance oscillated across two consecutive cycles. Relative to CT0, Bmall peaked at CT12 (FC= $3.2\pm0.07$ ) and CT36 (FC= $2.3\pm0.3$ ). As shown in figure 5.2 A, abundance at both CTs were statistically greater than the signals MESOR and passed ANOVA parameter tests (ANOVA,P=0.0007) (Multiple comparison: 0v12, P=0.02 12v24, P=0.0002)). Similarly, these parameters were conserved in chondrocytes of the xiphoid cartilage and liver; suggesting transcription of positive-limb genes is greatest within the animals subjective 'rest-phase' (Figure 5.2 B,C). Notably, Bmall oscillation in the hip failed formal test of rhythmicity. Discrepancies in the concentration of RNA isolated from hip cartilage are depicted in figure 5.3. Apart from CT28, RNA concentrations of explants processed in group C between CT20 and CT48 are considerably higher than the time-point average. As a tissue with low cellularity, larger RNA yields typically indicate bone and growth plate contamination though, no correlation is observed between replicates with a yield <100ng/ $\mu$ L and the abundance of biomarkers for osteosynthesis (Alpl), osteoclast (Trap) and osteoblast (*Runx2*) differentiation and chondrocyte hypertrophy (*Col10a1*) (Figure 5.3 Bi-Biii). Thus, variability is likely a batch effect and these samples were removed from the data set presented in Figure 5.2. Interestingly, the phase of *Bmall* was advanced by 4 hours in the liver comparative to knee chondrocytes; peaking at CT8 (FC=5.7) and CT32 (FC=6.4); supporting the concept of tissue-specific clock function. Collectively, these findings indicate that the temporal resolution of this model is sufficient to detect the free-running rhythmicity of Bmall in multiple peripheral tissues. Therefore, confirming a functional molecular clock mechanism in our model.

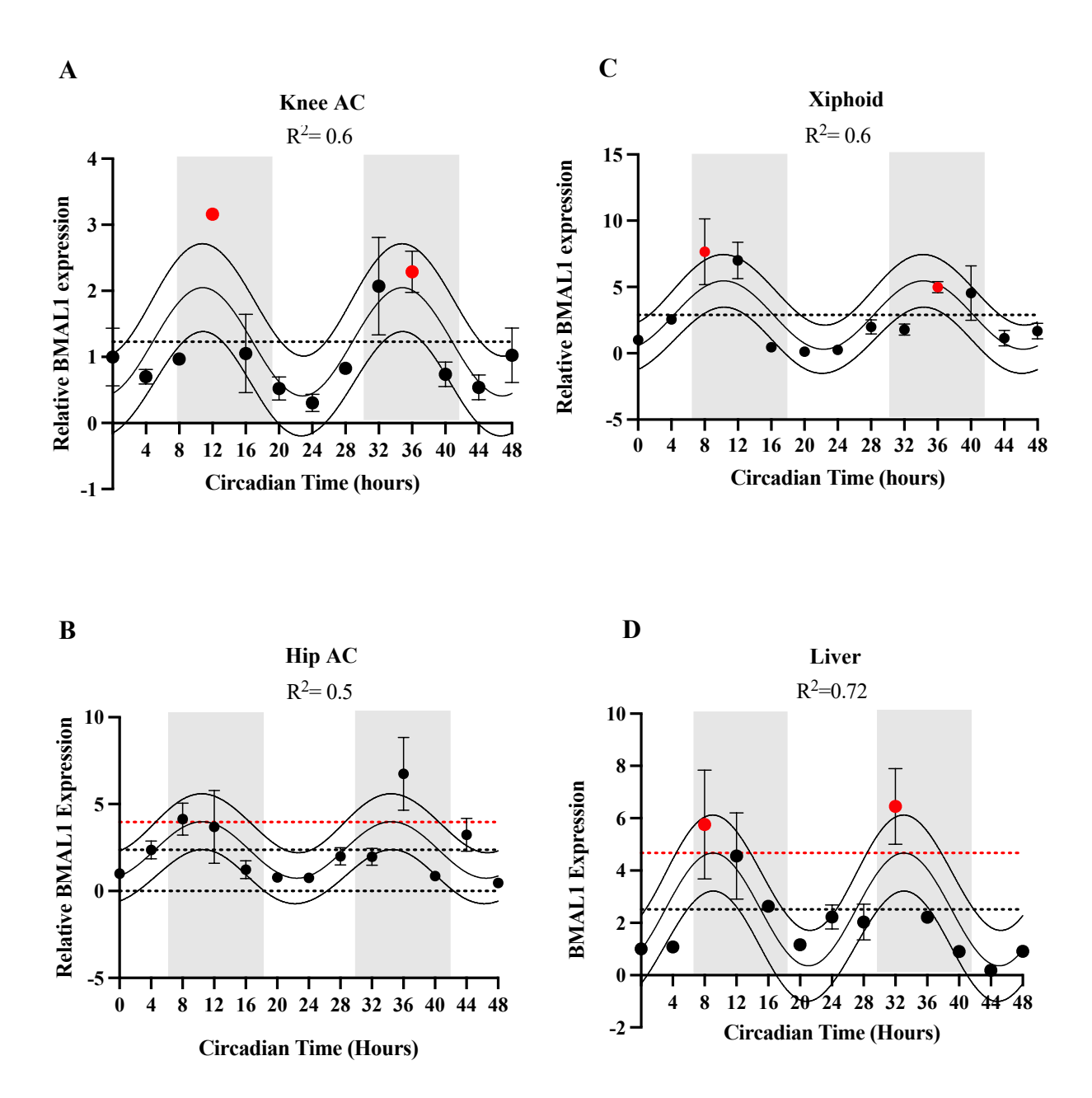


Figure 5. 2 Demonstrating autonomous *Bmal1* oscillation in mouse tissues by RT-qPCR. Expression of *Bmal1* mRNA was measured in (A) knee AC, (B) hip AC, (C) xiphoid cartilage and (D) liver by RT-qPCR, normalised to either *Gapdh* or *18s* Rhythmicity detected by Cosinor fit analysis. Red data points indicate amplitudes significantly greater than MESOR. Red line and black line depict predicted amplitude and MESOR respectively. Grey regions represent animals subjective rest-phase. Data presented relative to circadian time 0 mean +/- SD, N=3

Biological replicates per time point.

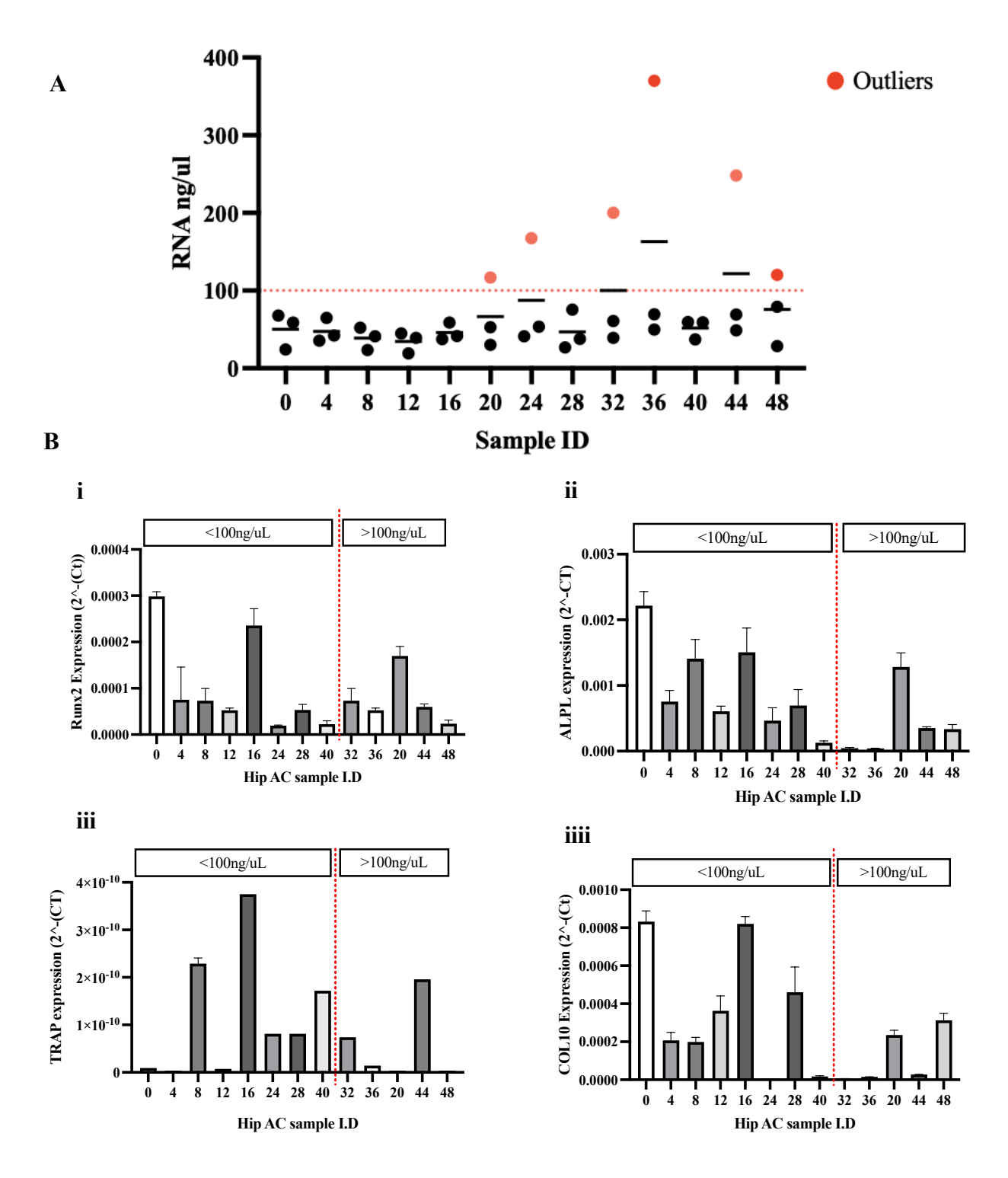


Figure 5. 3 Evaluating bone and muscle contamination in hip AC.

(A) RNA yields of biological replicates used in murine hip articular cartilage time series (ng/uL). Biological replicates with yields >100ng/μL were excluded from data sets. (B) Relationship between yield and growth plate contamination was assessed by measuring biomarkers *Runx2* (Bi) *Alpl* (Bii) *Trap* (Biii) *Col10a1* (Biiii) by RT-qPCR, normalized to 18s rRNA. Data presented as Mean +/- SD, N=3 technical replicates.

#### 5.3.4 Identifying circadian miRNAs by small-RNA-sequencing in mouse knee cartilage

# 5.3.4.1 Developing a statistical model for identifying circadian miRNAs in small RNA sequencing data sets *in-vivo*.

To date, a protocol for the evaluation of oscillating miRNAs in genome-wide data-sets has yet to be defined. As shown in chapter 3, circadian mRNA and miRNA may be identified in small scale data sets utilising cosinor and ANOVA analysis. Notably, both parametric models are only capable of identifying signals with a sinusoidal waveform. As summarised in figure 5.4, the detection power in small RNA-seq data-sets was increased using RAIN in tandem with cosinor analysis. RAIN is a non-parametric model capable of detecting arbitrary waveforms (i.e. spiked or sawtooth shaped curves) with a known period (24-hours)(235). In this way, our model may accommodate variation in miRNA half-life and clearance.

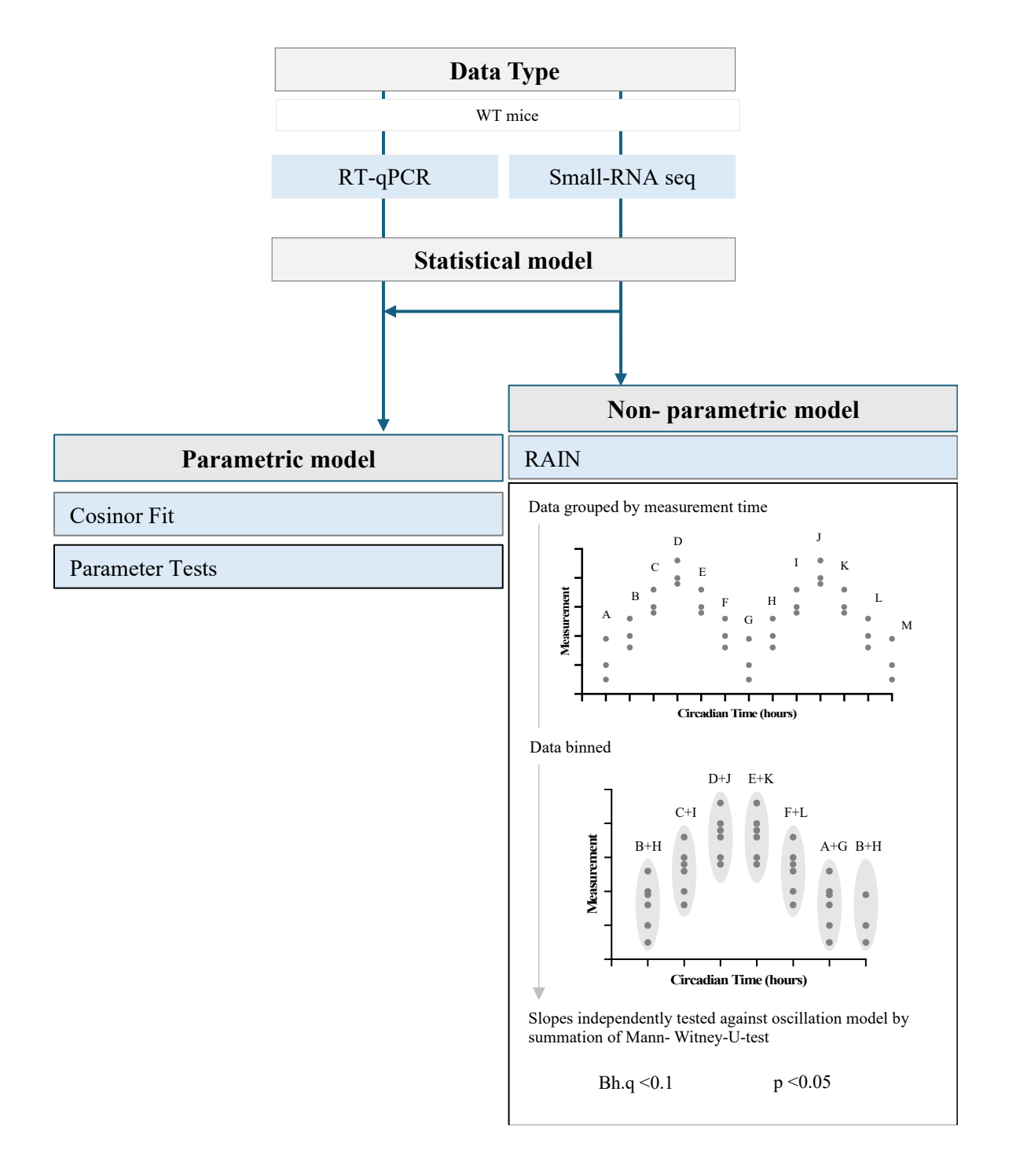


Figure 5. 4 Schematic diagram for the statistical analysis of time series data determined by qPCR and small-RNA-sequencing in mice.

#### 5.3.4.2 Global analysis of small-RNA-sequencing data

To gain insight into circadian regulation of cartilage microRNAs on a global scale, smallRNA-sequencing analysis was performed on knee cartilage harvested from mice kept in DD conditions over a 48hour period. At each 4-hour time bin, cartilage was harvested from 4 animals (2 male, 2 female), each replicate consisting of tissue of both hind legs. Replicates were processed in groups (Group A-D), with each group containing one sample from each time bin. Sample RNA quality was evaluated, and the 3 replicates with highest RIN and RNA concentrations were selected for sequencing. As summarised in figure 5.5, sample quality varied considerably across the time series. RNA concentration ranged from 4.7 ng/uL-164ng/μL and the average RIN value for each group was <6 (Group A:5.3, Group B:4.3, Group C:5.5 Group D:5.4). As result, time bins contain samples from different processing groups.

In this model, average read counts ranged from 6,377,216 (CT4) to 16,228,593 (CT0) after processing and, CT12 yielded the greatest number of clean reads (17,712,904). Following database alignment, tRNA accounted for 27.2% of total reads whilst other sRNAs accounted for 32.2% during the 48hour period. Of these piwi-interacting RNAs (piRNA) were the most dominant class of sRNAs followed by mature miRNAs (Figure 5.6). In agreement, we observed two distinct peaks at 22nt and 30nt when comparing sequence length distribution for mapped reads from the biological replicates of each time point.

Prior to RAIN analysis biological and technical variance was assessed by PCA and cluster analysis. Here, biological sample grouping accounted for 37% of the variability in the data set. To minimise this, batch effect correction (BEC) was performed. Significantly, variability from batch effects improved to 20% after BEC. Meanwhile, variability introduced by circadian time was maintained and, visual the clustering within circadian timepoint improved suggesting that the natural variability expected across the time series has not been over-corrected for in BEC. Following normalisation and count filtering, 430 mature miRNAs were universally expressed across all 13-time bins. miR-140-3p was most abundant, followed by miR-26a-5p and miR-16-5p (Appendix Table 3.1) and, significantly overrepresented comparative to the miR-140-5p and, abundance of miR-455-3p was 2.8-fold greater than miR-455-5p (Figure 5.8).

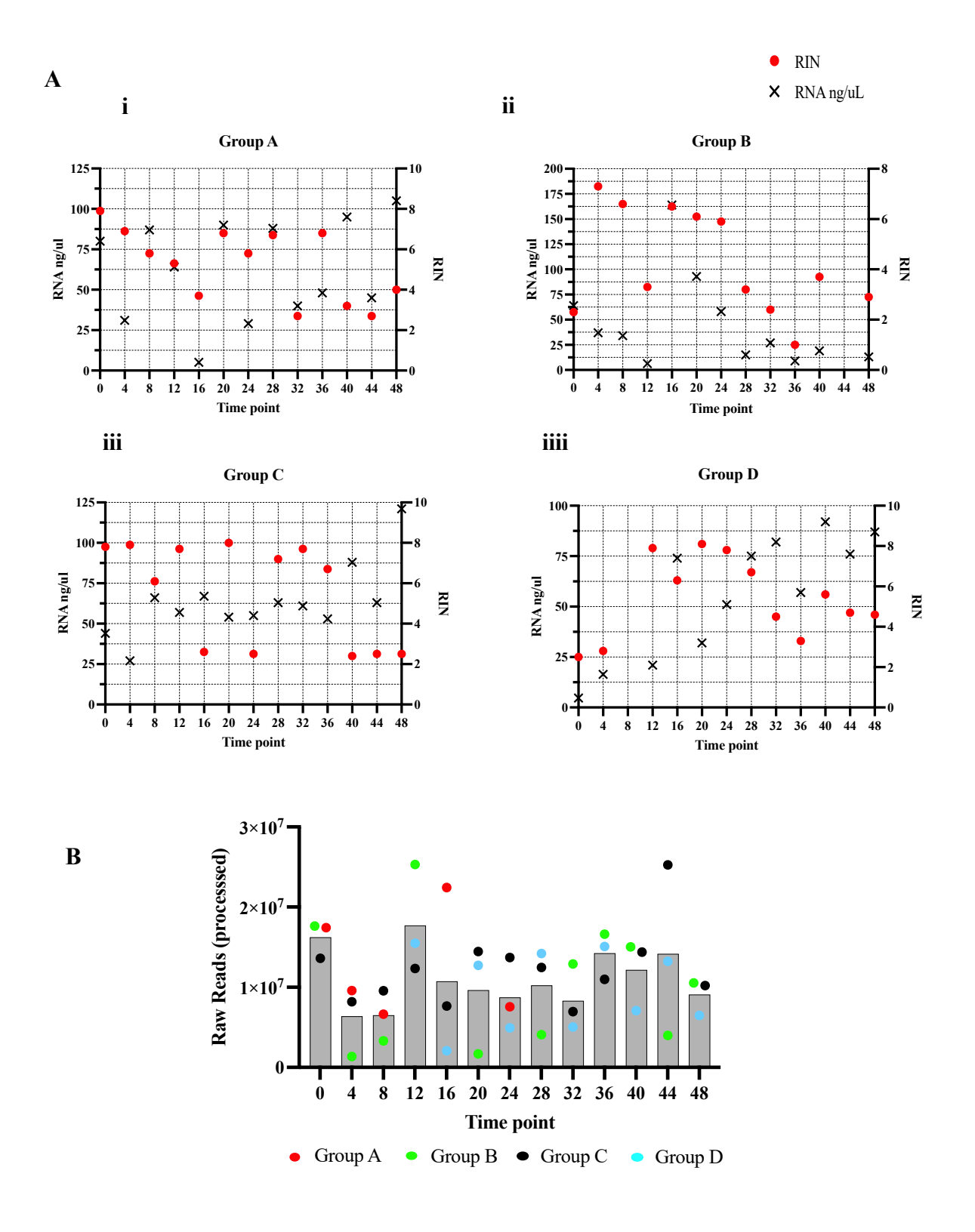


Figure 5. 5 Quality control of knee AC samples for small-RNA seq analysis.

AC was harvested from the tibial plateau of 4 WT mice every 4 hours/48hours. Samples were processed in groups A-D. 3 biological replicates were selected for processing by evaluating sample quality. (A(i-iiii)). Compares total RNA concentration and RIN of biological replicates in each group. (B) Read counts of biological replicates within in each time point. (N=3)

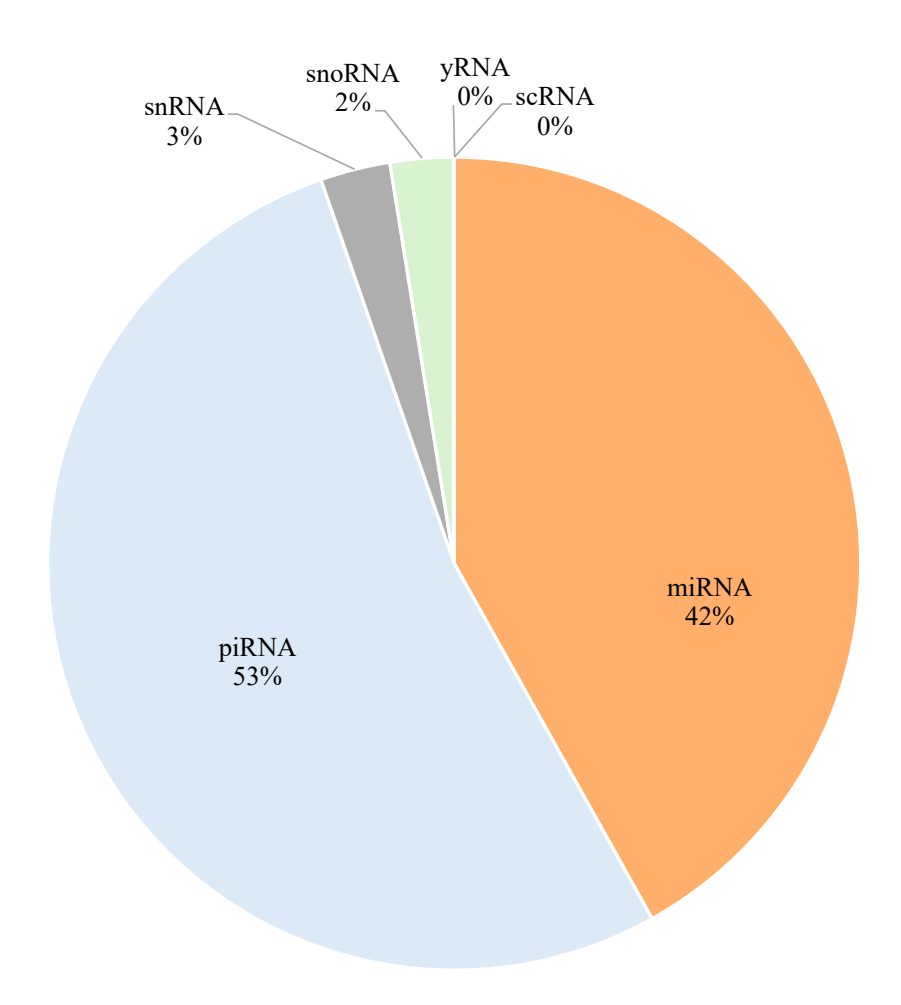


Figure 5. 6 Distribution of small RNAs in knee articular cartilage.

Pie chart indicates proportion of piwi-interacting RNAs (piRNA), microRNAs (miRNA), small nuclear RNA (snRNA), small nucleolar (snoRNA), Y RNAs, (yRNA), small cytoplasmic RNA (scRNA) as a percentage of total small RNAs.

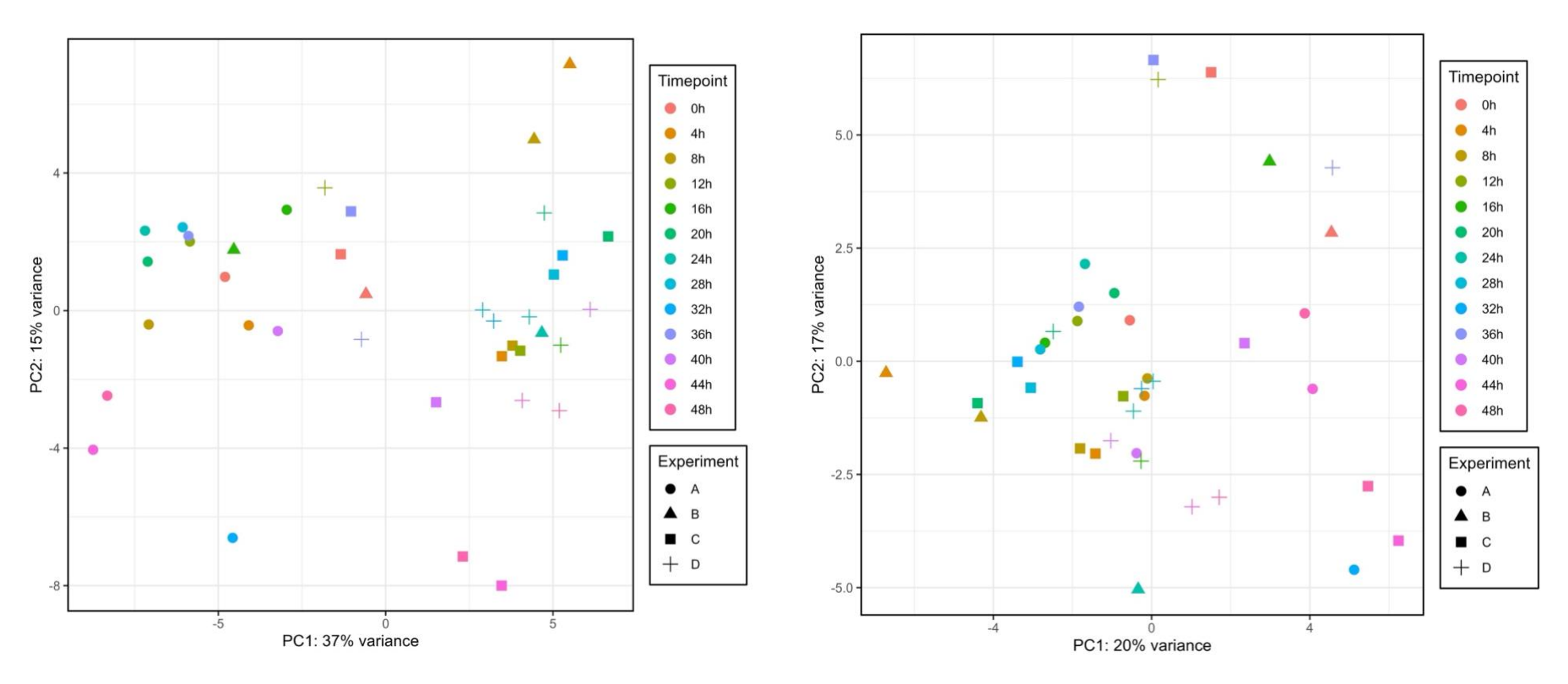


Figure 5. 7 Principal component analysis of small-RNA sequencing data. Axes of variation in small-RNA sequencing data was determined by PCA and clustering analysis.

PCA plots of small-RNA-seq data show the characteristics of biological samples according to technical group and time of harvest before (left) and after (right) batch correction.

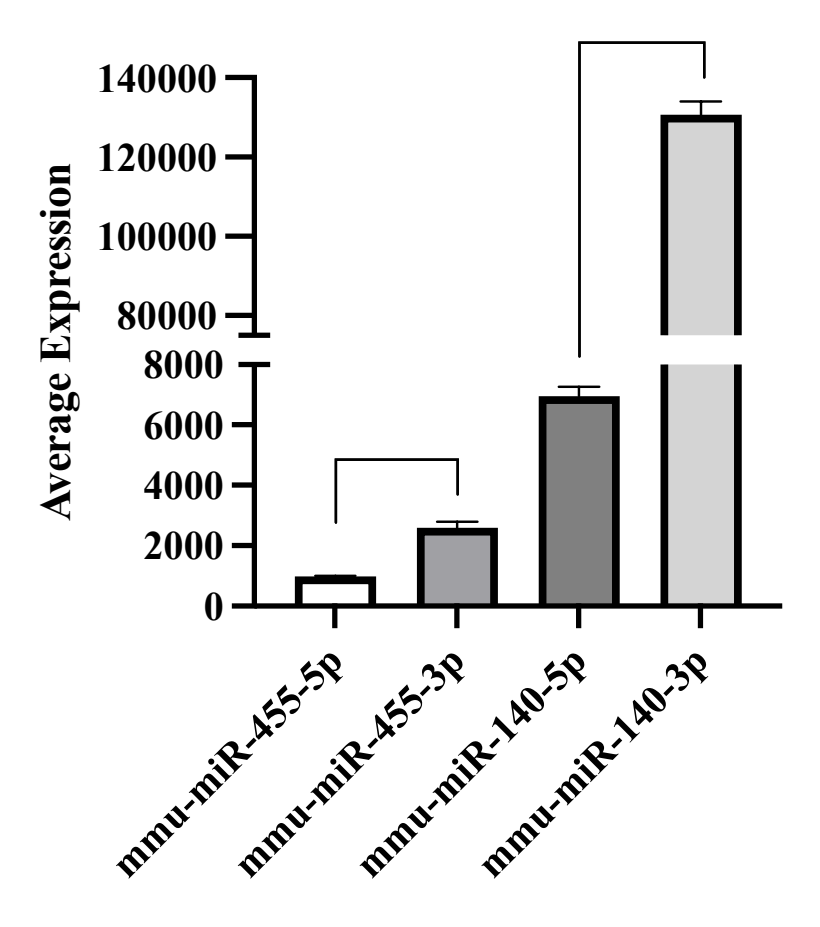


Figure 5. 8 Average abundance of key miRNAs in mouse cartilage.

Expression of miR-455 and miR-140 was determined by small-RNA-seq analysis. Data represented as mean  $\pm$  SD, unpaired t-test P<0.0001 \*\*\*\* (N=3)

#### 5.3.4.3 RAIN analysis

To identify endogenous circadian miRNAs in mouse knee cartilage at the genome-level scale, small RNA sequencing data was analysed using the RAIN algorithm with the aid of Dr Michel Dudek (University of Manchester). As summarised in table 5.2, 3.9% of detected miRNAs oscillated with a period of ~24 hours (BHQ <0.1) under DD conditions. Notably, table 5.2 depicts cosinor analysis results, to be discussed later. Of these, miR-196a-5p had the highest average expression, whilst miR-196a-3p was excluded during data filtering. Oscillation was also observed in several lowly expressed miRNAs including miR-212-3p, miR-505-3p and miR-23a-5p. Grouping miRNAs according to the CT of their peak abundance indicated 13 miRNAs peaked during the animal's subjective rest-phase (Figure 5.9). Here, the expression of miR-134-5p, miR-17-5p, miR-23a-5p and miR-337-5p was greatest at CT12. Previously we have demonstrated *Bmal1* mRNA peaks at CT12 in knee AC using RT-qPCR, suggesting these miRNAs oscillate in-phase with positive limb transcription factors.

The miR-30 family is formed of 5 miR, forming 6 distinct mature miRNAs. As depicted in figure 5.10, miR-30a-5p had the highest average expression and, 5p arms were consistently overrepresented in mouse knee AC. Analysis of data using RAIN identified oscillation in miR-30c-2-3p, miR-30d-3p and miR-30a-5p abundance in AC. Notably, significant inter-group variation was observed in this data, despite batch correction. For instance, at CT8 average expression of miR-30a-5p was  $10496 \pm 730$ . Therefore, the outcome of RAIN analysis is likely an underestimation. Indeed, further data analysis under a less stringent threshold of P<0.05, forecasted an additional 69 circadian miRNAs; including miR-455-5p (P=0.01), miR-146a-5p (P=0.01), miR-18a-5p (P=0.034), miR-20a-5p (P=0.007), miR-30d-5p (P=0.02), miR-30b-5p (P=0.02) and miR-30c-5p (P=0.03) (Appendix, table 4.2). Interestingly, miR-17-5P, miR-18a and miR-20a are members of the miR-17/92 cluster and oscillated in-phase (appendix Figure 4.1). Indeed, peak expression of 77% of miRNAs peaked during the animal's subjective rest-phase (Figure 5.9) As discussed in chapter 3, abundance of miR-455-5p in SW1353 did not pass cosinor tests for oscillation; suggesting miR-455-5p is differentially regulated between humans and mice.

To understand phase relationships of the miR-30 family, data was fitted with an estimated waveform by cosinor analysis. As shown in figure 5.11, rhythmicity was observed in all oscillating miR-30 family members. Using cosinor the amplitude of miR-30c-2-3p, miR-30d-

3p and miR-30b-5p were statistically greater than the MESOR (Appendix figure 4.2). With the exception of miR-30e, 5p arms of the miR-30 family miRNA share a conserved seed sequence (GUAAACA). Here, predicted waveform suggested the abundance of 5p strands were greatest during the animal's active phase, between CT4-CT8 (Fig. 5.11 A). Markedly, average expression of miR-30d-5p and miR-30a-5p were statistically similar (T-test, p=0.9) and oscillated in-phase over two circadian cycles. Interestingly, discrepancies between RAIN and Cosinor interpretations of miRNA signal parameters were recognized. Under RAIN, miR-30c-2-3p and miR-30d-3p oscillated in phase, peaking at CT8. Whereas under cosinor, miR-30c-2-3p peaked between CT4-8 whilst miR-30d-3p expression was greatest at CT16. Given this, comparison between rain findings and cosinor were repeated for all rhythmic miR. This was performed on miRNAs with Q<0.1, to minimize the scale of data analysis (For cosinor graphs, see appendix 4.2). Here, 11 miRNAs passed both RAIN and cosinor tests for oscillation, though peak CTs predicted by RAIN and cosinor were only the same for only miR-17-5p and miR-511-3p (Table 5.2)

								RAIN		COSINOR		
miRbase ID	microRNA ID	Genomic location		Mature sequence	Cross-Species Conservation	Average Expression	pVal.x	вно	Peak CT	Pass?	$\mathbb{R}^2$	Peak CT
MIMAT0005438	mmu-miR-30c-2- 3p	chr1	2329171- 23291784	C <u>UGGGAGA</u> AGGCUGUUUACUCU	+	161.5	6.62E-05	0.028	8	+	0.3	4
MIMAT0017019	mmu-miR-23a-5p	chr19	13836587-13836659	G <u>GGGUUCC</u> UGGGGAUGGGAUUU	+	52.2	0.00050647	0.0446	12	+	0.3	20
MIMAT0011213	mmu-miR-2137	chrX	72992079-7299214	G <u>CCGGCGG</u> GAGCCCCAGGGAG		374.9	0.00048748	0.046	8	+	0.4	16
MIMAT0017281	mmu-miR-511-3p	chr13	58392779-58392886	A <u>AUGUGUA</u> GCAAAAGACAGGAU		116.6	0.00053222	0.046	16	+	0.3	16
MIMAT0004670	mmu-miR-7a-1- 3p	chr13	58392779-58392886	CAACAAAUCACAGUCUGCCAUA		198.6	0.00053222	0.046	16		0.2	
MIMAT0000659	mmu-miR-212-3p	chr11	75173388-75173478	U <u>AACAGU</u> CUCCAGUCACGGCCA		19.6	0.00075049	0.054	16		0.2	
MIMAT0000146	mmu-miR-134-5p	chr12	109734139-109734209	U <u>GUGACU</u> GGUUGACCAGAGGGG	+	68.1	0.00160271	0.086	12	+	0.3	4
MIMAT0009426	mmu-miR-1955- 5p	chr2	92191977-92192074	A <u>GUCCCA</u> GGAUGCACUGCAGCUU		10.4	0.00200903	0.086	8	+	0.3	12
MIMAT0004644	mmu-miR-337-5p	chr12	109585789-109585885	C <u>GGCGUCA</u> UGCAGGAGUUGAUU		95	0.00187584	0.086	12	+	0.3	4
MIMAT0004656	mmu-miR-345-3p	chr12	108836973-108837068	C <u>CUGAACU</u> AGGGGUCUGGAGAC		155.4	0.0017612	0.086	16	+	0.3	0
MIMAT0003513	mmu-miR-505-3p	chr12	109585789-109585885	C <u>GUCAACA</u> CUUGCUGGUUUUCU		17.3	0.00326324	0.095	20		0.1	
MIMAT0000128	mmu-miR-30a-5p	Chr1	3272269-23272339	U <u>GUAAACA</u> UCCUCGACUGGAAG	+	8764.6	0.00313271	0.095	4		0.2	
MIMAT0017011	mmu-miR-30d-3p	Chr15	68341217-68341238	C <u>UUUCAGU</u> CAGAUGUUUGCUGC	+	16.7	0.00272187	0.095	8	+	0.2	16
MIMAT0000518	mmu-miR-196a- 5p *	chr11 chr15	96265164-96265265 102973350-102973434	U <u>AGGUAGU</u> UUCAUGUUGUUGGG	+	11670.8	0.00334385	0.095	8	+	0.3	4
MIMAT0000649	mmu-miR-17-5p	chr14	15043671-115043754	C <u>AAAGUGC</u> UUACAGUGCAGGUAG	+	895.4	0.00275424	0.095	12	+	0.2	12

Table 5. 2 Identification of the circadian miRNAome in mouse knee cartilage in-vivo.

Table summarising microRNAs with statistically significant (bhq > 0.1) circadian oscillation over a 48hour period as determined by RAIN analysis of small-RNAseq data. Left to right: miRbase ID, genomic location, mature sequence (seeds underlined), human cross species conservation, average expression, RAIN analysis results and cosinor results.

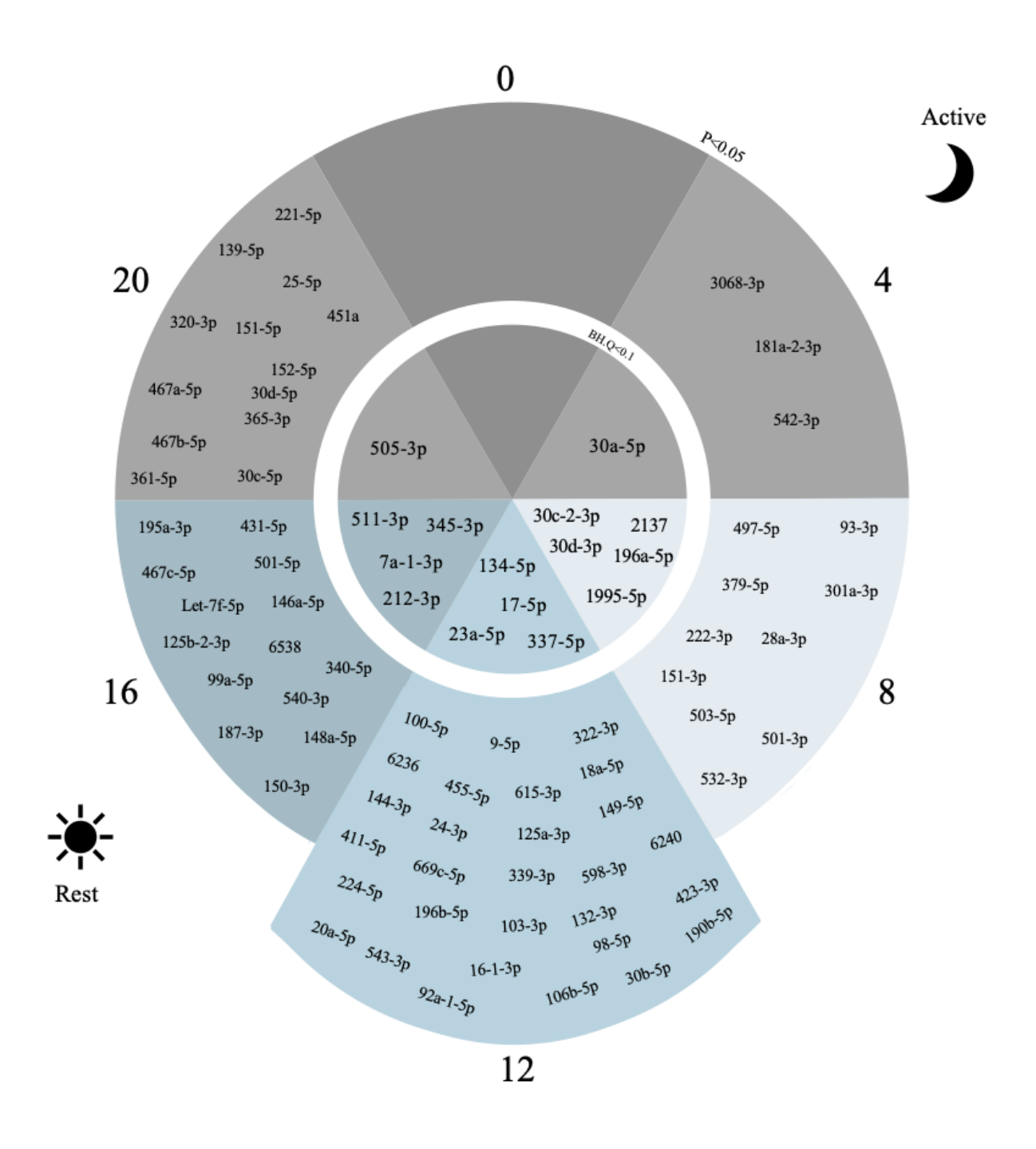


Figure 5. 9 Periodic functions of circadian microRNAs in mouse knee cartilage.

74 circadian microRNAs were grouped depending on the circadian time of their peak expression. Inner circle represents circadian miRNAs identified under bh.q<0.1 threshold, outer circle represents circadian miRNA identified under p<0.05 threshold. Dark regions indicate mouse subjective daytime and period of activity. Light regions indicates subjective night-time.

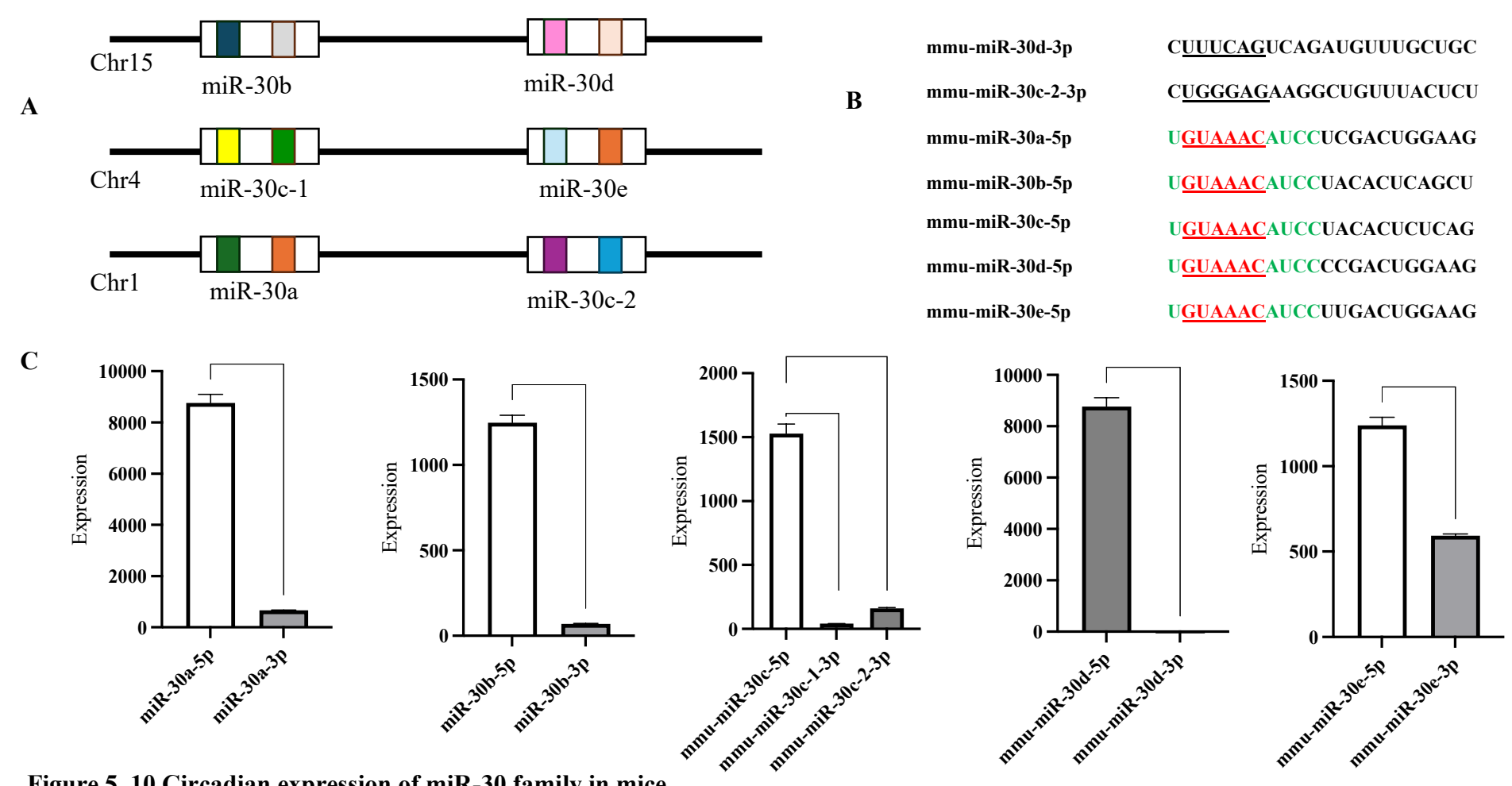


Figure 5. 10 Circadian expression of miR-30 family in mice.

(A) Genomic location of miR-30 family members. (B) Mature sequences of oscillating miR-30 family members. Mature 5p strands derived from miR-30 share conserved seeds. The sequences that arise from the 5' arms of miR-30c-1 and miR-30c-2 5p arms share the same mature miRNA sequence and named miR-30c-5p. underlined regions represent 6mer seed sequences. Red and green represent conserved nucleotides. (C) Average expression of miR-30 family in mouse knee AC over 48 hours determined by small-RNA seq. Data presented as mean +/- SD(N=36). Unpaired test, P<0.0001 \*\*\*\*

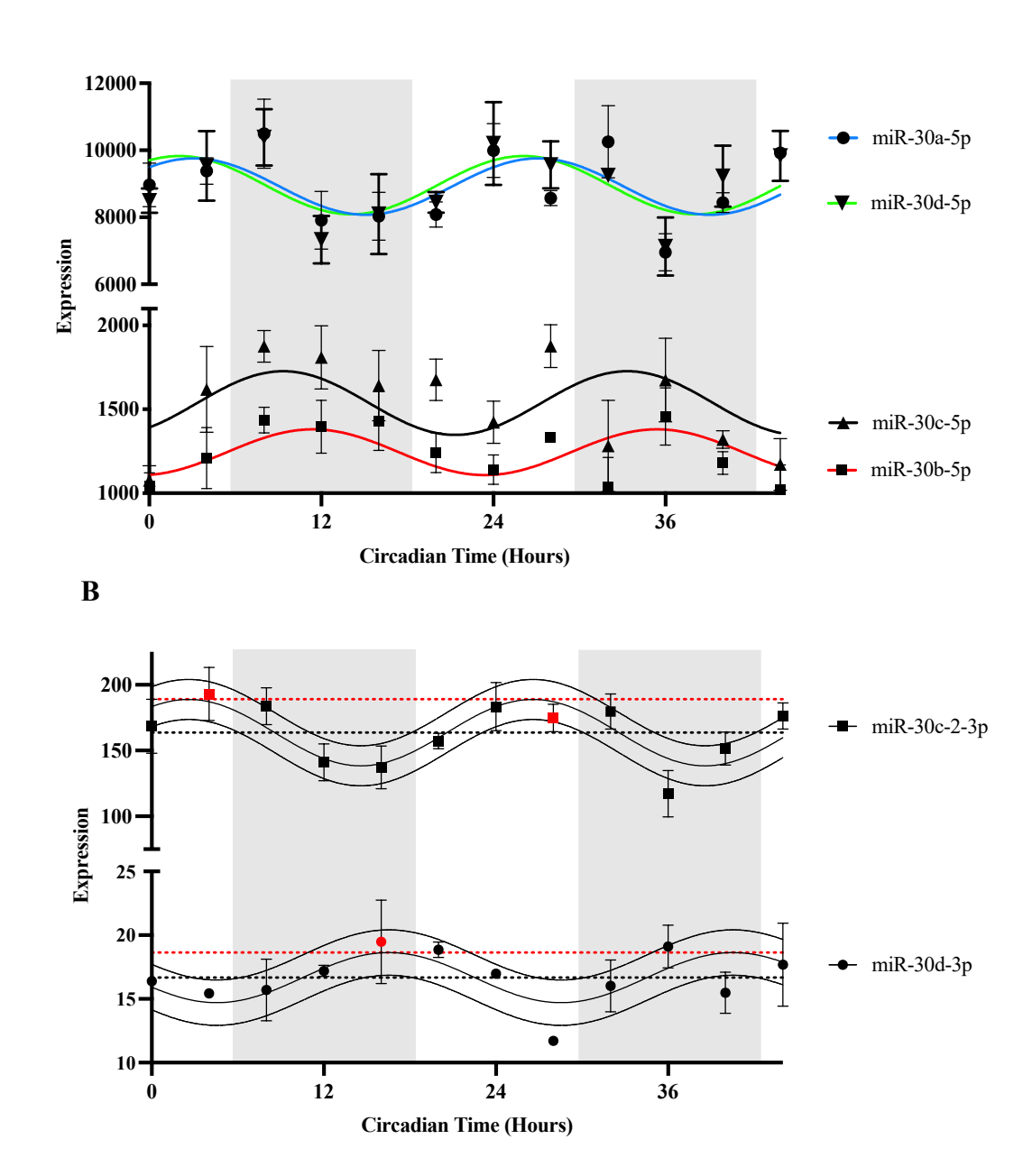


Figure 5. 11 Cosinor analysis of miR-30.

Expression of (A) miR-30a-5p, miR-30d-5p, miR-30c-5p, miR-30b-5p and (B) miR-30c-2-3p and miR-30d-3p in mouse knee AC was measured by small-RNA-seq. Circadian rhythmicity detected by Cosinor fit analysis. Grey regions represent animals subjective rest-phase. Red line and black line depict predicted amplitude and MESOR respectively. Red data points indicate amplitude statistically greater than the MESOR. data presented as average processed reads +/-SD. N=3 biological replicates per time point.

# 5.3.4.4 Time dependent expression of miRNAs by RT-qPCR in knee, hip, and xiphoid cartilage

Circadian transcriptomes are often tissue specific. Therefore, the temporal expression of circadian miRNAs identified section 5.3.4.3 was quantified in AC extracted from the femoral head by RT-qPCR. Experiments were not replicated in the cartilage extracted from the xiphoid, given its structural and functional distinction to knee and hip AC. Oscillation was determined by cosinor analysis. To minimise experimental scale, 3 miRNAs were selected: miR-17-5p, miR-196a-5p and miR-30c-2-3p. Mature sequences of these miRNAs are conserved between mouse and humans, enabling further studies in the cross-species conservation of miRNAomes using the SW1353 chondrosarcoma model at a later date. Given the inter-group variance discussed previously, RT-qPCR was performed on N=3 technical replicates (Group A).

Time dependent expression of candidate miRNAs are summarised in figure 5.12. Abundance of miR-196a-5p and miR-17-5p was regulated by the circadian clock in knee AC. In agreement with sRNA-seq data, miR-196a-5p visually oscillated over two circadian cycles and abundance at CT28 was greater than the MESOR. Figure 5.12 Bi depicts two peaks in miR-196a-5p expression in hip AC though, these peaks are likely not reflecting circadian regulation given previous limitations with the hip AC model. Across the time series, circadian expression of miR-17-5p was statistically significant in AC of the knee and hip. Notably, cosinor analysis of miR-17-5p RT-qPCR data contrasted those observed in section 5.3.4.3. Relative to CT0, miR-17-5p abundance was greatest as CT4 and CT28, correlating to the animal's subjective daytime. whilst miRNA abundance was greatest at CT12 in sRNA-seq data. In both AC models, abundance of miR-30c-2-3p was quantified over one 24-hour interval. Due to technical error, CT28-CT48 were undetermined. Respectively, at the highest point, relative expression of miR-30c-2-3p was 4.2-fold and 5.5-fold greater than CT0 in the knee and hip (Figure 5.12 Aiii, Biii). However, neither points were significantly greater than the MESOR.

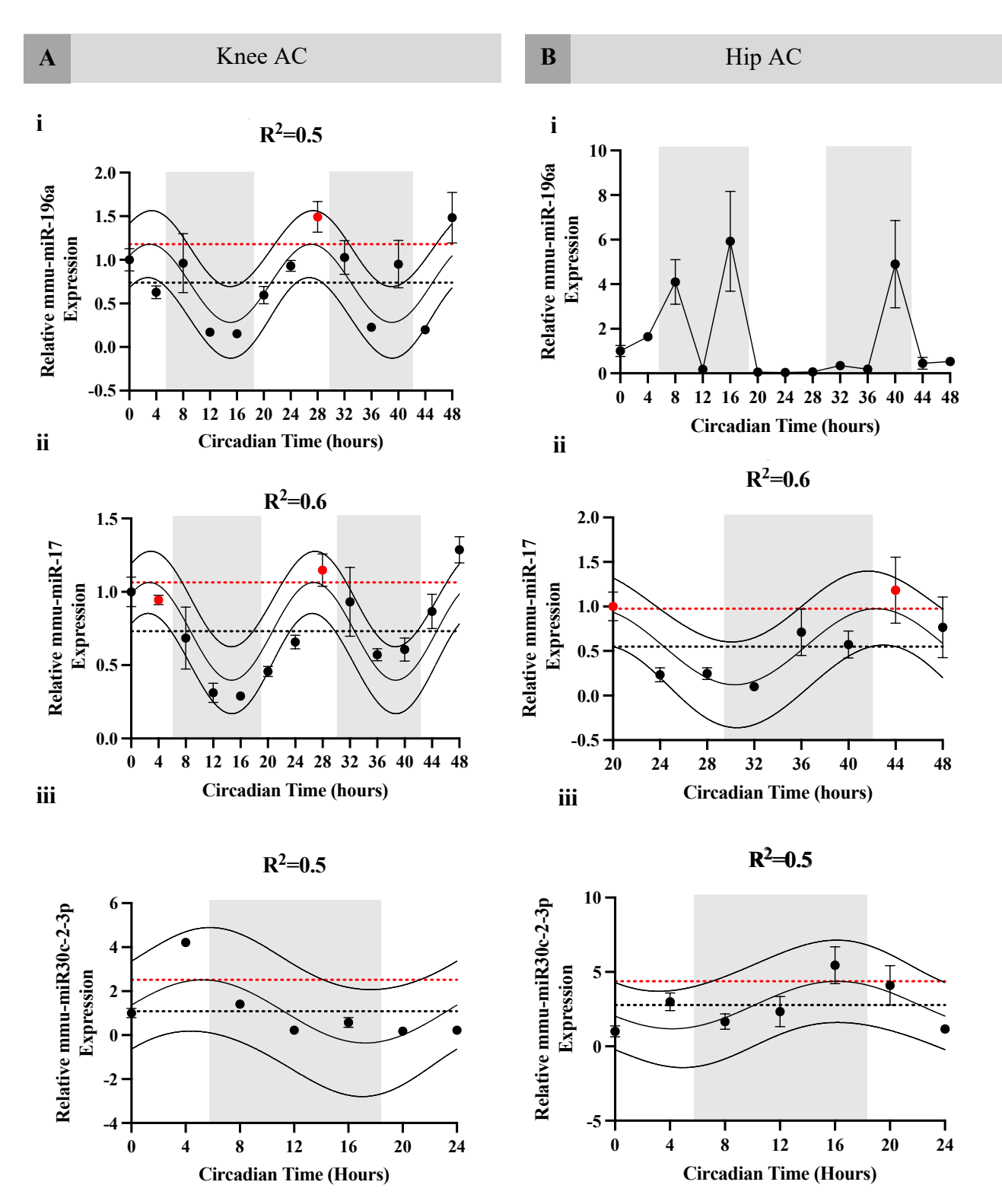


Figure 5. 12 Determining time dependent expression of miR-196a-5p, miR-17-3p, miR-30c-2-3p in mouse knee and hip AC by RT-qPCR.

Expression of mature miRNAs was measured in (Ai-iii) knee AC and (Bi-iii) hip AC by RT-qPCR, normalised to either *GAPDH* or *18s rRNA*. Rhythmicity detected by Cosinor fit analysis. Red line and black line depict predicted amplitude and MESOR respectively. Grey regions represent animals subjective rest-phase. Data presented relative to circadian time 0 mean +/-SD, N=3 technical replicates per time point.

#### 5.3.4.5 GO-term analysis of rhythmic miRNA targets

To understand the functional and biological pathways associated with circadian microRNAs, predicted mRNA targets of miR-17-5p, miR-196a-5p and miR-30c-2-3p were identified using miRTarBase (https://awi.cuhk.edu.cn/~miRTarBase/miRTarBase\_2025/php/contact.php) and Targetscanmouse (https://www.targetscan.org/mmu\_80/). Here, miR-30c-2-3p had the greatest number of predicted targets (5779), followed by miR-17-5p (467) and miR-196a-5p (311). The functions of theses gene sets were explored by gene ontology (GO) analysis using Enrichr software. Enriched terms were categorised into terms relating to 'extracellular-matrix' 'cartilage and bone', 'miRNA biogenesis and mechanism of action' 'inflammation' and 'circadian rhythm'.

In AC, RUNX2, SOX5, SOX6, SOX11, SMAD4 and SIRT6 are known regulators of homeostasis and predicted targets of miR-30c-2-3p. GO analysis identified enrichment for 455 terms across biological processes (BP), molecular function (MF) and cellular components (CC) (P<0.05). As shown in table 5.3, overrepresented terms for miR-30c-2-3p included: proteoglycan biosynthetic processes, regulation of chondrocyte differentiation and negative regulation of catabolism. Further GO analysis identified 13 targets were involved in regulation of circadian rhythm; including PER1, PER2, PER3 and CRY2. For miR-17-5p, 777 terms were enriched including ontologies related to regulation of bone development and osteoblast differentiation. 15 genes were associated with regulation of inflammatory response including MMP3, PPARG, TNF, APP, NR1D1 and RORA (Table 5.4). Notably, RORA and NR1D1 are key regulators of the chondrocyte molecular clock. Finally, comparatively fewer terms were enriched for miR-196a-3p though four key ECM macromolecules were estimated targets: COL1A1, COL2A1, COL1A2 COL1AA1 (Table 5.5)

Gene Ontology	Log10(p-value)	Gene		
Extracellular matrix				
Regulation Of Cell-Matrix Adhesion (GO:0001952)	2.6	GSK3B, , ROCK2,, PIK3CBCXCL1, CORD01C, CCR7, HOXA7, CLASP1, CCL25, JUP, DAPK3,CASK,PLET1, PTK2, CDK6, ADMA15, PTPRA,		
Proteoglycan Biosynthetic Process (GO:0030166)	1.6	HS3ST3B1, BMPR2, CANT1, B3GAT2, B3GAT1, XYLT2, XYLT1, EXTL1, CHST10, NDST3, PXYLP1, BMPR1B, EXTL3, GAL3ST3, B4GALT7		
Cartilage and Bone				
Regulation Of Osteoblast Differentiation (GO:0045667)	1.1	BMPR2, TWIST1, LRP3, RORB, LIMD1, PRKACA, TRPM4, WNT4, GDF10, SDA4D, PTCH1, SUCO, SOX11, TMEM64, RUNX2, PTK2, CCNA2, SKI, CDK5, PPARG, IL6ST, BMPR1B, DDR2, BMPR1A		
Positive Regulation Of Cartilage Development (GO:0061036)	1.5	BMPR2, MDK, ZBTB16, GD56, BMPR1B, SOX6, HOXA11, LOXL2, SOX9		
Positive Regulation Of Chondrocyte Differentiation (GO:0032332)	2.1	ZBTB16, BMPR1B, GDF6, SOX6, HOXA11, LOXL2, SOX5		
miRNA biogenesis and MOA				
Regulation Of pre-miRNA Processing (GO:2000631)	1.6	TRUB1, LIN28B, LIN28A, DGCR8		
Negative Regulation Of miRNA Transcription (GO:1902894)	1.4	NCORI, SRF, PPARG, PPARA, ESRI, RELA, NFATC4, PPARD		
Inflammation	'			
Regulation Of Transforming Growth Factor Beta Receptor Signalling Pathway (GO:0017015)	2.0	TNXB, FAM89B, TGFB1I1, LTPBP4, PEG10, PRDM16, NKX2-1, BCL9L, CREBBBP, SMAD4, CDKN2B, SMAD3, SMURF1, PDPK1, SOX11, DKK3 SMAD7, HIPK2, LATS1, SKI, BCL9, CILP, CD109, PPARG, PPARA, DAND5		

Interleukin-1-Mediated Signalling Pathway (GO:0070498)	1.6	RPS6KA4, IRAK1, ILIR1, TOPLLIP, IRAK3, IRAK4, MAP3K7, RELA, MYD88, MAPK3
Cellular Response To Interleukin-6 (GO:0071354)	1.4	PTPRT, SMAD4, FER, PID1, STAT3, IL6ST, JAK2, RELA, JAK1
Negative Regulation Of Catabolic Process (GO:0009895)	1.9	ALK, CDK5RAP3, PRKCG, CSNK2A1, RPS7, APOA2, IRAK3, SIRT6, NELL1, PPARA
Circadian rhythms		
Entrainment Of Circadian Clock By Photoperiod (GO:0043153)	2.3	CRTC1, FBXL17, RBM4B, PML, PPP1CA, PER2, PPP1CB, PER1, RBM4, PER3, CRY2, BHLH40, SIK1

Table 5. 3 GO term analysis oof miR-30-2-3p targets.

Table of predicted targets of miR-30c-2-3p with significantly enrichment for extracellular matrix, cartilage and bone, miRNA biogenesis, circadian rhythms, and inflammation gene ontologies and log10(p-value). The cut off for statistical relevance at p-<0.05 corresponding to  $-\log(p-adj)\sim1.3$ .

Gene Ontology	Log10(p- value)	Gene
Extracellular matrix		
Regulation Of Cell-Matrix Adhesion (GO:0001952)	1.7	MACF1 LIMCHI NASA1 NF1 GPM6B
Regulation Of Collagen Biosynthetic Process (GO:0032965)	2.1	BMP4 VIM RUNXI
Cartilage and Bone		
Regulation Of Cartilage Development (GO:0061035)	2.2	BMP4 BMPR2 TRPS1
Chondrocyte Differentiation (GO:0002062)	1.5	BMP4 MEF2C BMPR2

Regulation Of Bone	2.6	BMP4 MEF2C BMPR2 BMP2K S1PR1 GPM6B		
Mineralization (GO:0030500)	2.0	DIMI 7 MET 2C DIMI KZ DMF 2K SIFKI GFM0D		
Regulation Of Osteoblast	4.5	BMP SKI MEF2C BMPR2 ZHX3 BAMBI CRIMI		
Differentiation (GO:0045667)	4.5	TMEM64 TP63 PPARG		
miRNA biogenesis and MOA				
Regulation Of miRNA				
Transcription (GO:1902893)	1.9	BMP4 STAT3 PPARG TNF ESR1		
miRNA-mediated Gene				
Silencing (GO:0035195)	1.7	AGO4 AJUBA TNRC6B		
Inflammation				
D. 1.1. OOL G		RB1 APP ATAT3 MMP3 NR1D2 RORA TNF FOXP1		
Regulation Of Inflammatory	3.3	CYLD BCL6 CAMK2N1 PPARG TLR7 EXTL3		
Response (GO:0050727)		MGLL		
Positive Regulation Of				
Interleukin-6 Production	1.5	APP STAT3 TLR7 PTPN11 TNF		
(GO:0032755)				
Regulation Of Transforming				
Growth Factor Beta Receptor	2.2	SKI ZEB2 BAMBI CAVI BRMSIL EP300 PPARG		
Signalling Pathway	2.3	ZBTB7A		
(GO:0017015)				
Positive Regulation Of NIK/NF-				
kappaB Signalling	1.5	APP EP300 TLR7 TNF		
(GO:1901224)				
Stress-Induced Premature	2.0	CDVNIA MADVIA		
Senescence (GO:0090400)	2.0	CDKN1A MAPK14		

# Table 5. 4 GO term analysis of miR-17-5p targets.

Table of predicted targets of miR-17-5p with significantly enrichment for extracellular matrix, cartilage and bone, miRNA biogenesis and inflammation gene ontologies and log10(p-value). The cut off for statistical relevance at p-<0.05 corresponding to  $-log(p-adj)\sim1.3$ .

Gene Ontology	Log10(p- value)	Gene		
Extracellular matrix	1			
Collagen Fibril	2.4	COL1A1 COL2A1 COL1A2 COL14A1		
Organisation(GO:0030199)	2.4	COLIAI COLIAI COLIAI COLIAI		
Cartilage and Bone				
Regulation Of Osteoblast	1.9	BMPR2, SOX11, IGF1 ,SMAD6, HDAC9		
Differentiation (GO:0045667)				
Cellular Response To				
Mechanical Stimulus	1.4	MAPK8, MAP3K1,HABP4		
(GO:0071260)				
miRNA biogenesis and MOA				
pre-miRNA Processing	3.1	LIN29D LIN29A DICEDI		
(GO:0031054)	3.1	LIN28B, LIN28A, DICER1		
mRNA 3'-UTR Binding	3.2	RBM47, CELF2, IGF2BP1, IGF2BP3, LARP4,		
(GO:0003730)	3.2	CPEB3, RBMS3		
Inflammation				
Cellular Response To				
Transforming Growth Factor	1.7	TGFBR3, USP15,COL3A1, COL1A2, SMAD6		
Beta Stimulus (GO:0071560)				
Negative Regulation Of				
Interleukin-1 Beta Production	1.2	ELF4, IGF1		
(GO:0032691)				
Positive Regulation Of BMP				
Signaling Pathway	1.7	BMP2, RBPJ, SOX11		
(GO:0030513)				

# Table 5. 5 GO term analysis oof miR-196a-5p targets.

Table of predicted targets of miR-196a-5p with significantly enrichment for extracellular matrix, cartilage and bone, miRNA biogenesis and inflammation gene ontologies and log10(p-value). The cut off for statistical relevance at p-<0.05 corresponding to  $-log(p-adj) \sim 1.3$ .

#### 5.3.4.6 Exploring mechanisms of circadian miRNA regulation in cartilage

DROSHA and DICER1 are critical mediators in the biosynthesis of mature miRNAs. Here DROSHA aids cleavage of pri-miRNAs into pre-miRNAs and, DICER1 aids processing of pre-miRNAs into mature miRNAs. Diurnal oscillation of miRNA processing machinery is reported in the SCN, retina and liver of mice(173). Additionally, several pre-miRNA transcripts and their mature miRNA counterparts' show circadian oscillation in-vitro. Thus, expression dynamics of Dicer, Drosha and pre-miR-30c-2 were analysed in in mouse cartilage by RTqPCR to identify mechanisms of circadian microRNAs expression. *In-vivo*, oscillation of Dicer1 has been reported in central and peripheral clock-controlled tissues including the liver As shown in Figure 5.13, oscillation was not observed in either *Dicer1* or *Drosha* in cartilage of the knee and in the hip indicating that our RT-qPCR data is not consistent with previous reports. Given both are rate limiting enzymes in miRNA biogenesis, oscillation of miRNAs is likely induced at the level of transactivation or at an alternate point in miRNA processing. To this end we measured the time dependent expression of pre-miR-30c-2 in knee AC. To minimise the effects of inter-animal variation, pre-miR-30c-2 was measured separately in two groups (group C, group D). In group C, two peaks in expression were observed at CT4 and CT28 (Figure 5.14). However, expression dynamics were not circadian in either group C or group D and, suggesting oscillation of miR-30-c-2-3p is likely introduced in strand selection process or in miRNA clearance.



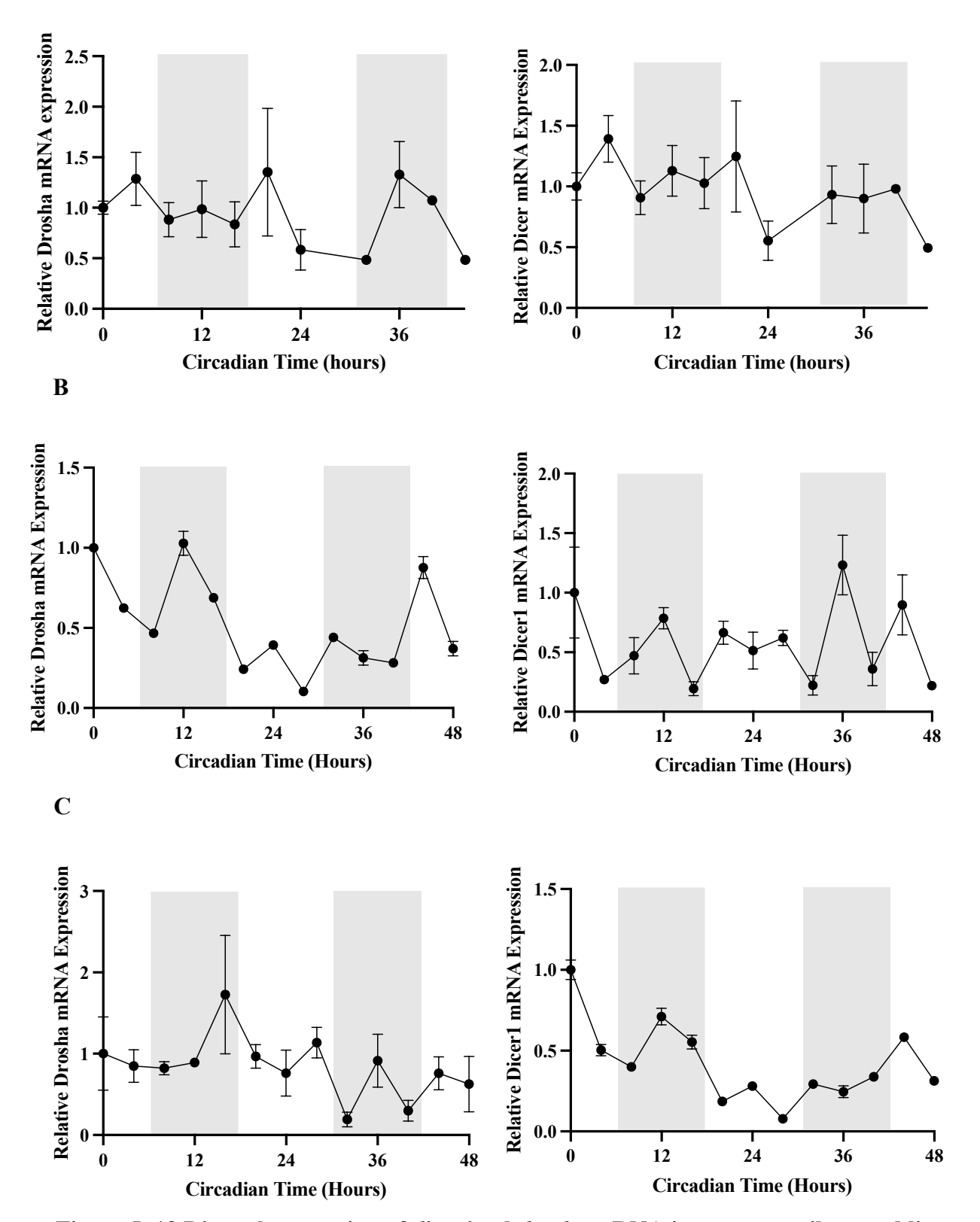


Figure 5. 13 Diurnal expression of dicer1 and drosha mRNA in mouse cartilage and liver.

Time dependent expression of *Dicer1* and *Drosha* mRNA in mouse (A) knee AC, (B) hip AC and (C) liver tissues were determined by RT-qPCR. Data normalised to either *Gapdh* or *18s rRNA*. Grey regions represent animals subjective rest-phase. Data presented relative to circadian time 0 mean +/- SD, N=3 technical replicates per time point.

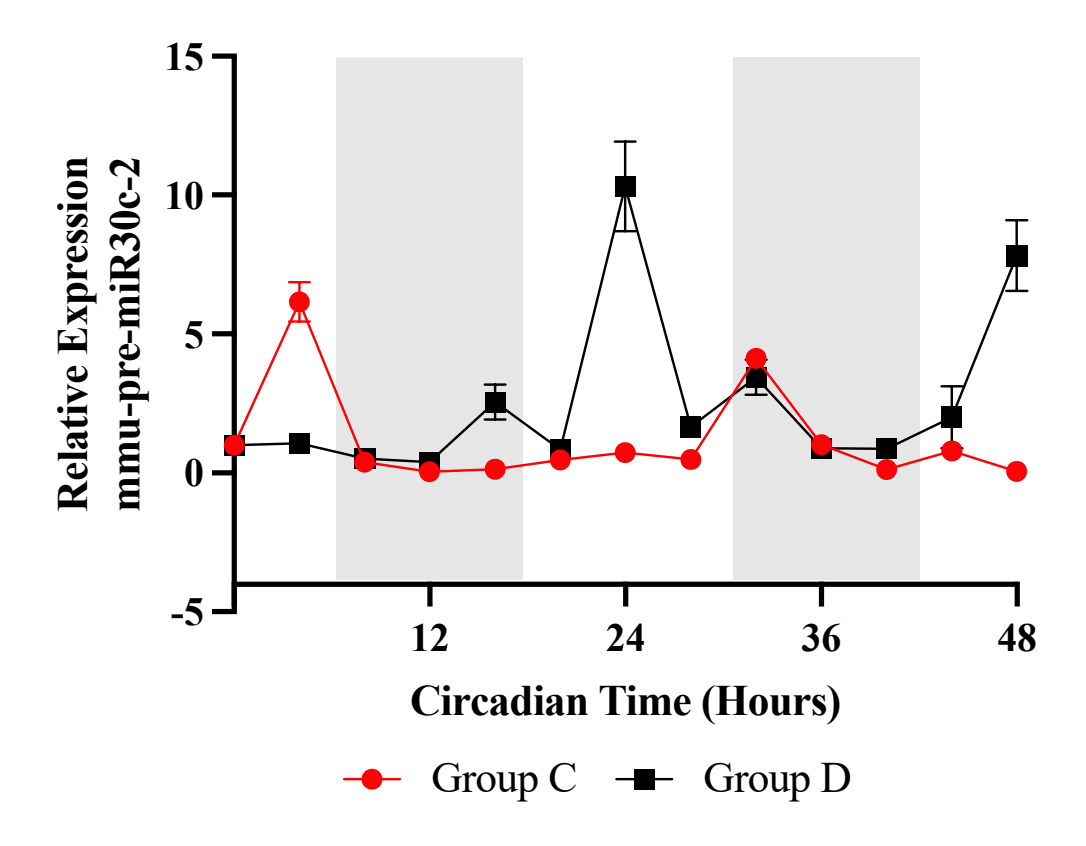


Figure 5. 14 Diurnal expression of pre-miR-30c-2 in mouse knee cartilage.

Time dependent expression of pre-miR-30c-2 in group C and group D were determined by RT-qPCR. Data normalised to *gapdh*. Grey regions represent animals subjective rest-phase. Data presented relative to circadian time 0 mean +/- SD, N=3 technical replicates per time point.

#### 5.4 Discussion

This chapter presents the first daily profile of mature miRNA transcription in AC and has determined the efficacy of RAIN for the detection of circadian miRNAs. Using RAIN, ~19.5% of detected miRNAs exhibited autonomous 24-hour oscillation under DD conditions. This included the 5p arms of the miR-30 family which, despite sharing the same seed sequence, were differentially regulated by the clock. Importantly, oscillation in miR-30a-5p was not identified by cosinor analysis. Similar discrepancies between RAIN and traditional parametric models are reported previously(235). Given the variation in miRNA decay dynamics, this is likely due to RAINs capacity to detect arbitrary waveforms; indicating the importance of model selection when identifying circadian components. Oscillation of several AC miRNAs are conserved in the mammalian SCN including mR-132-3p and miR-17-5p(170,181). Interestingly, the absence of oscillation in miR-132-3p is reported by changue et al in the eyestalk of the Chinese mitten crab (*E. sineisis*). Thus, the abundance of these miRNAs is likely highly relevant to the function of the mammalian central and peripheral tissues. In mammalian models, miR-132-3p oscillated in anti-phase within the SCN comparative to this AC model. In the same study, no significant changes in the expression of miR-16-1 were observed, whilst miR-16-1 was regulated by the circadian clock in this chapter. Therefore, we propose miRNAs are differentially regulated by the circadian clock to support the local needs to the tissue, as observed with circadian transcriptomes.

To elaborate on this, daily abundance of core clock genes and several circadian miRNAs were compared between different mouse tissues *in-vivo*. Consistent with Dudek *et al* oscillation of

*Bmal1* mRNA in hip and xiphoid cartilage is greatest in the subjective rest-period of mice(271). To date, dynamics of Bmall have not been directly acknowledged in knee AC. Here Bmall rhythmicity in the xiphoid, hip and knee peaked in-phase; indicating synchronisation by communal zeitgebers. Peak expression of liver Bmall was comparable but, opposed other publications. Koronowski et al reported high expression at CT20 under LD conditions; the same parameters were identified in heart, kidney, and white adipose tissue(275,276). Therefore, discrepancies are likely due to experiments beginning at different points in the mouses circadian cycle. miR-196a-5p was not rhythmic in hip AC; whilst regulation of miR-17-5p was conserved between knee and hip tissues and oscillated in antiphase. These findings indicate that whilst the basic clock mechanism is conserved across both anatomical locations, divergent miRNAomes have evolved. This is perhaps to accommodate different biophysical demands. Indeed, daily joint loading cycles are an emerging AC zeitgeber and, miR-17 is a mechanosensitive miRNA(277). Therefore, differences in miRNA abundance could be induced by zeitgeber entrainment; though further studies are needed to pinpoint the exact mechanisms. Similarly, to Gossan et al analysis in this hip model was limited by variation in sample quality(128). This was not due to bone contamination, indicated by low abundance osteosynthesis, bone cell differentiation and chondrocyte hypertrophy biomarkers. As discussed by Karim et al, distribution and phenotype of chondrocytes varies between AC zones in the hip(278). Thus, variance in depth and weight of hip explants may have been a contributory factor and further optimisation of this model is required.

Several rhythmic miRNA identified here directly regulate key cartilage transcription factors involved in AC homeostasis and joint disease (summarised in figure 5.15). Indeed, putative targets of miR-17-5p, miR-30c-2-3p and miR-196a-5p were enriched in pathways related to chondrocyte differentiation, catabolism, and inflammatory response. *In-vitro*, miR-30a-5p is known to supress translation of *SOX4/9*, *MMP3*, *HIF-2a* and *RUNX2(279,280)*. In the present study, expression of miR-30a-5p was greatest in the active-period; suggesting ECM turnover, cell proliferation and apoptosis pathways are repressed during activity to optimise tissue remodelling. Previous cartilage micro-arrays indicate that several putative targets of the miRNAome are clock controlled genes. For example, *SMAD3* is regulated by the circadian TTFL, and is supressed by miR-17-5p in AC(271,281). In the same model, 78.6% of oscillating proteolysis genes peaked in the rest-phase. Concomitantly, it is within this period that the majority of the mouse miRNAome peaks in knee AC. Therefore, we hypothesise that abundances of mRNA and miRNA are clustered to temporally compartmentalise cellular

functions. Moreover, this suggests oscillation in miRNAs is not a result of target-lead miRNA degradation, rather mRNA and miRNAs are likely regulated by a shared clock mechanism.

Previous studies propose a role for Dicerl in circadian regulation of miRNAs. Grant et al. reported oscillation of *Dicer1* in several tissues (i.e. SCN, liver, bone-marrow) and, has been implicated in the circadian regulation of miR-146a and miR-125a(173). As with section 3.3.7, this chapter disagrees with these findings, given miR-146a oscillation in was detected despite the stable expression of *Dicer1* or *Drosha* in liver and AC tissues. Thus, the miRNAome is not reflecting upstream oscillation in the miRNA processing machinery in this model. An alternate hypothesis is miRNAs expression is regulated by periodic binding of clock transcription factors within the miRNA locus. In some instances, this is reflected in oscillation within the intermediates of miRNA biogenesis, though is largely dependent on their metabolic stability. Indeed REV-ERBa is the circadian regulators of miR-122 transcription and pre-miR-122 is highly circadian in hepatocytes (171). Previously, 127 Bmall binding sites have been identified in chromosome 1 and, here we indicate that miR-30c-2-3p and *Bmal1* oscillate in antiphase in knee AC, though pre-miRNA was stably expressed (250). Similarly, in-vitro, CLOCK protein directly binds to the miR-17 promotor and pre-miR-17 expression is not rhythmic(181). Therefore, the absence of oscillation in pre-miR-30c is not sufficient to reject the hypothesis that miR-30c loci is transcribed in a circadian fashion and highlights a need for a more robust understanding of the stability and turnover of precursor and mature miRNAs in chondrocytes.

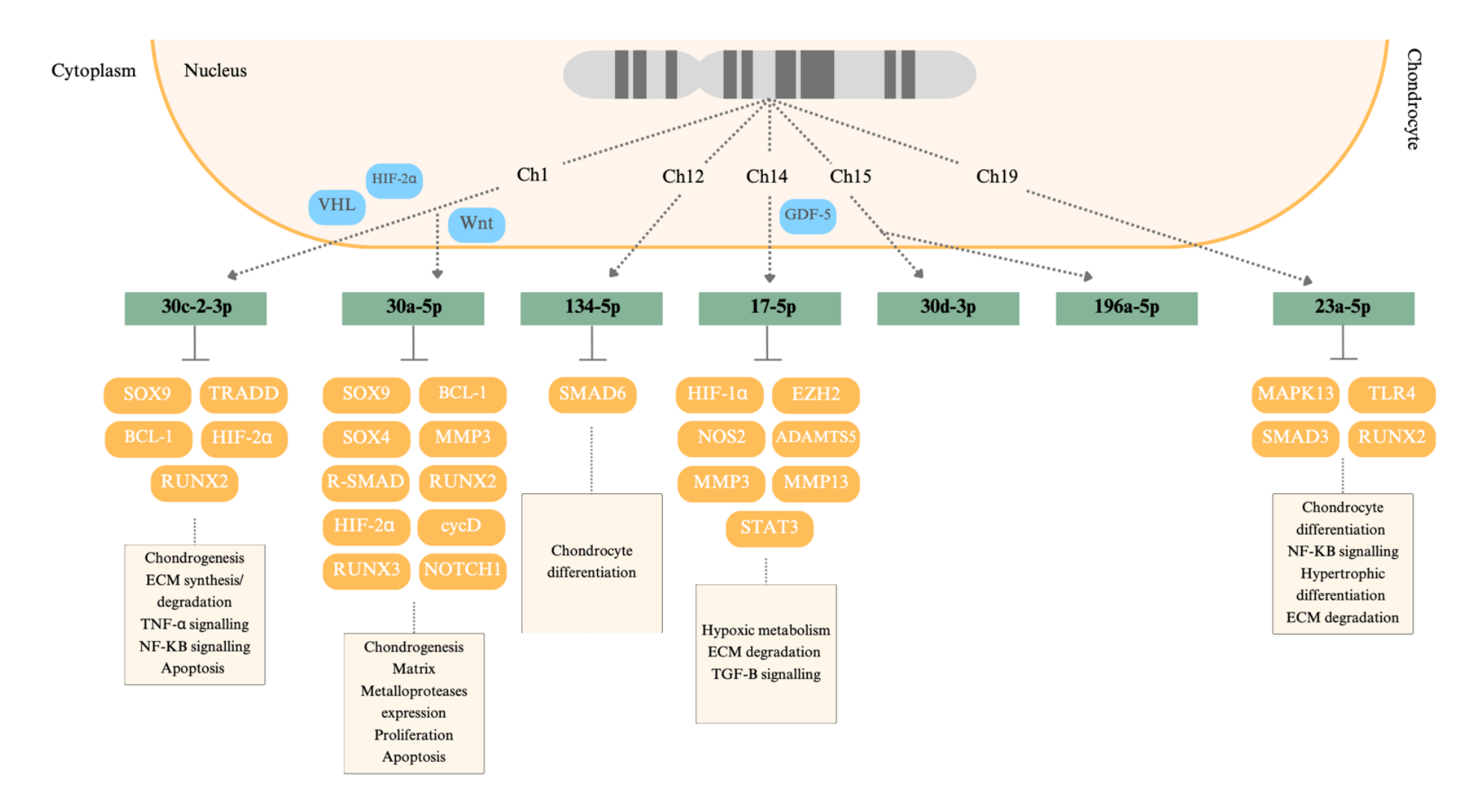


Figure 5. 15 Oscillating microRNAs target key regulators of cartilage development, homeostasis, and diseases.

Schematic demonstrating the experimentally validated targets, and their associated pathways, of circadian microRNAs identified by small-RNA sequencing in mouse knee AC

## Chapter 6: General discussion and future direction

OA is a degenerative and debilitating disease of the synovial joints, causing chronic pain and loss of mobility. Currently, OA affects ~7.6% of the global population, though an intervention for its prevention and treatment remains to be developed(282). This has been limited by the complex disease pathogenesis, given its propensity to affect multiple joint structures. As reviewed here, the degeneration of AC is a hallmark of OA. Often, this is driven by an imbalance in cartilage anabolism and catabolism - leading to increased expression of proinflammatory mediators, degradation of the ECM and eventual loss of AC. Separately, miRNAs and the circadian clock mechanism are key regulators of chondrocyte gene expression and, their dysfunction is an emerging effector of AC destruction(134,154,283). Given this, chronotherapy and miRNA therapeutics emerge as viable treatment strategy for joint diseases; though this is restricted by a limited understanding of their roles in AC physiology.

Previously, inter-regulation between both mechanisms has been reported. In the central clock, miR-132-3p modulates clock-gene expression and, is directly induced by photic cues via a MAPK/CREB-dependent mechanism(284). Therefore, the aim of this thesis has been to explore the extent of cross-talk between the circadian clock and miRNAs in AC. Here, circadian regulation of miRNAs has been examined in a human and mouse AC model. Additionally, several core clock genes were identified and validated as direct targets of hsamiR-455-3p and hsa-miR-455-5p. To the best of our knowledge, this thesis is the first to report the utility of the RAIN algorithm for the genome-wide detection of rhythmic behaviour in small-RNAs. Therefore, this research also reports practical guideline for the evaluation of oscillating miRNAs in samples of low RNA yield by small-RNA sequencing.

### 6.1 Circadian regulation of miRNA expression in cartilage

The peripheral circadian clock is an important regulator of cartilage physiology and function. In comparable transcriptomic and proteomic models, the daily abundances of ~4% of mRNAs and ~12% of proteins were rhythmically expressed in AC; including those involved in chondrocyte differentiation, energy production and regulation of ECM synthesis(132,237). In this way, metabolic processes involved in tissue homeostasis are segregated to an optimal time of day. Within this thesis, the output functions of the mammalian circadian clock has been extended to include post-transcriptional regulation of gene expression *in-vitro* and *in-vivo*.

#### 6.1.1 In-vitro

Our group and others have previously reported key roles for miR-140 and miR-455 in skeletal development and, both co-ordinately regulate AC homeostasis. Briefly, miR-140 is specifically expressed in the developing cartilage tissue of mouse embryos and, functionally supresses *HDAC-4* to promote chondrocyte differentiation(201). Under physiological conditions, miR-140 transcription is regulated by SOX9 and directly regulates, *Adamt5*, *Mmp13*, *Smad3* and *Dnpep* - which are implicated in AC catabolism (197,217). Similarly, miR-455 was co-expressed with miR-140 in an ATDC5 chondrogenesis model and, directly regulates translation of genes related to AC degeneration (i.e. *HDAC2*, *HDAC8*, *HIF-2α*). (238,253)Indeed, both miRNAs are abnormally expressed in joint diseases and, growth retardation and OA like pathologies are reported in separate miR-140<sup>-/-</sup> and miR-455<sup>-/-</sup> mice models (238,285). Given their relevance, understanding the transcriptional regulation of both is highly relevant. Thus, both were selected for the *in-vitro* identification of oscillating miRNAs in SW1353 chondrocyte like cells.

Following dexamethasone synchronisation in SW1353 cells, miR-140-3p oscillated robustly over 24-hours and peaked in the subjective 'active-period', whilst expression of miR-455-3p and miR-455-5p failed cosinor and ANOVA tests of rhythmicity. Significantly, mmu-miR-140-3p was stably expressed in the *in-vivo* mouse knee AC. This observation may be model dependent or may , indicate that miR-140 is differentially regulated between man and mouse.

In agreement with Gossan *et al*, *wwp2* was stably expressed in this model; suggesting mechanisms linking miR-140 and the chondrocyte clock occur independently of the *wwp2* host-gene promotor(237). Largely, circadian physiology is thought to be regulated in by transcriptional events within E-box regions and, 3127 BMAL1:CLOCK DNA binding sites were identified in the mammalian genome(261). However, *BMAL1* abundance peaked in phase with miR-140-3p in SW1353 cells, indicating this daily rhythm is not induced by the positive-limb transcription factors. Further, despite reports by Grant *et al* the abundance of *DICER1* and *DROSHA* were not transcriptionally regulated in these data, thus rhythmicity is not an effect of oscillation in biogenesis machinery(173). Concomitantly, abundance of *CRY1* and *CRY2* peaked 4 hours prior to miR-140 and are known regulators of the vitamin D receptor (VDR)(251). In primary osteoblasts, miR-140 transcription is induced by vitamin D via the VDR and, vitamin D was able to synchronise clock gene expression in ADSCs(286). Thus,

miR-140 oscillation may be indirectly regulated by the negative limb, through its periodic induction of Vitamin D/VDR pathway. Further, vitamin D deficiencies are highly prevalent in the aged population and, are strongly associated with progression of knee OA(287). It may be suggested that the effects of vitamin D deficiencies are mediated through decreased transcription and daily abundances of miR-140 and therefore, increased expression of its catabolic targets in OA.

Notably, daily abundances of intermediates of the miRNA biogenesis (i.e. pre-miR-140, miR-140-3p) pathway were not explored in this study. Further, autonomous expression of core clock genes and miR-140 were not reliably detected in the second 24-hours period due to decreased SW1353 cell viability. This was later determined to be a factor of time and so, we recommend utility of the amended model reported in section 3.3.8 in future *in-vitro* models.

#### 6.1.2 *In-vivo*

A proposed overview of the output mechanisms of the circadian clock in murine AC is shown in figure 6.1. Here, RAIN analysis of small-RNA sequencing data determined ~19.5% of detected AC miRNAs oscillated with a period of 24-hours *in-vivo*. Notably, the top 15 miRNAs identified were re-analysed using the cosinor model to provide a graphical interpretation of the small-RNA sequencing data. However, discrepancies between the outcomes of RAIN and cosinor models were identified. Likely, this reflects the cosinor models' susceptibility to signal noise. As discussed in Chapter 5, consistently low RIN scores (average range 4.3-5.5) and RNA yields were identified and, batch effects introduced a major sources of noise within this timeseries; a common limitation associated extracting high-quality RNA from tissues of low cellularity and high ECM composition(288). Given this, interpretations of the miRNAome within this chapter are derived from the outcomes of RAIN and reiterate the importance of model selection in chronobiology.

Interestingly, a significant portion of the miRNAome are regulators of AC physiology and their dysfunction has been associated with OA- including the miR-30 family and miR-17/92 cluster. Thus, daily fluctuations in their abundance are likely highly relevant to their function. As discussed, the miR-30 family are associated with autophagy, apoptosis, oxidative-stress, and inflammation pathways in multiple tissues(289). Indeed, miR-30b is significantly increased in OA chondrocytes and, downregulated the expression of *COL2A1* and *ACAN(290)*. Here, 5p

arms of the miR-30 family were consistently overrepresented and, with the exception of miR-30e-5p, oscillated in knee AC. Interestingly, despite being functionally related, the daily expression dynamics of the miR-30 family varied in this model. For instance, miR-30d-3p fold-change was greatest at CT8, whilst miR-30d-5p peaked 16 hours later. Similarly, abundance of miR-30a-5p and miR-30c-5p was highest in the rodents active-phase (i.e. CT18-CT6), whilst miR-30b-5p was greatest during the rest-phase. Our data suggests that the murine miR-30 family are differentially regulated by the molecular clock, likely to diversify their biological functions. Indeed, miR-30a-5p directly supresses translation of *SOX9*, *MMP3* and *RUNX2 invitro*; suggesting ECM turnover, cell proliferation and apoptosis pathways are repressed during activity to optimise tissue remodelling (279,280,291). In this way, miRNAs emerge as an important complement of the circadian clock function and a potential interface between clock dysfunction and disease.

Concomitantly, miR-17-5p and miR-18a-5p were co-regulated by the chondrocyte clock and both play pivotal role in OA progression. Under physiological conditions, miR-17-5p aids anabolic and catabolic balance by restricting HIF-1α signalling and, directly targeting catabolic factors (i.e. *MMP3/13, ADAMTS5* and *NOS2*)(292,293). Consistent with this, GO analysis of predicted gene off miR-17-5p were enriched for terms associated with chondrocyte differentiation, regulation of inflammatory response and collagen biosynthesis. Also, miR-18a coordinated chondrocyte hypertrophy *in-vivo* and *in-vitro* by targeting *TGFB1*, *SMAD2* and *SMAD3*(294). Therefore, the therapeutic potential of the miR-17/82 cluster has recently been explored(295). Endogenous induction of miR-17 expression by GDF-5 prevented OA *in-vitro*. Further, in rat model of OA, combined supplementation of IL-1B and miR-18a antagomir supressed chondrocyte hypertrophy. However, despite their evident significance, utilisation of miRNAs clinically has been restricted by a limited understanding of their regulation and therefore, their deregulation in AC. To this end, this study provides an additional mechanism by which miRNAs are regulated which in turn, adds an important dimension to miRNA therapies.

In light of this, future work will determine the systemic and localised entrainment factors of the miRNAome. Canonically, peripheral clocks are synchronised by endogenous zeitgebers coordinated by the central clock; including glucocorticoid signalling(296). Because AC is avascular and has no direct innervation, a role for daily cycles in body temperature and locomotor activity may be explored. *In-vitro*, incubation of AC of PER2::luc mice under

antiphase temperature cycles, drove oscillations in PER2 into antiphase (237) Further, it has been determined that miR-140 and miR-17 are mechanosensitive miRNA associated with bone formation(277). Given both zeitgebers are evoked by the day/night cycles, their integration into the miRNAome may aid synchronisation to the external environment (297).

Critically, this study has also determined that rhythmicity in miR-17-5p is a shared mechanism between knee and hip AC by RT-qPCR, whilst oscillation in miR-196a-5p and miR-30c-2-3p was not detected. In agreement with this, analysis of published data-sets revealed similar divergence between the circadian mRNA transcriptomes of intervertebral disk and xiphoidal processes; indicating that the circadian outputs may be influenced by the anatomical location of cartilage. Notably, we are unable to reliably determine if the peak abundances of miR-17-5p is conserved between both AC models, due to poor hip sample quality.

On a broader level, the AC miRNAome hosted several recognised clock-regulated miRNAs including miR-146a, miR-132-3p and miR-17-5p(169,181,298). In the SCN of mice and synchronised fibroblasts, miR-17-5p transcription is directly regulated by CLOCK protein. Comparatively, differential expression parameters of both miRNAs were observed between prior studies and ours. Therefore, the output function of the clock is highly conserved and, the miRNAome dynamically evolves to meet tissue specific needs. The next iteration of this study may be validation of this hypothesis in neighbouring tissues. For this, brain, liver, and spleen were harvested in parallel to this AC time series and, preliminary validation of an autonomous molecular clock in the liver has been identified for future miRNAome studies. Significantly, several miRNAs in the miRNAome are known to themselves regulate the core clock genes. miR-17-5p directly supressed the expression of *Clock* and *Npas2* in the SCN and, miR-30a interferes with protein abundance of *Per2*; suggesting rhythmic miRNAs may modulate the expression of core clock genes in a negative feedback loop(166,181).

## 6.2 The role of miRNA-455 in the chondrocyte circadian clock

It is understood that over one-third of human genes are regulated by miRNAs(299). Therefore, miRNAs are likely implicated in the molecular clock and its output pathways. *Lee* et al. determined circadian rhythms are significantly shortened in Dicer-deficient mice and, several species of miRNA directly regulate clock genes including *Bmall*, *Per* and *Rora(166)*.

Importantly, circadian dysfunction is a hallmark of several diseases including OA and, cytokine expression observed in OA has recently been associated with altered clock gene expression. However, the pathological mechanism leading to clock dysfunction remain poorly understood. To this end, integration of miRNAs within the chondrocyte time keeping has been explored, using hsa-miR-455-3p and hsa-miR-455-5p. As summarised in figure 6.2 these data extend the miR-455 interactome to include transcriptional regulators of the chondrocyte clock. Notably, a non-oscillating miRNA was selected for this model in order to limit the effects of daily fluctuations in abundance. Future studies might aim to identify clock targets of circadian miRNAs identified within this thesis.

Conversely, several studies have implicated altered cytokine expression with circadian dysfunction observed in OA. Exposure to IL-1B dampened rhythmic expression of Cry1 in cartilage explants of the Cry1-luc reporter mouse and, disruption was inhibited by pre-study treatment with IKK1/2 inhibitor indicating involvement of the NF $\kappa$ B pathway (141). Similarly, Pferdehirt Et~al reported a rapid loss of Per2 oscillation in Per2:luc explants following IL-1 $\alpha$  and ECM degradation (142)

Using a luciferase reporter system, we have identified *CLOCK*, *PER2*, *CRY2* and RORA as target genes of miR-455-5p. CLOCK, PER and CRY transcription factors form the backbone of the mammalian time keeping system. Here, BMAL1:CLOCK heterodimers directly induce transcription of the negative limb regulators PER and CRY, which in turn, co-supress BMAL1:CLOCK. A time delay between the transcription of *Per* and the accumulation of PER is a key facet of the feedback loop, indicating a role for miRNAs in the clock mechanism. In *Dicer*-mutant cells, period is shortened due to accelerated PER synthesis in the upswing of the rhythm and, overexpression of *Per1* and *Per2* 3'UTR caused period shortening in MEFs(166). Taken the findings of this study, it is possible that miR-455-5p may contribute to the negative limb time delay by regulating PER translation. Further, our findings determine two mechanisms by which miR-455-5p may regulate the positive limb and therefore, clock output functions. Here, overexpression of miR-455-5p decreased luciferase activity of CLOCK-3'UTR and RORA 3'UTR construct. Thus, miR-455-5p may modulate the formation of the positive limb heterodimer and rhythmic expression of *Bmal1*.

Using in-silico analysis, we identified 11 core clock genes as putative targets of 455-3p and, validated *NPAS2* as a direct target. miR-455-3p significantly reduced luciferase activity in the

CLOCK 3'UTR and RORA 3'UTR reporter suggesting direct targeting. Though, we were unable to validate the specificity due to unsuccessful site-directed mutagenesis and these data are likely an underestimation of the miR-455 circadian interactome. In the SCN, NPAS2 directly coordinates the circadian transcriptome by forming heterodimers with BMAL1, though its function in chondrocyte clock is poorly understood. Mengatto et al indicated that NPAS2 aids temporal expression of ECM macromolecules (300). Further, phase shift in gut microbiome taxonomy was observed in Npas2 cKO mice; thus, NPAS2 is a likely mediator of tissue physiology and circadian entrainment (301). NPAS2 abundance is decreased in OA; suggesting a role for post-transcriptional mechanisms. With our findings, it is conceivable that this is mediated by deregulated expression of miR-455-3p. Notably, no significant effects in the average expression of NPAS2 were observed in AC of miR-455 knockout mice or, following overexpression of miR-455 in SW1353 chondrosarcomas in-vitro. Similarly, mRNA and protein levels of circadian genes were only mildly affected by *Dicer1* mutant mice. This illustrates miR-455-3p as a subtle modulator rather than a specific regulator of NPAS2 and; exploring the role of miR-455 in determining the phase and amplitude of clock gene oscillation would be valuable.

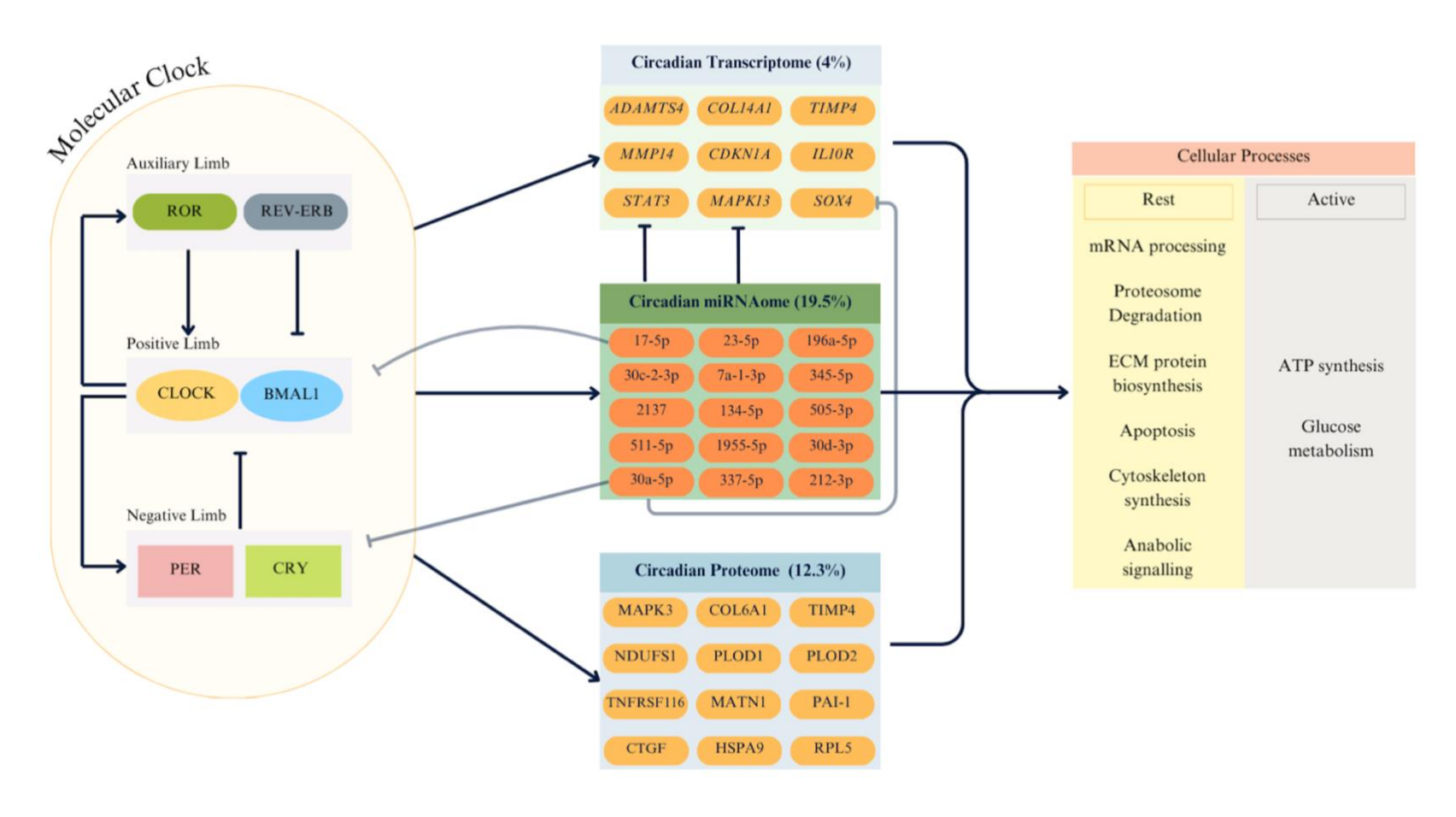


Figure 6. 1 Schematic of the proposed output mechanisms of the circadian clock in chondrocytes.

The molecular clock is a conserved transcription/translation feedback loop formed of core clock genes *CLOCK, BMAL1, CRY, PER, RORA* and REV-ERB. In mouse cartilage, the circadian clock coordinates homeostasis by regulating daily abundance of key AC genes. This regulation has been observed at the level of the transcript, protein and in regulators of gene expression including microRNAs. microRNAs are small non-coding RNAs that negatively regulate gene expression at the post transcriptional level and are known to directly target the 3'UTR of the core clock genes.

Chapter 1:

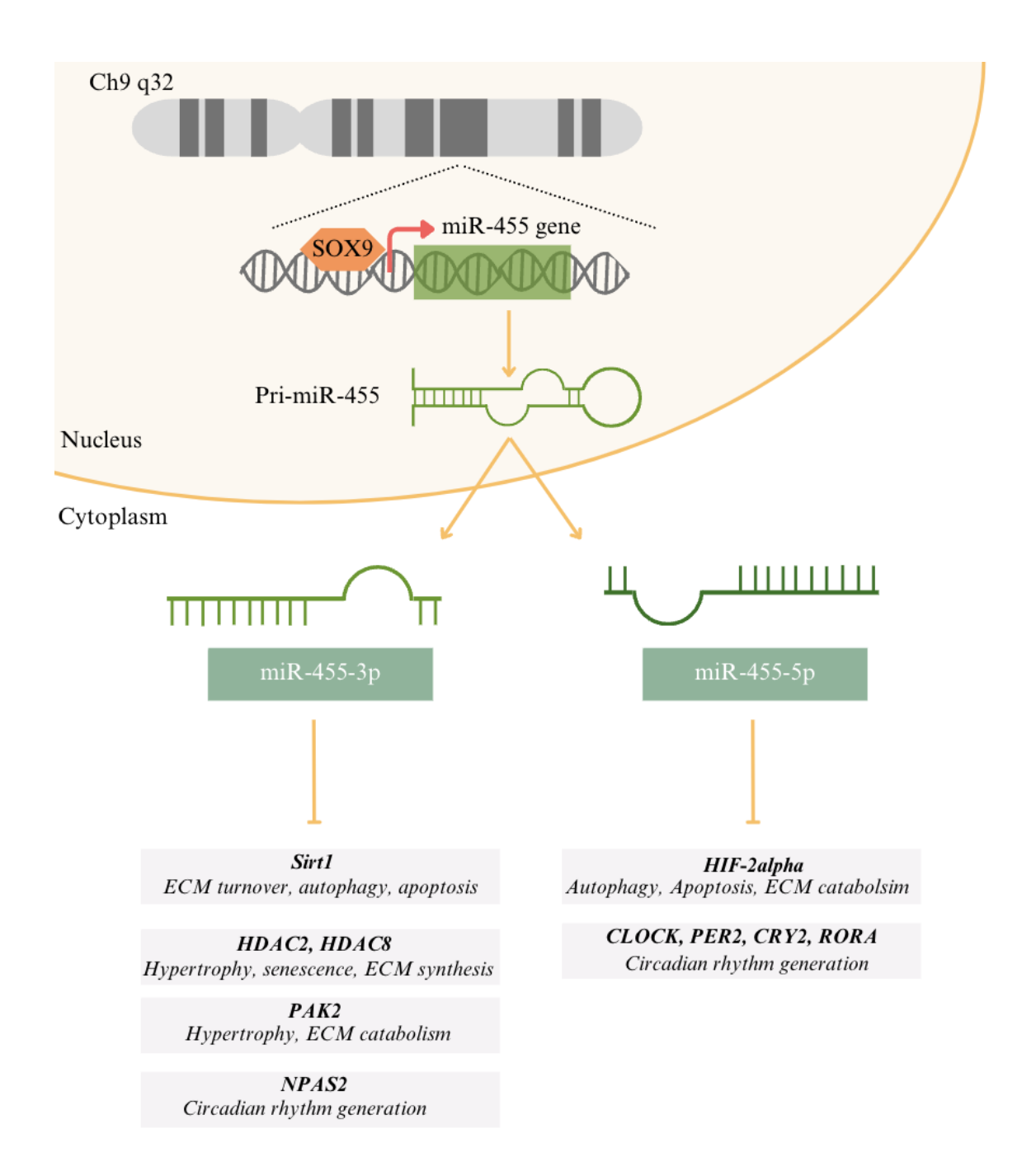


Figure 6. 2 Schematic of the proposed interactome of miR-455 in chondrocytes and its associated physiological processes.

Chapter 1:

- 1. Zhang Y, Jordan JM. Epidemiology of Osteoarthritis. Clin Geriatr Med. 2010 Aug;26(3):355–69.
- 2. Sarzi-Puttini P, Cimmino MA, Scarpa R, Caporali R, Parazzini F, Zaninelli A, et al. Osteoarthritis: An Overview of the Disease and Its Treatment Strategies. Semin Arthritis Rheum. 2005 Aug;35(1):1–10.
- 3. Frisbie DD. Synovial Joint Biology and Pathobiology. In: Equine Surgery. Elsevier; 2012. p. 1096–114.
- 4. van Weeren R. Joint physiology. In: Equine Sports Medicine and Surgery. Elsevier; 2014. p. 213–22.
- 5. Samvelyan HJ, Hughes D, Stevens C, Staines KA. Models of Osteoarthritis: Relevance and New Insights. Calcif Tissue Int [Internet]. 2021;109(3):243–56. Available from: https://doi.org/10.1007/s00223-020-00670-x
- 6. DAVIES D V. The structure and functions of the synovial membrane. Br Med J. 1950 Jan 14;1(4645):92–5.
- 7. D. Smith M. The Normal Synovium. Open Rheumatol J. 2011 Dec 30;5(1):100–6.
- 8. FitzGerald O, Bresnihan B. Synovial membrane cellularity and vascularity. Ann Rheum Dis. 1995 Jun 1;54(6):511–5.
- 9. Marcelino J, Carpten JD, Suwairi WM, Gutierrez OM, Schwartz S, Robbins C, et al. CACP, encoding a secreted proteoglycan, is mutated in camptodactyly-arthropathy-coxa vara-pericarditis syndrome. Nat Genet. 1999 Nov;23(3):319–22.
- 10. Chijimatsu R, Saito T. Mechanisms of synovial joint and articular cartilage development. Cellular and Molecular Life Sciences. 2019 Oct 14;76(20):3939–52.
- Becerra J, Andrades JA, Guerado E, Zamora-Navas P, López-Puertas JM, Reddi AH.
   Articular Cartilage: Structure and Regeneration. Tissue Eng Part B Rev. 2010
   Dec;16(6):617–27.
- 12. Sophia Fox AJ, Bedi A, Rodeo S a. The basic science of articular cartilage: structure, composition, and function. Sports Health [Internet]. 2009;1(6):461–8. Available from: http://www.ncbi.nlm.nih.gov/pubmed/23015907%5Cnhttp://www.ncbi.nlm.nih.gov/pubmed/23015907
- 13. Saito T. The superficial zone of articular cartilage. Inflamm Regen. 2022 Dec 2;42(1):14.

- 14. Rolauffs B, Williams JM, Grodzinsky AJ, Kuettner KE, Cole AA. Distinct horizontal patterns in the spatial organization of superficial zone chondrocytes of human joints. J Struct Biol. 2008 May;162(2):335–44.
- 15. Gilbert SJ, Blain EJ. Cartilage mechanobiology: How chondrocytes respond to mechanical load. In: Mechanobiology in Health and Disease. Elsevier; 2018. p. 99–126.
- Brittberg M, Lindahl A, Nilsson A, Ohlsson C, Isaksson O, Peterson L. Treatment of deep cartilage defects in the knee with autologous chondrocyte transplantation. N Engl J Med [Internet]. 1994;331(14):889–95. Available from: http://www.ncbi.nlm.nih.gov/pubmed/8078550
- 17. Wong M, Wuethrich P, Eggli P, Hunziker E. Zone-specific cell biosynthetic activity in mature bovine articular cartilage: A new method using confocal microscopic stereology and quantitative autoradiography. Journal of Orthopaedic Research. 1996 May;14(3):424–32.
- 18. Havelka S, Horn V, Spohrová D, Valouch P. The calcified-noncalcified cartilage interface: the tidemark. Acta Biol Hung. 1984;35(2–4):271–9.
- 19. Palmer D, Strain WD, Webb B. 242. Turning of the Tide: Does Tidemark Advancement Perpetuate Osteoarthritis. Rheumatology. 2014 Apr;53(suppl\_1):i150–i150.
- 20. Wang W, Ye R, Xie W, Zhang Y, An S, Li Y, et al. Roles of the calcified cartilage layer and its tissue engineering reconstruction in osteoarthritis treatment. Front Bioeng Biotechnol. 2022 Aug 31;10.
- 21. Zizak I, Roschger P, Paris O, Misof BM, Berzlanovich A, Bernstorff S, et al. Characteristics of mineral particles in the human bone/cartilage interface. J Struct Biol. 2003 Mar;141(3):208–17.
- 22. Boushell MK, Hung CT, Hunziker EB, Strauss EJ, Lu HH. Current strategies for integrative cartilage repair. Connect Tissue Res. 2017 Sep 3;58(5):393–406.
- 23. Arkill KP, Winlove CP. Solute transport in the deep and calcified zones of articular cartilage. Osteoarthritis Cartilage. 2008 Jun;16(6):708–14.
- 24. Schultz M, Molligan J, Schon L, Zhang Z. Pathology of the Calcified Zone of Articular Cartilage in Post-Traumatic Osteoarthritis in Rat Knees. PLoS One. 2015 Mar 25;10(3):e0120949.
- 25. Lodish H, Berk A, Zipursky S. Collagen: The fibrous Proteins of the Matrix. In: Molecular Cell Biology. 2000. p. Section 22.3.
- 26. Eyre D. Collagen of articular cartilage. Arthritis Res. 2002;4(1):30.

- 27. Poole AR, Kobayashi M, Yasuda T, Laverty S, Mwale F, Kojima T, et al. Type II collagen degradation and its regulation in articular cartilage in osteoarthritis. Ann Rheum Dis. 2002 Nov 1;61(Supplement 2):78ii–81.
- 28. Responte DJ, Natoli RM, Athanasiou KA. Collagens of articular cartilage: Structure, function, and importance in tissue engineering. Crit Rev Biomed Eng. 2007;35(5):363–411.
- 29. Xue-Xi Z, Zhi-Hua M, Jian-Hua Y, Yang X. Determination of collagen and proteoglycan concentration in osteoarthritic and healthy articular cartilage by Fourier transform infrared imaging and partial least square. Vib Spectrosc. 2015;78:49–53.
- 30. Zhou T, Yang X, Chen Z, Zhou Y, Cao X, Zhao C, et al. A novel COL2A1mutation causing spondyloepiphyseal dysplasia congenita in a Chinese family. J Clin Lab Anal. 2021 Apr 16;35(4).
- 31. Bowers SLK, Meng Q, Kuwabara Y, Huo J, Minerath R, York AJ, et al. Col1a2-Deleted Mice Have Defective Type I Collagen and Secondary Reactive Cardiac Fibrosis with Altered Hypertrophic Dynamics. Cells. 2023 Aug 30;12(17):2174.
- 32. Bayliss MT, Venn M, Maroudas a, Ali SY. Structure of proteoglycans from different layers of human articular cartilage. Biochem J. 1983;209(2):387–400.
- 33. Yanagishita M. Function of proteoglycans in the extracellular matrix. Vol. 43, Pathology International. 1993. p. 283–93.
- 34. Loret B, Simões FMF. Articular cartilage with intra- and extrafibrillar waters: a chemomechanical model. Mechanics of Materials. 2004 May;36(5–6):515–41.
- 35. Mow VC, Kuei SC, Lai WM, Armstrong CG. Biphasic Creep and Stress Relaxation of Articular Cartilage in Compression: Theory and Experiments. J Biomech Eng. 1980 Feb 1;102(1):73–84.
- 36. Maroudas A. Biophysical chemistry of cartilaginous tissues with special reference to solute and fluid transport1. Biorheology. 1975 Aug 1;12(3–4):233–48.
- 37. Xie L, Lin ASP, Kundu K, Levenston ME, Murthy N, Guldberg RE. Quantitative imaging of cartilage and bone morphology, reactive oxygen species, and vascularization in a rodent model of osteoarthritis. Arthritis Rheum. 2012 Jun;64(6):1899–908.
- 38. Goldring MB. Chondrogenesis, chondrocyte differentiation, and articular cartilage metabolism in health and osteoarthritis. Ther Adv Musculoskelet Dis [Internet]. 2012;4(4):269–85. Available from: http://journals.sagepub.com/doi/10.1177/1759720X12448454

- 39. Lefebvre V, Dvir-Ginzberg M. SOX9 and the many facets of its regulation in the chondrocyte lineage. Connect Tissue Res. 2017 Jan 2;58(1):2–14.
- 40. Santamaria S. ADAMTS-5: A difficult teenager turning 20. Int J Exp Pathol. 2020 Feb 27;101(1–2):4–20.
- 41. Sanchez C, Bay-Jensen AC, Pap T, Dvir-Ginzberg M, Quasnichka H, Barrett-Jolley R, et al. Chondrocyte secretome: a source of novel insights and exploratory biomarkers of osteoarthritis. Osteoarthritis Cartilage. 2017 Aug;25(8):1199–209.
- 42. Archer W Charles. The chondrocyte. Int J Biochem Cell Biol. 2003;(4):401–4.
- 43. Palazzo C, Nguyen C, Lefevre-Colau MM, Rannou F, Poiraudeau S. Risk factors and burden of osteoarthritis. Vol. 59, Annals of Physical and Rehabilitation Medicine. Elsevier Masson SAS; 2016. p. 134–8.
- 44. Yao Q, Wu X, Tao C, Gong W, Chen M, Qu M, et al. Osteoarthritis: pathogenic signaling pathways and therapeutic targets. Signal Transduct Target Ther. 2023;8(1).
- 45. Blasioli DJ, Kaplan DL. The Roles of Catabolic Factors in the Development of Osteoarthritis. Tissue Eng Part B Rev. 2014 Aug;20(4):355–63.
- 46. van der Kraan PM, van den Berg WB. Chondrocyte hypertrophy and osteoarthritis: role in initiation and progression of cartilage degeneration? Osteoarthritis Cartilage. 2012 Mar;20(3):223–32.
- 47. Jaswal AP, Bandyopadhyay A. Re-examining osteoarthritis therapy from a developmental biologist's perspective. Biochem Pharmacol. 2019 Jul;165:17–23.
- 48. Malemud CJ. Inhibition of MMPs and ADAM/ADAMTS. Biochem Pharmacol. 2019 Jul;165:33–40.
- 49. Kapila S, Wang W, Uston K. Matrix Metalloproteinase Induction by Relaxin Causes Cartilage Matrix Degradation in Target Synovial Joints. Ann N Y Acad Sci. 2009 Apr 10;1160(1):322–8.
- 50. Wang WM, Lee S, Steiglitz BM, Scott IC, Lebares CC, Allen ML, et al. Transforming Growth Factor-β Induces Secretion of Activated ADAMTS-2. Journal of Biological Chemistry. 2003 May;278(21):19549–57.
- 51. Sun Z, Yin Z, Liu C, Liang H, Jiang M, Tian J. IL-1β promotes ADAMTS enzymemediated aggrecan degradation through NF-κB in human intervertebral disc. J Orthop Surg Res. 2015 Dec 6;10(1):159.
- 52. Davidson RK, Waters JG, Kevorkian L, Darrah C, Cooper A, Donell ST, et al. Expression profiling of metalloproteinases and their inhibitors in synovium and cartilage. Arthritis Res Ther. 2006 Jul 19;8(4):R124.

- 53. Sanchez-Adams J, Leddy HA, McNulty AL, O'Conor CJ, Guilak F. The Mechanobiology of Articular Cartilage: Bearing the Burden of Osteoarthritis. Curr Rheumatol Rep. 2014 Oct 3;16(10):451.
- 54. Wang M, Sampson ER, Jin H, Li J, Ke QH, Im HJ, et al. MMP13 is a critical target gene during the progression of osteoarthritis. Arthritis Res Ther. 2013;15(1):R5.
- 55. Hamada D, Maynard R, Schott E, Drinkwater CJ, Ketz JP, Kates SL, et al. Suppressive Effects of Insulin on Tumor Necrosis Factor–Dependent Early Osteoarthritic Changes Associated With Obesity and Type 2 Diabetes Mellitus. Arthritis & Rheumatology. 2016 Jun 26;68(6):1392–402.
- Vincent TL. Il-1 in osteoarthritis: Time for a critical review of the literature [Internet].
  Vol. 8, F1000Research. F1000 Research Ltd; 2019 [cited 2021 Jun 4]. Available from: /pmc/articles/PMC6589928/
- 57. Jacques C, Gosset M, Berenbaum F, Gabay C. The Role of IL-1 and IL-1Ra in Joint Inflammation and Cartilage Degradation [Internet]. Vol. 74, Vitamins and Hormones. Vitam Horm; 2006 [cited 2021 Jun 4]. p. 371–403. Available from: https://pubmed.ncbi.nlm.nih.gov/17027524/
- 58. Araki Y, Tsuzuki Wada T, Aizaki Y, Sato K, Yokota K, Fujimoto K, et al. Histone Methylation and STAT-3 Differentially Regulate Interleukin-6–Induced Matrix Metalloproteinase Gene Activation in Rheumatoid Arthritis Synovial Fibroblasts. Arthritis & Rheumatology. 2016 May 27;68(5):1111–23.
- 59. Naito S, Shiomi T, Okada A, Kimura T, Chijiiwa M, Fujita Y, et al. Expression of ADAMTS4 (aggrecanase-1) in human osteoarthritic cartilage. Pathol Int. 2007 Nov 4;57(11):703–11.
- 60. Huang K, Wu L. Aggrecanase and Aggrecan Degradation in Osteoarthritis: A Review. Journal of International Medical Research. 2008 Dec 1;36(6):1149–60.
- 61. Naito S, Shiomi T, Okada A, Kimura T, Chijiiwa M, Fujita Y, et al. Expression of ADAMTS4 (aggrecanase-1) in human osteoarthritic cartilage. Pathol Int. 2007 Nov 4;57(11):703–11.
- 62. Bondeson J, Wainwright S, Hughes C, Caterson B. The regulation of the ADAMTS4 and ADAMTS5 aggrecanases in osteoarthritis: a review. Clin Exp Rheumatol. 2008;26(1):139–45.
- 63. Szentléleky E, Szegeczki V, Karanyicz E, Hajdú T, Tamás A, Tóth G, et al. Pituitary Adenylate Cyclase Activating Polypeptide (PACAP) Reduces Oxidative and

- Mechanical Stress-Evoked Matrix Degradation in Chondrifying Cell Cultures. Int J Mol Sci. 2019 Jan 4;20(1):168.
- 64. Nagase H, Kashiwagi M. Aggrecanases and cartilage matrix degradation. Arthritis Res Ther. 2003;5(2):94.
- 65. Li T, Peng J, Li Q, Shu Y, Zhu P, Hao L. The Mechanism and Role of ADAMTS Protein Family in Osteoarthritis. Biomolecules. 2022 Jul 8;12(7):959.
- 66. Dupuis LE, McCulloch DR, McGarity JD, Bahan A, Wessels A, Weber D, et al. Altered versican cleavage in ADAMTS5 deficient mice; A novel etiology of myxomatous valve disease. Dev Biol. 2011 Sep;357(1):152–64.
- 67. Dupuis LE, Osinska H, Weinstein MB, Hinton RB, Kern CB. Insufficient versican cleavage and Smad2 phosphorylation results in bicuspid aortic and pulmonary valves. J Mol Cell Cardiol. 2013 Jul;60:50–9.
- 68. Molnar V, Matišić V, Kodvanj I, Bjelica R, Jeleč Ž, Hudetz D, et al. Cytokines and Chemokines Involved in Osteoarthritis Pathogenesis. Int J Mol Sci. 2021 Aug 26;22(17):9208.
- 69. Rigoglou S, Papavassiliou AG. The NF-κB signalling pathway in osteoarthritis. Int J Biochem Cell Biol. 2013 Nov;45(11):2580–4.
- 70. Yao Q, Wu X, Tao C, Gong W, Chen M, Qu M, et al. Osteoarthritis: pathogenic signaling pathways and therapeutic targets. Vol. 8, Signal Transduction and Targeted Therapy. Springer Nature; 2023.
- 71. Fields JK, Günther S, Sundberg EJ. Structural Basis of IL-1 Family Cytokine Signaling. Front Immunol. 2019 Jun 20;10.
- 72. Boraschi D, Italiani P, Weil S, Martin MU. The family of the interleukin-1 receptors. Immunol Rev. 2018 Jan 16;281(1):197–232.
- 73. Martel-Pelletier J, Mccollum R, Dibattista J, Faure M, Chin JA, Fournier S, et al. The interleukin-1 receptor in normal and osteoarthritic human articular chondrocytes. Identification as the type I receptor and analysis of binding kinetics and biologic function. Arthritis Rheum. 1992 May 9;35(5):530–40.
- 74. Attur M, Statnikov A, Samuels J, Li Z, Alekseyenko AV, Greenberg JD, et al. Plasma levels of interleukin-1 receptor antagonist (IL1Ra) predict radiographic progression of symptomatic knee osteoarthritis. Osteoarthritis Cartilage. 2015 Nov;23(11):1915–24.
- 75. Araki Y, Tsuzuki Wada T, Aizaki Y, Sato K, Yokota K, Fujimoto K, et al. Histone Methylation and STAT-3 Differentially Regulate Interleukin-6–Induced Matrix

- Metalloproteinase Gene Activation in Rheumatoid Arthritis Synovial Fibroblasts. Arthritis & Rheumatology. 2016 May 27;68(5):1111–23.
- 76. Torzilli PA, Bhargava M, Chen CT. Mechanical Loading of Articular Cartilage Reduces IL-1-Induced Enzyme Expression. Cartilage. 2011 Oct 16;2(4):364–73.
- 77. Magnusson K, Scurrah K, Ystrom E, Ørstavik RE, Nilsen T, Steingrímsdóttir ÓA, et al. Genetic factors contribute more to hip than knee surgery due to osteoarthritis a population-based twin registry study of joint arthroplasty. Osteoarthritis Cartilage. 2017 Jun;25(6):878–84.
- 78. Spector TD, Cicuttini F, Baker J, Loughlin J, Hart D. Genetic influences on osteoarthritis in women: a twin study. BMJ. 1996 Apr 13;312(7036):940–3.
- 79. Zhai G, Stankovich J, Ding C, Scott F, Cicuttini F, Jones G. The genetic contribution to muscle strength, knee pain, cartilage volume, bone size, and radiographic osteoarthritis: A sibpair study. Arthritis Rheum. 2004 Mar;50(3):805–10.
- 80. Skousgaard SG, Skytthe A, Möller S, Overgaard S, Brandt LPA. Sex differences in risk and heritability estimates on primary knee osteoarthritis leading to total knee arthroplasty: a nationwide population based follow up study in Danish twins. Arthritis Res Ther. 2016 Dec 11;18(1):46.
- 81. Zhai G, Hart DJ, Kato BS, MacGregor A, Spector TD. Genetic influence on the progression of radiographic knee osteoarthritis: a longitudinal twin study. Osteoarthritis Cartilage. 2007 Feb;15(2):222–5.
- 82. Magnusson K, Turkiewicz A, Englund M. Nature vs nurture in knee osteoarthritis the importance of age, sex and body mass index. Osteoarthritis Cartilage. 2019 Apr 1;27(4):586–92.
- 83. Sacitharan PK. Ageing and Osteoarthritis. In 2019. p. 123–59.
- 84. Shane Anderson A, Loeser RF. Why is osteoarthritis an age-related disease? Best Pract Res Clin Rheumatol. 2010 Feb;24(1):15–26.
- 85. Felson DT. The epidemiology of knee osteoarthritis: Results from the framingham osteoarthritis study. Semin Arthritis Rheum. 1990 Dec;20(3):42–50.
- 86. JORDAN JM, HELMICK CG, RENNER JB, LUTA G, DRAGOMIR AD, WOODARD J, et al. Prevalence of Hip Symptoms and Radiographic and Symptomatic Hip Osteoarthritis in African Americans and Caucasians: The Johnston County Osteoarthritis Project. J Rheumatol. 2009 Apr;36(4):809–15.

- 87. Greene MA, Loeser RF. Aging-related inflammation in osteoarthritis. Osteoarthritis Cartilage [Internet]. 2015 Nov;23(11):1966–71. Available from: https://linkinghub.elsevier.com/retrieve/pii/S1063458415000217
- 88. Singh T, Newman AB. Inflammatory markers in population studies of aging. Ageing Res Rev. 2011 Jul;10(3):319–29.
- 89. Penninx BWJH, Abbas H, Ambrosius W, Nicklas BJ, Davis C, Messier SP, et al. Inflammatory markers and physical function among older adults with knee osteoarthritis. J Rheumatol. 2004 Oct;31(10):2027–31.
- 90. Morrisette-Thomas V, Cohen AA, Fülöp T, Riesco É, Legault V, Li Q, et al. Inflammaging does not simply reflect increases in pro-inflammatory markers. Mech Ageing Dev. 2014 Jul;139:49–57.
- 91. Goekoop RJ, Kloppenburg M, Kroon HM, Frölich M, Huizinga TWJ, Westendorp RGJ, et al. Low innate production of interleukin-1β and interleukin-6 is associated with the absence of osteoarthritis in old age. Osteoarthritis Cartilage. 2010 Jul;18(7):942–7.
- 92. de Hooge ASK, van de Loo FAJ, Bennink MB, Arntz OJ, de Hooge P, van den Berg WB. Male IL-6 gene knock out mice developed more advanced osteoarthritis upon aging. Osteoarthritis Cartilage. 2005 Jan;13(1):66–73.
- 93. Li YS, Xiao W feng, Luo W. Cellular aging towards osteoarthritis. Mech Ageing Dev. 2017 Mar;162:80–4.
- 94. Hou A, Chen P, Tang H, Meng H, Cheng X, Wang Y, et al. Cellular senescence in osteoarthritis and anti-aging strategies. Mech Ageing Dev. 2018 Oct;175:83–7.
- 95. Price JS, Waters JG, Darrah C, Pennington C, Edwards DR, Donell ST, et al. The role of chondrocyte senescence in osteoarthritis. Aging Cell. 2002 Oct 15;1(1):57–65.
- 96. Coppé JP, Patil CK, Rodier F, Sun Y, Muñoz DP, Goldstein J, et al. Senescence-Associated Secretory Phenotypes Reveal Cell-Nonautonomous Functions of Oncogenic RAS and the p53 Tumor Suppressor. PLoS Biol. 2008 Dec 2;6(12):e301.
- 97. Korenčič A, Košir R, Bordyugov G, Lehmann R, Rozman D, Herzel H. Timing of circadian genes in mammalian tissues. Sci Rep. 2014 Jul 22;4(1):5782.
- 98. Fagiani F, Di Marino D, Romagnoli A, Travelli C, Voltan D, Di Cesare Mannelli L, et al. Molecular regulations of circadian rhythm and implications for physiology and diseases. Signal Transduct Target Ther. 2022 Feb 8;7(1):41.
- 99. Dibner C, Schibler U, Albrecht U. The mammalian circadian timing system: Organization and coordination of central and peripheral clocks. Annual Review of Physiology. 2009.

- 100. Asher G, Sassone-Corsi P. Time for Food: The Intimate Interplay between Nutrition, Metabolism, and the Circadian Clock. Cell. 2015 Mar;161(1):84–92.
- 101. Dudek M, Pathiranage DRJ, Bano-Otalora B, Paszek A, Rogers N, Gonçalves CF, et al. Mechanical loading and hyperosmolarity as a daily resetting cue for skeletal circadian clocks. Nat Commun. 2023 Nov 14;14(1):7237.
- 102. Herzog ED, Hermanstyne T, Smyllie NJ, Hastings MH. Regulating the Suprachiasmatic Nucleus (SCN) Circadian Clockwork: Interplay between Cell-Autonomous and Circuit-Level Mechanisms. Cold Spring Harb Perspect Biol. 2017 Jan 3;9(1):a027706.
- 103. Hastings MH, Maywood ES, Brancaccio M. Generation of circadian rhythms in the suprachiasmatic nucleus. Nat Rev Neurosci. 2018 Aug 22;19(8):453–69.
- 104. Welsh DK, Takahashi JS, Kay SA. Suprachiasmatic nucleus: Cell autonomy and network properties. Annual Review of Physiology. 2009.
- 105. Herzog ED, Geusz ME, Khalsa SBS, Straume M, Block GD. Circadian rhythms in mouse suprachiasmatic nucleus explants on multimicroelectrode plates. Brain Res. 1997 May;757(2):285–90.
- 106. Buhr ED, Takahashi JS. Molecular components of the mammalian circadian clock. Handb Exp Pharmacol. 2013;217(217):3–27.
- 107. Reischl S, Vanselow K, Westermark PO, Thierfelder N, Maier B, Herzel H, et al. β-TrCP1-Mediated Degradation of PERIOD2 Is Essential for Circadian Dynamics. J Biol Rhythms. 2007 Oct 1;22(5):375–86.
- 108. Preitner N, Damiola F, Luis-Lopez-Molina, Zakany J, Duboule D, Albrecht U, et al. The orphan nuclear receptor REV-ERBα controls circadian transcription within the positive limb of the mammalian circadian oscillator. Cell. 2002;110(2):251–60.
- 109. Sato TK, Panda S, Miraglia LJ, Reyes TM, Rudic RD, McNamara P, et al. A functional genomics strategy reveals rora as a component of the mammalian circadian clock. Neuron. 2004;
- 110. DeBruyne JP, Weaver DR, Reppert SM. CLOCK and NPAS2 have overlapping roles in the suprachiasmatic circadian clock. Nat Neurosci. 2007 May 8;10(5):543–5.
- 111. Cox KH, Takahashi JS. Circadian clock genes and the transcriptional architecture of the clock mechanism. J Mol Endocrinol. 2019 Nov;63(4):R93–102.
- 112. Yeung J, Mermet J, Jouffe C, Marquis J, Charpagne A, Gachon F, et al. Transcription factor activity rhythms and tissue-specific chromatin interactions explain circadian gene expression across organs. Genome Res. 2018 Feb;28(2):182–91.

- 113. Yan J, Wang H, Liu Y, Shao C. Analysis of gene regulatory networks in the mammalian circadian rhythm. PLoS Comput Biol. 2008;
- 114. Damiola F, Le Minli N, Preitner N, Kornmann B, Fleury-Olela F, Schibler U. Restricted feeding uncouples circadian oscillators in peripheral tissues from the central pacemaker in the suprachiasmatic nucleus. Genes Dev. 2000;
- 115. Hara R, Wan K, Wakamatsu H, Aida R, Moriya T, Akiyama M, et al. Restricted feeding entrains liver clock without participation of the suprachiasmatic nucleus. Genes to Cells. 2001 Mar 7;6(3):269–78.
- 116. Yang N, Meng QJ. Circadian clocks in articular cartilage and bone: A compass in the sea of matrices. J Biol Rhythms. 2016;31(5):415–27.
- 117. Turek FW, Joshu C, Kohsaka A, Lin E, Ivanova G, McDearmon E, et al. Obesity and Metabolic Syndrome in Circadian *Clock* Mutant Mice. Science (1979). 2005 May 13;308(5724):1043–5.
- 118. Simmons DJ. Diurnal periodicity in epiphyseal growth cartilage. Nature. 1962;
- 119. Igarashi K, Saeki S, Shinoda H. Diurnal rhythms in the incorporation and secretion of <sup>3</sup> H-proline and <sup>3</sup> H-galactose by cartilage cells and osteoblasts in various bone-forming sites in growing rats. Orthodontic Waves. 2013 Mar 1;72(1):11–5.
- 120. Yu S, Tang Q, Xie M, Zhou X, Long Y, Xie Y, et al. Circadian BMAL1 regulates mandibular condyle development by hedgehog pathway. Cell Prolif. 2020 Jan 20;53(1).
- 121. Song X, Ma T, Hu H, Zhao M, Bai H, Wang X, et al. Chronic Circadian Rhythm Disturbance Accelerates Knee Cartilage Degeneration in Rats Accompanied by the Activation of the Canonical Wnt/β-Catenin Signaling Pathway. Front Pharmacol. 2021 Nov 11;12.
- 122. Akagi R, Akatsu Y, Fisch KM, Alvarez-Garcia O, Teramura T, Muramatsu Y, et al. Dysregulated circadian rhythm pathway in human osteoarthritis: NR1D1 and BMAL1 suppression alters TGF-β signaling in chondrocytes. Osteoarthritis Cartilage. 2017 Jun;25(6):943–51.
- 123. Dudek M, Yang N, Ruckshanthi JPD, Williams J, Borysiewicz E, Wang P, et al. The intervertebral disc contains intrinsic circadian clocks that are regulated by age and cytokines and linked to degeneration. Ann Rheum Dis. 2017;76(3):576–84.
- 124. Dudek M, Morris H, Rogers N, Pathiranage DR, Chan D, Kadler KE, et al. The clock transcription factor BMAL1 is a key regulator of extracellular matrix homeostasis and cell fate in the intervertebral disc. 2023.

- 125. Dudek M, Gossan N, Yang N, Im HJ, Ruckshanthi JPD, Yoshitane H, et al. The chondrocyte clock gene Bmall controls cartilage homeostasis and integrity. Journal of Clinical Investigation. 2016 Jan 4;126(1):365–76.
- 126. Yoo SH, Yamazaki S, Lowrey PL, Shimomura K, Ko CH, Buhr ED, et al. PERIOD2::LUCIFERASE real-time reporting of circadian dynamics reveals persistent circadian oscillations in mouse peripheral tissues. Proc Natl Acad Sci U S A [Internet]. 2004 Apr 13 [cited 2021 Jun 9];101(15):5339–46. Available from: /pmc/articles/PMC397382/
- 127. Gossan N, Zeef L, Hensman J, Hughes A, Bateman JF, Rowley L, et al. The circadian clock in murine chondrocytes regulates genes controlling key aspects of cartilage homeostasis. Arthritis Rheum. 2013;
- 128. Sekiya I, Vuoristo JT, Larson BL, Prockop DJ. *In vitro* cartilage formation by human adult stem cells from bone marrow stroma defines the sequence of cellular and molecular events during chondrogenesis. Proceedings of the National Academy of Sciences. 2002 Apr 2;99(7):4397–402.
- 129. Liu B, Cheng H, Ma W, Gong F, Wang X, Duan N, et al. Common variants in the GNL3 contribute to the increasing risk of knee osteoarthritis in Han Chinese population. Sci Rep. 2018;
- 130. Chen G, Zhao H, Ma S, Chen L, Wu G, Zhu Y, et al. Circadian Rhythm Protein Bmall Modulates Cartilage Gene Expression in Temporomandibular Joint Osteoarthritis via the MAPK/ERK Pathway. Front Pharmacol. 2020;11(September):1–12.
- 131. Dudek M, Angelucci C, Pathiranage D, Wang P, Mallikarjun V, Lawless C, et al. Circadian time series proteomics reveals daily dynamics in cartilage physiology. Osteoarthritis Cartilage. 2021 May 1;29(5):739–49.
- 132. Chang J, Garva R, Pickard A, Yeung CYC, Mallikarjun V, Swift J, et al. Circadian control of the secretory pathway maintains collagen homeostasis Europe PMC Funders Group. Nat Cell Biol. 2020;22(1):74–86.
- 133. Rogers N, Meng QJ. Tick tock, the cartilage clock. Osteoarthritis Cartilage. 2023 Nov;31(11):1425–36.
- 134. Fu S, Kuwahara M, Uchida Y, Kondo S, Hayashi D, Shimomura Y, et al. Circadian production of melatonin in cartilage modifies rhythmic gene expression. Journal of Endocrinology. 2019;

- 135. Snelling SJB, Forster A, Mukherjee S, Price AJ, Poulsen RC. The chondrocyte-intrinsic circadian clock is disrupted in human osteoarthritis. Chronobiol Int. 2016 May 27;33(5):574–9.
- 136. Yang W, Kang X, Liu J, Li H, Ma Z, Jin X, et al. Clock gene Bmal1 modulates human cartilage gene expression by crosstalk with Sirt1. Endocrinology. 2016;157(8):3096–107.
- 137. Bekki H, Duffy T, Okubo N, Olmer M, Alvarez-Garcia O, Lamia K, et al. Suppression of circadian clock protein cryptochrome 2 promotes osteoarthritis. Osteoarthritis Cartilage. 2020 Jul;28(7):966–76.
- 138. Dernie F, Adeyoju D. A matter of time: Circadian clocks in osteoarthritis and the potential of chronotherapy. Exp Gerontol. 2021 Jan;143:111163.
- 139. Thielen N, van der Kraan P, van Caam A. TGFβ/BMP Signaling Pathway in Cartilage Homeostasis. Cells. 2019 Aug 24;8(9):969.
- 140. Guo B, Yang N, Borysiewicz E, Dudek M, Williams JL, Li J, et al. Catabolic cytokines disrupt the circadian clock and the expression of clock-controlled genes in cartilage via an NFκB-dependent pathway. Osteoarthritis Cartilage. 2015 Nov;23(11):1981–8.
- 141. Pferdehirt L, Damato AR, Dudek M, Meng QJ, Herzog ED, Guilak F. Synthetic gene circuits for preventing disruption of the circadian clock due to interleukin-1–induced inflammation. Sci Adv. 2022 May 27;8(21).
- 142. Khapre R V., Kondratova AA, Susova O, Kondratov R V. Circadian clock protein BMAL1 regulates cellular senescence in vivo. Cell Cycle. 2011 Dec 28;10(23):4162–9.
- 143. Gabay O, Sanchez C, Dvir-Ginzberg M, Gagarina V, Zaal KJ, Song Y, et al. Sirtuin 1 enzymatic activity is required for cartilage homeostasis in vivo in a mouse model. Arthritis Rheum. 2013 Jan 27;65(1):159–66.
- 144. Gossan N, Boot-Handford R, Meng QJ. Ageing and osteoarthritis: a circadian rhythm connection. Biogerontology. 2015 Apr 31;16(2):209–19.
- 145. Nakahata Y, Sahar S, Astarita G, Kaluzova M, Sassone-Corsi P. Circadian Control of the NAD + Salvage Pathway by CLOCK-SIRT1. Science (1979). 2009 May;324(5927):654–7.
- 146. Chang HC, Guarente L. SIRT1 Mediates Central Circadian Control in the SCN by a Mechanism that Decays with Aging. Cell. 2013 Jun;153(7):1448–60.
- 147. Ramsey KM, Yoshino J, Brace CS, Abrassart D, Kobayashi Y, Marcheva B, et al. Circadian Clock Feedback Cycle Through NAMPT-Mediated NAD <sup>+</sup> Biosynthesis. Science (1979). 2009 May;324(5927):651–4.

- 148. Berenbaum F. Osteoarthritis as an inflammatory disease (osteoarthritis is not osteoarthrosis!). Osteoarthritis Cartilage. 2013 Jan;21(1):16–21.
- 149. SHERMAN B, WYSHAM W, PFOH B. Age-Related Changes in the Circadian Rhythm of Plasma Cortisol in Man\*. J Clin Endocrinol Metab. 1985 Sep;61(3):439–43.
- 150. Joseph F, Chan BY, Durham BH, Ahmad AM, Vinjamuri S, Gallagher JA, et al. The Circadian Rhythm of Osteoprotegerin and Its Association with Parathyroid Hormone Secretion. J Clin Endocrinol Metab. 2007 Aug 1;92(8):3230–8.
- 151. Guo B, Yang N, Borysiewicz E, Dudek M, Williams JL, Li J, et al. Catabolic cytokines disrupt the circadian clock and the expression of clock-controlled genes in cartilage via an NFkB-dependent pathway. Osteoarthritis Cartilage. 2015;23(11):1981–8.
- 152. Gebert LFR, MacRae IJ. Regulation of microRNA function in animals. Nat Rev Mol Cell Biol. 2019 Jan 14;20(1):21–37.
- 153. Gu J, Rao W, Huo S, Fan T, Qiu M, Zhu H, et al. MicroRNAs and long non-coding RNAs in cartilage homeostasis and osteoarthritis. Front Cell Dev Biol. 2022 Dec 13;10.
- 154. Liu B, Shyr Y, Cai J, Liu Q. Interplay between miRNAs and host genes and their role in cancer. Brief Funct Genomics. 2019 Jul 22;18(4):255–66.
- 155. O'Brien J, Hayder H, Zayed Y, Peng C. Overview of microRNA biogenesis, mechanisms of actions, and circulation. Front Endocrinol (Lausanne). 2018;9(AUG):1–12.
- 156. Gulyaeva LF, Kushlinskiy NE. Regulatory mechanisms of microRNA expression. J Transl Med. 2016 Dec 20;14(1):143.
- 157. Vilimova M, Pfeffer S. Post-transcriptional regulation of polycistronic <scp>microRNAs</scp>. WIREs RNA. 2023 Mar 14;14(2).
- 158. Lao TD, Huyen Le TA. MicroRNAs: Biogenesis, functions and potential biomarkers for early screening, prognosis and therapeutic molecular monitoring of nasopharyngeal carcinoma. Vol. 8, Processes. MDPI AG; 2020.
- 159. Ha M, Kim VN. Regulation of microRNA biogenesis. Nat Rev Mol Cell Biol. 2014 Aug 16;15(8):509–24.
- 160. Gu W, Xu Y, Xie X, Wang T, Ko JH, Zhou T. The role of RNA structure at 5' untranslated region in microRNA-mediated gene regulation. RNA. 2014 Sep;20(9):1369–75.
- 161. Ørom UA, Nielsen FC, Lund AH. MicroRNA-10a Binds the 5'UTR of Ribosomal Protein mRNAs and Enhances Their Translation. Mol Cell. 2008 May;30(4):460–71.

- 162. MacFarlane LA, R. Murphy P. MicroRNA: Biogenesis, Function and Role in Cancer. Curr Genomics. 2010 Nov 1;11(7):537–61.
- 163. Sadakierska-Chudy A. MicroRNAs: Diverse Mechanisms of Action and Their Potential Applications as Cancer Epi-Therapeutics. Biomolecules. 2020 Sep 7;10(9):1285.
- 164. Meijer HA, Kong YW, Lu WT, Wilczynska A, Spriggs R V., Robinson SW, et al. Translational Repression and eIF4A2 Activity Are Critical for MicroRNA-Mediated Gene Regulation. Science (1979). 2013 Apr 5;340(6128):82–5.
- 165. Chen R, D'Alessandro M, Lee C. MiRNAs are required for generating a time delay critical for the circadian oscillator. Current Biology. 2013 Oct 21;23(20):1959–68.
- 166. Kinoshita C, Okamoto Y, Aoyama K, Nakaki T. MicroRNA: A Key Player for the Interplay of Circadian Rhythm Abnormalities, Sleep Disorders and Neurodegenerative Diseases. Clocks Sleep. 2020 Jul 23;2(3):282–307.
- 167. Cheng HYM, Papp JW, Varlamova O, Dziema H, Russell B, Curfman JP, et al. microRNA Modulation of Circadian-Clock Period and Entrainment. Neuron. 2007;
- 168. Mendoza-Viveros L, Chiang CK, Ong JLK, Hegazi S, Cheng AH, Bouchard-Cannon P, et al. miR-132/212 Modulates Seasonal Adaptation and Dendritic Morphology of the Central Circadian Clock. Cell Rep. 2017 Apr 18;19(3):505–20.
- 169. Alvarez-Saavedra M, Antoun G, Yanagiya A, Oliva-Hernandez R, Cornejo-Palma D, Perez-Iratxeta C, et al. miRNA-132 orchestrates chromatin remodeling and translational control of the circadian clock. Hum Mol Genet. 2011;
- 170. Gatfield D, Le Martelot G, Vejnar CE, Gerlach D, Schaad O, Fleury-Olela F, et al. Integration of microRNA miR-122 in hepatic circadian gene expression. Genes Dev [Internet]. 2009 Jun 1 [cited 2022 Dec 1];23(11):1313–26. Available from: http://genesdev.cshlp.org/content/23/11/1313.full
- 171. Shende VR, Neuendorff N, Earnest DJ. Role of miR-142-3p in the Post-Transcriptional Regulation of the Clock Gene Bmall in the Mouse SCN. PLoS One. 2013 Jun 5;8(6):e65300.
- 172. Yan Y, Salazar TE, Dominguez JM, Nguyen D V., Li Calzi S, Bhatwadekar AD, et al. Dicer Expression Exhibits a Tissue-Specific Diurnal Pattern That Is Lost during Aging and in Diabetes. PLoS One. 2013 Nov 7;8(11):e80029.
- 173. Zhao X, Zhu X, Cheng S, Xie Y, Wang Z, Liu Y, et al. MiR-29a/b/c regulate human circadian gene & amp;lt;italic>hPER1</italic&amp;gt; expression by targeting its 3&amp;prime;UTR. Acta Biochim Biophys Sin (Shanghai). 2014 Apr 1;46(4):313–7.

- 174. Yoo SH, Kojima S, Shimomura K, Koike N, Buhr ED, Furukawa T, et al. *Period2* 3′-UTR and microRNA-24 regulate circadian rhythms by repressing PERIOD2 protein accumulation. Proceedings of the National Academy of Sciences. 2017 Oct 17;114(42).
- 175. Mauvoisin D, Wang J, Jouffe C, Martin E, Atger F, Waridel P, et al. Circadian clock-dependent and -independent rhythmic proteomes implement distinct diurnal functions in mouse liver. Proceedings of the National Academy of Sciences. 2014 Jan 7;111(1):167–72.
- 176. Chen L, Zhang B, Yang L, Bai YG, Song JB, Ge YL, et al. BMAL1 Disrupted Intrinsic Diurnal Oscillation in Rat Cerebrovascular Contractility of Simulated Microgravity Rats by Altering Circadian Regulation of miR-103/CaV1.2 Signal Pathway. Int J Mol Sci. 2019 Aug 14;20(16):3947.
- 177. Hong Z, Feng Z, Sai Z, Tao S. PER3, a novel target of miR-103, plays a suppressive role in colorectal cancer in vitro. BMB Rep. 2014 Sep 30;47(9):500–5.
- 178. Shende VR, Goldrick MM, Ramani S, Earnest DJ. Expression and Rhythmic Modulation of Circulating MicroRNAs Targeting the Clock Gene Bmall in Mice. PLoS One. 2011 Jul 22;6(7):e22586.
- 179. Zhang W, Wang P, Chen S, Zhang Z, Liang T, Liu C. Rhythmic expression of miR-27b-3p targets the clock gene *Bmal1* at the posttranscriptional level in the mouse liver. The FASEB Journal. 2016 Jun 14;30(6):2151–60.
- 180. Gao Q, Zhou L, Yang SY, Cao JM. A novel role of microRNA 17-5p in the modulation of circadian rhythm. Sci Rep. 2016 Jul 21;6(1):30070.
- 181. Zhou W, Li Y, Wang X, Wu L, Wang Y. MiR-206-mediated dynamic mechanism of the mammalian circadian clock. BMC Syst Biol. 2011 Dec 9;5(1):141.
- 182. Zou Y, Lin X, Bu J, Lin Z, Chen Y, Qiu Y, et al. Timeless-Stimulated miR-5188-FOXO1/β-Catenin-c-Jun Feedback Loop Promotes Stemness via Ubiquitination of β-Catenin in Breast Cancer. Molecular Therapy. 2020 Jan;28(1):313–27.
- 183. Zhou L, Miller C, Miraglia LJ, Romero A, Xu S, Mure LS, et al. A genome-wide microRNA screen identifies the microRNA-183/96/182 cluster as a modulator of circadian rhythms. Proceedings of the National Academy of Sciences. 2021 Jan 5;118(1).
- 184. Nagel R, Clijsters L, Agami R. The miRNA-192/194 cluster regulates the *Period* gene family and the circadian clock. FEBS J. 2009 Oct 14;276(19):5447–55.
- 185. Hong Z, Feng Z, Sai Z, Tao S. PER3, a novel target of miR-103, plays a suppressive role in colorectal cancer in vitro. BMB Rep. 2014 Sep 30;47(9):500–5.

- 186. Yuan P, Yang T, Mu J, Zhao J, Yang Y, Yan Z, et al. Circadian clock gene NPAS2 promotes reprogramming of glucose metabolism in hepatocellular carcinoma cells. Cancer Lett. 2020 Jan;469:498–509.
- 187. Zheng X, Wu K, Liao S, Pan Y, Sun Y, Chen X, et al. MicroRNA-transcription factor network analysis reveals miRNAs cooperatively suppress RORA in oral squamous cell carcinoma. Oncogenesis. 2018 Oct 8;7(10):79.
- 188. Wang Y, Lv K, Chen H, Zhao M, Ji G, Zhang Y, et al. Functional annotation of extensively and divergently expressed miRNAs in suprachiasmatic nucleus of *Clock* Δ19 mutant mice. Biosci Rep. 2018 Dec 21;38(6).
- 189. Horii R, Honda M, Shirasaki T, Shimakami T, Shimizu R, Yamanaka S, et al. MicroRNA-10a Impairs Liver Metabolism in Hepatitis C Virus-Related Cirrhosis Through Deregulation of the Circadian Clock Gene Brain and Muscle Aryl Hydrocarbon Receptor Nuclear Translocator-Like 1. Hepatol Commun. 2019 Dec 26;3(12):1687–703.
- 190. Lee KH, Kim SH, Lee HR, Kim W, Kim DY, Shin JC, et al. MicroRNA-185 oscillation controls circadian amplitude of mouse Cryptochrome 1 via translational regulation. Mol Biol Cell. 2013 Jul 15;24(14):2248–55.
- 191. Kobayashi T, Lu J, Cobb BS, Rodda SJ, Mcmahon AP, Schipani E, et al. Dicerdependent pathways regulate chondrocyte proliferation and differentiation. 2008;105(6).
- 192. McAlinden A, Varghese N, Wirthlin L, Chang LW. Differentially Expressed MicroRNAs in Chondrocytes from Distinct Regions of Developing Human Cartilage. PLoS One. 2013 Sep 9;8(9):e75012.
- 193. Papaioannou G, Inloes JB, Nakamura Y, Paltrinieri E, Kobayashi T. let-7 and miR-140 microRNAs coordinately regulate skeletal development. Proceedings of the National Academy of Sciences. 2013 Aug 27;110(35).
- 194. Jouan Y, Bouchemla Z, Bardèche-Trystram B, Sana J, Andrique C, Ea HK, et al. Lin28a induces SOX9 and chondrocyte reprogramming via HMGA2 and blunts cartilage loss in mice. Sci Adv. 2022 Aug 26;8(34).
- 195. Eberhart JK, He X, Swartz ME, Yan YL, Song H, Boling TC, et al. MicroRNA Mirn140 modulates Pdgf signaling during palatogenesis. Nat Genet. 2008 Mar 10;40(3):290–8.
- 196. Nakamura Y, He X, Kato H, Wakitani S, Kobayashi T, Watanabe S, et al. Sox9 is upstream of microRNA-140 in cartilage. Appl Biochem Biotechnol. 2012;166(1):64–71.

- 197. Paddy P, Submitted T, The FOR, Of D, Of D. MICRORNA-455 IN CARTILAGE AND SKELETAL DEVELOPMENT. 2021;
- 198. Yang J, Qin S, Yi C, Ma G, Zhu H, Zhou W, et al. MiR-140 is co-expressed with Wwp2-C transcript and activated by Sox9 to target Sp1 in maintaining the chondrocyte proliferation. FEBS Lett. 2011;
- 199. Miyaki S, Sato T, Inoue A, Otsuki S, Ito Y, Yokoyama S, et al. MicroRNA-140 plays dual roles in both cartilage development and homeostasis. 2010;1173–85.
- 200. Tuddenham L, Wheeler G, Ntounia-Fousara S, Waters J, Hajihosseini MK, Clark I, et al. The cartilage specific microRNA-140 targets histone deacetylase 4 in mouse cells. FEBS Lett. 2006 Jul 24;580(17):4214–7.
- 201. Karlsen TA, Jakobsen RB, Mikkelsen TS, Brinchmann JE. MicroRNA-140 targets RALA and regulates chondrogenic differentiation of human mesenchymal stem cells by translational enhancement of SOX9 and ACAN. Stem Cells Dev. 2014;
- 202. Pais H, Nicolas FE, Soond SM, Swingler TE, Clark IM, Chantry A, et al. Analyzing mRNA expression identifies Smad3 as a microRNA-140 target regulated only at protein level. RNA. 2010;
- 203. Guérit D, Philipot D, Chuchana P, Toupet K, Brondello JM, Mathieu M, et al. Sox9-Regulated miRNA-574-3p Inhibits Chondrogenic Differentiation of Mesenchymal Stem Cells. PLoS One. 2013 Apr 23;8(4):e62582.
- 204. Cong L, Zhu Y, Tu G. A bioinformatic analysis of microRNAs role in osteoarthritis. 2017;25(155):1362–71.
- 205. Coutinho De Almeida R, Ramos YFM, Mahfouz A, Den Hollander W, Lakenberg N, Houtman E, et al. RNA sequencing data integration reveals an miRNA interactome of osteoarthritis cartilage. Ann Rheum Dis. 2019 Feb 1;78(2):270–7.
- 206. Yang Z, Wang J, Pan Z, Zhang Y. miR-143-3p regulates cell proliferation and apoptosis by targeting IGF1R and IGFBP5 and regulating the Ras/p38 MAPK signaling pathway in rheumatoid arthritis. Exp Ther Med. 2018 Feb 28;
- 207. Zacharjasz J, Mleczko AM, Bąkowski P, Piontek T, Bąkowska-Żywicka K. Small Noncoding RNAs in Knee Osteoarthritis: The Role of MicroRNAs and tRNA-Derived Fragments. Int J Mol Sci. 2021 May 27;22(11):5711.
- 208. Li ZC, Han N, Li X, Li G, Liu YZ, Sun GX, et al. Decreased expression of microRNA-130a correlates with TNF-α in the development of osteoarthritis. Int J Clin Exp Pathol. 2015;8(3):2555–64.

- 209. Yin X, Wang JQ, Yan SY. Reduced miR-26a and miR-26b expression contributes to the pathogenesis of osteoarthritis via the promotion of p65 translocation. Mol Med Rep. 2017;
- 210. Xie Q, Wei M, Kang X, Liu D, Quan Y, Pan X, et al. Reciprocal inhibition between *miR-26a* and NF-κB regulates obesity-related chronic inflammation in chondrocytes. Biosci Rep. 2015 Jun 1;35(3).
- 211. Iliopoulos D, Malizos KN, Oikonomou P, Tsezou A. Integrative MicroRNA and proteomic approaches identify novel osteoarthritis genes and their collaborative metabolic and inflammatory networks. PLoS One. 2008;
- 212. Yamasaki K, Nakasa T, Miyaki S, Ishikawa M, Deie M, Adachi N, et al. Expression of microRNA-146a in osteoarthritis cartilage. Arthritis Rheum. 2009;
- 213. Wang JH, Shih KS, Wu YW, Wang AW, Yang CR. Histone deacetylase inhibitors increase microRNA-146a expression and enhance negative regulation of interleukin-1β signaling in osteoarthritis fibroblast-like synoviocytes. Osteoarthritis Cartilage. 2013 Dec;21(12):1987–96.
- 214. Zhang F, Wang J, Chu J, Yang C, Xiao H, Zhao C, et al. MicroRNA-146a Induced by Hypoxia Promotes Chondrocyte Autophagy through Bcl-2. Cellular Physiology and Biochemistry. 2015;37(4):1442–53.
- 215. Li J, Huang J, Dai L, Yu D, Chen Q, Zhang X, et al. MiR-146a, an IL-1β responsive miRNA, induces vascular endothelial growth factor and chondrocyte apoptosis by targeting Smad4. Arthritis Res Ther. 2012;
- 216. Tardif G, Hum D, Pelletier JP, Duval N, Martel-Pelletier J. Regulation of the IGFBP-5 and MMP-13 genes by the microRNAs miR-140 and miR-27a in human osteoarthritic chondrocytes. BMC Musculoskelet Disord. 2009;10(1):1–11.
- 217. Papathanasiou I, Balis C, Trachana V, Mourmoura E, Tsezou A. The synergistic function of miR-140–5p and miR-146a on TLR4-mediated cytokine secretion in osteoarthritic chondrocytes. Biochem Biophys Res Commun. 2020 Feb;522(3):783–91.
- 218. Y. Hao DTMRSCDYoungN. CHARACTERISATION OF MICE LACKING MIR-140 AND ITS HOST GENE WWP2. Osteoarthritis Cartilage. 2018;26.
- 219. Zhang M, Liu L, Xiao T, Guo W. [Detection of the expression level of miR-140 using realtime fluorescent quantitative PCR in knee synovial fluid of osteoarthritis patients]. Zhong Nan Da Xue Xue Bao Yi Xue Ban. 2012 Dec;37(12):1210–4.
- 220. Duan L, Liang Y, Xu X, Xiao Y, Wang D. Recent progress on the role of miR-140 in cartilage matrix remodelling and its implications for osteoarthritis treatment [Internet].

- Vol. 22, Arthritis Research and Therapy. BioMed Central; 2020 [cited 2021 Jun 4]. p. 1–9. Available from: https://doi.org/10.1186/s13075-020-02290-0
- 221. Tao SC, Yuan T, Zhang YL, Yin WJ, Guo SC, Zhang CQ. Exosomes derived from miR-140-5p-overexpressing human synovial mesenchymal stem cells enhance cartilage tissue regeneration and prevent osteoarthritis of the knee in a rat model. Theranostics. 2017;
- 222. Swingler TE, Niu L, Smith P, Paddy P, Le L, Barter MJ, et al. The function of microRNAs in cartilage and osteoarthritis. Clin Exp Rheumatol. 2019;37(5):40–7.
- 223. Shi S, Zhang L, Wang Q, Wang Q, Li D, Sun W, et al. Targeting Cartilage miR-195/497 Cluster for Osteoarthritis Treatment Regulates the Circadian Clock. Gerontology. 2024;70(1):59–75.
- 224. Ko JY, Wang FS, Lian WS, Fang HC, Kuo SJ. Cartilage-specific knockout of miRNA-128a expression normalizes the expression of circadian clock genes (CCGs) and mitigates the severity of osteoarthritis. Biomed J. 2024 Apr;47(2):100629.
- 225. Swingler TE, Horne R, Meng Q, Clark IM. microRNA-455 is regulated in a circadian manner and targets a number of components of the circadian rhythm. Osteoarthritis Cartilage [Internet]. 26(2018):S164–5. Available from: https://doi.org/10.1016/j.joca.2018.02.358
- 226. Diendorfer A, Khamina K, Pultar M, Hackl M. miND (miRNA NGS Discovery pipeline): a small RNA-seq analysis pipeline and report generator for microRNA biomarker discovery studies. F1000Res. 2022 Feb 24;11:233.
- 227. Andrews S. FASTQC. A quality control tool for high throughput sequence data. 2010;
- 228. Ewels P, Magnusson M, Lundin S, Käller M. MultiQC: summarize analysis results for multiple tools and samples in a single report. Bioinformatics. 2016 Oct 1;32(19):3047–8.
- 229. Zerbino DR, Achuthan P, Akanni W, Amode MR, Barrell D, Bhai J, et al. Ensembl 2018. Nucleic Acids Res. 2018 Jan 4;46(D1):D754–61.
- 230. Friedländer MR, Chen W, Adamidi C, Maaskola J, Einspanier R, Knespel S, et al. Discovering microRNAs from deep sequencing data using miRDeep. Nat Biotechnol. 2008 Apr;26(4):407–15.
- 231. Sweeney BA, Petrov AI, Burkov B, Finn RD, Bateman A, Szymanski M, et al. RNAcentral: a hub of information for non-coding RNA sequences. Nucleic Acids Res. 2019 Jan 8;47(D1):D221–9.

- 232. Love MI, Huber W, Anders S. Moderated estimation of fold change and dispersion for RNA-seq data with DESeq2. Genome Biol. 2014 Dec 5;15(12):550.
- 233. Zhang Y, Parmigiani G, Johnson WE. ComBat-seq: batch effect adjustment for RNA-seq count data. NAR Genom Bioinform. 2020 Sep 1;2(3).
- 234. Thaben PF, Westermark PO. Detecting Rhythms in Time Series with RAIN. J Biol Rhythms. 2014 Dec 17;29(6):391–400.
- 235. Chen EY, Tan CM, Kou Y, Duan Q, Wang Z, Meirelles GV, et al. Enrichr: interactive and collaborative HTML5 gene list enrichment analysis tool. BMC Bioinformatics. 2013 Dec 15;14(1):128.
- 236. Gossan N, Zeef L, Hensman J, Hughes A, Bateman JF, Rowley L, et al. The circadian clock in murine chondrocytes regulates genes controlling key aspects of cartilage homeostasis. Arthritis Rheum. 2013 Aug;65(9):2334–45.
- 237. Ito Y, Matsuzaki T, Ayabe F, Mokuda S, Kurimoto R, Matsushima T, et al. Both microRNA-455-5p and -3p repress hypoxia-inducible factor-2α expression and coordinately regulate cartilage homeostasis. Nat Commun. 2021 Jul 6;12(1):4148.
- 238. Zhang Z, Hou C, Meng F, Zhao X, Zhang Z, Huang G, et al. MiR-455-3p regulates early chondrogenic differentiation via inhibiting Runx2. FEBS Lett. 2015 Nov 30;589(23):3671–8.
- 239. Sun Y, Zhao J, Wu Q, Zhang Y, You Y, Jiang W, et al. Chondrogenic primed extracellular vesicles activate miR-455/SOX11/FOXO axis for cartilage regeneration and osteoarthritis treatment. NPJ Regen Med. 2022 Sep 16;7(1):53.
- 240. Xie F, Xiao P, Chen D, Xu L, Zhang B. miRDeepFinder: a miRNA analysis tool for deep sequencing of plant small RNAs. Plant Mol Biol. 2012 Sep 31;80(1):75–84.
- 241. Luzak B, Siarkiewicz P, Boncler M. An evaluation of a new high-sensitivity PrestoBlue assay for measuring cell viability and drug cytotoxicity using EA.hy926 endothelial cells. Toxicology in Vitro. 2022 Sep;83:105407.
- 242. Gossan N, Boot-Handford R, Meng QJ. Ageing and osteoarthritis: a circadian rhythm connection. Biogerontology. 2015;16(2):209–19.
- 243. Fourier C, Ran C, Sjöstrand C, Waldenlind E, Steinberg A, Belin AC. The molecular clock gene cryptochrome 1 ( *CRYI* ) and its role in cluster headache. Cephalalgia. 2021 Nov 13;41(13):1374–81.
- 244. Kim M, de la Peña JB, Cheong JH, Kim HJ. Neurobiological Functions of the Period Circadian Clock 2 Gene, *Per2*. Biomol Ther (Seoul). 2018 Jul 1;26(4):358–67.

- 245. Woods S, Charlton S, Cheung K, Hao Y, Soul J, Reynard LN, et al. microRNA-seq of cartilage reveals an overabundance of miR-140-3p which contains functional isomiRs. RNA. 2020 Nov;26(11):1575–88.
- 246. Shende VR, Goldrick MM, Ramani S, Earnest DJ. Expression and Rhythmic Modulation of Circulating MicroRNAs Targeting the Clock Gene Bmall in Mice. PLoS One. 2011 Jul 22;6(7):e22586.
- 247. Marzi MJ, Ghini F, Cerruti B, de Pretis S, Bonetti P, Giacomelli C, et al. Degradation dynamics of microRNAs revealed by a novel pulse-chase approach. Genome Res. 2016 Apr;26(4):554–65.
- 248. Vágó J, Katona É, Takács R, Dócs K, Hajdú T, Kovács P, et al. Cyclic uniaxial mechanical load enhances chondrogenesis through entraining the molecular circadian clock. J Pineal Res. 2022 Nov 2;73(4).
- 249. Rey G, Cesbron F, Rougemont J, Reinke H, Brunner M, Naef F. Genome-Wide and Phase-Specific DNA-Binding Rhythms of BMAL1 Control Circadian Output Functions in Mouse Liver. PLoS Biol. 2011 Feb 22;9(2):e1000595.
- 250. Kriebs A, Jordan SD, Soto E, Henriksson E, Sandate CR, Vaughan ME, et al. Circadian repressors CRY1 and CRY2 broadly interact with nuclear receptors and modulate transcriptional activity. Proceedings of the National Academy of Sciences. 2017 Aug 15;114(33):8776–81.
- 251. Gutierrez-Monreal MA, Cuevas-Diaz Duran R, Moreno-Cuevas JE, Scott SP. A Role for 1α,25-Dihydroxyvitamin D 3 in the Expression of Circadian Genes. J Biol Rhythms. 2014 Oct 17;29(5):384–8.
- 252. Chen W, Chen L, Zhang Z, Meng F, Huang G, Sheng P, et al. MicroRNA-455-3p modulates cartilage development and degeneration through modification of histone H3 acetylation. Biochim Biophys Acta Mol Cell Res. 2016;
- 253. Hu S, Zhao X, Mao G, Zhang Z, Wen X, Zhang C, et al. MicroRNA-455-3p promotes TGF-β signaling and inhibits osteoarthritis development by directly targeting PAK2. Exp Mol Med. 2019 Oct 4;51(10):1–13.
- 254. Qian Z, Gao X, Jin X, Kang X, Wu S. Cartilage-specific deficiency of clock gene Bmall accelerated articular cartilage degeneration in osteoarthritis by up-regulation of mTORC1 signaling. Int Immunopharmacol. 2023 Feb;115:109692.
- 255. Swingler TE, Niu L, Pontifex MG, Vauzour D, Clark IM. The microRNA-455 Null Mouse Has Memory Deficit and Increased Anxiety, Targeting Key Genes Involved in Alzheimer's Disease. Int J Mol Sci. 2022 Jan 5;23(1):554.

- 256. Cheng JH, Wang CJ, Su SH, Huang CY, Hsu SL. Next-generation sequencing identifies articular cartilage and subchondral bone miRNAs after ESWT on early osteoarthritis knee. Oncotarget. 2016 Dec 20;7(51):84398–407.
- 257. Swingler TE, Wheeler G, Carmont V, Elliott HR, Barter MJ, Abu-Elmagd M, et al. The expression and function of microRNAs in chondrogenesis and osteoarthritis. Arthritis Rheum. 2012;64(6):1909–19.
- 258. Akagi R, Akatsu Y, Fisch KM, Alvarez-Garcia O, Teramura T, Muramatsu Y, et al. Dysregulated circadian rhythm pathway in human osteoarthritis: NR1D1 and BMAL1 suppression alters TGF-β signaling in chondrocytes. Osteoarthritis Cartilage. 2017;25(6):943–51.
- 259. Rong Z, Zheng K, Chen J, Jin X. Function and regulation of ULK1: From physiology to pathology. Gene. 2022 Oct;840:146772.
- 260. Koike N, Yoo SH, Huang HC, Kumar V, Lee C, Kim TK, et al. Transcriptional Architecture and Chromatin Landscape of the Core Circadian Clock in Mammals. Science (1979). 2012 Oct 19;338(6105):349–54.
- 261. Nagel R, Clijsters L, Agami R. The miRNA-192/194 cluster regulates the Period gene family and the circadian clock. FEBS Journal. 2009;276(19):5447–55.
- 262. Rosensweig C, Reynolds KA, Gao P, Laothamatas I, Shan Y, Ranganathan R, et al. An evolutionary hotspot defines functional differences between CRYPTOCHROMES. Nat Commun. 2018 Mar 19;9(1):1138.
- 263. Park J, Lee K, Kim H, Shin H, Lee C. Endogenous circadian reporters reveal functional differences of *PERIOD* paralogs and the significance of PERIOD:CK1 stable interaction. Proceedings of the National Academy of Sciences. 2023 Feb 7;120(6).
- 264. Bekki H, Duffy T, Okubo N, Olmer M, Alvarez-Garcia O, Lamia K, et al. Suppression of circadian clock protein cryptochrome 2 promotes osteoarthritis. Osteoarthritis Cartilage. 2020;
- 265. Paige Paddy. microRNA-455 in cartilage and skeletal development. University of East Anglia; 2021.
- 266. Akashi M, Takumi T. The orphan nuclear receptor RORα regulates circadian transcription of the mammalian core-clock Bmall. Nat Struct Mol Biol. 2005 May 10;12(5):441–8.
- 267. Liang T, Chen T, Qiu J, Gao W, Qiu X, Zhu Y, et al. Inhibition of nuclear receptor RORα attenuates cartilage damage in osteoarthritis by modulating IL-6/STAT3 pathway. Cell Death Dis. 2021 Sep 28;12(10):886.

- 268. Chen Z, Wang H, Xia Y, Yan F, Lu Y. Therapeutic Potential of Mesenchymal Cell–Derived miRNA-150-5p–Expressing Exosomes in Rheumatoid Arthritis Mediated by the Modulation of MMP14 and VEGF. The Journal of Immunology. 2018 Oct 15;201(8):2472–82.
- 269. Zhang Y, Li S, Jin P, Shang T, Sun R, Lu L, et al. Dual functions of microRNA-17 in maintaining cartilage homeostasis and protection against osteoarthritis. Nat Commun. 2022;13(1):1–14.
- 270. Dudek M, Gossan N, Yang N, Im HJ, Ruckshanthi JPD, Yoshitane H, et al. The chondrocyte clock gene Bmall controls cartilage homeostasis and integrity. Journal of Clinical Investigation. 2016;126(1):365–76.
- 271. Yu C, Huang Z, Xu Y, Zhang B, Li Y. Deep sequencing of microRNAs reveals circadian-dependent microRNA expression in the eyestalks of the Chinese mitten crab Eriocheir sinensis. Sci Rep. 2023 Mar 31;13(1):5253.
- 272. Le Bleu HK, Kamal FA, Kelly M, Ketz JP, Zuscik MJ, Elbarbary RA. Extraction of high-quality RNA from human articular cartilage. Anal Biochem. 2017 Feb;518:134–8.
- 273. Zhang X, Wang C, Zhao J, Xu J, Geng Y, Dai L, et al. miR-146a facilitates osteoarthritis by regulating cartilage homeostasis via targeting Camk2d and Ppp3r2. Cell Death Dis. 2017 Apr 6;8(4):e2734–e2734.
- 274. Koronowski KB, Kinouchi K, Welz PS, Smith JG, Zinna VM, Shi J, et al. Defining the Independence of the Liver Circadian Clock. Cell. 2019 May;177(6):1448-1462.e14.
- 275. Abe YO, Yoshitane H, Kim DW, Kawakami S, Koebis M, Nakao K, et al. Rhythmic transcription of Bmal1 stabilizes the circadian timekeeping system in mammals. Nat Commun. 2022 Aug 23;13(1):4652.
- 276. Chen Z, Zhang Y, Liang C, Chen L, Zhang G, Qian A. Mechanosensitive miRNAs and Bone Formation. Int J Mol Sci. 2017 Aug 2;18(8):1684.
- 277. Karim A, Amin AK, Hall AC. The clustering and morphology of chondrocytes in normal and mildly degenerate human femoral head cartilage studied by confocal laser scanning microscopy. J Anat. 2018 Apr 28;232(4):686–98.
- 278. Liu X, Yang B, Zhang Y, Guo X, Yang Q, Liu X, et al. miR-30a-5p inhibits osteogenesis and promotes periodontitis by targeting Runx2. BMC Oral Health. 2021 Dec 11;21(1):513.
- 279. Jiang L hong, Zhang H da, Tang J hai. MiR-30a: A Novel Biomarker and Potential Therapeutic Target for Cancer. J Oncol. 2018 Aug 6;2018:1–9.

- 280. Zhang M, Liu Q, Mi S, Liang X, Zhang Z, Su X, et al. Both miR-17-5p and miR-20a Alleviate Suppressive Potential of Myeloid-Derived Suppressor Cells by Modulating STAT3 Expression. The Journal of Immunology. 2011 Apr 15;186(8):4716–24.
- 281. Steinmetz JD. Global, regional, and national burden of osteoarthritis, 1990–2020 and projections to 2050: a systematic analysis for the Global Burden of Disease Study 2021. The lancet Rheumatology . 5(9):e508–22.
- 282. Balaskas P, Clegg P, Welting T, Peffers M. Defining the role and mechanisms of microRNAs in cartilage ageing and disease. Osteoarthritis Cartilage [Internet]. 26(2018):S165. Available from: https://doi.org/10.1016/j.joca.2018.02.360
- 283. Aten S, Hansen KF, Snider K, Wheaton K, Kalidindi A, Garcia A, et al. miR-132 couples the circadian clock to daily rhythms of neuronal plasticity and cognition. Learning and Memory. 2018;25(5):214–29.
- 284. Miyaki S, Nakasa T, Otsuki S, Grogan SP, Higashiyama R, Inoue A, et al. MicroRNA-140 is expressed in differentiated human articular chondrocytes and modulates interleukin-1 responses. Arthritis Rheum. 2009 Sep 27;60(9):2723–30.
- 285. Luo W, Liu L, Yang L, Dong Y, Liu T, Wei X, et al. The vitamin D receptor regulates miR-140-5p and targets the MAPK pathway in bone development. Metabolism. 2018 Aug;85:139–50.
- 286. Wang Z, Zhu Z, Pan F, Zheng S, Parameswaran V, Blizzard L, et al. Long-term effects of vitamin D supplementation and maintaining sufficient vitamin D on knee osteoarthritis over 5 years. Arthritis Res Ther. 2023 Sep 23;25(1):178.
- 287. Pagani S, Maglio M, Sicuro L, Fini M, Giavaresi G, Brogini S. RNA Extraction from Cartilage: Issues, Methods, Tips. Int J Mol Sci. 2023 Jan 20;24(3):2120.
- 288. Mao L, Liu S, Hu L, Jia L, Wang H, Guo M, et al. miR-30 Family: A Promising Regulator in Development and Disease. Biomed Res Int. 2018 May 29;2018:1–8.
- 289. Li L, Yang C, Liu X, Yang S, Ye S, Jia J, et al. Elevated expression of microRNA-30b in osteoarthritis and its role in ERG regulation of chondrocyte. Biomedicine & Pharmacotherapy. 2015 Dec;76:94–9.
- 290. Zhang H, Wang Y, Yang G, Yu H, Zhou Z, Tang M. MicroRNA-30a regulates chondrogenic differentiation of human bone marrow-derived mesenchymal stem cells through targeting Sox9. Exp Ther Med. 2019 Oct 30;
- 291. Taguchi A, Yanagisawa K, Tanaka M, Cao K, Matsuyama Y, Goto H, et al. Identification of Hypoxia-Inducible Factor-1α as a Novel Target for *miR-17-92* MicroRNA Cluster. Cancer Res. 2008 Jul 15;68(14):5540–5.

- 292. Zhang Y, Li S, Jin P, Shang T, Sun R, Lu L, et al. Dual functions of microRNA-17 in maintaining cartilage homeostasis and protection against osteoarthritis. Nat Commun. 2022 Dec 1;13(1).
- 293. Lian C, Tao T, Su P, Liao Z, Wang X, Lei Y, et al. Targeting miR-18a sensitizes chondrocytes to anticytokine therapy to prevent osteoarthritis progression. Cell Death Dis. 2020 Nov 3;11(11):947.
- 294. Lian C, Tao T, Su P, Liao Z, Wang X, Lei Y, et al. Targeting miR-18a sensitizes chondrocytes to anticytokine therapy to prevent osteoarthritis progression. Cell Death Dis. 2020 Nov 3;11(11):947.
- 295. Pezük P, Mohawk JA, Wang LA, Menaker M. Glucocorticoids as Entraining Signals for Peripheral Circadian Oscillators. Endocrinology. 2012 Oct 1;153(10):4775–83.
- 296. Husse J, Eichele G, Oster H. Synchronization of the mammalian circadian timing system: Light can control peripheral clocks independently of the SCN clock. BioEssays. 2015 Oct 7;37(10):1119–28.
- 297. Wang Q, Bozack SN, Yan Y, Boulton ME, Grant MB, Busik J V. Regulation of Retinal Inflammation by Rhythmic Expression of MiR-146a in Diabetic Retina. Investigative Opthalmology & Visual Science. 2014 Jun 26;55(6):3986.
- 298. Li M, Marin-Muller C, Bharadwaj U, Chow K, Yao Q, Chen C. MicroRNAs: Control and Loss of Control in Human Physiology and Disease. World J Surg. 2009 Apr 22;33(4):667–84.
- 299. Mengatto CM, Mussano F, Honda Y, Colwell CS, Nishimura I. Circadian Rhythm and Cartilage Extracellular Matrix Genes in Osseointegration: A Genome-Wide Screening of Implant Failure by Vitamin D Deficiency. PLoS One. 2011 Jan 11;6(1):e15848.
- 300. O'Neil D, Jochum MD, Goodspeed D, Gozalez-Rodriguez P, Shope C, Aagaard KM. Deletion of Npas2 in the liver alters the functional gut microbiome at light/dark timepoints. Am J Obstet Gynecol. 2022 Jan;226(1):S196.

Gene	Primer	Sequence 5'-3'	Probe	
18s rRNA	F	GCCGCTAGAGGTGAAATTCTTG	6-FAM- ACCGGCGCAAGACGGA-	
	R	CATTCTTGGCAAATGCTTTCG	TAMRA	
GAPDH	F	ACCCACTCCTCCACCTTTGA	#77	
G/H DII	R	CCACCACCTGTTGCTGTAG		
YWHAZ	F	TCCAGGGACAGAGTCTCAGC	#74	
1 1111112	R	AGCTCATTTTATCCATGAC		
BMAL1	F	TCCTTCCAGTGGCCTACTATC	#2	
Divir (L)	R	GGGTTCTCACCAAGAATAGAAGAA		

## Appendix Table 1. 1 RT-qPCR primer and probe universal probe library

Human			
Gene	Primer	Sequence 5'-3'	
GAPDH	F	ACCCACTCCTCCACCTTTGA	
GAFDH	R	CCACCACCTGTTGCTGTAG	
BMAL1	F	TCCTTCCAGTGGCCTACTATC	
DWALI	R	GGGTTCTCACCAAGAATAGAAGAA	
CLOCK	F	ACCTCGCAGAATGTCACAGGCA	
CLOCK	R	CTGAACCATCGACTTCGTAGCG	
CRY1	F	GGTTGCCTGTTTCCTGACTCGT	
CKTT	R	GACAGCCACATCCAACTTCCAG	
CRY2	F	GGACAAGCACTTGGAACGGAAG	
CK12	R	ACAAGTCCCACAGGCGGTAGTA	
PER1	F	TCAACTGCCTGGACAGCATCCT	
LKI	R	TCAGAGGCTGAGGAGGTGGTAT	
RORA	F	CACCAGCATCAGGCTTCTTTCC	
KOKA	R	GTATTGGCAGGTTTCCAGATGCG	
NPAS2	F	AAGTGCTGGGAACCTCAGGCTA	
NI ASZ	R	AGCCAGATCCACTGCTGACCTT	
DICER	F	TCCGATGGTTCTCGAAGG	
DICER	R	GCAAAGCAGGCTTTTCAT	
DROSHA	F	GAAACTTCGCCACCTCCTAGCA	
DROSHA	R	CTCCACCGTTACTTCTCGTCTC	
WWP2	F	GGTGCGATACTTTGTGGACCAC	
** ** 1	R	GATACTTCCACCGAAAACTGCGG	
MMP13	F	CCTTGATGCCATTACCAGTCTCC	
1711711 13	R	AAACAGCTCCGCATCAACCTGC	
SOX9	F	GTACCCGCACTTGCACAAC	
5011)	R	TCTCGCTCTCGTTCAGAAGCT	

## Appendix Table 1. 2 Human RT-qPCR primer and probe Sybr green.

Mouse			
Gene	Primer	Sequence 5'-3'	
GAPDH	F	AAGAGGGATGCTGCCCTTAC	
GAI DII	R	CCATTTTGTCTACGGGACGA	
18S	F	GCCGCTAGAGGTGAAATTCTTG	
103	R	CATTCTTGGCAAATGCTTTCG	
BMAL1	F	GCAACTACAGTGGCCCTTTG	
DWI/YE1	R	GGGCCCAAATTCCCACATCT	
DICER	F	AGCAGTGCTGAGAAGAGGAAGG	
DICER	R	CCGCTTTTCTCCACAGTGATGC	
DROSHA	F	GAAACTTCGCCACCTCCTAGCA	
DROSHA	R	GAATCCTTGGCTACTCAGCTCC	
RUNX2	F	CACCGTCTTTACAAATCCGCCAC	
KUNAZ	R	CGCTCGGAAAAGGACAAACTCC	
ALPL	F	CCAGAAAGACACCTTGACTGTGG	
ALIL	R	TCTTGTCCGTGTCGCTCACCAT	
COL10A1	F	GCATCTCCCAGCACCAGA	
COLIUAI	R	CCATGAACCAGGGTCAAGAA	
TRAP	F	GGTCAGCAGCTCCCTAGAAG	
TICH.	R	GGAGTGGGAGCCATATGATTT	

Appendix Table 1. 3 Mouse RT-qPCR primer and probe Sybr green

hsa-miR-455-5p					
Gene	Primer	rimer sequence 5'-3'			
	F	TTGTTTAAACGAGCTC GCACTAGTATAGCCTCATCCG			
CLOCK A	R	CGACTCTAGACTCGAG CAAGAGCAATTCAAATGG			
CLOCK A	Mut1	TTTTGGTAGGCTGACAATAGGATCCTTACCCATGCGGATGAGGC			
	Mut2	GAAATGCTGAAATGACATGCCAACATTTCAGGCTAGCTTTAAAACACTCAGAATAATTCTTGAAATTATTATA			
	F	TTGTTTAAACGAGCTC TGCACTTCCCTCAAG			
CLOCK B	R	CGACTCTAGACTCGAG CCGCCAAATTTAAGAACTT			
	Mut1	AAATAGAGGCATCAGGATCCATTGGTCATACTGGCCTTTGAC			
	F	TTGTTTAAACGAGCTC CCTTGCCTCTAAAGTCAG			
PER2	R	CGACTCTAGACTCGAG TTGGCATCACGTAAACAAA			
	Mut1	TGAAGCTACAGTTAACAATCAGTGAGGGATCCTTAAATGATAAAAATAATGCTGATGGTAAACA			
PER3 A	F	TTGTTTAAACGAGCTC TGCCACCTACAGGTTGT			
PER3 A	R	CGACTCTAGACTCGAG GATCTACAAGGATGAAGGC			
DED2 D	F	TTGTTTAAACGAGCTC GTAGCTATCAGGATCATTGCG			
PER3 B	R	CGACTCTAGACTCGAG CTCCTCATGCTCTGACA			
	F	TTGTTTAAACGAGCTC TCCACAAGTTTGGGTC			
CRY1	R	CGACTCTAGACTCGAG TCCACAAGTTTGGGTC			
	Mut1	CAGAGGCTACAATACCAATTTGGATTACGGATCCTATCTAAAACATTATTATCAAAGAGTGCAAAGTT			
CDV2 A	F	TTGTTTAAACGAGCTC CCACCGCAGCAGCAG			
CRY2 A	R	CGACTCTAGACTCGAG GGCGTGCTACAGGTAC			

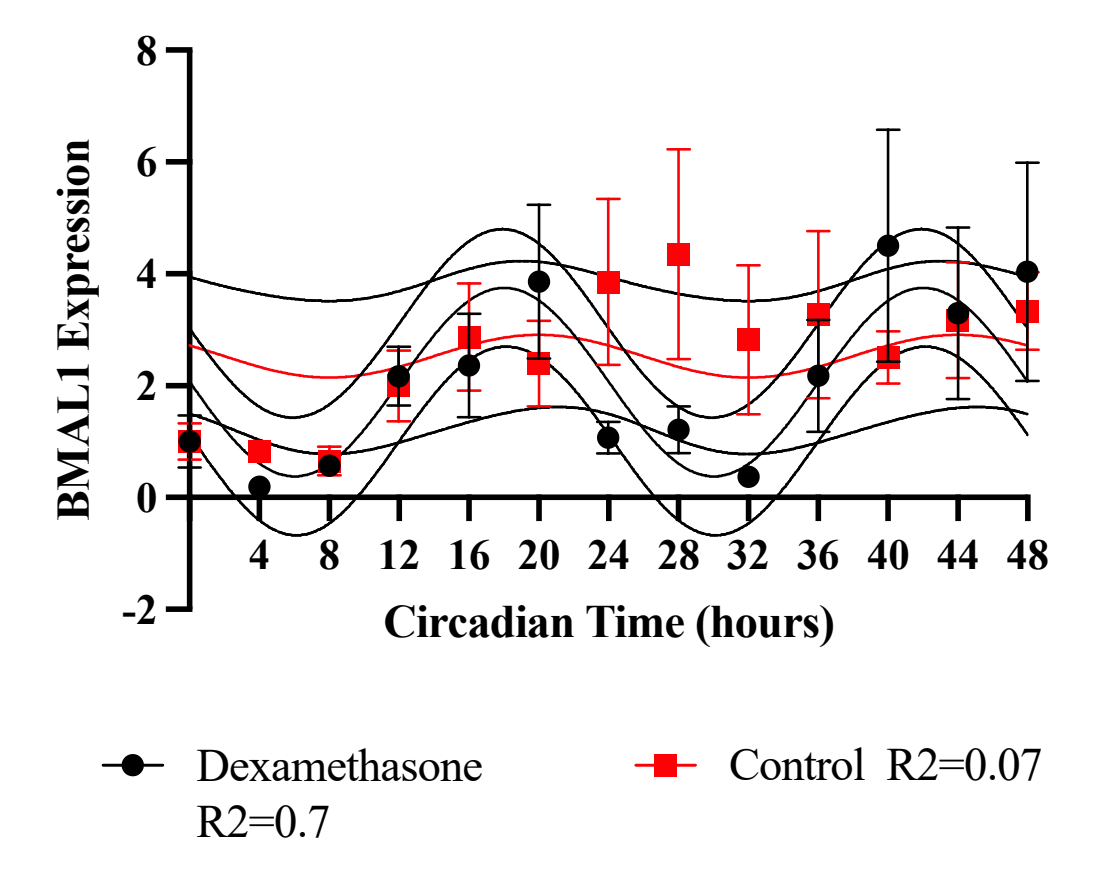
	Mut1	CATGCACACACACAGGATCCCCACTCCCTCTGC
	F	TTGTTTAAACGAGCTC CAGTAGCTGAGCTCCAA
CRY2 B	R	CGACTCTAGACTCGAG GCGCTGCTAGTGAA
	Mut1	GAAGGAAGAGGTGGGAGGATCCGGCCACTCCTGGAATG
	F	TTGTTTAAACGAGCTC TACATAACATGTGATTGC
RORA A	R	CGACTCTAGACTCGAG ACTGATCTCACCTACAC
	Mut1	CTGTTGCAATTGCGTTTCTGGATCCATTATTTGATCTATAATATAAAGTTGTTTTCATGGGG
RORA B	F	TTGTTTAAACGAGCTC GCACGATTTAGCATCCT
KOKA B	R	CGACTCTAGACTCGAG TTACAGAAGGCTGAGT

Appendix Table 1. 4 Circadian clock gene 3'UTR cloning Wild-type and mutant primers for miR-455-5p assay

hsa-miR-45	hsa-miR-455-3p				
Gene	Primer sequence 5'-3'				
CLOCK A	F	TTGTTTAAACGAGCTCGGGAATCAGAAAGGCACT			
CLOCK A	R	CGACTCTAGACTCGAG TGTAGTGAAGGCATAGCCA			
	F	TTGTTTAAACGAGCTCACGGAAGGAATAGCACACA			
CLOCK B	R	CGACTCTAGACTCGAG TATCCTGAATAACTGTGCC			
	Mut1	TAACCAAAGTATTCTTTTTCTGGATCCTTTTTGTGCAAAAATATTCAAGAGCAATTCAAATGGAAAT			
CLOCK C	F	TTGTTTAAACGAGCTC CTTATTCTGGGTGGTACTT			
CLOCK C	R	CGACTCTAGACTCGAG GTCTGCGTAGAGTACTATT			
	F	TTGTTTAAACGAGCTC ACTCCATTCTGGGACCA			
PER1	R	CGACTCTAGACTCGAG TGGATCCTAGGCTGG			
	Mut1	ATAGGAGAAGAAGCCTCTCAGGATCCCCTGGAGATGGTCCCAGAATG			
PER2 A	F	TTGTTTAAACGAGCTCTTCCCAGGGTGTTTGGATCA			
TERE II	R	CGACTCTAGACTCGAG CATGAAAAGAATGAGGGCTG			
PER 2 B	F	TTGTTTAAACGAGCTCTCTGCCTCCCAGGTTCAAGC			
TER 2 D	R	CGACTCTAGACTCGAG AAGTCAACTGCTTGGCACGC			
PER3	F	TTGTTTAAACGAGCTCGCTTCTTACCCAGTGCTGTT			
LENJ	R	CGACTCTAGACTCGAGTGATCTGCAGGGGTGTGAAT			
CRY2	F	TTGTTTAAACGAGCTCGACCTGGAGCAG			
	R	CGACTCTAGACTCGAGGAGGCCACTCC			
RORA A	F	TTGTTTAAACGAGCTCCAGACTTTCTACAGAGTC			

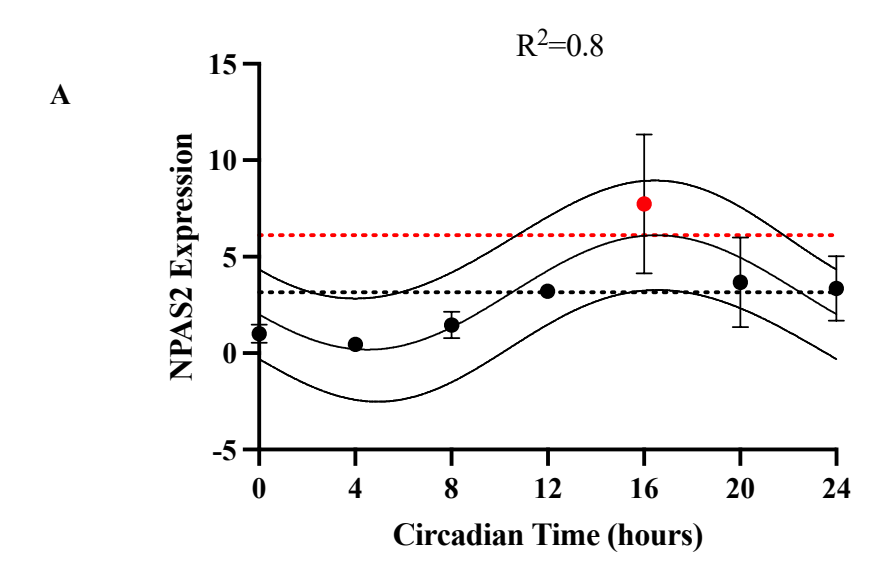
	R	CGACTCTAGACTCGAGCCTCACCCTATCCATCG
Mut 1 ATGCACACCAGTCACCG		ATGCACACCAGTCACCGATTATTGCGTGCACCTCTGTTGTTACTGACAGATTGGTG
	Mut2	CCCTTTTCATGCCATCCTGCGGATCCGCAATAATCGGTGAAAAAAT
	Mut3	AGAATTCCAAGTTGAGACCGGCTAGCTATTTAACTACTGAATTGTGTAAAATGAGCTTCTCCTCC
RORA B	F	TTGTTTAAACGAGCTCCATACAATGTTGAACCAGTT
KOKA B	R	CGACTCTAGACTCGAGTATGCTGACAGTTAGCATCT
HLF	F	TTGTTTAAACGAGCTC GCGTCTTGGATTAGCCTTTG
IILI	R	CGACTCTAGACTCGAG TAGCACCGATATCAACCTCA
DBP	F	TTGTTTAAACGAGCTCCCGCCTTGCTGAGACTTACG
DDI	R	CGACTCTAGACTCGAGTGTTCGTCTCATGCGCGTC
	F	TTGTTTAAACGAGCTCATCTCTGGAGTGCAGCGC
NPAS2	R	CGACTCTAGACTCGAGGCTGCTGTTACTGTGGT
	Mut1	CTCCAACAGATCTCTGACCGGATCCTTCTCCAATACAAAGGAAAGA

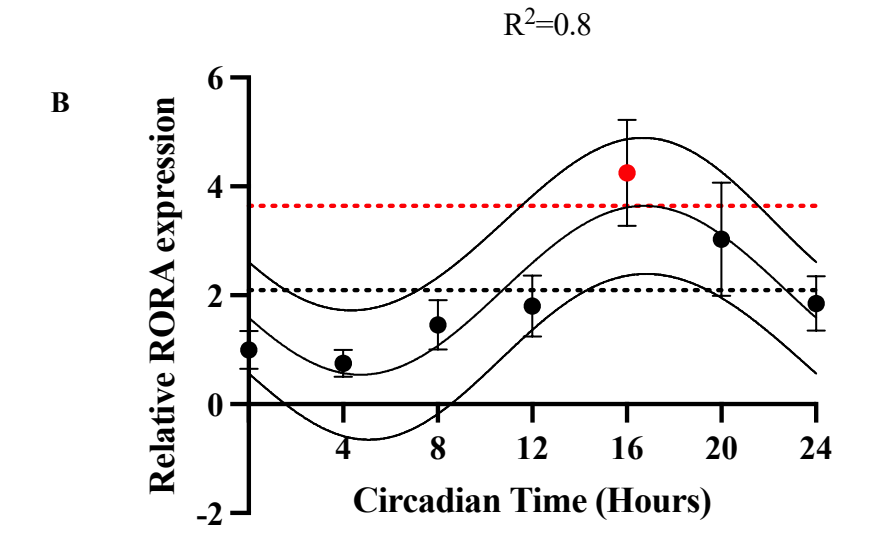
Appendix Table 1. 5. Circadian clock gene 3'UTR cloning Wild-type and mutant primers for miR-455-3p assay.



Appendix Figure 2. 1 Comparing cosinor analysis of *BMAL1* abundance in non-synchronised and synchronised SW1353 cells.

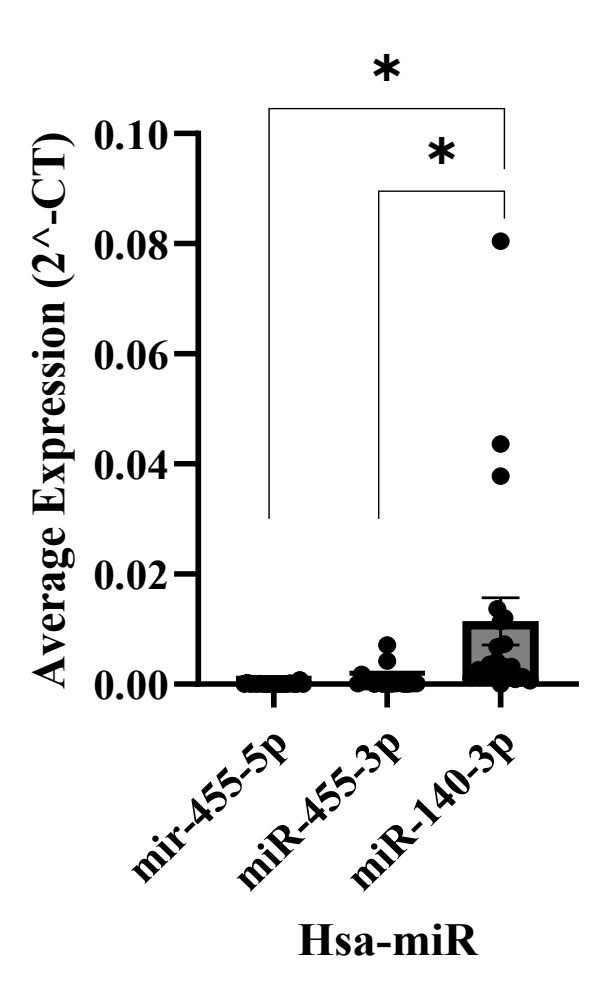
Time dependent expression of *BMAL1* in SW1353 cells synchronised in 100nM dexamethasone or non-synchronised vehicle control. Oscillation in *BMAL1* abundance evaluated by cosinor analysis. Data presented relative to circadian time 0 mean +/- SD, N=3.





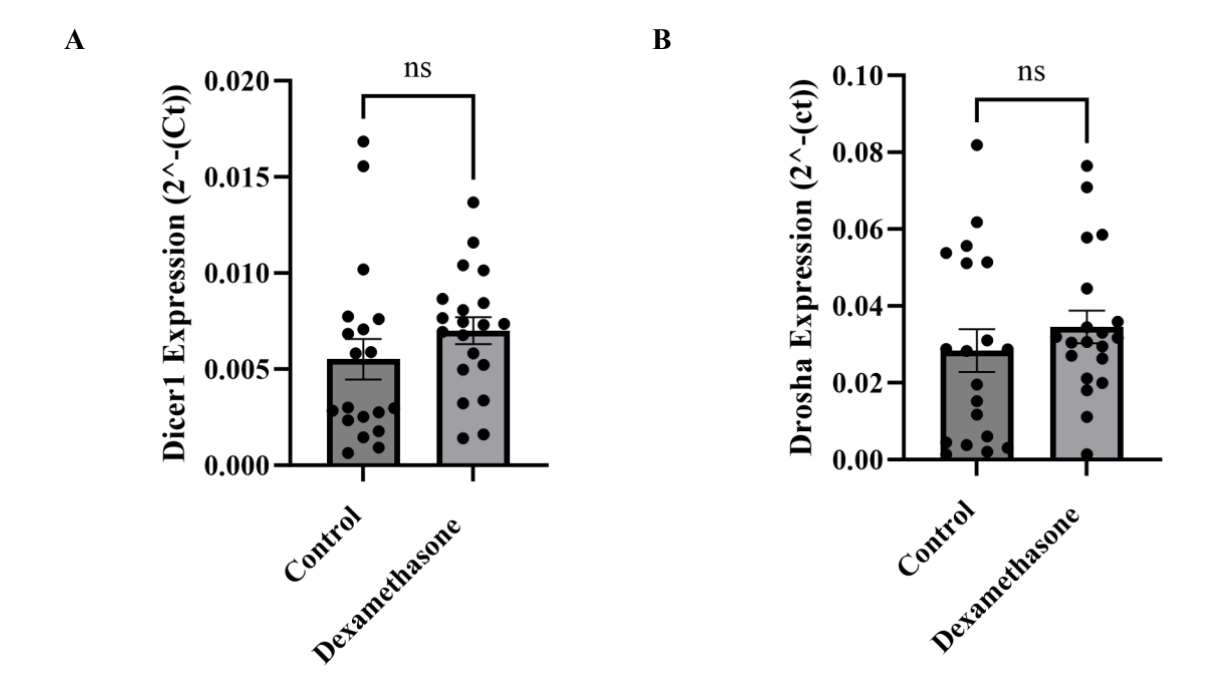
## Appendix Figure 2. 2 Rhythmic expression of NPAS2 and ROR $\alpha$ genes of the molecular circadian clock in SW1353.

Time dependent expression of (A) NPAS2 (B)  $ROR\alpha$  in SW1353 synchronised in 100nM dexamethasone. Differences determined by two-way ANOVA and multiple comparisons. Oscillation in BMAL1 abundance evaluated by cosinor analysis. Red data points indicate amplitudes significantly greater than MESOR. Red line and black line depict predicted amplitude and MESOR respectively Data presented relative to circadian time 0 mean +/- SD, N=3.



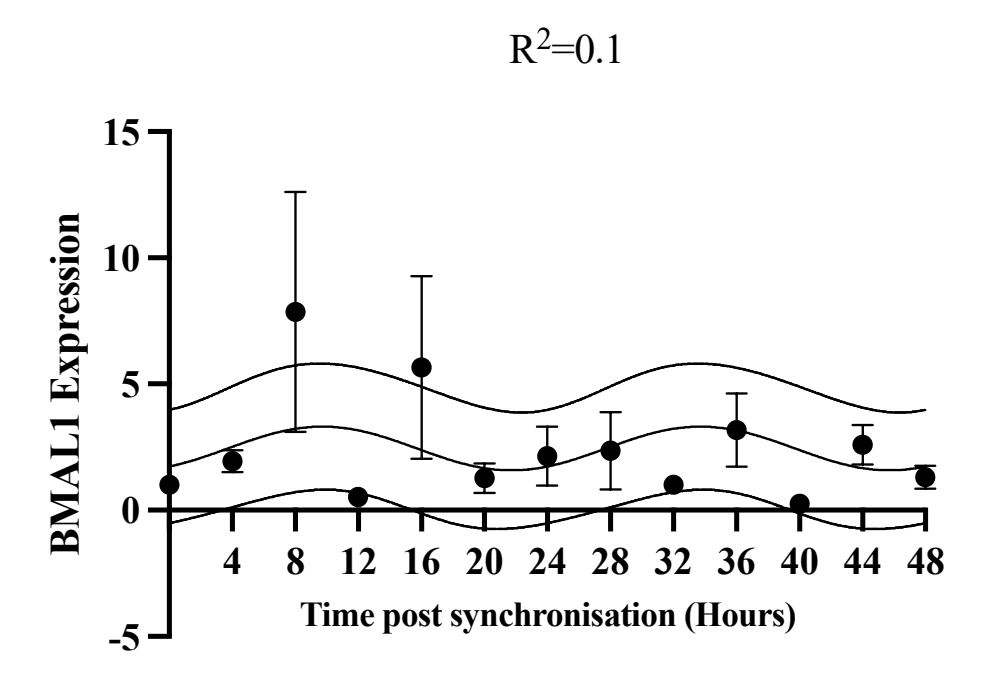
## Appendix Figure 2. 3 Average abundance of miR-140 and miR-455 in SW1353 chondrosarcoma cells.

Average expression of microRNAs in SW1353 cells non-synchronized vehicle control over a 48hours. Expression of hsa-miR-455-3p, hsa-miR-455-5p and hsa-miR-140-3p was determined by RT-qPCR, normalized to *GAPDH* housekeeper gene. Data presented as mean +/- SD, Difference determined by multiple comparisons test P<0.05, \*\*P<0.01\*\*\* p < 0.001.(N=39)



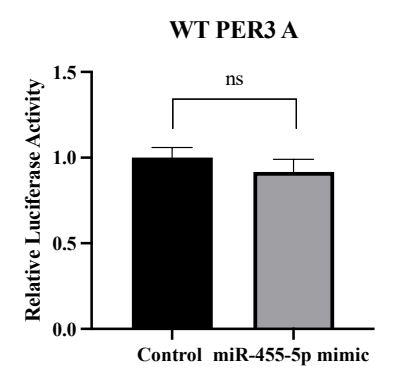
Appendix Figure 2. 4 Effects of dexamethasone on DICER1 and DROSHA abundance in chondrocytes.

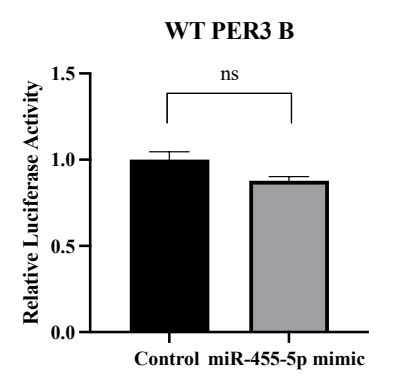
Average expression of (A) DICER1 and (B) DROSHA mRNA in SW1353 chondrosarcomas synchronised in either 100nM dexamethasone or vehicle control. Data presented as mean  $\pm$ SD. Difference determined by students T-test P<0.05, \*\*P<0.01\*\*\* p<0.001.(N=39)

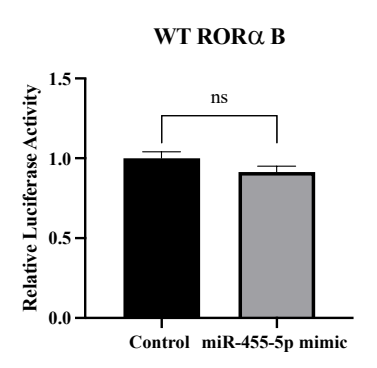


Appendix Figure 2. 5 Oscillation of BMAL1 in SW1353 chondrosarcoma cells synchronised in 50% FCS.

SW1353 chondrosarcoma cells were synchronised in DMEM containing 50% foetal calf serum for 2 hours and rested in low serum and RNA was extracted by TRIZOL every 4 hours for 48hours. The first harvest is designated circadian time 0. Expression of *BMAL1* mRNA was measured by RT-qPCR, normalised to *18S* housekeeper gene mRNA. Rhythmicity detected by Cosinor fit analysis. Red line and black line depict predicted amplitude and MESOR respectively. Data presented relative to circadian time 0 mean +/- SD, N=3 Biological replicates per time point. \*p<0.05 \*\*p<0.005 \*\*p<0.001.

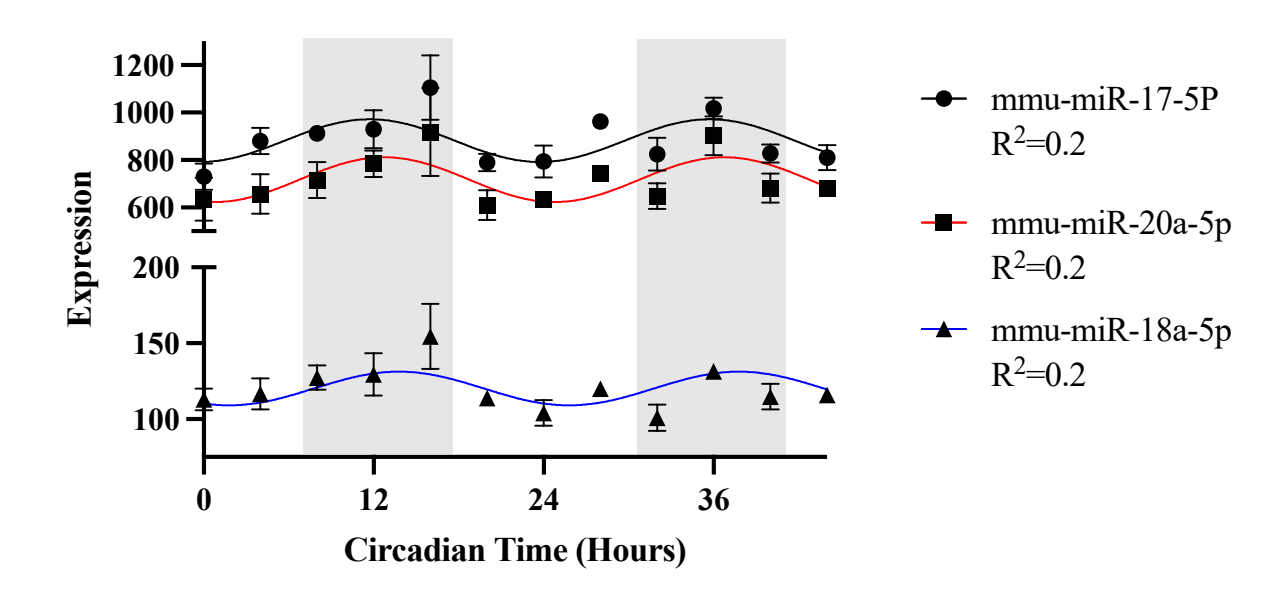






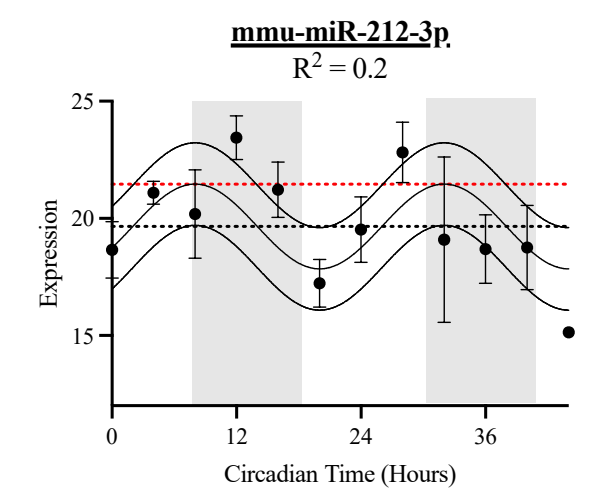
#### Appendix Figure 3. 1 Identifying miR-455-5p clock targets by dual-glo luciferase assay. .

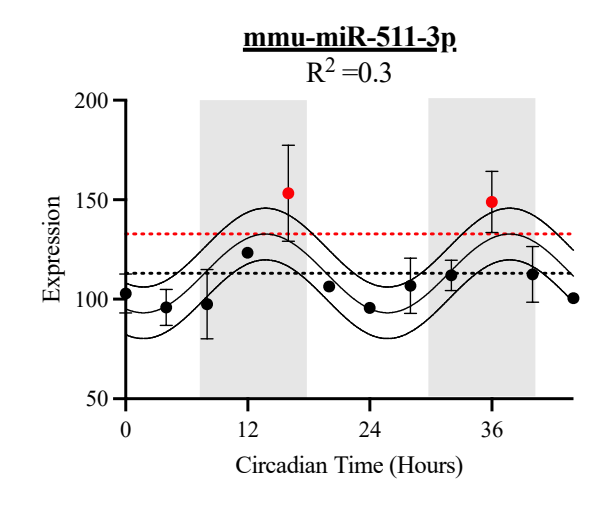
Dual-luciferase reporter assays were performed to assess interaction of hsa-miR-455-5p and targeting sequences in the 3'UTR of circadian mRNA. Reporter plasmids containing sections of the 3'UTR with predicted seed sites were cloned into pmirGLO. Plasmids were transfected into DF1 with miR-455-5p mimic or negative control for 48hours. Relative luciferase activity was normalised to Renilla luciferase. Results presented as miR-455-5p fold change over negative control. Data presented as mean +/ SD(N=5), two-tailed unpaired t-test. \* p < 0.05, \*\*\* p < 0.01, \*\*\* p < 0.005



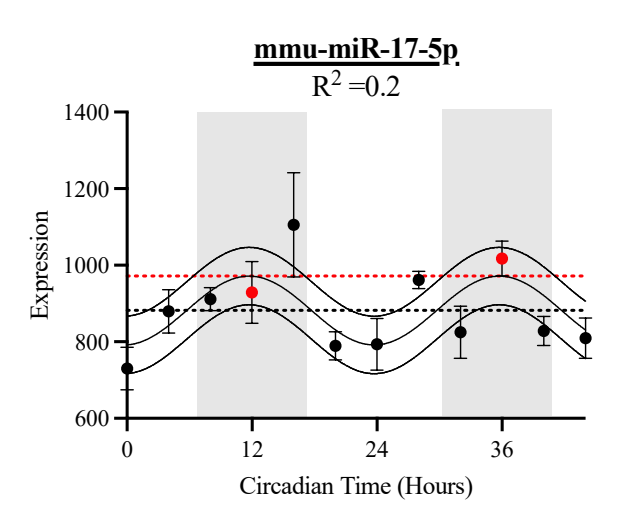
#### Appendix Figure 4. 1. Circadian expression of miR-17/92 cluster in knee AC.

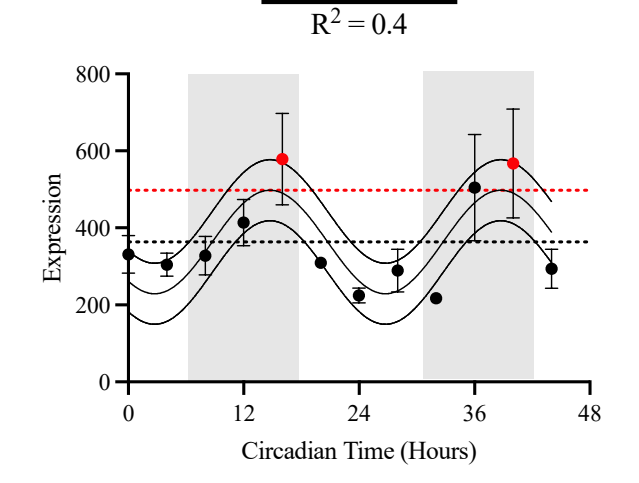
Cosinor analysis of daily abundances of miR-17-5p, miR-20a-5p, miR-18a-5p as determined by small RNA sequencing. Grey regions represent animals subjective rest-phase. Data presented as average processed reads +/- SD. N=3 biological replicates.

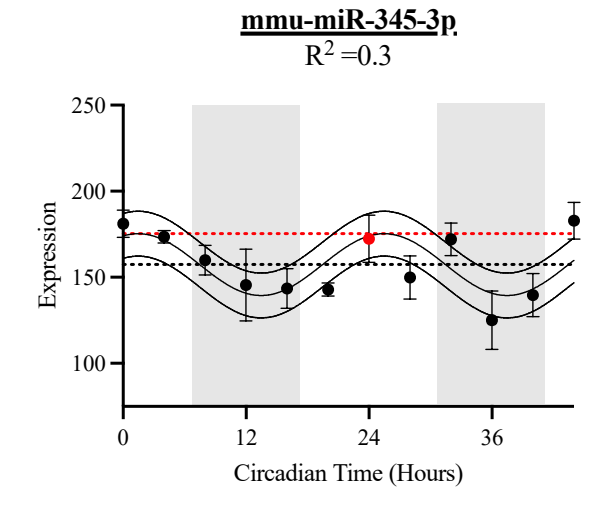


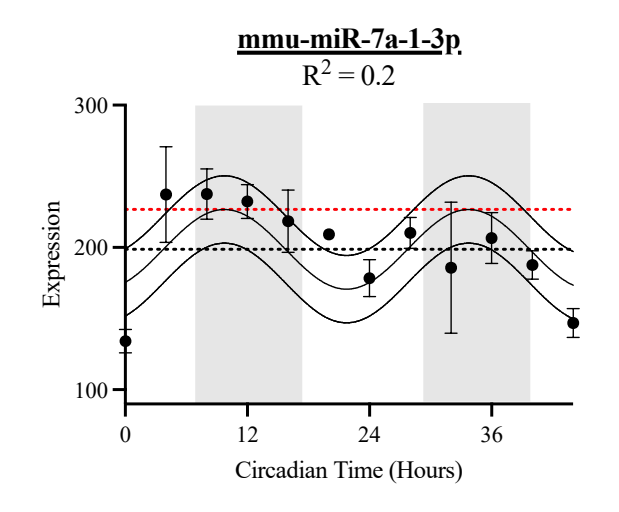


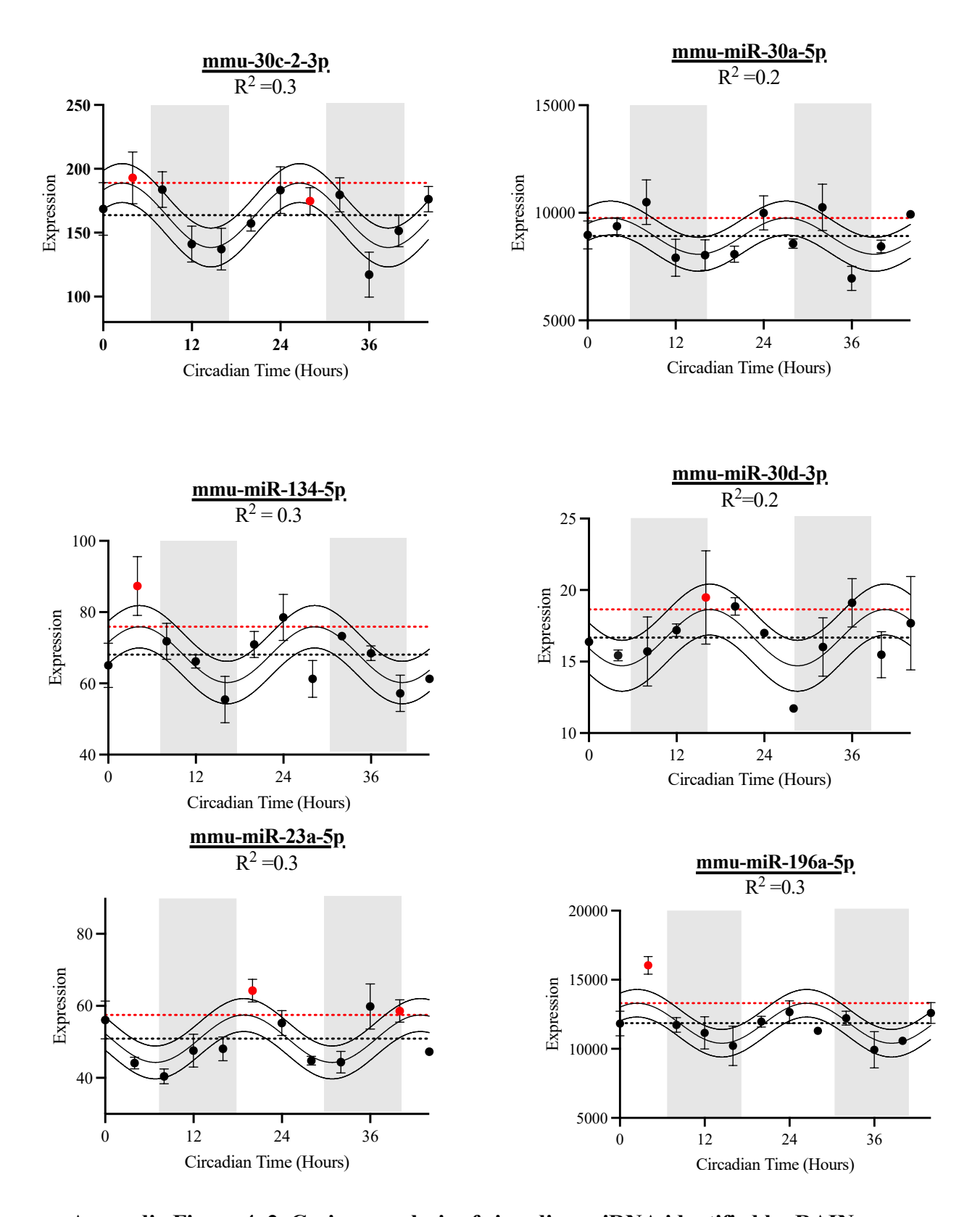
mmu-miR-2137











Appendix Figure 4. 2. Cosinor analysis of circadian miRNA identified by RAIN.

Cosinor analysis of oscillating microRNAs as determined by RAIN analysis. Grey regions represent animals subjective rest-phase. Red line and black line depict predicted amplitude and MESOR respectively. Red data points indicate amplitude statistically greater than the MESOR. data presented as average processed reads +/- SD. N=3 biological replicates per time point.

	miRNA	Average
	IIIKNA	PRM
1	mmu-miR-140-3p	106523.52
2	mmu-miR-26a-5p	65621.44
3	mmu-miR-16-5p	54232.05
4	mmu-miR-99a-5p	39607.71
5	mmu-miR-21a-5p	33478.84
6	mmu-let-7i-5p	32946.85
7	mmu-miR-181a-5p	26653.94
8	mmu-let-7c-5p	24908.33
9	mmu-miR-125b-5p	24193.19
10	mmu-let-7f-5p	24069.90
11	mmu-miR-191-5p	19641.88
12	mmu-miR-24-3p	19623.88
13	mmu-miR-103-3p	19282.97
14	mmu-miR-92a-3p	19264.28
15	mmu-miR-27b-3p	18849.88
16	mmu-miR-93-5p	18722.36
17	mmu-miR-23a-3p	17733.10
18	mmu-miR-29a-3p	17727.88
19	mmu-miR-451a	15291.40
20	mmu-miR-143-3p	14661.43
21	mmu-miR-23b-3p	14591.50
22	mmu-miR-25-3p	13987.96
23	mmu-miR-133a-3p	13888.90
24	mmu-miR-125a-5p	12617.14
25	mmu-let-7b-5p	10828.57

26	mmu-miR-486a-5p	10754.93
27	mmu-miR-486b-5p	10724.40
28	mmu-miR-126a-3p	10689.69
29	mmu-miR-181b-5p	10337.68
30	mmu-miR-196a-5p	9900.76
31	mmu-miR-223-3p	9209.09
32	mmu-miR-199a-5p	9075.93
33	mmu-miR-199a-3p	8772.89
34	mmu-miR-196b-5p	8753.03
35	mmu-miR-199b-3p	8745.90
36	mmu-miR-26b-5p	8541.27
37	mmu-let-7j	7923.66
38	mmu-miR-30a-5p	7421.47
39	mmu-miR-100-5p	7382.68
40	mmu-miR-30d-5p	7263.59
41	mmu-miR-22-3p	6882.89
42	mmu-miR-140-5p	6851.66
43	mmu-miR-19b-3p	6251.87
44	mmu-miR-497a-5p	6021.52
45	mmu-miR-221-3p	5865.68
46	mmu-miR-101a-3p	5820.68
47	mmu-miR-148a-3p	5681.10
48	mmu-miR-27a-3p	5409.28
49	mmu-miR-378a-3p	5352.73
50	mmu-let-7g-5p	4350.27
65	mmu-miR-455-3p	2389.21
93	mmu-miR-455-5p	855.34

# Appendix Table 4. 1 Abundance of microRNAs in mouse knee AC determined by small-RNA sequencing.

Table summarising average abundance of microRNAs in mouse knee cartilage (N=39).

ID	p.Value	BHQ	Peak CT
mmu-miR-100-5p	0.004	0.11	12
mmu-miR-195a-3p	0.005	0.12	16
mmu-miR-221-5p	0.005	0.12	20
mmu-miR-411-5p	0.005	0.12	12
mmu-miR-431-5p	0.006	0.13	16
mmu-miR-139-5p	0.007	0.13	20
mmu-miR-24-3p	0.007	0.13	12
mmu-miR-20a-5p	0.007	0.13	12
mmu-miR-144-3p	0.007	0.13	12
mmu-miR-6236	0.008	0.14	12
mmu-miR-501-5p	0.009	0.14	16
mmu-miR-497a-5p	0.009	0.14	8
mmu-miR-3068-3p	0.009	0.14	4
mmu-miR-543-3p	0.008	0.14	12
mmu-miR-151-5p	0.011	0.14	20
mmu-miR-467c-5p	0.013	0.14	16
mmu-miR-146a-5p	0.011	0.14	16
mmu-miR-92a-1-5p	0.014	0.14	12
mmu-miR-181a-2-3p	0.013	0.14	4
mmu-miR-93-3p	0.011	0.14	8
mmu-miR-339-3p	0.013	0.14	12
mmu-miR-379-5p	0.012	0.14	8
mmu-miR-455-5p	0.011	0.14	12
mmu-miR-196b-5p	0.012	0.14	12
mmu-miR-669c-5p	0.012	0.14	12
mmu-miR-301a-3p	0.012	0.14	8
mmu-miR-9-5p	0.013	0.14	12
mmu-miR-615-3p	0.014	0.14	12
mmu-let-7f-5p	0.015	0.15	16
mmu-miR-125a-3p	0.016	0.15	12
mmu-miR-16-1-3p	0.016	0.15	12
mmu-miR-125b-2-3p	0.017	0.15	16
mmu-miR-6240	0.018	0.16	12
mmu-miR-28a-3p	0.018	0.16	8
mmu-miR-598-3p	0.019	0.16	12

ID	p.Value	BHQ	Peak CT
mmu-miR-103-3p	0.019	0.16	12
mmu-miR-103-3p	0.020	0.16	12
mmu-miR-106b-5p	0.021	0.17	12
mmu-miR-98-5p	0.022	0.17	20
mmu-miR-451a	0.022	0.17	16
mmu-miR-6538	0.023	0.17	8
mmu-miR-30d-5p	0.022	0.17	20
mmu-miR-320-3p	0.023	0.17	12
mmu-miR-30b-5p	0.024	0.18	12
mmu-miR-132-3p	0.027	0.19	20
mmu-miR-152-5p	0.028	0.19	20
mmu-miR-467a-5p	0.028	0.19	20
mmu-miR-467b-5p	0.029	0.19	12
mmu-miR-149-5p	0.032	0.21	8
mmu-miR-222-3p	0.032	0.21	16
mmu-miR-99a-5p	0.033	0.21	12
mmu-miR-322-3p	0.032	0.21	12
mmu-miR-18a-5p	0.034	0.22	20
mmu-miR-361-5p	0.036	0.22	20
mmu-miR-25-5p	0.036	0.22	20
mmu-miR-30c-5p	0.038	0.23	20
mmu-miR-365-3p	0.039	0.23	16
mmu-miR-340-5p	0.039	0.23	8
mmu-miR-503-5p	0.040	0.23	4
mmu-miR-542-3p	0.041	0.23	12
mmu-miR-423-3p	0.041	0.23	8
mmu-miR-151-3p	0.044	0.23	16
mmu-miR-150-3p	0.044	0.23	8
mmu-miR-501-3p	0.043	0.23	16
mmu-miR-187-3p	0.044	0.23	12
mmu-miR-190b-5p	0.042	0.23	12
mmu-miR-224-5p	0.047	0.25	16
mmu-miR-148a-5p	0.049	0.25	8
mmu-miR-532-3p	0.049	0.25	16
mmu-miR-540-3p	0.019	0.16	12

# Appendix Table 4. 2 Identification of the circadian miRNAome in mouse knee cartilage in-vivo (P>0.05).

Table summarising circadian microRNAs identified by a statistical threshold of P<0.05 using RAIN analysis of small-RNAseq data.